Aus dem Lehrstuhl für Physiologische Chemie
Lehrstuhl der Ludwig-Maximilians-Universität München

Dissertation

zum Erwerb des Doctor of Philosophy (Ph.D.)

an der Medizinischen Fakultät der
Ludwig-Maximilians-Universität München

Characterization of a novel ISWI chromatin remodeler in Saccharomyces cerevisiae

vorgelegt von:
Ameirika .

aus:

Malang / Indonesien

Jahr:
2024

Mit Genehmigung der Medizinischen Fakultät der
Ludwig-Maximilians-Universität München

Erstes Gutachten von:	Prof. Dr. Andreas G. Ladurner
Zweites Gutachten von:	Prof. Dr. Peter B. Becker
Drittes Gutachten von:	Prof. Dr. Maria del Sagrario Robles Martinez
Viertes Gutachtes:	Prof. Dr. Robert Schneider

Dekan: **Prof. Dr. med. Thomas Gudermann**

Datum der Verteidigung:

05.12.2024

Table of Contents

Abstract

Eukaryotic DNA is organized and packaged together with histone proteins to form chromatin. The compaction of chromatin structure consequently hinders access to the DNA with important implications for DNA-related processes such as transcription, replication, or DNA repair. To mediate access to DNA, histone modifications and chromatin remodelers are required to modulate chromatin structure. Chromatin remodelers have pivotal functions by utilizing the energy generated from ATP hydrolysis to reposition or evict nucleosomes or exchange histones. The ISWI-type remodeler is one of the four remodeler complex families and is highly conserved from yeast to humans. In *Saccharomyces cerevisiae*, two ISWI homologs, Isw1 and Isw2, both form multi-subunit complexes. The Isw1 remodeler is further grouped into two different complexes that share the catalytic ATPase subunit with different Ioc-associated subunits, namely Isw1a and Isw1b. Here, Isw1a consists of Isw1 and Ioc3, while Isw1b comprises Isw1, Ioc2 and Ioc4. Moreover, aside from the Ioc subunits, Esc8 has been suggested as another protein interacting with Isw1 according to protein-protein analysis in yeast, as well as its homology to Ioc3. However, an interaction between Esc8 and Isw1 remains to be confirmed, as do any possible functions as a chromatin remodeler. For this reason, a combination of biochemical i*n vitro* assays and AlphaFold structural analysis of the protein complex were utilized in this research to investigate the formation and functions of the Isw1-Esc8 protein complex as chromatin remodelers.

In this research, the Isw1c complex was endogenously purified from *S. cerevisiae* using TAP affinity purification, thus confirming the interaction between Isw1 and Esc8. Furthermore, a higher yield of the Isw1c protein complex was purified from a yeast strain containing the *pCUP1-ESC8* in an *ioc2*Δ *ioc3*Δ strain background. This purified complex was further tested in numerous biochemical assays, including DNA and nucleosome binding assays, ATP hydrolysis assays, and nucleosome sliding assays. These assays collectively demonstrated that Isw1c exhibits all the basic hallmarks of a chromatin remodeler. Specifically, Isw1c can bind to DNA and nucleosomes containing at least one DNA overhang. Like other Isw1 remodelers, the Isw1c ATPase activity is nucleosome-stimulated. Moreover, Isw1c has the ability to slide nucleosomes, preferably from the end position to the middle position. Also, by employing genome-wide *in vitro* reconstitution of nucleosome assays, Isw1c displayed the ability to generate regularly spaced and phased nucleosome arrays.

In addition to the basic characteristics of chromatin remodelers, I discovered that the recruitment of Isw1c and its remodeling activity are influenced by differently modified nucleosomes. Here, Isw1c showed a slight preference for binding to unmodified nucleosomes compared to acetylated nucleosomes. Remarkably, Isw1c demonstrated a preference for sliding nucleosomes containing histone H4K5,8,12ac over unmodified ones.

Moreover, the formation of the Isw1c complex was analyzed using a predicted structure generated by the AlphaFold tool. Superimposing the AlphaFold predicted structures of Isw1c onto the crystal structure of Isw1a revealed notable differences in the interaction of Esc8 or Ioc3 with Isw1 despite this homology. Specifically, the Esc8 protein appeared to primarily attach to the SLIDE domain of Isw1 to form the Isw1c

complex. Additionally, the structural analysis showed that Esc8 possesses three out of the four-helix structures of the HLB domain found in Ioc3 (α8, α10, and α11) but lacks an HSSB loop and HLB- α9, consistent with a previous study. Using co-immunoprecipitation assays, the deletion of the SLIDE domain in Isw1 resulted in no interaction with Esc8. This finding implies that the SLIDE domain is essential for Isw1 to interact with Esc8 and for the formation of the Isw1c complex. Furthermore, protein-protein interaction analyses of Esc8 deletion mutants and Isw1 revealed that the N-terminus of Esc8 likely plays a crucial role in stabilizing the protein, and the absence of about 100 amino acids at the C-terminus of Esc8 somewhat sustains the association with Isw1 and its ability to mobilize nucleosomes.

In summary, this research reveals that Isw1c, composed of Isw1 and Esc8, is a novel Isw1 chromatin remodeler in *S. cerevisiae*, expanding the known group of Isw1 chromatin remodelers. Furthermore, it provides new insights and a deeper understanding of the structural formation of the Isw1c complex and the molecular mechanisms underlying Isw1c's role as chromatin remodelers *in vitro*.

Zusammenfassung

Die eukaryotische DNA wird zusammen mit Histonproteinen organisiert und verpackt, um Chromatin zu bilden. Die Verdichtung der Chromatinstruktur behindert folglich den Zugang zur DNA, was wichtige Auswirkungen auf DNA-bezogene Prozesse wie Transkription, Replikation oder DNA-Reparatur hat. Um den Zugang zur DNA zu vermitteln, sind Histon-Modifikationen und Chromatin-Remodelers erforderlich, um die Chromatinstruktur zu modulieren. Chromatin-Remodeler haben zentrale Funktionen, indem sie die durch ATP-Hydrolyse erzeugte Energie nutzen, um Nukleosomen neu zu positionieren oder zu verdrängen oder Histone auszutauschen. Der ISWI-Remodeler ist eine der vier Remodeler-Komplex-Familien und ist von der Hefe bis zum Menschen hoch konserviert. In *Saccharomyces cerevisiae* bilden zwei ISWI-Homologe, Isw1 und Isw2, beide Komplexe mit mehreren Untereinheiten. Der Isw1-Remodeler wird außerdem in zwei verschiedene Komplexe unterteilt, die die katalytische ATPase-Untereinheit mit verschiedenen Ioc-assoziierten Untereinheiten teilen, nämlich Isw1a und Isw1b. Dabei besteht Isw1a aus Isw1 und Ioc3, während Isw1b aus Isw1, Ioc2 und Ioc4 besteht. Darüber hinaus wurde neben den Ioc-Untereinheiten Esc8 als ein weiteres Protein vorgeschlagen, das mit Isw1 interagiert, und zwar aufgrund von Protein-Protein-Analysen in Hefe sowie seiner Homologie zu Ioc3. Eine Interaktion zwischen Esc8 und Isw1 muss jedoch noch bestätigt werden, ebenso wie eine mögliche Funktion als Chromatin-Umgestalter. Aus diesem Grund wurde in dieser Studie eine Kombination aus biochemischen *In-vitro*-Assays und AlphaFold-Strukturanalyse des Proteinkomplexes verwendet, um die Bildung und die Funktionen des Isw1-Esc8-Proteinkomplexes als Chromatin-Remodeler zu untersuchen.

In dieser Untersuchung wurde der Isw1c-Komplex mit Hilfe der TAP-Affinitätsreinigung endogen aus *S. cerevisiae* gereinigt, wodurch die Interaktion zwischen Isw1 und Esc8 bestätigt wurde. Außerdem wurde eine höhere Ausbeute des Isw1c-Proteinkomplexes aus einem Hefestamm gereinigt, der den *pCUP1-ESC8* in einem *ioc2*Δ *ioc3*Δ-Stamm-Hintergrund enthält. Dieser gereinigte Komplex wurde in zahlreichen biochemischen Assays getestet, darunter DNA- und Nukleosomen-Bindungstests, ATP-Hydrolyse-Assays und Nukleosomen-Gleit-Assays. Diese Tests zeigten insgesamt, dass Isw1c alle grundlegenden Merkmale eines Chromatin-Remodelers aufweist. Insbesondere kann Isw1c an DNA und Nukleosomen binden, die mindestens einen DNA-Überhang enthalten. Wie andere Isw1-Remodeler wird auch die ATPase-Aktivität von Isw1c durch Nukleosomen stimuliert. Darüber hinaus hat Isw1c die Fähigkeit, Nukleosomen zu verschieben, vorzugsweise von der Endposition in die Mittelposition. Bei genomweiten *In-vitro*-Rekonstruktionsversuchen von Nukleosomen zeigte Isw1c außerdem die Fähigkeit, regelmäßig angeordnete und phasenweise angeordnete Nukleosomenarrays zu erzeugen.

Zusätzlich zu den grundlegenden Eigenschaften von Chromatin-Remodelern entdeckte ich, dass die Rekrutierung von Isw1c und seine Remodeling-Aktivität durch unterschiedlich modifizierte Nukleosomen beeinflusst werden. Hier zeigte Isw1c eine leichte Vorliebe für die Bindung an unmodifizierte Nukleosomen im Vergleich zu acetylierten Nukleosomen. Bemerkenswerterweise zeigte Isw1c eine Vorliebe für gleitende Nukleosomen, die Histon H4K5,8,12ac enthalten, gegenüber unmodifizierten Nukleosomen.

Außerdem wurde die Bildung des Isw1c-Komplexes anhand einer mit dem AlphaFold-Tool erstellten Strukturvorhersage analysiert. Die Überlagerung der von AlphaFold vorhergesagten Strukturen von Isw1c mit der Kristallstruktur von Isw1a ergab trotz dieser Homologie bemerkenswerte Unterschiede bei der Interaktion von Esc8 oder Ioc3 mit Isw1. Insbesondere schien das Esc8-Protein hauptsächlich an die SLIDE-Domäne von Isw1 zu binden, um den Isw1c-Komplex zu bilden. Darüber hinaus zeigte die Strukturanalyse, dass Esc8 drei der vier Helixstrukturen der HLB-Domäne von Ioc3 besitzt (α8, α10 und α11), aber keine HSSB-Schleife und HLB-α9, was mit einer früheren Studie übereinstimmt. Die Deletion der SLIDE-Domäne in Isw1 führte in Co-Immunopräzipitationstests zu keiner Interaktion mit Esc8. Dieses Ergebnis deutet darauf hin, dass die SLIDE-Domäne für die Interaktion von Isw1 mit Esc8 und für die Bildung des Isw1c-Komplexes unerlässlich ist. Darüber hinaus ergaben Protein-Protein-Wechselwirkungsanalysen von Esc8-Deletionsmutanten und Isw1, dass der N-Terminus von Esc8 wahrscheinlich eine entscheidende Rolle bei der Stabilisierung des Proteins spielt und dass das Fehlen von etwa 100 Aminosäuren am C-Terminus von Esc8 die Assoziation mit Isw1 und seine Fähigkeit, Nukleosomen zu mobilisieren, etwas aufrechterhält.

Zusammenfassend lässt sich sagen, dass diese Forschungsarbeit zeigt, dass Isw1c, bestehend aus Isw1 und Esc8, ein neuartiger Isw1-Chromatin-Remodeler in *S. cerevisiae* ist und die bekannte Gruppe der Isw1-Chromatin-Remodeler erweitert. Darüber hinaus liefert sie neue Erkenntnisse und ein tieferes Verständnis der strukturellen Bildung des Isw1c-Komplexes und der molekularen Mechanismen, die der Rolle von Isw1c als Chromatin-Remodeler *in vitro* zugrunde liegen.

Übersetzt mit DeepL.com

List of Figures

List of Tables

List of Abbreviations

Å	Angstrom
aa	Amino acids
ADP	Adenosine diphosphate
ATP	Adenosine triphosphate
bp	Base pairs
CBP	Calmodulin binding peptide
cEMSA	Competitive electrophoretic mobility shift assay
CHD	Chromodomain helicase DNA binding
ChIP-qPCR	Chromatin immunoprecipitation quantitative polymerase chain reaction
ChIP-seq	Chromatin immunoprecipitation sequencing
Co-IP	Co-immunoprecipitation
Cryo-EM	Cryogenic electron microscopy
cSliding Assay	Competitive nucleosome sliding assay
CUT&RUN	Cleavage under targets and release using nuclease
D. Melanogaster	*Drosophila Melanogaster*
DNA	Deoxyribonucleic acid
dsDNA	Double stranded DNA
E. coli	*Escherichia coli*
EMSA	Electrophoretic mobility shift assay
Esc8	Establishes silent chromatin 8
fmol	femtomole
GST	Glutathione S-transferase
H2A.Z	Histone variant H2A.Z
H3K36me0	Unmethylated histone H3K36
H3K36me3	Trimethylated histone H3K36
H3K4me0	Unmethylated histone H3K4
H3K4me3	Trimethylated histone H3K4
H3K9,14ac	Acetylated histone H3K9,14ac
H4K16ac	Acetylated histone H4K16
H4K5,8,12ac	Acetylated histone H4K5,8,12
HAT	Histone acetyltransferase
HDAC	Histone deacetylase
HDM	Histone demethylase
HIS	Histidine
HMT	Histone methyltransferase
HRV	Human rhinovirus
INO80	Inositol requiring 80
Ioc	Iswi one complex
IPTG	Isopropyl β-D-1-thiogalactopyranoside
ISWI	Imitation switch
LB	Lysogeny broth
kb	Kilo base pairs
Kda	Kilo dalton
MBP	Maltose binding protein
Min	Minute
NADH	Nicotinamide adenine dinucleotide

NCP	Nucleosome core particle
Ni-NTA	Nickel-nitrilotriacetic acid
OD600	Optical density 600
PAE	Predicted aligned error
PAGE	Polyacrylamide gel electrophoresis
PCR	Polymerase chain reaction
PDB	Protein data bank
Pi	Inorganic phosphate
pLDDT	Predicted local distance difference test
PTMs	Post-translational modifications
RNA	Ribonucleic acid
Rpm	Revolutions per minute
RT	Room temperature
S. cerevisiae	*Saccharomyces cerevisiae*
SDS-PAGE	Sodium dodecyl sulfate- Polyacrylamide gel electrophoresis
Sec	second
SWI/SNF	Switch/sucrose non-fermentable
TAP	Tandem affinity purification
v/v	Volume by volume
w/v	Weight by volume
X. laevis	*Xenopus laevis*
YPD	Yeast extract peptone dextrose

1. Introduction

1.1 Structure of chromatin and nucleosomes

In 1882, the term “chromatin” was first proposed by Walther Flemming, referring to the fibrous scaffold or the stainable substance in the nucleus after treatment with staining dyes **(Flemming, 1882; Meshorer & Plath, 2020; Paweletz, 2001)**. It was not until 1973, nearly 100 years later, that the structure of chromatin was first visualized by electron microscopy (EM) **(Fig. 1)** **(Olins & Olins, 1974; Woodcock et al., 1976)**. The appearance of each 10 nm chromatin fiber was then described as a beads-on-a-string **(Olins & Olins, 1974; Olins & Olins, 2003; Woodcock et al., 1976)**. After scrutinizing the nucleohistone (or v bodies), it was discovered that there were two of each type of histone molecule in complex with a double-stranded DNA **(Olins & Olins, 1974)**. Additionally, folded or helical DNA wrapped around spherical bodies occurred based on non-covalent interactions, representing how DNA packaging processes **(Olins & Olins, 1974)**. Given these observations using an electron microscope and some biophysical assays, these characteristics become a model of chromatin. In the same year, Kornberg proposed a model of chromatin structure with some more detail. It contains the repeating unit of 200 base pairs of DNA complexed with two copies each of four histones **(Kornberg, 1974)**. This chromatin structure was subsequently confirmed with electron microscopy and biochemical studies **(Oudet et al., 1975)**. In 1975, the term “nucleosome” was introduced to describe the fundamental repeating unit of chromatin structure **(Oudet et al., 1975)**. Additionally, the nomenclature for histone proteins was standardized at the Ciba Foundation symposium on “The structure and function of chromatin,” held in the same year **(Bradbury, 1977)**. At present, these histone proteins are known as histones H1, H2A, H2B, H3, and H4.

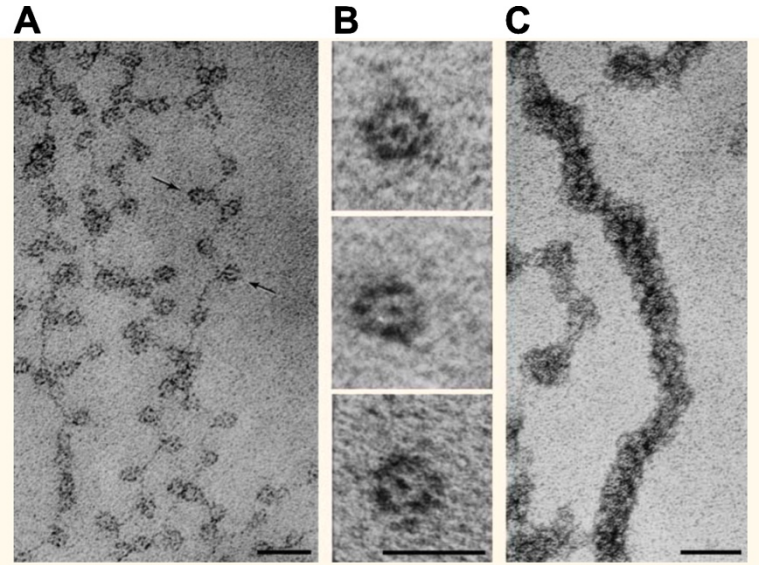

Figure 1. Structure of chromatin under electron microscopy. **(A)** Chromatin structure forms in beads-on-a-string. Size marker of 30 nm. **(B)** Mononucleosomes upon nuclease-digested chromatin. Size marker of 10 nm. **(C)** The 30 nm higher-order fiber structure of chromatin. The Figure is adapted from Olins & Olins, 2003.

After the first visualization of chromatin structure by electron microscopy, numerous studies have revealed three-dimensional structures of nucleosomes, starting from low-resolution to high-resolution images, for the past four decades. Over the course of research, X-ray scattering or diffraction has emerged as a prominent technique for solving the structure of nucleosomes. With X-ray diffraction and electron microscopy, the low-resolution structure of nucleosome core particles (NCPs) was reported as a flat disk shape with a diameter of 110 Å and thickness of 57 Å, and a DNA wrapped around 1.75 turns of left-handed superhelix around the histone core **(Finch et al., 1977)**. In addition, the 7 Å resolution of the NCP structure showed that several regions of DNA were rather bending or kinking adjacent to the points of contact with histones (H3 and H4), and not all DNA was equally bent into the superhelix **(Richmond et al., 1984)**. Later, in 1997 and 2003, the high-resolution crystal structures of NCPs, containing the palindromic DNA in complexed with recombinant *Xenopus laevis* histones, were solved at 2.8 Å and 1.9 Å resolution **(Davey et al., 2002; Luger et al., 1997; Richmond & Davey, 2003)**. Given that extensive research, the nucleosome core particle is therefore described as 147±2 bp of DNA wrapped around 1.65 turns of left-handed superhelix around a flat, disk-shaped histone octamer containing two copies of each histone protein of H2A, H2B, H3, and H4 **(Fig. 2A-C)**.

The contacts between histones and DNA superhelix are specified according to their superhelical location (SHL) **(Luger et al., 1997; Richmond et al., 1984; Zhou et al., 2019).** The center of the nucleosomal DNA is positioned at the pseudo-two-fold axis and referred to as the nucleosome dyad or super-helical location zero, SHL0 **(Luger et al., 1997)**. Here, 147 bp nucleosomal DNA in NCP can be divided into two "gyres" consisting of 72 bp and 73 bp halves **(Richmond et al., 1984)**. At each super-helical location (SHL), this shows the position of the major groove of DNA facing inward the histone octamer and reflects each successive turn of the DNA helix **(Luger et al., 1997; Richmond et al., 1984)**. The numbering of the SHL increases with the distance relative to the nucleosome dyad (SHL0), which can be from SHL-7 to SHL0 and from SHL0 to SHL +7 **(Fig. 2D)**.

In addition to ongoing research uncovering nucleosome structure, histone octamer structure was first solved using X-ray crystallography at 3.1 Å resolution, addressing how eight histone proteins are arranged and assembled inside the NCP **(Arents et al., 1991)**. Structurally, the core of histones is organized into a tripartite assembly, with the histone H3-H4 tetramer positioned at the center and flanked by the histone H2A-H2B dimer on each side **(Arents et al., 1991; Cutter & Hayes, 2015)**. This finding is consistent with a previous study that proposed the arrangement of each histone protein with H2A-H2B-H4-H3-H3-H4-H2B-H2B following the DNA superhelix starting from SHL-7 to SHL+7 **(Cutter & Hayes, 2015; Klug et al., 1980)**. The association between heterodimers of histones H3-H4 and heterodimers of histones H2A-H2B is described by the formation of a "handshake" arrangement through the histone fold motif shared between each histone protein **(Arents et al., 1991)**. This histone fold contains three alpha-helices connected with two intervening loops (α1-L1-α2-l2-α3) **(Arents et al., 1991; McGinty & Tan, 2015)**. Besides the globular structure of histone, there is an unstructured and flexible tail located at the N-terminus to all histone proteins and at the C-terminus only for histone H2A extending out from the nucleosomes **(Davey et al., 2002)**. Histone tails are positively charged and contain residue sites that are the target of post-translational modifications **(Bannister & Kouzarides, 2011; Luger et al., 1997)**. Functionally, histone tails are important for

the stability of nucleosome structure, and the modifications of histone tails play a crucial role in regulating the chromatin structure that influences cellular processes such as transcription, replication, and DNA repair **(Bannister & Kouzarides, 2011; Biswas et al., 2011; Ghoneim et al., 2021; Iwasaki et al., 2013; Kouzarides, 2007; Millan-Zambrano et al., 2022)**.

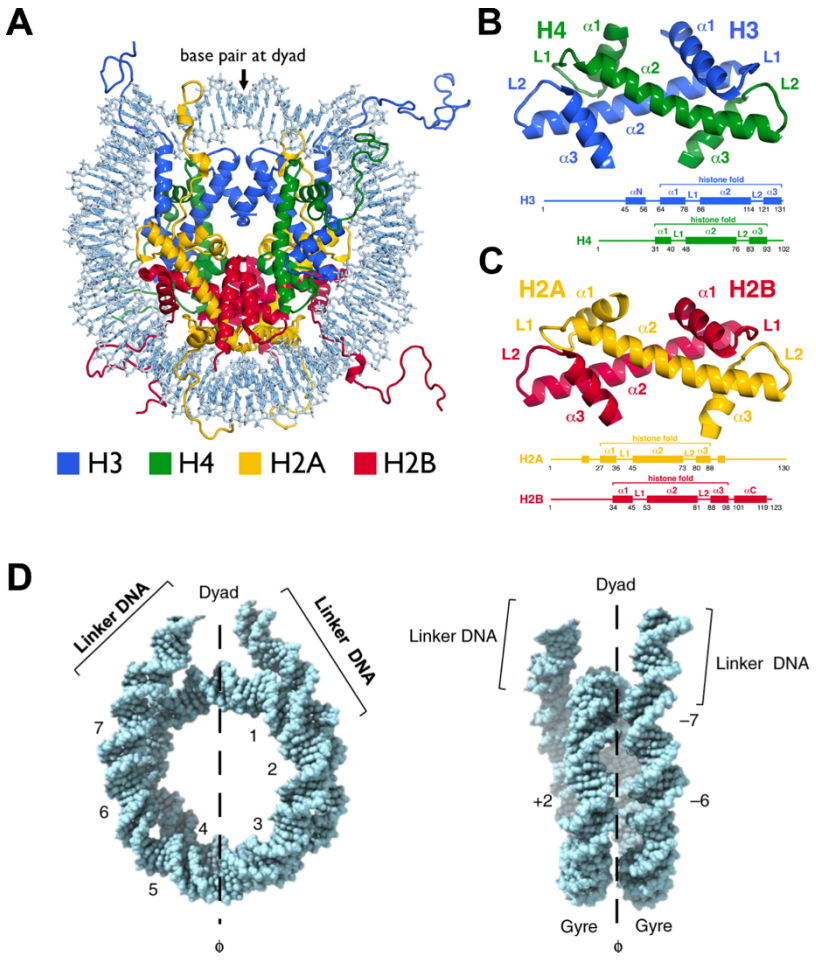

Figure 2. Three-dimensional structure of nucleosome core particle. **(A)** Crystal structure of the nucleosome core particle at 1.9 Å resolution (PDB ID: #1KX5). **(B)** H3-H4 heterodimer. **(C)** H2A-H2B heterodimer. **(D)** Superhelical axis of nucleosome. Figures 2A-C are adapted from McGinty & Tan, 2015 and Figure 2D is adapted from Zhou et al., 2019.

1.2 The complexity of the higher-order structure of chromatin

Eukaryotic genomic DNA is folded and packaged with histone proteins to form chromatin. For the genomic DNA to fit inside the nucleus, this process involves different levels of compaction and arrangement of the linear array of nucleosomes to form the higher-order structure chromatin **(Woodcock & Dimitrov, 2001)**. To achieve that, the nucleosome arrays (primary chromatin structure) are folded and compacted into 30 nm chromatin fiber, which is categorized as the secondary chromatin structure. Of the many proposed models available, there are two most prominent models for the 30-nm fiber structure: (1) solenoid model or one-start helix and (2) two-start helix **(Fig. 3A-D)**. However, it is necessary to note that the *in vivo* existence of this model is under debate despite years of intensive efforts **(Grigoryev & Woodcock, 2012; Maeshima, Hihara, & Eltsov, 2010; Tremethick, 2007; van Holde & Zlatanova, 1995, 2007)**.

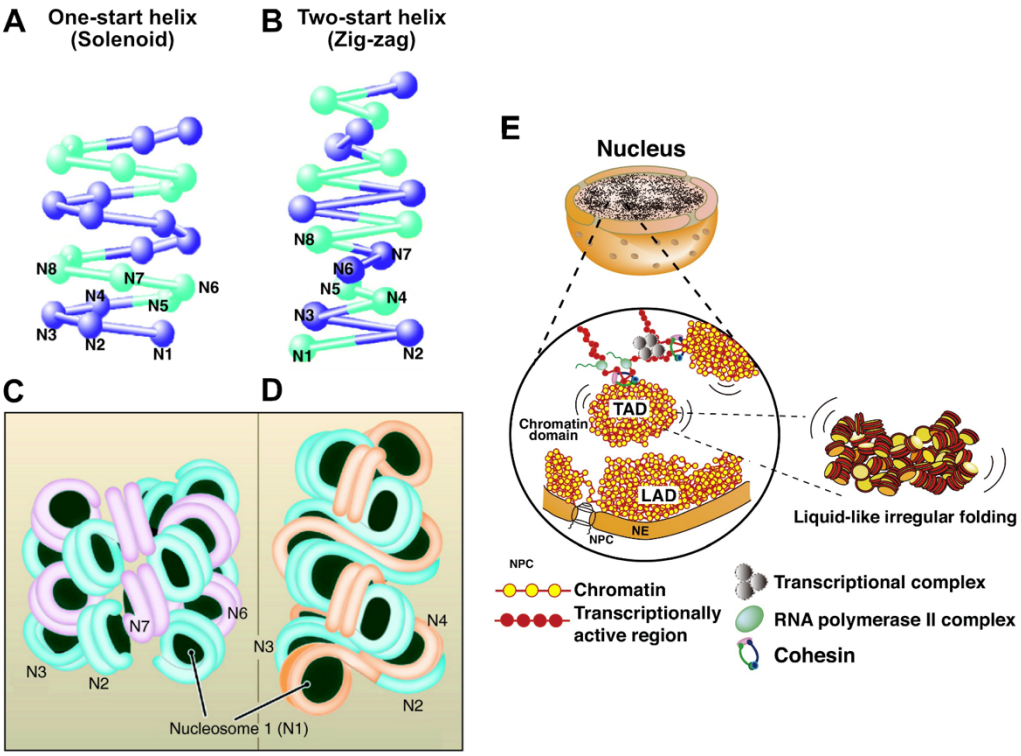

Figure 3. The higher-order structure of chromatin. **(A, C)** One-start helix or solenoid model. **(B, D)** Two-start helix or zig-zag model. These two models are the 30-nm chromatin fibers. **(E)** Irregularly folded 10-nm chromatin fibers and chromatin domain of topologically associating domain (TAD). Another chromatin region, the lamina-associated chromatin domain (LAD), presumably consists of the heterochromatin region at the nuclear periphery. Figures 3A-D are adapted from Li & Reinberg 2011, and Figure 3E is adapted from Maeshima et al., 2019.

Much evidence has mostly been observed according to *in vitro* studies of isolated chromatin fragments under certain conditions using electron microscopy or X-ray diffraction. The solenoid model, or one-start helix, was the first model proposed by John Finch and Aaron in 1976. Using electron microscopy and X-ray, this model is illustrated where the neighboring nucleosomes are connected by linker DNA and positioned adjacent to each other in the fiber, folding into a one-start helix **(Finch et al., 1977; Li & Reinberg, 2011; van Holde & Zlatanova, 2007; Widom & Klug, 1985)**. In every helical turn, around 6 to 8 nucleosomes are closed in contact at the central axis symmetry **(Finch et al., 1977)**. Additionally, histone H1 is required for the stabilization of the structure **(Finch et al., 1977; Thoma et al., 1979)**. In the second model, the two-start helix is illustrated with the arrangement of nucleosomes in the zig-zag chain formation in such a way that the first nucleosome is in close contact with the third nucleosome while the second nucleosome is with the fourth nucleosome connected by the linker DNA **(Williams et al., 1986; Woodcock et al., 1984; Worcel et al., 1981)**. Moreover, the crystal structure of a tetranucleosome shows that two stacks of nucleosomes with linker DNA interweave to form a zigzag structure, thus providing more compelling evidence for this model **(Schalch et al., 2005)**. Nonetheless, despite all these studies that observed the 30 nm fiber structure, it remains controversial how these models possibly represent the native chromatin.

Furthermore, other studies have reported the observation of irregular chromatin fibers in extracted nuclei **(van Holde & Zlatanova, 2007; Woodcock et al., 1993)**. Here, rather than having a 30nm chromatin structure, it is described as dynamic and irregularly folded 10-nm nucleosome fibers, resembling a liquid-like structure **(Fig. 3E)** **(Joti et al., 2012; Nishino et al., 2012)**. Consequently, it is speculated that the 30-nm chromatin fibers found using electron microscopy are likely to be *in vitro* artifacts due to the low ionic strength buffer condition **(Maeshima et al., 2014)**. Several reviews offer detailed analyses for further insights into this liquid-like chromatin structure **(Maeshima, Hihara, & Takata, 2010; Maeshima et al., 2019; Maeshima et al., 2016; Maeshima et al., 2014)**.

1.3 Chromatin regulators

The compaction of chromatin limits the accessibility of DNA sequences. However, packaging eukaryotic DNA into a chromatin structure is essential for numerous cellular functions such as transcription, DNA replication, and DNA repair. Given those DNA-cellular processes, the dynamic state of chromatin undergoes structural changes with decondensation to mediate DNA accessibility as required. Histone-modifying enzymes and chromatin remodelers are two key classes of chromatin regulators that facilitate these structural changes, thereby regulating gene expression and other cellular processes. By functions, the histone-modifying enzymes catalyze the addition and removal of histone post-translational modifications, and the chromatin remodelers utilize the energy from ATP hydrolysis to slide, evict, or modify nucleosomes **(Clapier & Cairns, 2009; Marmorstein & Trievel, 2009)**. The following sections will elaborate on the factors modulating the chromatin organization.

1.3.1 Histone post-translational modifications

Histone octamers consist of the four core histones H2A, H2B, H3 and H4. Each histone protein features a globular structure with a flexible N-terminal tail protruding from the nucleosome core particle. All these histones are subjected to post-translational modifications (PTMs), predominantly on their N-terminal tails and also their globular domains. In 1960, the pioneering work of Vincent Allfrey marked the initial identification of histones acetylation and methylation **(Allfrey et al., 1964)**. The interest in discovering new histone modifications associated with biological functions has increased in the past decades. Particularly in *S. cerevisiae*, numerous PTMs have been identified, biochemically dissected and genetically validated using a wide range of approaches, including acetylation, methylation, phosphorylation, ubiquitylation, sumoylation, acylation, and many more **(Fig. 4)** **(Chou et al., 2023; Millar & Grunstein, 2006)**. Many of these histone modification sites are conserved from yeast to humans.

Furthermore, two mechanisms may occur following the histone modifications. First, it involves the disruption of histone-DNA or nucleosome-nucleosome interaction, which consequently impacts chromatin organization **(Bannister & Kouzarides, 2011; Kouzarides, 2007; Zhang et al., 2016)**. Second, the modified histones can serve as a binding platform for the recruitment of non-histone proteins like chromatin remodelers **(Bannister & Kouzarides, 2011; Kouzarides, 2007)**.

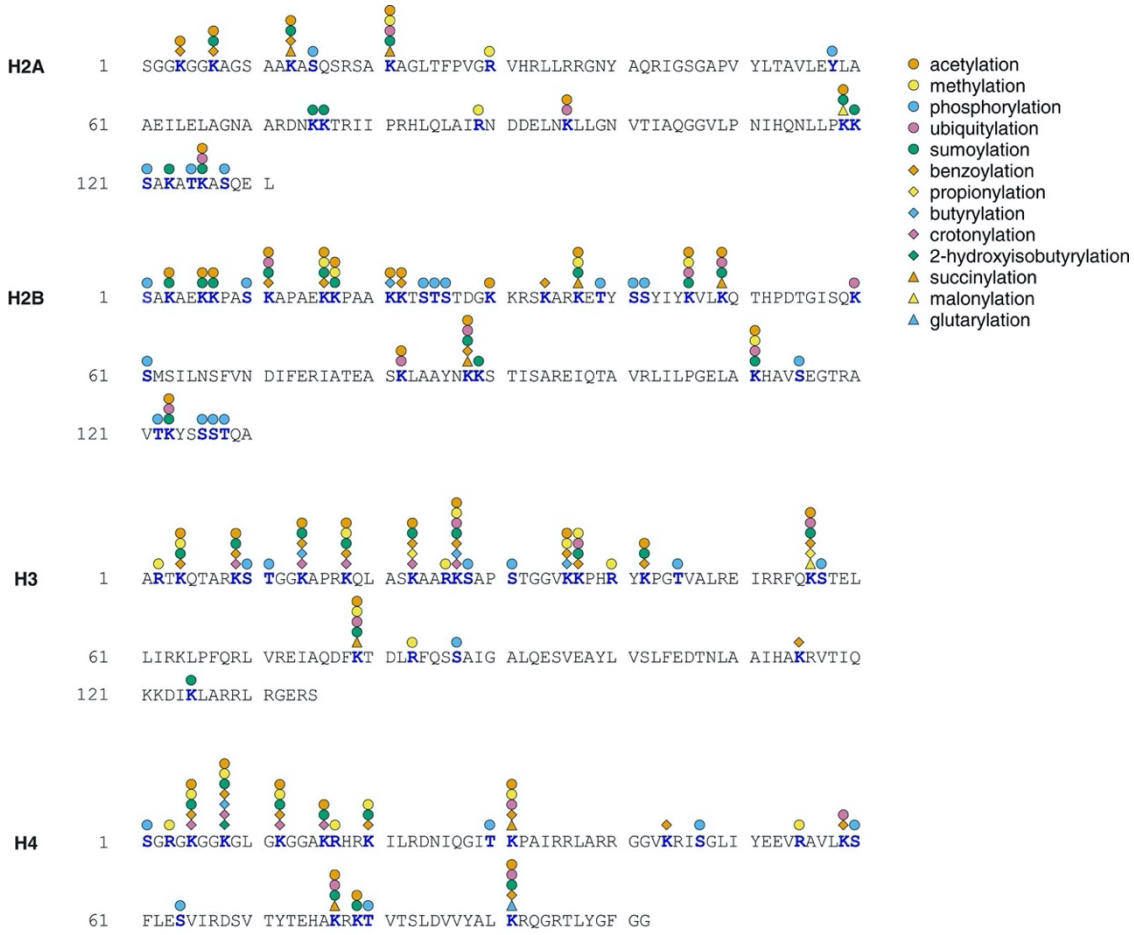

Figure 4. A schematic map for post-translational modifications on histones found in *Saccharomyces cerevisiae*. The Figure is modified and adapted from Chou et al., 2023.

1.3.1.1 Histone acetylation

Histone acetylation and deacetylation are highly associated with “open chromatin” and “closed chromatin” and are regulated by two families of enzymes, known as histone acetyltransferases (HATs) and histone deacetylases (HDACs). **(Allfrey et al., 1964; Pokholok et al., 2005)**. These enzymes mostly target specific lysine residue sites.

In histone acetylation, HATs catalyze the transfer of the acetyl group to the ε-amino group of lysine side chains of the histone, resulting in the neutralization of the positive charge of lysine residues **(Bannister & Kouzarides, 2011; Roth et al., 2001)**. This process is thought to loosen the interactions between histone-DNA, histone-histone within adjacent nucleosomes, and between histones and regulatory proteins **(Roth et al., 2001)**. Nevertheless, while histone acetylation may weaken interactions with some non-histone proteins, it can also enable and stabilize interactions between bromodomain-containing proteins and acetylated chromatin **(Matangkasombut & Buratowski, 2003)**. Moreover, it is also important to note that an *in vitro* study of nucleosomal arrays found that the association between histone and DNA remains stable with the increase of histone acetylation **(Mutskov et al., 1998)**. Nonetheless, histone acetylation may cause a less compact chromatin structure by preventing the folding of nucleosomal arrays into higher-order chromatin fiber **(Horn & Peterson,**

2002; Tse et al., 1998). Thus, it has been proposed that histone acetylation and deacetylation regulate transcription by modifying the complex structure of the chromatin fiber **(Kurdistani & Grunstein, 2003)**. This less compact chromatin structure facilitates easier accessibility to DNA for proteins that are involved in transcription **(Bannister & Kouzarides, 2011)**.

Certain acetylated lysine residues of histones can also provide a binding platform for the recruitment of various chromatin-regulatory factors such as chromatin remodelers, and transcriptional regulators **(Bannister & Kouzarides, 2011)**. For instance, the bromodomain of the Sth1 subunit of the yeast RSC remodeler complex is recruited by acetylated histone H3K14 (H3K14ac)-containing nucleosomes at the transcription start sites and repositions the nucleosomes providing access for polymerase II to start transcription **(Carey et al., 2006; Chen et al., 2020; Kasten et al., 2004)**. Similarly, the Bdf1 subunit of yeast SWR1 remodeler, containing a bromodomain, associates with nucleosomes bearing acetylation on the N-terminal tails of histones H2A and H4 by NuA4 **(Altaf et al., 2010; Matangkasombut & Buratowski, 2003)**. In addition to remodelers, the TAF250 subunit of the general transcription factor TFIID, which contains two tandem bromodomains, specifically interacts with multiple acetylated histone H4 (K5, K8, K12, and K16) residues to recognize specific chromatin-bound promoters **(Jacobson et al., 2000)**.

The opposite of histone acetylation by HATs is histone deacetylation. HDACs catalyze the removal of acetyl groups from the lysine residues of histones and restore the positive charge of lysine on histones **(Kurdistani & Grunstein, 2003)**. This modification promotes the compaction of chromatin structure, thereby blocking access to DNA **(Bannister & Kouzarides, 2011)**. In heterochromatin, silent mating-type cassettes and telomeres are formed with hypoacetylated nucleosomes, which are transcriptionally inactive or known as silent chromatin **(Braunstein et al., 1993; Braunstein et al., 1996).** For example, deacetylated histone H4K16ac by Sir2 is essential at the centromere region for kinetochore function and chromosome segregation **(Choy et al., 2011)**.

Many sites of lysine in histones can be acetylated and deacetylated. Of all the acetylated histones, there are highly conserved acetylation sites in histone H3 at lysine residues K9, K14, K18, K23, and K27, and the histone H4 at lysine residues K5, K8, K12, and K16 **(Kurdistani et al., 2004)**. Some of these histone acetylation sites are well-correlated with transcriptional activation and thus preferentially enriched at the promoter region or the 5' end of transcribed genes **(Fig 5)** **(Liu et al., 2005)**. For example, hyperacetylated or histone H4 acetylated at four lysine sites of K5, K8, K12, and K16 (H4K5, K8, K12, K16ac) by the acetyltransferase Esa1 are highly enriched at the start sites of active genes and correlated with transcription rates **(Pokholok et al., 2005)**. In addition to that, each modification site of histone H4K5ac, H4K8ac, H4K12ac, and H4K16ac is broadly positioned from the 5' to 3' of actively transcribed regions **(Liu et al., 2005)**. Similarly, the acetylation of histones H3K9 and H3K14 catalyzed by acetyltransferase Gcn5 is found to localize at the start site of active genes **(Liu et al., 2005; Pokholok et al., 2005)**.

Among those highly conserved acetylation sites on histone H3 and H4, the deacetylation and acetylation of H4K16 play important roles in the establishment telomeric heterochromatin in *S. cerevisiae*, including the nucleation and the spreading

steps, as well as the formation of boundaries to prevent heterochromatin spreading **(Millar et al., 2004; Oppikofer et al., 2013)**. In general, this telomeric silent chromatin is formed through the assembly of the Silent Information Regulator (SIR) proteins complex, including Sir2, Sir3, and Sir4, which binds to histones H3 and H4 **(Hecht et al., 1995; Hecht et al., 1996; Strahl-Bolsinger et al., 1997; Thompson et al., 1994).** Additionally, the protein Rap1, which specifically recognizes and binds to the C_{1-3} A repeats at the telomere, plays a role in recruiting the Sir complex to initiate heterochromatin formation **(Moretti et al., 1994)**. The Rap1 protein recruits the Sir3 and Sir4, while the Sir2 interacts only with Sir4, forming the Sir protein complex **(Moazed et al., 1997; Moretti et al., 1994; Strahl-Bolsinger et al., 1997)**. Sir2 is a NAD-dependent histone deacetylase **(Imai et al., 2000; Landry et al., 2000)**. Functionally, Sir2 has a role to deacetylate H4K16-containing nucleosome, and this process is necessary to further recruit Sir3, and with Sir4, to promote the spreading of the heterochromatin state **(Hecht et al., 1996; Imai et al., 2000; Johnson et al., 2009; Renauld et al., 1993)**. In contrast, the acetylation of H4K16-containing nucleosome by histone acetyltransferase Sas2 is found to inhibit the recruitment of Sir3 and is proposed to create a boundary element that limits the spreading of telomeric heterochromatin between the sub-telomeric chromatin and euchromatin **(Kimura et al., 2002; Oppikofer et al., 2011; Suka et al., 2002)**. In addition, other protein such as the Bdf1 bromodomains (Independently of TFIID), which interact with acetylated H4, have been identified to have a function in limiting heterochromatic spreading of SIR protein **(Ladurner et al., 2003)**. The study revealed that the loss of acetyl-histone binding function of Bdf1 leads Sir3 to spread into euchromatin, resulting in transcriptionally silenced **(Ladurner et al., 2003)**.

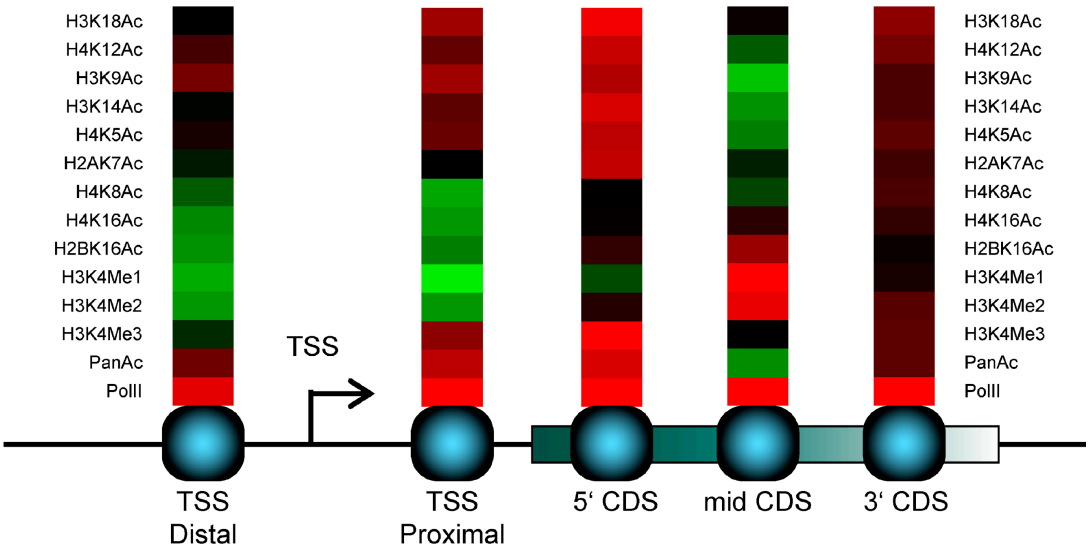

Figure 5. Localization of histone acetylation and methylation of nucleosomes in actively transcribed genes. Red indicates enrichment, and green indicates depletion. Additionally, black represents non-significant cells (false discovery rate of 95% on *t-test p-values*). The Figure is adapted from Liu et al., 2005.

1.3.1.2 Histone methylation

Histone methylation is another extensively studied histone modification known for its distinct complexity level compared to histone acetylation **(Kouzarides, 2007)**.

This modification primarily occurs on lysine and arginine side chains of histone proteins **(Bannister & Kouzarides, 2011; Bannister et al., 2002)**. Notably, histone methylation demonstrates specificity toward histone residues **(Kouzarides, 2007)**. Particularly in yeast, histone methyltransferases exclusively modify specific histone residues **(Millar & Grunstein, 2006)**. Adding to the complexity, lysine residues can be mono-, di-, or trimethylated, whereas arginine residues can be monomethylated, demethylated asymmetrically, or demethylated symmetrically **(Bannister & Kouzarides, 2011; Bannister et al., 2002; Kouzarides, 2007)**. Nonetheless, unlike histone acetylation, histone methylation does not alter the electrostatic charge of lysine or arginine side chains, which directly affects chromatin folding **(Separovich & Wilkins, 2021)**. Conversely, the methylation on specific residues of the histone tails generates docking sites for various chromatin regulatory factors that subsequently evoke change in the chromatin folding structure to mediate a downstream process such as transcription **(Chou et al., 2023; Martin & Zhang, 2005; Separovich & Wilkins, 2021).** Histone methylation can be associated with both activation or repression of transcription depending on where the methylation sites **(Kouzarides, 2007)**.

Histone methylation and demethylation are regulated by histone methyltransferases (HMTs) and histone demethylases (HDMs) **(Zhang et al., 2016)**. With two targets of side chains, HMTs can be classified into two groups: lysine methyltransferases (KMTs) and protein arginine methyltransferases (PRMTs) **(Liu et al., 2023)**. In addition to that, KMTs are further divided into SET domain-containing and non-SET domain-containing **(Liu et al., 2023)**. Also, there are two groups of histone demethylation, including Jumonji domain-containing HDMs demethylate (JMJC) and lysine-specific demethylase 1 or 2 (LSD) **(Hyun et al., 2017; Shi & Tsukada, 2013; Zhang et al., 2016)**. Mechanistically, KMTs catalyze the transfer of up to three methyl groups of S-adenosyl-L-methionine (SAM) to histone lysine (ε-amino group) to form mono- (me1), di- (me2), or trimethylated (me3) while PRMTs catalyze the transfer of one or two methyl groups to the histone arginine (ω-guanidino group) resulting either monomethylarginines (MMA), asymmetric dimethylarginines (ADMA) or symmetric dimethylarginines (SDMA) **(Bannister & Kouzarides, 2011; Bedford & Richard, 2005; Di Lorenzo & Bedford, 2011)**. Together, this modification consists of levels of complexity distinctive from other histone modifications.

Methylations of histones H3K4, H3K36, and H3K79 are predominantly involved in transcriptional activation and highly conserved in eukaryotes, including in *S. cerevisiae* **(Kouzarides, 2007)**. On active genes, the three states of histone H3K4 methylation are distributed in a “gradient” pattern with tri-methylated enriched at the transcription start site, whereas di-methylated at the middle of coding regions, and mono-methylated is mostly observed at the 3’ end of genes **(Liu et al., 2005; Pokholok et al., 2005; Separovich & Wilkins, 2021; Soares et al., 2017)**. Strikingly, all these methylations are catalyzed by the sole histone methyltransferase Set1, and each pattern is generated corresponding to the amount of time for the Set1 complex (COMPASS) to stay along the gene **(Briggs et al., 2001; Miller et al., 2001; Soares et al., 2017)**. Each modification level has distinct transcription functions by facilitating the recruitment of chromatin effector proteins **(Buratowski & Kim, 2010)**. One example is the enrichment of histone H3K4me3 near the promoter directly correlated with the initiation of transcription **(Chou et al., 2023; Liu et al., 2005)**. This methylated histone particularly recruits the transcription factor of TFIID via the TAF3 subunit and

the preinitiation complex to activate gene expression **(Beacon et al., 2021)**. Aside from that, the human ATPase chromatin remodeling CHD1 has an interaction with histone H3K4me3 through the chromodomain **(Sims et al., 2005)**.

In contrast with histones H3K4me1 and H3K4me3, the histones H3K36me1 and H3K36me3 are primarily found at the 5' end and toward the 3' end of active genes, respectively **(Pokholok et al., 2005)**. The histone H3K36me2 remains positioned over the mid-coding region **(Pokholok et al., 2005)**. In budding yeast, methylation of histone H3K36 by Set2 is highly connected with transcription elongation **(Krogan et al., 2003; Schaft et al., 2003)**. This event can be explained when the histone methyltransferase Set2 is recruited by the serine 2 phosphorylated RNA Polymerase II during transcription elongation to catalyze methylation of histone H3K36 **(Kizer et al., 2005; Li et al., 2003; Xiao et al., 2003)**. After the modification, this modified histone plays a crucial role as a platform site for histone deacetylase Rpd3S to prevent cryptic transcription initiation by retaining a hypoacetylated state at coding regions **(Carrozza et al., 2005; Li et al., 2007; Li et al., 2009; Venkatesh & Workman, 2013)**. Moreover, the histone H3K36me3 recruits a chromatin remodeler yeast Isw1b via the PWWP domain of the Ioc4 subunit with functions to maintain chromatin integrity during transcription elongation and suppress cryptic transcription **(Li et al., 2022; Maltby et al., 2012; Smolle et al., 2012)**.

Methylation of histone H3K79 is situated on the globular domain and mediated by histone methyltransferase Dot1 **(Nguyen & Zhang, 2011)**. This methylation was initially found to involve establishing the heterochromatin formation; however, it was later identified that this modification has a function in gene expression **(Chou et al., 2023)**. Unlike histones H3K4 and H3K36 methylation, the genome distribution profile for all methylation states of histone H3K79 in *S. cerevisiae* shows one uniform pattern and is primarily accumulated across the gene bodies of actively transcribed genes **(Pokholok et al., 2005; Separovich & Wilkins, 2021)**. However, a different distribution of histone H3K79 methylation states is observed in two actively transcribed human genes, including *CDK9* and *KPNB1* **(Wood et al., 2018)**. All methylation states are concentrated close to the transcription start site, except that histone H3K79me1 has a broader distribution than the other two forms **(Wood et al., 2018)**. Apart from that, there is a lack of information about the correlation between histone H3K79 methylation in transcription **(Wozniak & Strahl, 2014)**.

Other highly conserved histone methylations implicated in repression transcription are histones H3K9, H3K27, and H4K20 **(Kouzarides, 2007)**. Nonetheless, all these histone methylations are predominantly identified in higher eukaryotes but not present in *S. cerevisiae* **(Kouzarides, 2007; Oh et al., 2022; Zhao & Garcia, 2015).** While only histone H3K9 methylation mediated by histone methyltransferase Clr4 is found in *Schizosaccharomyces pombe* **(Allshire & Ekwall, 2015; Bannister et al., 2001; Nakayama et al., 2001)**. Notably, histone H3K9 methylation is recognized as an epigenetic mark for transcriptional silencing that has an important role in the establishment and maintenance of heterochromatin **(Padeken et al., 2022)**. Both histones H3K9me2 and H3K9me3 can serve as a binding site for the heterochromatin protein 1 family protein, chromodomain-containing protein of Swi6, Chp2, and Chp1 **(Maksimov et al., 2018; Nakayama et al., 2001; Sadaie et al., 2004; Sadaie et al., 2008)**. All these proteins have different roles in heterochromatin assembly. For example, Swi6 recruits cohesin to facilitate the

segregation of chromosomes at the centromere region **(Bernard et al., 2001; Nonaka et al., 2002)**. Apart from that, histone demethylase Epe1 and histone deacetylase Clr3 harbor heterochromatic loci by interacting with Swi6 **(Yamada et al., 2005; Zofall & Grewal, 2006)**. Another protein, Chp2, associates with SHREC histone deacetylase complex and removes the acetyl group from histone H3K14 acetylation that limits access of RNA polymerase II to heterochromatin and represses the transcription **(Maksimov et al., 2018; Motamedi et al., 2008)**. Moreover, RNA interference (RNAi) is involved in the establishment of centromeric heterochromatin **(Alper et al., 2012)**. This process requires the interaction between Chp1 with Ago1, Tas3, and siRNAs to form a complex so-called RITS complex **(Sadaie et al., 2004; Verdel et al., 2004)**.

Hypomethylated histone is a prominent feature observed in repressed euchromatin genes and silent chromatin regions in yeast **(Millar & Grunstein, 2006)**. One study identified hypomethylation of histone H3K79 within the globular domain of histone H3 and proposed that the recruitment of Sir silencing protein complex to this nucleosome blocks the binding of the histone methyltransferase Dot1 **(Ng et al., 2003)**. Another instance is found in *S. pombe*, where the Lid2 histone demethylase plays a crucial role in hypomethylating histone H3K4me3 within heterochromatin regions **(Li et al., 2008)**. In summary, heterochromatin is characterized by hypomethylated nucleosomes interacting with the Sir2 complex protein **(Bi, 2014)**.

1.3.2 Chromatin remodelers

In eukaryotes, the dynamic balance between DNA packaging and DNA access is vital for intricate processes such as gene regulation, genome stability, and genome repair, all of which are essential for the proper functioning of living organisms. These processes involve organizing the genome into stable chromatin architecture while ensuring accessibility to regulatory factors, requiring that the chromatin structure be both dynamic and plastic. Much evidence has emerged that chromatin remodelers are powerful molecular machines that play crucial roles in generating stability and plasticity of chromatin organization. Nonetheless, different remodelers create distinct nucleosome organizations corresponding to cellular functional states **(Eustermann et al., 2023)**. They can act in nucleosome positioning, removal, and histone variant deposition **(Clapier & Cairns, 2009)**. For example, a recent paper proposed that DNA packaging to form chromatin is a multilevel self-organization process **(Misteli, 2020)**. At the first level of chromatin organization, remodelers establish and specify nucleosome positioning patterns to have regularly spaced and phased nucleosomes **(Eustermann et al., 2023)**. Additionally, remodelers can generate nucleosome organization prerequisites for transcription by removing the nucleosomes from the promoter region **(Eustermann et al., 2023)**. Overall, it is known that chromatin remodelers utilize energy from ATP hydrolysis to slide, eject, destabilize, or restructure nucleosomes **(Clapier & Cairns, 2009)**.

1.3.2.1 Classification of chromatin remodelers with their shared features

Chromatin remodeler can be classified into four distinct families, including SWI/SNF (switch/sucrose non-fermentable), ISWI (imitation switch), CHD (chromodomain helicase DNA binding), and INO80 (inositol requiring 80) **(Clapier & Cairns, 2009)**. These families share a similar ATPase domain, containing two regions, so-called Dexx and HELIC **(Clapier & Cairns, 2009; Tyagi et al., 2016)**. These two

parts of the ATPase domain are connected with a short insertion for SWI/SNF, ISWI, and CHD and a long insertion for INO80 **(Clapier & Cairns, 2009; Tyagi et al., 2016)**. In general, the ATPase domain is responsible for ATP hydrolysis coupling with DNA translocation mechanisms to disrupt the interaction between histone and DNA contact **(Clapier et al., 2017; Nodelman & Bowman, 2021)**. Besides the ATPase domain, there are other basic properties shared by these families, such as (1) the domains that are involved in binding affinity to the nucleosome, (2) domains that recognize histone modifications, (3) domains and/or proteins that regulate the ATPase domain and (4) domains and/or proteins interacting with other chromatin or transcription factors **(Clapier & Cairns, 2009)**.

1.3.2.2 Specialized domains and subunit proteins in chromatin remodeler

In addition to their shared features, each member of the chromatin remodeler groups contains distinct flanking domains adjacent to its catalytic ATPase domain, as illustrated in **Figure 6** **(Clapier & Cairns, 2009; Reyes et al., 2021)**. They also feature unique associated subunits **(Clapier & Cairns, 2009)**. It is important to note that while chromatin remodelers are highly conserved from yeast to humans, there are differences in the protein domain composition **(Clapier & Cairns, 2009)**. Given the additional associated proteins, some remodelers can form large multi-subunit complexes, while others exist as monomers **(Murawska & Brehm, 2011)**.

The SWI/SNF remodelers contain about 9 to 16 subunits **(Chen et al., 2023)**. Apart from its catalytic ATPase domain, this remodeler consists of helicase SANT (HSA) and a post-HSA at the N-terminus, along with a bromodomain at the C-terminus **(Clapier & Cairns, 2009)**. Other conserved proteins, such as actin and/or actin-related proteins, are found to interact with the N-terminus HSA domain of the SWI/SNF catalytic subunit **(Tyagi et al., 2016)**.

In contrast with SWI/SNF complexes, the ISWI remodelers are rather small complexes composed of 2 to 4 subunits **(Clapier & Cairns, 2009; Tyagi et al., 2016)**. The prominent features of the ISWI remodeler are the HAND-SANT-SLIDE (HSS) domains located at the C-terminus region and the additional two regulatory autoinhibition domains, NegC and AutoN, situated in between the ATPase domain **(Clapier & Cairns, 2012; Reyes et al., 2021)**. The specialized accessory proteins contain various chromatin binding domains, including DNA-binding histone fold motifs, plant homeodomain (PHD), and bromodomain, as well as DNA binding motifs **(Clapier & Cairns, 2009)**.

Among all the remodelers, CHD remodelers can form monomer and multiprotein complexes **(Murawska & Brehm, 2011)**. The CHD remodelers are characterized by the presence of two tandem chromodomains at the N-terminus adjoining the catalytic ATPase domain **(Marfella & Imbalzano, 2007; Woodage et al., 1997)**. In addition, CHD complexes comprise 1 to 10 associated subunits **(Clapier & Cairns, 2009)**. With the absence and presence of additional domains, the CHD family is further classified into three subfamilies: Chd1-Chd2, Chd3-Chd4, and Chd5-Chd9 **(Hall & Georgel, 2007; Marfella & Imbalzano, 2007; Sims & Wade, 2011; Trujillo et al., 2022)**. The first subfamily of Chd1-Chd2 consists of the sole Chd family identified in *S. cerevisiae*, Hrp1 and Hrp3 in *S. pombe,* as well as the Chd1 and Chd2 proteins present in higher eukaryotes **(Jae Yoo et al., 2002; Y. H. Jin et al., 1998;**

Yong Hwan Jin et al., 1998; Marfella & Imbalzano, 2007; Woodage et al., 1997). The signature motif in this subfamily is a DNA-binding domain localized at the C-terminus region **(Stokes & Perry, 1995)**. The second subfamily includes human Chd3 and Chd4 proteins (or known with Mi-2α and Mi-2β, respectively) and flies Mi-2 protein that lacks the DNA-binding domain but contains a pair of plant homeodomain (PHD) at the N-terminal part **(Woodage et al., 1997)**. The third subfamily members are Chd5-Chd9 proteins. The proteins in this subfamily have additional signature motifs at the C-terminus regions, such as paired Brahma and Kismet (BRK) domain, SANT domain, CR domain, and a DNA-binding domain **(Hall & Georgel, 2007; Marfella & Imbalzano, 2007)**. Nonetheless, it is worth mentioning that not all members of this subfamily share these domains **(Murawska & Brehm, 2011)**.

The last family member of the remodeler is INO80, the largest remodeler complex containing about 15 subunits of protein **(Bao & Shen, 2007; Shen et al., 2000)**. Besides a long insertion region connected between the ATPase domain, this component has an important role as a scaffold for two DNA helicase RubV-like subunits (e.g., Rbv1/2 in yeast, Reptin and Pontin in flies, and RUVBL1/2 in humans), as well as actin and actin-related proteins **(Clapier & Cairns, 2009; Jonsson et al., 2004; Tosi et al., 2013)**. Additionally, the ATPase catalytic subunit also contains the HSA domain at the C-terminus, which can interact with the nuclear actin and actin-related proteins **(Szerlong et al., 2008)**.

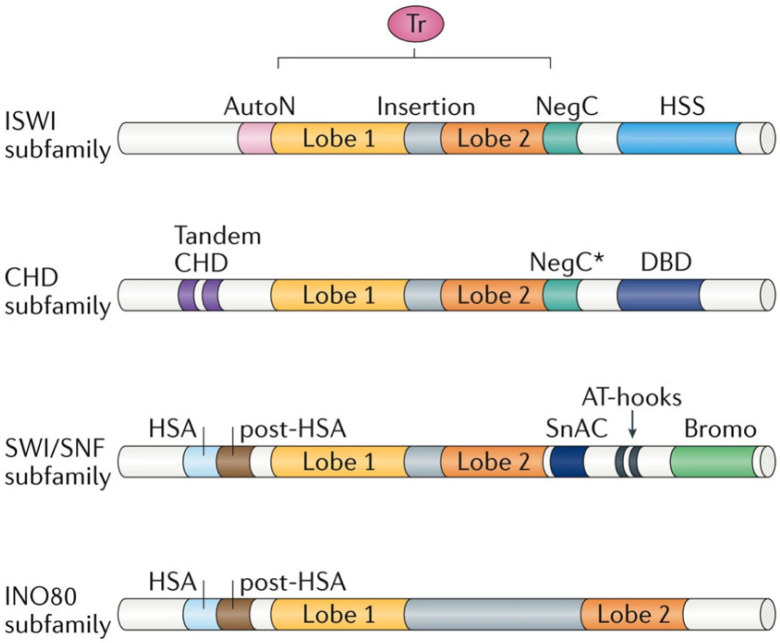

Figure 6. Domain compositions of chromatin remodelers. The four subfamilies of remodelers can be classified based on the length of the insertion region between the ATPase domain and the conserved accessory domains residing from the catalytic domain. The Figure is adapted from Clapier et al., 2017.

1.3.2.3 Functions of specialized domains in chromatin remodelers

The variant domains and specialized subunit proteins likely contribute to remodeler recruitment to chromatin and functional diversity, influencing their implications in cellular processes. For example, the SWI/SNF remodeler is known to interact with acetylated lysine histone tails via bromodomain, providing evidence for

the recruitment of this remodeler to chromatin **(Awad & Hassan, 2008; Dhalluin et al., 1999; Hassan et al., 2002; Sudarsanam & Winston, 2000)**. Additionally, associated proteins such as actin and/or actin-related proteins have been proposed to promote remodeler complex assembly, modulate ATPase activity, and facilitate DNA translocation and chromatin remodeling activities **(Mohrmann & Verrijzer, 2005; Szerlong et al., 2008; Szerlong et al., 2003; Yang et al., 2007)**. These discrete functions of the specialized domains and their associated subunits are apparent to influence the recruitment of SWI/SNF chromatin remodelers at specific loci and their role in facilitating access for regulatory proteins to nucleosome DNA through nucleosome sliding and ejection, as well as the removal of histone dimers **(Clapier et al., 2017; Lin et al., 2020; Singh et al., 2023)**. This process can occur during transcriptional activation, where the SWI/SNF remodelers establish nucleosome-free regions at the enhancers and promoters **(Hassan et al., 2001; Martin et al., 2023; Rawal et al., 2018)**.

Some ISWI remodeler complexes have an associated subunit protein containing the PHD finger domain and/or bromodomain **(Bartholomew, 2014)**. The PHD finger motif of human and *Drosophila* NURF exhibits preferential interaction with trimethylation of histone H3 lysine 4 (H3K4me3) **(Li et al., 2006; Wysocka et al., 2006)**. Since histone H3K4me3 is primarily enriched at the transcription start sites of active genes, the association of NURF to H3K4me3 at the promoter region suggests the potential implication in modulating transcription initiation **(Wysocka et al., 2006)**. Indeed, this finding is in line with both *in vitro* and *in vivo* studies that reveal NURF repositions nucleosomes at the enhancer elements and promoter regions to generate access for transcription factors during transcription initiation **(Mizuguchi et al., 1997) (Badenhorst et al., 2002; Hamiche et al., 1999; Kang et al., 2002; Kwon et al., 2016; Xiao et al., 2001)**. Apart from the perturbation of nucleosomes, other *Drosophila* ISWI remodeler ACF participates in chromatin assembly and remodeling nucleosomes **(Fyodorov & Kadonaga, 2002; Ito et al., 1997; Ito et al., 1999)**. Moreover, the bromodomain of human NURF is found to bind with the acetylated histone 3 lysine 16 (H3K16ac) **(Ruthenburg et al., 2011)**. In *S. cerevisiae* ISWI, the PWWP domain-Ioc4 of Isw1b interacts with nucleosomes containing histone H3K36me3 to maintain chromatin structure by preventing the initiation of cryptic transcription during transcription elongation **(Li et al., 2022; Smolle et al., 2012)**. Another domain at the C-terminus of ISWI, the HSS contributes to nucleosome recognition and DNA binding modules **(Grune et al., 2003)**.

In the CHD remodeler, each subfamily contains a pair of tandem chromodomain in addition to the ATPase domain, yet they have different structural motifs. In general, CHD chromodomains recognize and interact with methylated lysine residues of histone H3 **(Becker & Workman, 2013)**. An *in vitro* study reported that the tandem chromodomains of human CHD1 selectively bind with both histones H3K4me2 and H3K4me3, marks correlated with actively transcribed genes **(Flanagan et al., 2005)**. Additionally, this interaction has been confirmed by a crystal structure of histone H3K4me3 bound to CHD1 **(Flanagan et al., 2005)**. In contrast with human CHD1, the *Drosophila* CHD1 chromodomains can bind to all histone modification states of histone H3K4, including mono-, di, and tri-methylation **(Morettini et al., 2011)**. The evidence that yeast CHD1 chromodomains interact with histone H3K4 methylation has sparked a debate of contradiction in several studies. Initially, one study revealed that the second chromodomain (CD2) of yeast CHD1 specifically interacts with histone

H3K4me2, suggesting a correlation with transcriptional regulation **(Pray-Grant et al., 2005)**. However, fluorometric titration experiments did not detect the association between yeast CHD1 with all three histone methylation states **(Flanagan et al., 2005; Sims et al., 2005)**. This result is also supported by a genetic study where the localization of yeast CHD1 in active genes is unaffected despite deleting the Set1, an enzyme that catalyzes histone H3K4 methylation **(Sims et al., 2005)**. Two years later, a structural comparative study on the crystal structure of CHD1 dual chromodomain between humans and *S. cerevisiae* hypothesized that the nonexistence of yeast chromodomains binding to histone H3K4 methylation is due to the differences in the folding of insert 1 region within chromodomain 1 **(Flanagan et al., 2007)**. Although the yeast chromodomain of CHD1 is likely not to interact with histone H3K4 methylation, it has been identified that the chromodomains are important and required in transcription elongation **(Simic et al., 2003)**.

The signature subunits of the INO80 remodeler are the two RuvB-like proteins DNA helicases, nuclear actin, and actin-related proteins. RuvB is a bacterial ATPase helicase that is required for Holliday junction migration, a process for the formation of heteroduplex DNA during homologous recombination and recombination repair of DNA damage **(Iwasaki et al., 1992; Parsons et al., 1992; Wald et al., 2022; West & Connolly, 1992)**. The two RuvB-like proteins DNA helicases in the INO80 remodeler complex are homologs to bacterial RuvB, implying the potential implication of the INO80 complex in DNA repair **(Jha & Dutta, 2009; Morrison, 2017)**. The presence of the RuvB-like proteins as components of the INO80 complex is identified to be essential for the complexes' structural integrity and the functions of the INO80 chromatin remodeling **(Jonsson et al., 2004)**. This has been demonstrated by the absence of yeast Rvb proteins leads to the loss of Arp5 (actin-related protein), which is crucial in the DNA binding activity and nucleosome mobilization activity of the INO80 remodeler **(Jonsson et al., 2004; Shen et al., 2003)**. Act1, Arp4, Arp5, and Arp8 are members of the actin and actin-related proteins in the yeast INO80 complex **(Shen et al., 2000).** Notably, all these proteins are found to be essential for the formation of the INO80 complex and influence how the INO80 functions. In the formation of this complex, it has been proposed that there is an ordered assembly of Arps **(Shen et al., 2003)**. Some evidence reported that Arp5 requires Rvb to bind with Ino80, whereas other actin-related proteins of Act1, Arp4, and Arp8 interact with the HSA domain **(Jonsson et al., 2004; Shen et al., 2003)**. In addition to that, the deletion of Arp8 in the INO80 complex leads to the missing of both actin and Arp4 **(Shen et al., 2003)**. Another potential function of Arps is to mediate the interaction of the INO80 complex with nucleosomes. For example, both yArp4 and yArp8 generally can bind to all four core histones **(Harata et al., 1999; Shen et al., 2003)**. For certain specific targets, yArp4 is shown to be responsible for the yINO80 complex interacting directly with phosphorylated histone H2A on Ser129 in response to DNA damage, which links the involvement of yINO80 in the repair of DNA damage **(Downs et al., 2004; van Attikum et al., 2004)**. An *in vivo* study has revealed that yArp4 binds to the promoter region, suggesting a functional implication of INO80 in transcriptional regulation **(Harata et al., 2002)**. Furthermore, yeast and human Arp8 prefer to associate with $(H3/H4)_2$ tetramer **(Gerhold et al., 2012; Saravanan et al., 2012; Shen et al., 2003)**. Besides that, Arp proteins affect the functional integrity of INO80 as a chromatin remodeler in which deleting Arp5 and Arp8 significantly abolishes the binding activity to DNA as well as the nucleosome-mobilizing activities **(Shen et al., 2003)**.

After all, each specialized domain in both associated subunits and ATPase subunits contributes to how the chromatin remodelers act. Given that, the remodelers can be categorized based on their distinct functions in nucleosome assembly, chromatin access, and nucleosome editing, as shown in **Figure 7** **(Clapier et al., 2017)**. However, it is noteworthy that the depicted figure is a simplified version of the classification whereby there are exception cases for ISWI and CHD to contribute to chromatin access and not only in nucleosome assembly **(Clapier et al., 2017)**.

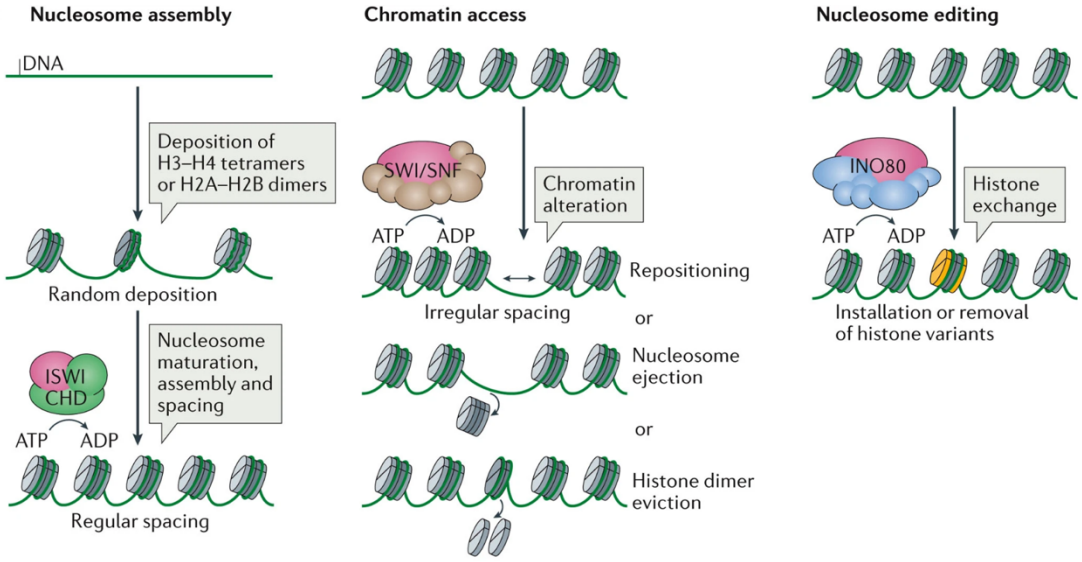

Figure 7. Representative schematic of distinct roles of chromatin remodelers to assemble and modify chromatin structure. The pink division in the remodeler represents the catalytic ATPase domain. The subunit of the remodeler group is indicated in different colors: green for ISWI and CHD, brown for SWI/SNF, and blue for INO80. The Figure is adapted from Clapier et al., 2017.

1.4 ISWI chromatin remodeler

The ISWI ATPase was first identified in *Drosophila* based on its similarity to *Drosophila brahma*, the catalytic ATPase subunit of the SWI/SNF-related chromatin remodeler **(Elfring et al., 1994)**. Thus far, the *Drosophila* ISWI forms six distinct complexes by sharing the sole catalytic ATPase subunit, including nucleosome remodeling factor (NURF), ATP-utilizing chromatin assembly and remodeling factor (ACF), chromatin-accessibility complex (CHRAC), remodeling and spacing factor (RSF), Toutatis-containing chromatin remodeling complex (ToRC) and nucleolar remodeling complex (NoRC) **(Ito et al., 1997; LeRoy et al., 1998; Strohner et al., 2001; Tsukiyama & Wu, 1995; Varga-Weisz et al., 1997)**. Each complex exhibits biochemical activities to modify the structure of chromatin in distinct ways. Typically, *Drosophila* ISWI (dACF and dCHRAC) participates in the assembly of chromatin structure by sliding nucleosomes as well as generating regularly spacing nucleosomes and phasing nucleosome arrays **(Baldi et al., 2018; Eberharter et al., 2001; Langst et al., 1999; Scacchetti et al., 2018; Yang et al., 2006)**. However, dNURF has different functions that alter the chromatin structure by sliding the nucleosomes, thereby allowing access to transcription factors for the promoters to facilitate transcription **(Kang et al., 2002; Mizuguchi et al., 1997; Tsukiyama & Wu, 1995)**. The following members of dISWI, both dRSF and dNoRC, contribute to establishing heterochromatic structures. Particularly, dNoRC mediates the silencing of ribosomal gene transcription by recruiting histone deacetylase and DNA methyltransferase to the

rDNA promoter, thus establishing the silent chromatin region **(Santoro et al., 2002; Strohner et al., 2001; Zhou et al., 2002)**. Meanwhile, the dRSF is identified to play a role in facilitating the replacement of histone variant H2A in silent chromatin formation **(Hanai et al., 2008)**. The last member, dToRC, and histone chaperone NAP-1 are involved in nucleosome assembly **(Emelyanov et al., 2012)**. With all these functions, the absence of ISWI in *Drosophila* has been discovered to be lethal and to affect gene expression during development **(Deuring et al., 2000)**.

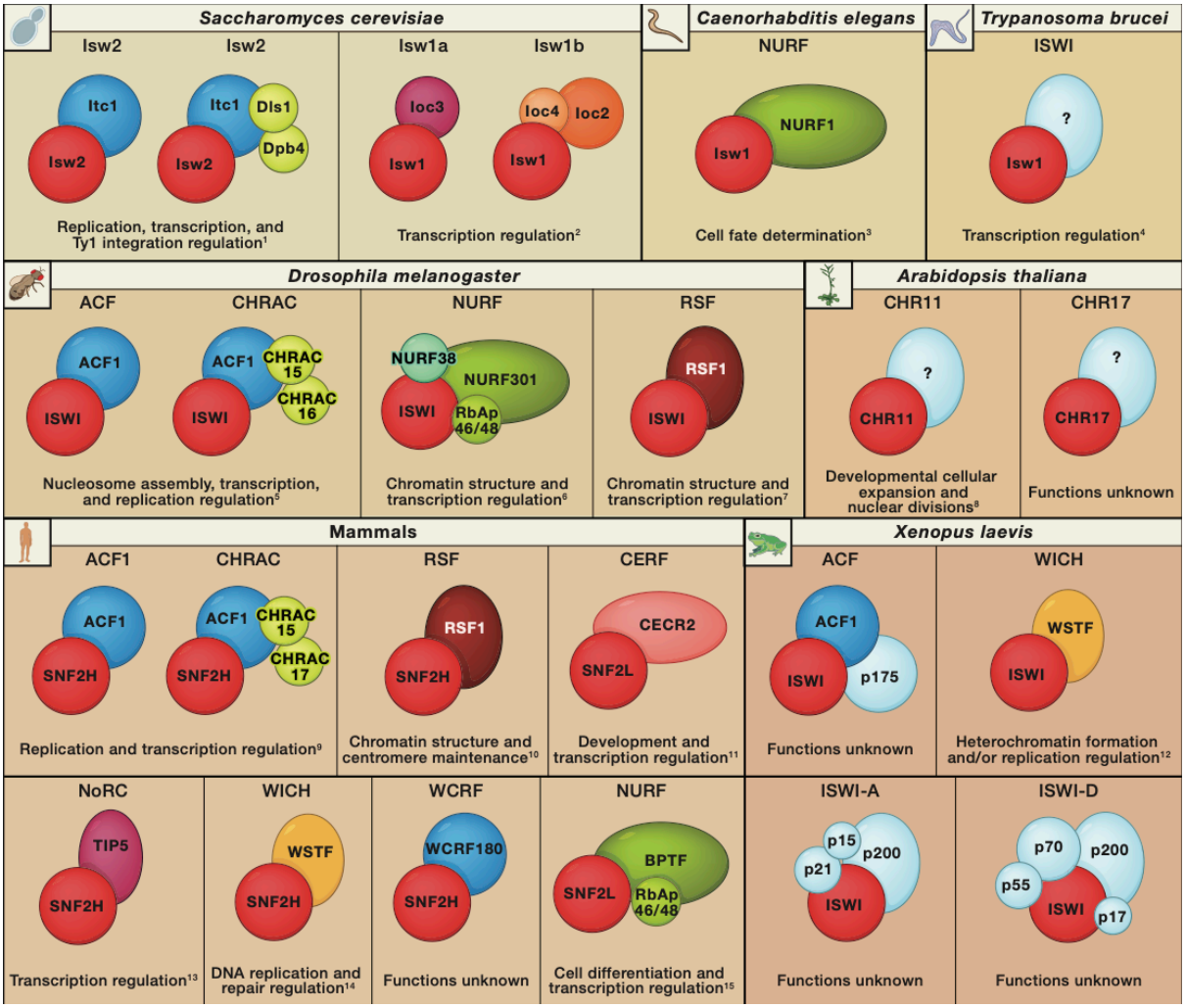

Figure 8. Chromatin remodeler ISWI conserved from yeast to human. The Figure is adapted from Yadon & Tsukiyama, 2011.

Afterward, the ISWI remodeler complexes have since been identified in other organisms such as yeast, frogs, nematode worms, plants, and mammals, signifying that remodelers are highly conserved from yeast to mammals **(Fig. 8)** **(Yadon & Tsukiyama, 2011)**. Among yeast, the ISWI remodelers from *Saccharomyces cerevisiae* have been extensively studied in both *in vitro* and *in vivo*. There are two complexes of ISWI remodeler named Isw1 and Isw2, which bind with different associated subunits and assemble into a total of 4 distinct complexes **(Tsukiyama et al., 1999; Vary et al., 2003)**. Unlike *S. cerevisiae*, the other popular yeast model organism, fission yeast *Schizosaccharomyces pombe,* strikingly has no ISWI remodeler but rather has two CHD1 subfamilies **(Flaus et al., 2006)**. Another yeast, *Myceliopthora thermophila* exhibits ISWI (MtISWI) with an identical sequence of about

68% to both Isw1 and Isw2 of *S. cerevisiae*, and it has been structurally crystalized with a resolution of 2.4 Å **(Yan et al., 2016)**. Lastly, the Isw2 from *Candida albicans* shares 61% identity and 77% similarity with Isw2 of *S. cerevisiae* **(Navarathna et al., 2016)**. Little information for the Isw2 molecular function in *C. albicans* **(Navarathna et al., 2016)**.

Moreover, one ISWI complex is found in parasites and worms, including TbISWI in *Trypanosoma brucei* **(Hughes et al., 2007; Stanne et al., 2015)**, TcISWI from *Trypanosoma cruzi* **(Diaz-Olmos et al., 2020),** and ISW-1 of *Caenorhabditis elegans* **(Andersen et al., 2006)**. Then, there are three ISWI complexes from the plant *Arabidopsis thaliana,* so-called CRA (CHR11/17-RLT1/2, ARID5), CDM (CHR11/17-DDP1/2/3-MS13), and CDD (CHR11/17-DDR1/3/4/5/DDW1) **(Tan et al., 2020).**

In higher organisms like *Xenopus laevis*, there are four ISWI complexes in egg extract such as xACF, xWICH, ISWI-A, and ISWI-D **(Bozhenok et al., 2002; Guschin et al., 2000)**. In humans, the ISWI family consists of two ATPase catalytic subunits, SMARCA1 (SNF2L) and SMARCA5 (SNF2H), which interact with one of seven regulatory subunits: BAZ1A, BAZ1B, BAZ2A, BAZ2B, BPTF, CECR2, and RSF1 **(Oppikofer et al., 2017)**. With the addition of these regulatory subunits, the ISWI family remarkably expands to a total of 16 complex members, including ACF1/ACF5 (SMARCA1/5-BAZ1A), CHRAC-1/5 (SMARCA1/5-BAZ1A, POLE3, CHRAC1), WICH-1/5 (SMARCA1/5-BAZ1B), NORC-1/5 (SMARCA1/5-BAZ2A), RSF-1/5 (SMARCA1/5-RSF1), BRF-1/5 (SMARCA1/5-BAZ2B), NURF-1/5 (SMARCA1/5-BPTF, RBBP4, RBBP7), and CERF-1/5 (SMARCA1/5-CECR2) **(Li et al., 2021; Oppikofer et al., 2017)**.

1.5 Yeast ISWI chromatin remodeler complexes

In *Saccharomyces cerevisiae*, Isw1 and Isw2 are two homologous ISWI ATPases of *Drosophila* ISWI **(Tsukiyama et al., 1999)**. However, unlike the lethal phenotype observed in *Drosophila* upon deletion of ISWI, budding yeast lacking ISWI under normal growth conditions exhibit no effect on cell viability and phenotype **(Deuring et al., 2000; Tsukiyama et al., 1999)**. The absence of yeast ISWI alone rather appears to impact the transcriptional regulation of various genes significantly **(Hughes et al., 2000; Vary et al., 2003)**. Depending on the yeast background, deletion of ISWI along with CHD1 can lead to more severe or less severe phenotype under stress conditions. After all, ISWI and CHD1 can have overlapping functions, yet later found there are some differences in the group of genes affected **(Smolle et al., 2012)**.

Isw1 and Isw2 are associated with different accessory proteins, forming four distinct ISWI complexes **(Dirscherl & Krebs, 2004)**. Isw1 forms two complexes named Isw1a, containing Isw1 and Ioc3, and Isw1b, comprising Isw1, Ioc2, and Ioc4 **(Tsukiyama et al., 1999; Vary et al., 2003)**. Notably, none of the associated proteins are shared between the Isw1 complexes **(Tsukiyama, 2002)**. The distinct compositions of the Isw1 complexes strongly suggest that they are responsible for each remodeler's specialized functions despite sharing the same catalytic ATPase subunit **(Vary et al., 2003)**. Biochemical studies have shown that Isw1a and Isw1b exhibit comparable nucleosome-stimulated ATPase activities, but they somewhat differ in nucleosome sliding and spacing **(Vary et al., 2003)**. Moreover, the deletion of *ISW1* and/or *CHD1* are to cause an increase in cryptic transcription **(Smolle et al.,**

2012). Subsequent evidence from genomic nucleosome organization reconstituted experiments revealed that Isw1a plays a crucial role in generating regular arrays **(Krietenstein et al., 2016)**. Given all that, Isw1a has a function in organizing nucleosomes, whereas Isw1b plays a crucial role in transcription elongation and termination **(Bhardwaj et al., 2020; Lafon et al., 2012; Mellor & Morillon, 2004; Morillon et al., 2003; Smolle et al., 2012)**.

Similar to Isw1, Isw2 also can form two complexes, with one containing Isw2 and imitation switch 2 complex subunit 1 (Itc1) and another complex named Isw2/yCHRAC, formed by the association of Isw2, Itc1, Dpb3-like subunit (Dls1) and Dpb4 **(Gelbart et al., 2001; Iida & Araki, 2004; McConnell et al., 2004; Tsukiyama et al., 1999)**. The Isw2-Itc1 is the first Isw2 complex to be identified and functionally characterized **(Goldmark et al., 2000; Tsukiyama et al., 1999)**. The Isw2-Itc1 complex exhibits function in parallel with the Sin3-Rpd3 histone deacetylase complex to repress early meiotic genes during mitotic growth via the recruitment by Ume6 **(Goldmark et al., 2000)**. Here, the WAC domain in Itc1 plays a role in targeting the DNA-bound factor such as Ume6 **(Donovan et al., 2021)**. After the binding, the transcription repression process can be explained wherein the Isw2 complex slides nucleosomes near the upstream sequence of the Ume6p and establishes a nuclease-inaccessible chromatin structure **(Goldmark et al., 2000)**. Consistent with this, the Isw2 complex can slide nucleosomes close to the promoter region but also to the specific regions *in vivo* **(Fazzio et al., 2005; Fazzio & Tsukiyama, 2003)**.

Moreover, the Isw2 complex is also reported to participate in the repression of some other genes independently from *UME6, such as INO1, SIP4,* and *REC104* **(Fazzio et al., 2001; Goldmark et al., 2000)**. It has been shown that the absence of Isw2 affects the nucleosome positioning at the promoter site of *INO1* and *PHO3*, causing increased accessibility of chromatin **(Fazzio et al., 2001; Kent et al., 2001)**. Another study demonstrates that the Isw2-Itc1 complex is required in maintaining the repressive chromatin structure of Mata-specific genes in Matα cells **(Ruiz et al., 2003)**.

In 2004, a novel Isw2 complex was first reported and named ISW2/yCHRAC **(Iida & Araki, 2004; McConnell et al., 2004)**. This complex comprises Isw2, Itc1, Dls1 and Dpb4 **(Iida & Araki, 2004; McConnell et al., 2004)**. The Dls1 and Dpb4 contain histone fold motifs and are found to be homologous to the smallest subunit of CHRAC complexes in higher eukaryotes **(McConnell et al., 2004)**. Using single-cell assays, ISW2/yCHRAC is proposed to be involved in maintaining or inheriting the proper configuration of chromatin structure during cell division, such as DNA replication **(Iida & Araki, 2004)**. In addition, it has been pointed out that there is limited evidence supporting the idea for ISW2/yCHRAC to establish silent chromatin **(Iida & Araki, 2004)**. Later in 2018, Cutler and colleagues first characterized the implication of Isw2 complex conjunction with Ino80 to regulate chromatin structure in ribosomal DNA, facilitate efficient firing of rDNA origin of replication, and contribute to the rDNA repeat copy number **(Cutler et al., 2018)**. More information about this ISW2/yCHRAC complex is the subunit of Dls1 responsible for transcription repression of some genes from meiotic cells and not for Mata-specific gene *STE2* and *STE6,* whereas the Dpb4 subunit is found to be exclusively recruited to extranucleosomal DNA **(McConnell et al., 2004)**. Despite that many studies showed that Isw2 predominantly functions in gene repression, Isw2 is also suggested to have a role in transcriptional activation of the *SUC2* locus **(Fazzio et al., 2001)**.

1.5.1 Type and domain compositions of the yeast Isw1 complexes

As previously mentioned, the *S. cerevisiae* Isw1 remodeler can be further categorized into two distinct complexes known as Isw1a and Isw1b **(Vary et al., 2003)**. Isw1a comprises Isw1 and Ioc3, whereas Isw1b consists of Isw1, Ioc2, and Ioc4 **(Fig. 9) (Vary et al., 2003)**. Like other chromatin remodelers, the functional activity of the Isw1 complex likely depends on its specialized domains and unique signature subunits. The following section will describe each specialized domain present in the Isw1 subunit and the Ioc subunits.

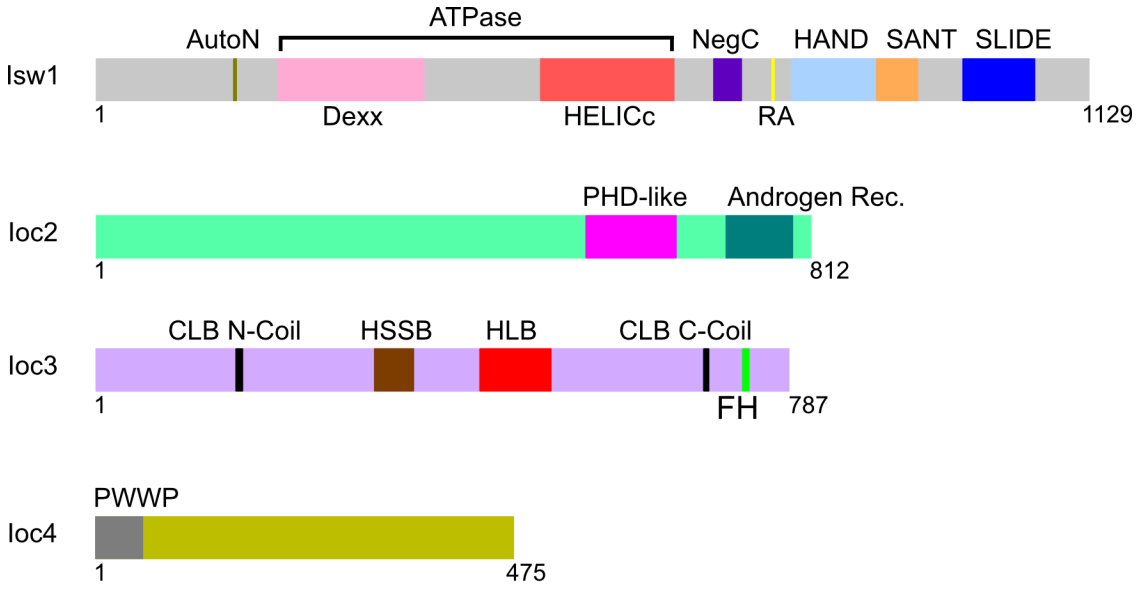

Figure 9. Domain compositions of Isw1a and Isw1b complexes. Isw1a contains Isw1 and Ioc3 subunits, while Isw1b consists of Isw1, Ioc2, and Ioc4 subunits.

1.5.1.1 ATPase subunit

Both Isw1a and Isw1b share Isw1 - a conserved SNF2-family catalytic ATPase subunit **(Vary et al., 2003)**. The ATPase subunit is separated by a short insertion sequence into two RecA-like domains, including the Dexx box helicases domain and the helicase superfamily C-terminal (HELICc) domain **(Clapier et al., 2017)**. Based on the cryo-EM structure of yeast Isw1-nucleosome, the ATPase domain of Isw1 interacts at the SHL2 position of nucleosomes **(Li et al., 2024; Yan et al., 2019)**. Moreover, this ATPase domain holds the essential key for the functional activities of Isw1, coupling ATP hydrolysis to modify or break histone-DNA contacts via a common DNA translocation mechanism **(Clapier et al., 2017)**. With all these capabilities, it achieves diverse outcomes of chromatin remodeling, such as nucleosome assembly, chromatin access, and nucleosome editing **(Clapier et al., 2017)**. The models of DNA translocation and the mechanistic understanding of chromatin remodeler in nucleosome sliding, spacing, and ejection have been extensively elucidated in various excellent reviews **(Clapier et al., 2017; Eustermann et al., 2023; Nodelman & Bowman, 2021; Zhou et al., 2016)**. Furthermore, a single mutation within the ATPase domain (ISWI-K227A) led to the inactivation of ATP hydrolysis in the presence of nucleosomes and resulted in the lack of regular spacing in nucleosome arrays **(Tsukiyama et al., 1999).** This study reveals how significant the role of this ATPase domain is for the functioning of the Isw1 complex.

Apart from the ATPase domain, the Isw1 subunit exhibits multiple functional domains. These are the C-terminal HAND-SANT-SLIDE (HSS) domain and two regulatory domains flanking within the ATPase, including the autoinhibitory N-terminal (AutoN) and the negative regulator of coupling (NegC), and the polybasic arginine anchor (RA) motif **(Clapier & Cairns, 2012; Lin et al., 2020; Yan et al., 2016)**. By function, the HSS domain primarily plays a crucial role in maintaining the integrity of the Isw1 complex by facilitating its formation and stability. The immunoprecipitation assays of TAP-tagged Isw1 in yeast strain mutants revealed that the SLIDE domain is required for association with Ioc3, whereas both the SANT and SLIDE domains are responsible for interaction with Ioc2 and Ioc4 **(Pinskaya et al., 2009)**. However, it is important to note that a weak interaction was observed between the Ioc3 and the Isw1Δ*SLIDE,* and no interaction occurred when both the SANT and SLIDE domains (Isw1Δ*C*) were deleted **(Pinskaya et al., 2009)**. This finding can render a hint that both the SANT and SLIDE domains of Isw1 may contribute to the interaction with Ioc3, leading to the formation of a stable Isw1a complex. Consistent with previous findings, the crystal structure of Isw1a lacking its ATPase showed that only the SLIDE domain is attached to the core of the Ioc3 subunit **(Yamada et al., 2011)**. Given all that, the intact formation of the Isw1 complex is essential for its ability to slide nucleosomes where deletion of either the SANT or SLIDE domain consequently abolishes Isw1 nucleosome remodeling activity **(Pinskaya et al., 2009; Yamada et al., 2011)**. Apart from that, structural studies of Isw1a revealed another ability for SANT and SLIDE domains to interact with minor grooves of the linker DNA, suggesting the involvement of both domains in the recruitment to nucleosomes **(Li et al., 2024; Yamada et al., 2011)**. Their interaction, however, is different from the *Drosophila* SANT and SLIDE domains despite the fact that they are structurally related to c-Myb DNA binding modules **(Grune et al., 2003; Pinskaya et al., 2009; Richmond, 2012)**.

Moreover, AutoN and NegC are two conserved regulatory domains situated on either side of the ATPase domain **(Clapier & Cairns, 2012)**. They were initially identified in *Drosophila* ISWI **(Clapier & Cairns, 2012)**. The AutoN domain exhibits sequence similarity to the basic patch of histone H4, while the NegC domain is characterized as a C-terminal bridge between ATPase lobes **(Clapier & Cairns, 2012)**. These domains primarily function to negatively regulate ATP hydrolysis and coupling ATP hydrolysis to DNA translocation, respectively, maintaining the inactive conformation of ISWI **(Clapier & Cairns, 2012)**. Activation of ISWI ATPase activity requires structural conformational changes involving two nucleosomal epitopes. Mechanistically, the inhibitory role of AutoN can be relieved when the histone H4 competes for interaction with the ATPase domain, displacing AutoN, whereas the interaction of HSS to extranucleosomal DNA alleviates the inhibitory role of NegC **(Clapier & Cairns, 2012)**. These mechanisms collectively form the concept of the "inhibition of inhibition" model in *Drosophila* ISWI **(Clapier & Cairns, 2012)**. In contrast, limited information is available on the functional roles of both domains in *S. cerevisiae*. However, one study revealed that deletion of the inhibitory L3 loop of the AutoN domain in Isw1 resulted in an active mutant capable of remodeling chromatin **(Yan et al., 2019)**. Furthermore, structural studies have reported that AutoN interacts with the first ATPase domain and somehow retains its association even after being released from the inactive conformation, and the NegC domain appears structurally disordered **(Li et al., 2024; Yan et al., 2019)**. An *in vivo* experiment found that deletion of both AutoN and NegC causes defective growth in cells with a sensitized background for chromatin misregulation **(Clapier & Cairns, 2012)**.

The recently identified feature of Isw1 is the RA motif, named after the two conserved amino acids of arginine (R) at residues 769 and 771 **(Li et al., 2024)**. Cryo-EM structure analysis of Isw1a bound to N1 nucleosome revealed that the RA motif can recognize the histones H2A and H2B acidic patch **(Li et al., 2024)**. Intriguingly, mutations of R769E or R771E fully abolish the ability of Isw1 in sliding nucleosomes and spacing nucleosomes **(Li et al., 2024)**. Collectively, the RA motif is suggested to play an important role in facilitating the basic nucleosome sliding activity **(Li et al., 2024)**.

1.5.1.2 Ioc subunits

The subunits Ioc2, Ioc3, and Ioc4 are uniquely distinct, and each contains auxiliary domains. The Ioc2 subunit contains a plant homeodomain (PHD)-finger-like motif (aa 557-659) **(Vary et al., 2003)**. Generally, the PHD finger motif is perceived as an epigenome reader histone that can recognize or read the unmodified histone tails and certain post-translational modifications on histone H3, such as H3K4me3 **(Musselman & Kutateladze, 2011; Sanchez & Zhou, 2011)**. Many studies found the association of PHD finger to histone H3 is connected with several processes, especially in gene regulation, nucleosome remodeling, and recombination **(Musselman & Kutateladze, 2011; Sanchez & Zhou, 2011)**. Given this information, the PHD motif of Ioc2 also has been proposed to have an interaction with histone H3K4me3. Other supporting studies have emerged from another ISWI remodeler in *Drosophila* NURF301, which has been characterized previously to have a role in binding specifically with histone H3K4me3 as a mark of the transcription start site of active genes **(Li et al., 2006; Wysocka et al., 2006)**. Conversely, one study using immunoblot analysis reported that histone H3K4me3 was not detected in the Isw1b-associated histones **(Maltby et al., 2012)**. After all, it remains unclear about the involvement of the PHD motif in the Ioc2 subunit for the Isw1b remodeler function.

The Ioc4 subunit interacts with Ioc2 and Isw1 to form the Isw1b complex. The specialized domain in the Ioc4 is the PWWP domain (amino acids 1-178) **(Vary et al., 2003)**, which has been well characterized for its functions. The PWWP domain is named from a Pro-Trp-Trp-Pro motif and belongs to the Royal superfamily **(Maurer-Stroh et al., 2003)**. This domain is characterized as a chromatin reader that contains a conserved aromatic cage that recognizes histone lysine modified containing nucleosome **(Qin & Min, 2014; Rona et al., 2016)**. In the Ioc4 subunit, the PWWP domain was identified to be responsible for the interaction and localization of Ioc4 to nucleosome-containing histone H3K36me3 in both *in vitro* and *in vivo* **(Smolle et al., 2012)**. Specifically, it has been found that the aromatic cage of the PWWP domain of Ioc4 mediates the preference interaction with histone H3K36me3 **(Li et al., 2022)**. Together, the PWWP domain of Ioc4-associated protein predominantly contributes to the Isw1b remodeler to preferably target the histone H3K36me3, which is methylated by Set2 and linked to transcriptional elongation **(Krogan et al., 2003; Maltby et al., 2012; Smolle et al., 2012).**

In contrast with other Ioc subunits, the Ioc3 of Isw1a exhibits multiple domains, including the N-terminal and C-terminal of coil-linker-DNA-binding (CLB), the HSS-binding loop (HSSB loop), the helical-linker-DNA-binding domain (HLB) and the finger helices (FH) **(Li et al., 2024; Yamada et al., 2011)**. As noted, both the CLB and HLB play an important role primarily in the binding of Ioc3 to DNA. Both the X-ray structure and cryo-EM structure of Isw1a revealed that both the N-coil and C-coil of CLB domains bind to the external-linker DNA, whereas the HLB is in close proximity with the internal-linker DNA **(Li et al., 2024; Yamada et al., 2011)**. Additionally, one study reported that the CLB domain also interacts with the HSS domain of Isw1 **(De Cian et al., 2012)**. Of note, the HLB domain of Ioc3 possesses a pivotal function in the recruitment of Isw1a to dinucleosomes and sensing DNA for nucleosome spacing **(Bhardwaj et al., 2020)**. With that role, the HLB domain is thus suggested to be involved in the nucleosome organization **(Bhardwaj et al., 2020)**. Consistent with a previous study, the cryo-EM structure of Isw1a bound to dinucleosomes showed that nucleosome spacing by Isw1a requires both the HSS of Isw1 and Ioc3-HLB to measure the length of entry DNA from the nucleosome edge **(Li et al., 2024)**. Moreover, the loss of the HLB domain in Ioc3, along with NuA4/SWR1, can affect the transcription of many genes correlated with nucleotide/nucleoside synthesis, metabolism, and respiration **(Bhardwaj et al., 2020)**. The HSSB loop is another distinguishing feature of the Ioc3 subunit and exhibits the ability to interact with the SLIDE and SANT domains of Isw1. This interaction is structurally described whereby the HSSB loop extends over the SLIDE α9 domain to the HSS α7 and SANT domain **(Yamada et al., 2011)**. Lastly, the recently identified FH domain consists of four arginine residues – Arg735, Arg738, Arg739, and Arg742 – which play a crucial role in nucleosome recognition **(Li et al., 2024)**.

1.5.2 Structural insights into Isw1 chromatin remodelers

The structure of the Isw1a complex has been resolved using various approaches, including high-resolution X-ray crystallography, cryogenic electron microscopy (Cryo-EM), and site-directed photo-crosslinking. These multiple studies have delved into the relationship between structures and functions of the Isw1 complex in nucleosome remodeling. In 2011, Yamada and colleagues were the first to solve the crystal structure of Isw1a lacking ATPase domain (HSS-Ioc3) alone or bound to two copies of DNA at resolutions of 3.25 Å and 3.6 Å, respectively **(Yamada et al., 2011)**. The formation of HSS-Ioc3 appears to be in an L-shaped dimension and has a rigid structure, with the SLIDE domain interacting with the Ioc3 core, the HLB domain extending from the core, and the HSSB stretched out close to the SLIDE and SANT domains **(Fig. 10A)** **(Yamada et al., 2011)**. When DNA is present; it can be observed that SLIDE, SANT, HLB, and CLB are in contact with DNA **(Yamada et al., 2011)**. Intriguingly, a model of Isw1a (HSS-Ioc3) binds dinucleosome and potentially functions as a “protein ruler” to establish the spacing between two nucleosomes is proposed based on the evidence from combinations of X-ray structure, cryo-EM structure, and site-directed photocrosslinking **(Yamada et al., 2011)**. Later on, a study using biochemical assays validated that Isw1a has preferences to interact and slide dinucleosomes rather than mononucleosomes **(Bhardwaj et al., 2020)**. Additionally, utilizing site-directed DNA and histone crosslinking, this study unveiled the allosteric changes in Isw1a and Ioc3 interactions with both dinucleosomes and mononucleosomes **(Bhardwaj et al., 2020)**.

Recently, Li and colleagues revealed the cryo-EM structure of Isw1a bound to the dinucleosome at a resolution of 5.4 Å **(Li et al., 2024)**. An intriguing discovery of this structure is that Isw1 and Ioc3 interact with two different nucleosomes (N1 and N2, respectively), as shown in **Figure 10B** **(Li et al., 2024)**. In addition to that, this structure highlights evidence for Isw1a to play a crucial role as a protein ruler to generate spacing between two adjacent nucleosomes **(Li et al., 2024)**.

The interaction of the Isw1a complex with nucleosome requires various actions derived from each domain present in both the Isw1 and Ioc3 subunits **(Li et al., 2024)**. First, the binding of Isw1 to the mobile (N1) nucleosome includes (1) the ATPase domain interacting with the mobile nucleosome, preceded by the release of AutoN inhibition, (2) the basic patch of the RA motif that recognizes the acidic patch of the nucleosome, causing unfold of NegC, and (3) the HSS domain binding with the entry linker DNA close to the nucleosome edge **(Li et al., 2024)**. All these steps are crucial because they provide the structural basis for the enzyme-sensing DNA linker **(Li et al., 2024)**. Second, the Ioc3 subunit senses and interacts with the neighboring nucleosome (N2), involving (1) the positive charge of the HLB and the CLB domain binding with the DNA, (2) the negative charge of Ioc3 interacting with the polybasic N-terminus of H4 tail, and (3) the C-terminus helix of Ioc3 (Finger helix) recognizing the H2A-H2B acidic patch of nucleosome **(Li et al., 2024)**. Ultimately, these interaction steps are necessary for the Isw1a complex to remodel nucleosomes and spacing nucleosomes.

Conversely to the extensive structural studies on Isw1a, the structure of the Isw1b complex has yet to be resolved. Nevertheless, the crystal structure of the Ioc4-PWWP domain has been determined at a resolution of 2.3 Å **(Li et al., 2022)**. Here, the unique feature of the PWWP domain is characterized by a long insertion motif and contains highly charged patches, including one acidic patch and two basic patches **(Li et al., 2022)**. With biochemical experiments, it has been shown that the Ioc4-PWWP can bind with histones and DNA through the acidic and basic patches identified previously in the PWWP domain **(Li et al., 2022)**. Resolving the structure of the Isw1b complex would be optimal for uncovering additional mechanisms underlying nucleosome remodeling.

Moreover, cryo-EM structures of the Isw1-nucleosome complex coupled with ADP and ADP-BeFx were determined at resolutions of 3.4 Å and 3.37 Å, respectively **(Yan et al., 2019)**. These structural represent the states of Isw1 after ATP hydrolysis and the transition state of Isw1 after binding ATP but not hydrolyzable, respectively. In both structures, Isw1 was found to bind to the nucleosome at SHL ± 2 **(Yan et al., 2019)**. Additional evidence from DNA footprinting supports this finding by showing that the Isw1 alone associates with the SHL-2 position **(Bhardwaj et al., 2020)**. Furthermore, this study discovered that the Isw1 protein undergoes structural conformational changes when it is activated following the interaction with nucleosomes. These changes include rotation of the lobe 2 ATPase domain for about 148 degrees, a disordered form of the NegC domain, and an association of the AutoN to the lobe 1 ATPase domain **(Yan et al., 2019)**. Similar to other remodelers, the local DNA distortion and translocation were detected after ATP hydrolysis, which is the typical feature of DNA translocation **(Yan et al., 2019)**.

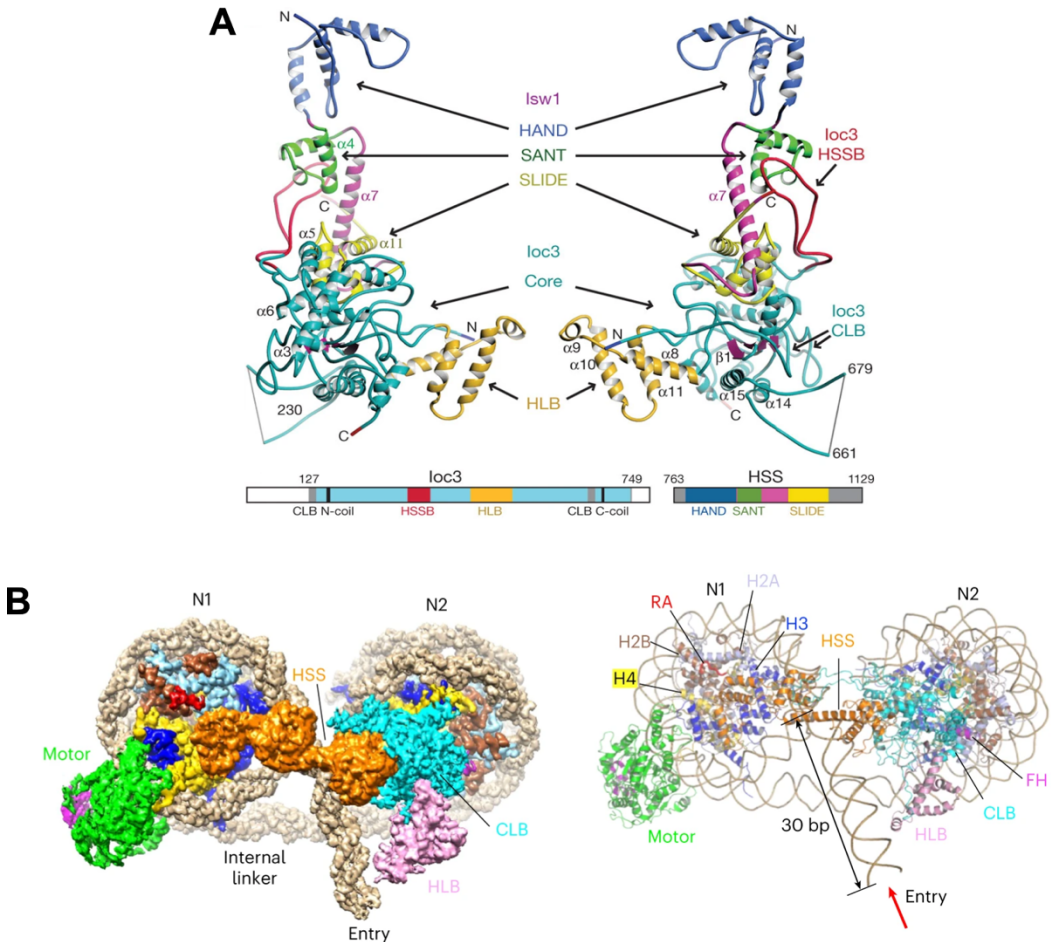

Figure 10. Crystal structure and cryo-EM structure of the Isw1a complex. **(A)** Crystal structure of Isw1a (HSS-Ioc3) at a resolution of 3.25 Å (PDB ID: #2Y9Y). **(B)** Cyro-EM structure of Isw1a with the dinucleosome at a resolution of 5.4 Å (PDB ID: #7X3T). Figure 10A is adapted from Yamada et al., 2011 and Figure 10B is adapted from Li et al., 2024.

1.5.3 *In vitro* functional studies of Isw1 chromatin remodelers

Isw1 remodelers require at least five mechanistic actions to alter chromatin structures, which include (1) recognition of DNA and/or nucleosomes, (2) ATP hydrolysis, (3) DNA translocation, (4) nucleosome repositioning and (5) nucleosome spacing and phasing. Nevertheless, certain Isw1 remodelers may exhibit variations in their actions depending on specific factors. In this section, I will present the evidence derived from numerous previous studies elucidating the mechanistic actions of the Isw1 monomer, Isw1a, and Isw1b.

1.5.3.1 Roles of Isw1 remodelers in DNA and nucleosome binding

The recruitment of the Isw1 complex to chromatin marks the initial step in its remodeling process. Isw1 alone lacks the ability to bind to DNA or nucleosome arrays in the absence of ATP **(Vary et al., 2003)**. In contrast, both Isw1a and Isw1b complexes interact efficiently with DNA or nucleosome arrays independent of ATP **(Vary et al., 2003)**. Nonetheless, Isw1a demonstrates a more robust binding activity compared to the Isw1b complex **(Vary et al., 2003)**. A couple of years later, an intriguing finding reported that different lengths of extranucleosomal DNA may

influence the binding activity of the Isw1 complex to nucleosomes. For instance, the Isw1a complex can bind to nucleosomes with extranucleosomal DNA at one site (entry/exit) or two sites (entry and exit), requiring an optimal length of about 33 bp **(Gangaraju & Bartholomew, 2007)**. Notably, the binding affinity of Isw1a appears to be higher for nucleosomes with two sites of extranucleosomal DNA **(Gangaraju & Bartholomew, 2007)**. In contrast, the Isw1b complex requires a shorter length of extranucleosomal DNA of about 13 to 19 bp **(Gangaraju & Bartholomew, 2007)**.

Moreover, various factors, such as discrete modified histone tails or histone variants, can also influence the recruitment of the Isw1 complex, providing insight into their positioning in genomic loci and potential functions *in vivo*. A recent study has revealed that Isw1a preferably interacts with nucleosomes containing histone variant H2A.Z **(Bergmann, 2021)**. Additionally, Isw1b is well-known for its preference to bind to histone H3K36me3 mononucleosome rather than unmethylated mononucleosome mediated by the PWWP-Ioc4 subunit, implying the role of Isw1b in transcriptional elongation **(Li et al., 2022; Maltby et al., 2012; Smolle et al., 2012)**.

Additional findings from structural and biochemical studies provide evidence supporting the role of Isw1a as a protein ruler in nucleosome spacing. Here, Isw1a exhibits a strong binding preference towards dinucleosomes compared to mononucleosomes **(Bhardwaj et al., 2020; Li et al., 2024; Yamada et al., 2011)**.

1.5.3.2 Roles of Isw1 remodelers in ATP hydrolysis and DNA translocation

All remodelers share a similar ATPase domain capable of hydrolyzing ATP and utilizing the energy to alter chromatin organization. The ATPase hydrolysis activity of remodeler complexes may vary depending on the substrates, such as DNA, histones, or nucleosomes. However, yeast ISWI remodelers seem to have similar ATPase activity stimulated by nucleosomes. Both Isw1a and Isw1b exhibit nearly equivalent nucleosome-stimulated ATPase activities **(Vary et al., 2003)**. In contrast, the Isw1 monomer lacks the ability to hydrolyze ATP in the presence of nucleosomes **(Vary et al., 2003)**. This activity is also observed in another member of yeast ISWI remodelers, Isw2, which requires all subunits to form a complex to be able to hydrolyze the ATP in the presence of nucleosomes **(Gelbart et al., 2001)**. Moreover, with the conserved ATPase motor shared within ISWI remodelers, they all possess the ability for DNA translocation, as described in several reviews **(Bowman, 2010; Clapier et al., 2017; Nodelman & Bowman, 2021; Yan & Chen, 2020; Zhou et al., 2016)**.

1.5.3.3 Roles of Isw1 remodelers in nucleosome sliding

The yeast ISWI remodelers modify chromatin structure by moving nucleosomes along the DNA sequence. This activity is necessary for the maturation of nucleosome assembly and providing access for the transcription machinery to DNA. Each Isw1 complex moves the nucleosome in different directionalities. The Isw1a complex prefers to slide end-positioned nucleosomes towards the central position of the DNA fragment with no closer than 15 bp from a DNA end as the final location from sliding **(Stockdale et al., 2006)**. On the other hand, Isw1b efficiently moves mid-positioned nucleosomes toward the end position **(Stockdale et al., 2006)**. Moreover, Isw1a exhibits a sliding preference for nucleosomes containing histone variant H2A.Z rather than histone H2A, which is consistent with its binding preference **(Bergmann, 2021).**

Notably, one study revealed that Isw1a demonstrates higher efficiency in sliding dinucleosomes (50N150N26) compared with mononucleosomes (0N70) despite the ATPase hydrolysis activity having no difference between the two substrates **(Bhardwaj et al., 2020)**.

1.5.3.4 Roles of Isw1 remodelers in nucleosome spacing and phasing

Both Isw1a and Isw1b exhibit nucleosome spacing activity during chromatin assembly, transforming irregular nucleosome arrays into regularly spaced nucleosome arrays. By definition, nucleosome spacing is referred to as the distances of the linker length between nucleosomes, which can be varied depending on the chromosomal loci and the functional state of the underlying DNA sequence **(Becker & Workman, 2013; Blank & Becker, 1996)**. *In vitro*, Isw1 complexes can establish regular nucleosome spacing with an average of about 175 bp **(Tsukiyama et al., 1999; Vary et al., 2003)**. Specifically, Isw1a generates spacing between nucleosomes of approximately 170 bp **(Kritenstein et al., 2017)**. In addition, Isw1a demonstrates greater activity in spacing nucleosome arrays than Isw1b **(Krietenstein et al., 2016; Vary et al., 2003)**.

The mechanism of nucleosome spacing by Isw1a has only begun to be understood, emerging from a structural model for Isw1a complex with dinucleosome, constructed based on the results from X-ray crystallography, cryo-EM, and site-directed photocrosslinking analyses **(Yamada et al., 2011).** This model suggests that the Isw1a complex interacts with two adjacent nucleosomes and acts as a "protein ruler" to determine the length of linker DNA at about 25 bp or 30 bp **(Gangaraju & Bartholomew, 2007; Yamada et al., 2011)**. Notably, the recognition of dinucleosomes and sensing DNA linker length is primarily dependent on the HLB domain of Ioc3 **(Bhardwaj et al., 2020)**. Moreover, other evidence, such as the preferred dinucleosome arrangement for Isw1a that reflects the nucleosomes positioned at the promoter and the ability of Isw1a to slide the +2 nucleosome towards the +1 nucleosome, further elucidates how Isw1a creates nucleosome spacing near promoters *in vivo* **(Bhardwaj et al., 2020)**. The *in vitro* system using a genome-wide *in vitro* reconstituted nucleosome system with purified Isw1a complex has further revealed the ability of Isw1a in +1 nucleosome positioning, nucleosome spacing, and nucleosome phasing, supporting previous studies on Isw1a complex functions **(Krietenstein et al., 2016; Oberbeckmann et al., 2021)**. Here, the term "nucleosome phasing" is characterized where all nucleosomes within nucleosome arrays are similarly positioned in the cell population at a genomic reference point **(Baldi et al., 2018; Blank & Becker, 1996; Chereji & Clark, 2018; Singh & Mueller-Planitz, 2021)**. In yeast, phased nucleosomes are mainly located at the transcription start sites or +1 nucleosomes downstream, related to transcription **(Jiang & Pugh, 2009a, 2009b)**. Furthermore, there is a proposed mechanistic model that suggests nucleosome spacing by Isw1a involves the simultaneous actions between two adjoining nucleosomes, with one nucleosome being mobile and moved while the other nucleosome remains in a steady state **(Bhardwaj et al., 2020).** Additionally, the recent cryo-EM structure of Isw1a interacting with dinucleosomes has shown detailed mechanistic aspects of Isw1a spacing activity involving distinct components of the Isw1a complex **(Li et al., 2024)**.

1.5.4 *In vivo* functional studies of Isw1 chromatin remodelers in transcription

Isw1a and Isw1b are implicated in transcriptional regulation in different manners. This was initially discovered through DNA microarray analysis, which revealed that the absence of Isw1a and Isw1b results in different expression profiles, implying independent roles for each complex **(Vary et al., 2003)**. Additionally, a study has reported that Isw1a and Isw1b have distinct transcription functions. ChIP-qPCR analysis at the inducible *MET16* locus demonstrated that Isw1a is located at the promoter region during gene repression, whereas Isw1b is detected at the coding region and the end region of actively transcribed genes **(Morillon et al., 2003)**. This study suggests that the Isw1a complex has a function to repress gene expression, and the Isw1b complex is involved in transcription elongation and termination **(Mellor & Morillon, 2004; Morillon et al., 2003)**. Intriguingly, this distinct role of Isw1a and Isw1b can be somewhat associated with the interaction of remodeler at specific nucleosome positions and the direction of nucleosome positioning on a genome-wide scale. For example, the role of Isw1a in transcriptional repression is suggested by the evidence where the Ioc3 is primarily enriched at transcription start sites (+1 nucleosome), and the deletion of *IOC3* leads to the nucleosome's shifted away from the nucleosome-depleted regions (NDRs), initiating transcription **(Yen et al., 2012)**. Moreover, the implication of Isw1b in transcription elongation and termination is found to be in line with its positions at the mid-region of genes (+2, +3, +4 nucleosomes) and 3' coding region (terminal nucleosome -1) **(Smolle et al., 2012; Yen et al., 2012)**. Another function of the Isw1 remodelers is to prevent cryptic transcription initiation within genes **(Smolle et al., 2012; Tirosh et al., 2010)**. This has been clearly shown by deleting *ISW1*, which allows transcription initiation from cryptic sites within genes and consequently results in an increased number of cryptic transcripts **(Smolle et al., 2012; Tirosh et al., 2010)**. When both *ISW1* and *CHD1* are deleted, an additive effect of a stronger cryptic transcript phenotype can be observed **(Smolle et al., 2012)**.

In addition to the previously known role of Isw1a, there is further a suggestion that it may contribute to the actively transcribed genes rather than solely having a role in inactive genes **(Smolle et al., 2012)**. However, despite numerous biochemical studies and structural studies on the Isw1a complex, there is limited understanding of the mechanisms by which Isw1a is involved in the activation and/or repression of transcription.

Conversely to Isw1a, the role of Isw1b in transcription has been extensively studied. Here, histone H3K3me3-containing nucleosome recruits the Isw1b complex via the PWWP domain of the Ioc4 subunit with functions to maintain chromatin integrity during transcription elongation and suppress cryptic transcription **(Li et al., 2022; Maltby et al., 2012; Smolle et al., 2012)**.

1.6 Aims of the research

To date, yeast Isw1 remodelers are well-recognized for their two protein complexes named Isw1a (Isw1-Ioc3) and Isw1b (Isw1-Ioc2-Ioc4) **(Tsukiyama et al., 1999; Vary et al., 2003)**. These two complexes typically share the same Isw1 catalytic ATPase subunit but exhibit different Ioc-associated subunits **(Vary et al., 2003)**. Different Ioc-associated subunits present in each Isw1 complex appear to have distinct regulatory functions. This may involve the recruitment of the complexes to specific genomic loci, regulating the enzymatic activity and influencing their interaction with other proteins or chromatin components **(Morillon et al., 2003; Smolle et al., 2012; Vary et al., 2003).** Thus far, many other studies have extensively characterized the proteins for their structural features, functional domains, and functions as ISWI chromatin remodelers both *in vitro* and *in vivo*.

Besides the Ioc-associated subunits, another yeast protein known as Esc8 has been proposed to interact with the Isw1 protein. This interaction was initially suggested based on a comprehensive analysis of protein interactions in yeast and the homology sequence of Esc8 to Ioc3 **(Cuperus & Shore, 2002; Gavin et al., 2002; Vary et al., 2003)**. Esc8 protein shares 26% identity and 42% similarity to Ioc3, the associated subunit in Isw1a **(Chen et al., 2016; Cuperus & Shore, 2002)**. In addition to the high similarity between Esc8 and Ioc3, many binding features of Ioc3 to Isw1 are retained in Esc8, providing further evidence that Esc8 could be another subunit of the Isw1 remodeler **(Yamada et al., 2011)**. Furthermore, the Esc8, together with Sir2 histone deacetylase, is known to play a role in gene silencing and silent chromatin cohesion **(Chen et al., 2016; Cuperus & Shore, 2002)**. Although it is known that Esc8 potentially interacts with Isw1, it remains unclear whether Esc8 and Isw1 can form a complex and whether this Isw1-Esc8 protein (Isw1c) complex may exhibit functions as a chromatin remodeler. Given this limited understanding, the primary aim of my PhD research is to characterize the function of the Isw1-Esc8 (Isw1c) complex *in vitro* as a novel ISWI chromatin remodeler from *Saccharomyces cerevisiae*.

Throughout my PhD research, I have addressed four research questions: (1) Does Isw1 interact with Esc8? (2) Does Isw1c function as a chromatin remodeler? (3) Do histone variants or histone modifications influence the Isw1c functions? and (4) How does Isw1 interact with Esc8 and vice versa?

To answer these questions, I utilized a combined approach of biochemical tools and structural predictions of AlphaFold. First, the Isw1-Esc8 protein (Isw1c) complex was endogenously purified from *S. cerevisiae* using the TAP affinity purification technique to confirm the interaction between Isw1 and Esc8 proteins. Second, a highly abundant purified Isw1c protein was prepared and acquired for biochemical assays to characterize its functions as a chromatin remodeler. These assays included ATP hydrolysis assay, DNA-binding assay, nucleosome-binding assay, nucleosome sliding assay, and genome-wide *in vitro* reconstitution of nucleosome assay. Third, various modified nucleosomes and histone variants were used as substrates to investigate further the distinct roles of the Isw1c remodeler in nucleosome sliding and binding activities. Fourth, an in-depth analysis of the AlphaFold structural prediction of Isw1c alongside the reference structure of Isw1a was conducted to gain comprehensive insights into the formation of the protein complex. Based on the sequence and structural analyses, deletion mutants of Isw1 and Esc8 were generated and

subsequently tested for their interaction with full-length Esc8 and Isw1 proteins using co-immunoprecipitation, respectively. Furthermore, an additional nucleosome sliding assay was carried out using the purified protein of the Isw1c mutant (Isw1-Esc8$_{\Delta C2}$) to assess its function in sliding nucleosomes.

2. Materials and Methods

2.1 Materials

2.1.1 Bacterial strains

Table 1. List of *Escherichia coli* strains

Strain	Genotype	Application
BL21 (DE3)	F⁻*omp*T *hsd*S$_B$ (r_B^-, m_B^-) *gal dcm* (DE3)	Protein expression
BL21 (DE3) pLysS	F⁻*omp*T *hsd*S$_B$ (r_B^-, m_B^-) *gal dcm* (DE3) pLysS(Cam^R)	Protein expression
DH5α	F⁻ φ80*lac*ZΔM15Δ(*lac*ZYA*arg*F)U169 *rec*A1 *end*A1 *hsd*R17(r_K^-, m_K^+) *pho*A *sup*E44 λ⁻*thi*-1 *gyr*A96 *rel*A1	Transformation
Rosetta (DE3)	F⁻*ompT hsdS*$_B$(r_B^- m_B^-) *gal dcm* (DE3) pRARE (Cam^R)	Protein expression
Rosetta (DE3) pLysS	F⁻ *ompT hsdS*$_B$(r_B^- m_B^-) *gal dcm* (DE3) pLysSRARE (Cam^R)	Protein expression

2.1.2 Yeast strains

Table 2. List of *Saccharomyces cerevisiae* strains

Strain	Parental strain	Genotype
BMA64	-	*MATα ura3-1 ade2-1 his3-11,5 trp1Δ leu2-3,112 can1-100*
BY4741	-	*MATa his3Δ1 leu2Δ0 met15Δ0 ura3Δ0*
MP3	BMA64	*MATα ura3-1 ade2-1 his3-11,5 trp1Δ leu2-3,112 can1-100 isw1Δ2961-3150*
MP4	BMA64	*MATα ura3-1 ade2-1 his3-11,5 trp1Δ leu2-3,112 can1-100 isw1Δ2641-3150*
YAA025	YMS357	*MATa his3Δ1 leu2Δ0 met15Δ0 ura3Δ0 ESC8-TAP-HIS3 ioc2Δ::URA3 ioc3Δ::HYG CUP1-ESC8-KanMX*
YAA026	YMS357	*MATa his3Δ1 leu2Δ0 met15Δ0 ura3Δ0 ESC8-TAP-HIS3 ioc2Δ::URA3 ioc3Δ::HYG ADH-ESC8-KanMX*
YAA027	YMS357	*MATa his3Δ1 leu2Δ0 met15Δ0 ura3Δ0 ESC8-TAP-HIS3 ioc2Δ::URA3 ioc3Δ::HYG GPD-ESC8-KanMX*
YAA028	YMS357	*MATa his3Δ1 leu2Δ0 met15Δ0 ura3Δ0 ESC8-TAP-HIS3 ioc2Δ::URA3 ioc3Δ::HYG TEF-ESC8-KanMX*
YAA029	YMS357	*MATa his3Δ1 leu2Δ0 met15Δ0 ura3Δ0 ESC8-TAP-HIS3 ioc2Δ::URA3 ioc3Δ::HYG GAL1-ESC8-KanMX*
YAA030	YMS357	*MATa his3Δ1 leu2Δ0 met15Δ0 ura3Δ0 ESC8-TAP-HIS3 ioc2Δ::URA3 ioc3Δ::HYG MET25-ESC8-KanMX*
YAA034	BY4741	*MATa his3Δ1 leu2Δ0 met15Δ0 ura3Δ0 esc8Δ1411-2145::TAP-URA3*
YAA035	BY4741	*MATa his3Δ1 leu2Δ0 met15Δ0 ura3Δ0 esc8Δ1816-2145::TAP-URA3*
YAA036	YMS249	*MATa his3Δ1 leu2Δ0 met15Δ0 ura3Δ0 esc8Δ::esc8Δ1-615-TAP-URA3*
YAA037	YMS249	*MATa his3Δ1 leu2Δ0 met15Δ0 ura3Δ0 esc8Δ::esc8Δ1-1008-TAP-URA3*
YAA039	BMA64	*MATα ura3-1 ade2-1 his3-11,5 trp1Δ leu2-3,112 can1-100 ESC8-TAP-URA3*

YAA040	MP3	*MATα ura3-1 ade2-1 his3-11,5 trp1Δ leu2-3,112 can1-100 isw1Δ2961-3150 ESC8-TAP-URA3*
YAA041	MP4	*MATα ura3-1 ade2-1 his3-11,5 trp1Δ leu2-3,112 can1-100 isw1Δ2641-3150 ESC8-TAP-URA3*
YMS060	S288C	*MATa his3Δ1 leu2Δ0 met15Δ0 ura3Δ0 IOC3-TAP-HIS3*
YMS194	S288C	*MATa his3Δ1 leu2Δ0 met15Δ0 ura3Δ0 ESC8-TAP-HIS3*
YMS249	BY4741	*MATa his3Δ1 leu2Δ0 met15Δ0 ura3Δ0 esc8Δ::KanMX*
YMS357	S288C	*MATa his3Δ1 leu2Δ0 met15Δ0 ura3Δ0 ESC8-TAP-HIS3 ioc2::URA3 ioc3::HYG*

2.1.3 Oligonucleotides sequences

Table 3. List of oligos sequences

Name	Sequence	Description
5' 601-R (no Bio)	TCACACCGAGTTCATCCCTT	A reverse primer for 5' end positioned nucleosomes
601-NCP 3'	CTGGAGAATCCCGGTGCCGA	A reverse primer for NCP nucleosomes
601-NCP 5'	ACAGGATGTATATATCTGACACGT GCC	A forward primer for Cy5-end positioned and NCP nucleosomes
Backbone_pYG048 _1	catTTTGTAGCGCTTTTTTGTAC	A reverse primer for generating *ESC8$_{\Delta N1}$* and *ESC8$_{\Delta N2}$*
Esc8_Backbone_g 1	gattttatgtaaccagcagctacacttcatggcatt caaaTTCAATTCATCATTTTTTTT	A reverse primer used for generating *ESC8$_{\Delta N1/2}$* and *ESC8$_{\Delta C1/2}$*
Esc8_Del_1	CATTCTGCGAAGAATATTCG	A forward primer used for generating *ESC8$_{\Delta N1}$*
Esc8_Del_2	CATCAAACTTTTCACGCC	A forward primer used for generating *ESC8$_{\Delta N2}$*
Esc8_Del_4.1	TCCTTCAGTACTGCCTGTAGGGG CAG	A reverse primer used for colony PCR
Esc8_Del_g1	caaacaagaaaataaggaacaagaaatttgag gtacaataATGCATTCTGCGAAGAAT ATTCG	A forward primer for generating *ESC8$_{\Delta N1}$*
Esc8_Del_g2	caaacaagaaaataaggaacaagaaatttgag gtacaataATGCATCAAACTTTTCAC GCC	A forward primer for generating *ESC8$_{\Delta N2}$*
Esc8_dN1-615_TAPa	caaacaagaaaataaggaacaagaaatttgag gtacaataATGCATTCTGCGAAGAAT ATTC	A forward primer for generating *ESC8$_{\Delta N1}$* with 40 bp overhang upstream the *ESC8*
Esc8_dN1-615_TAPb	gattttatgtaaccagcagctacacttcatggcatt caaaTACGACTCACTATAGGG	A reverse primer for generating *ESC8$_{\Delta N1}$* with 40 bp overhang downstream the *ESC8*
Esc8_dN2-1008_TAPa	caaacaagaaaataaggaacaagaaatttgag gtacaataATGCATCAAACTTTTCAC GC	A forward primer for generating *ESC8$_{\Delta N2}$* with 40 bp overhang upstream the *ESC8*
Esc8_dN2-1008_TAPb	gattttatgtaaccagcagctacacttcatggcatt caaaTACGACTCACTATAGGGC	A forward primer for generating *ESC8$_{\Delta N2}$* with 40 bp overhang downstream the *ESC8*
Esc8_seq1_F	TGAAATTCAAAGGCTCACTCAC	A forward primer for colony PCR and DNA sequencing
Esc8_seq2_F	CTGAACCTGTCATTTCAAGATGTG	A forward primer for DNA sequencing
Esc8_seq3_F	GGATTGGCAACGAATGCAGTTCA G	A forward primer for colony PCR and DNA sequencing
Esc8_TAPa_dC1	tttctacttaccaccattctggattggcaacgaatg cagtTCCATGGAAAAGAGAAG	A forward primer for generating *ESC8$_{\Delta C1}$-TAP-URA*

Esc8_TAPa_dC2	tcagcgcataactgctgcccctacaggcagtactgaaggaTCCATGGAAAAGAGAAG	A forward primer for generating *ESC8$_{\Delta C2}$*-TAP-URA
Esc8_TAPb	gattttatgtaaccagcagctacacttcatggcattcaaaTACGACTCACTATAGGG	A reverse primer for generating *ESC8$_{\Delta C1}$-TAP-URA* and *ESC8$_{\Delta C2}$-TAP-URA*
Esc8-Del 3.1	ACTGCATTCGTTGCCAATCCAGAATG	A reverse primer for colony PCR
Esc8-Seq1_F	TGAAATTCAAAGGCTCACTCAC	A forward primer for colony PCR and DNA sequencing
Esc8-Seq3-F	CTGAACCTGTCATTTCAAGATGTG	A forward primer for DNA sequencing
Esc8-TAPa	ggaaaaaagaagcttgaggcgtaatgccagaaaaggtctaTCCATGGAAAAGAGAAG	A forward primer for amplification of *TAP-URA* to generate *ESC8-TAP-URA* in Isw1 mutant yeast strains
Esc8-TAPb	gattttatgtaaccagcagctacacttcatggcattcaaaTACGACTCACTATAGGG	A reverse primer for amplification of *TAP-URA* to generate *ESC8-TAP-URA* in Isw1 mutant yeast strains
Esc8.Del_2	CATCAAACTTTTCACGCC	A forward primer for PCR colony
Esc8dN1_fwd	acaaaagctggaggaATGCATTCTGCGAAGAATATTC	A forward primer for amplification of *ESC8$_{\Delta N1}$* for generating *ESC8$_{\Delta N1}$-TAP-URA*
Esc8dN1_rev	tctcttttccatggaTAGACCTTTTCTGGCATT	A reverse primer for amplification of *ESC8$_{\Delta N1}$* for generating *ESC8$_{\Delta N1}$-TAP-URA*
Esc8dN2_fwd	caaaagctggaggaATGCATCAAACTTTTCAC	A forward primer for amplification of *ESC8$_{\Delta N2}$* for generating *ESC8$_{\Delta N2}$-TAP-URA*
Esc8dN2_Rev	cttctcttttccatggaTAGACCTTTTCTGGC	A reverse primer for amplification of *ESC8$_{\Delta N2}$* for generating *ESC8$_{\Delta N2}$-TAP-URA*
IRD700-601NCP F' LB	ACAGGATGTATATATCTGACACGTGCC	A forward primer for amplification of nucleosomal DNA used in reconstituted mononucleosomes IRD700-0N47
IRD800-601NCP F' LB	ACAGGATGTATATATCTGACACGTGCC	A forward primer for amplification of nucleosomal DNA used in reconstituted mononucleosomes IRD800-0N47
M13_rev	gtcatagctgtttcctg	A forward primer for DNA sequencing
M13	CAGGAAACAGCTATGACC	A forward primer for colony PCR outside Esc8
Mid-601-F (Cy5)	gggtctagaGGCAAGGTCGCTGTTCAATA	A forward primer for amplification of nucleosomal DNA used in reconstituted mononucleosomes Cy5-34N37
Mid-601-R (Bio)	gggggatccTATGTGATGGACCCTATACG	A reverse primer for amplification of nucleosomal DNA used in reconstituted mononucleosomes Cy5-34N37
o-Esc8-1	ggtagggtgatataaacgcgtgaac	A forward primer for colony PCR and DNA sequencing of *ESC8*
o-Esc8-2	atggcgctaaagattgtgatagg	A forward primer for DNA sequencing of *ESC8*
o-Esc8-3	ggctggtgaagaggaagacgatag	A reverse primer for colony PCR and DNA sequencing of *ESC8*
o-Esc8-4	gcagtcttttgaggttattattctgctcc	A forward primer for colony PCR of *ESC8*

o-ISW1-1	aactggttggtgtctctgcataag	A forward primer for DNA sequencing *ISW1*
o-ISW1-10	cggaagttgtctgagtataag	A forward primer for DNA sequencing *ISW1*
o-ISW1-3	ctagcatgcagaagaaatggtac	A forward primer for DNA sequencing *ISW1*
o-ISW1-6	aggagatgatattgatctggacga	A forward primer for DNA sequencing *ISW1*
o-ISW1-8	aagacatccagtgagcctgacc	A forward primer for DNA sequencing *ISW1*
o-ISW1-9	tggaccaagaaatccaaagcctg	A reverse primer for DNA sequencing *ISW1*
pBS1539_bb_Fwd_Esc8_2	gccagaaaaggtctaTCCATGGAAAAGAGAAGATGG	A forward primer for amplification of *TAP URA* to generate *ESC8-$_{\Delta N1}$-TAP-URA* and *ESC8-$_{\Delta N2}$-TAP-URA*
pBS1539_bb_Rev_Esc8_1	cttcgcagaatgcatTCCTCCAGCTTTTGTTCC	A reverse primer for amplification of *TAP-URA* to generate *ESC8-$_{\Delta N1}$-TAP-URA*
pBS1539_bb_Rev_Esc8_2	aaaagtttgatgcatTCCTCCAGCTTTTGTTCC	A reverse primer for amplification of *TAP-URA* to generate *ESC8-$_{\Delta N2}$-TAP-URA*
S1-ESC8-Fw	aaacaagaaaataaggaacaagaaatttgaggtacaataatgCGTACGCTGCAGGTCGAC	A forward primer for amplification of various promoters in exchange of native promoter of *ESC8*
S4-ESC8-Rv	cttgataaagtcatcgaccaagtctaaatcaataatttctgtCATCGATGAATTCTCTGTCG	A reverse primer for amplification of various promoters in exchange of native promoter of *ESC8*
TAP-Tag_Seq_R	GTAAGGAACAACAAGCGGC	A reverse primer for colony PCR and DNA sequencing

2.1.4 Plasmids

Table 4. List of plasmids

Name	**Vector backbone**	**Reference**	**Source**
pBS1539, TAP-URA	pBS1539	-	In this study
pCoofy4, 6xHisMBP-Esc8	pCoofy4	-	In this study
pCoofy4, 6xHisMBP-Isw1	pCoofy4	-	In this study
pETDuet-1, 6xHisEsc8	pETDuet-1	-	In this study
pETDuet-1, 6xHisEsc8-Isw1	pETDuet-1	-	In this study
pGEM, 3z/601	pGEM-3z	-	-
pGEX, GST-Alc1	pGEX	-	Dr. Gunnar Knobloch
pGEX6P-1, GST-Isw1	pGEX6P-1	-	In this study
pYM-N1, CUP1-KanMX4	pYM	**(Janke et al., 2004)**	Dr. Mathias Capella
pYM-N10, CYC1-KanMX4	pYM		
pYM-N14, GPD-KanMX4	pYM		
pYM-N18, TEF-KanMX4	pYM		
pYM-N22, GAL1-KanMX4	pYM		
pYM-N34, MET25-KanMX4	pYM		
pYM-N6, ADH-KanMX4	pYM		

2.1.5 Histone octamers

Table 5. List of histone octamers and the position of reconstituted mononucleosomes

Histone octamer	Species	Position	Source
H3K36me0	*Homo sapiens*	0N47	Dr. Philipp Voigt
H3K36me3			
Wild type$_{T32C}$	*Homo sapiens*	0N47	Dr. Till Bartke
H3K4me0			
H3K4me4			
H4K16ac			
H3K9,14ac			
H4K5,8,12ac			
H2A.Z			
Wild type	*Xenopus laevis*	0N47, 0N0, 34N37	Dr. Michaela Smolle

2.1.6 Enzymes and kits

Table 6. List of enzymes and kits

Description	Manufacturer, Catalogue No.
AcTEV™ Protease	Invitrogen, #12575015
mi-PCR Purification Kit	Metabion, #mi-PCR250
mi-Plasmid Miniprep Kit	Metabion, #mi-PMN250
OneTaq® DNA Polymerase	NEB, #M0480L
PCRBIO VeriFi™ Polymerase	PCR Biosystems, #PB10.42-05
Phusion™ High-Fidelity DNA Polymerase	NEB, #M0530L
Pierce™ HRV 3C Protease	Thermo Scientific™, #88946
PureYield™ Plasmid Midiprep System	Promega, #A2495
Pyruvate kinase/ Lactate Dehyrogenase	Sigma, #P0294
QIAquick PCR Purification Kit	Qiagen, #28106
QIAquick® PCR Purification kIT	Qiagen, #28106
T5 Exonuclease	NEB, #M0363S
Taq DNA Ligase	NEB, #M0208S
Trans-Blot Turbo RTA Midi 0.2 µm Nitrocellulose Transfer Kit	Bio-Rad, #1704271
Yeast DNA Extraction Kit	Thermo Scientific™, #78870
Zymolyase 100T	Zymo Research, #E1004

2.1.7 Antibodies

Table 7. List of antibodies

Name	Dilution used	Manufacturer, Catalogue No.
Goat Anti-Rat IgG Antibody, HRP conjugate	1:5000	Sigma-Aldrich, #AP136P
Peroxidase anti-peroxidase (PAP)	1:1000	Sigma-Aldrich, #P1291
Isw1 serum	1:50	Ashish Kumar Singh, #3C4

2.1.8 Sources of chemicals and consumables

Table 8. List of chemicals

Description	Manufacturer, Catalogue No.
1 kb DNA Ladder	NEB, N3200L
100 bp DNA Ladder	NEB, N3231S
37% Formaldehyde solution	Roth, #4979.1
6X DNA Loading dye	NEB, #B7024S
Acetone	Sigma, #34850
Acrylamide/Bis Solution, 37.5:1 (30% w/v)	Serva, #10688.02
Agar-Agar	Serva, #11396.04
Agarose	Sigma, #A9539
Ammonium Persulfate (APS)	Sigma, #09913
Ampicillin sodium salt	Serva, #13398.02
Amylose resin	NEB, #E8021S
ATP (for nucleosome sliding assay)	Sigma, #A1388
ATP (for ATP hydrolysis assay)	Sigma, #A3377
Bacto™ peptone	Otto Nordwald, #211830
Benzamidine HCl	Sigma, #434760
Benzonase nuclease	Sigma, #E1014
Bradford protein assay	Bio-Rad, #5000006
Bromophenol Blue	Sigma-Aldrich, #B8026
BSA	Biomol, #01400.100
Calcium Chloride ($CaCl_2$)	Sigma, #1023821000
Calmodulin Sepharose resin	Cytiva #17-0529-01
Coomassie Brilliant Blue R250	Serva, #35051.03
Copper	Sigma, #C1297
Deoxynucleotide (dNTP) Solution Mix	NEB, #N0447L
Dithiothreitol (DTT)	Sigma, #438219
EDTA	Sigma, #E1644
EGTA	Sigma, E4378
Ethanol, Molecular Biology Grade	Sigma, #32205-2.5L-M
Ethanol, Technical Grade	Kost, #642
Ethidium bromide	Thermo, #17898
G418 disulfate salt	Sigma, #A1720
Galactose	Sigma, 48260
Glacial acetic acid	Roth, T179.2
Glucose	VWR, #1.04074.5000
Glutathione Sepharose 4B	GE Healthcare, 17-52
Glycerol	Sigma, #G6279
Glycine	Sigma, #G7126
Heparin sodium salt	Sigma, #H-7005
HEPES	Roth, #6763.3
Hydrogen chloride (HCl)	Sigma, #30721
IgG Sepharose resin	Cytiva #17096901
Imidazole	Sigma, #1047161000
Immobilon Western HRP Substrate	Merck, #WBKLS0500
IPTG	Roth, #2316.5
Isopropanol, Molecular Biology Grade	Fisher Scientific, #11398461
Kanamycin	Serva, #26897.02
KOH	Merck, #1050335000
Leupeptin	Roth, #CN33.2
Linear acrylamide	Invitrogen, #AM9520
Lithium acetate (LiAc)	Sigma #L4158
Magnesium acetate (MgOAc)	Sigma, #M5661
Magnesium Chloride ($MgCl_2$)	Sigma, #M2670

Methanol	VWR, #20903.368
NADH	GERBU Biotechnik, #1051.0005
Ni-NTA resin	Qiagen, #30250
Non-fat dry milk powder	Frema, #4046006002033
Nonidet P-40 Substitute, NP-40 (Igepal)	Sigma, #74385
Orange G	Eurobio, #018072
PageRuler™ Plus Prestained Protein Ladder, 10 to 250 kDa	Thermo Scientific™, #26620
PEG8000	Sigma, #P5413
Pepstatin	Roth, #2936.2
Phenylmethylsulfonyl fluoride (PMSF)	Serva, #32395.04
Phosphoenolpyruvate (PEP)	Sigma, #860077
Polyethylene glycol (PEG) 3350	Sigma #P3640
Ponceau S	Serva, #33429.02
Potassium acetate (KOAc)	Merck, #1.04820.1000
Potassium chloride (KCl)	Sigma-Aldrich, #102513567
Potassium hydroxide (KOH)	Merck, #1.05033.5000
Protease Inhibitor Cocktail	Sigma, #P8215
Raffinose	Biosynth, #OR06197
SDS	Serva, #20765.03
Silver nitrate	Sigma, #1015120025
Single-stranded carrier DNA (2 mg/mL)	Sigma #D1626
Sodium acetate	Merck, #106268
Sodium Butyrate	Sigma, #8175000100
Sodium carbonate	Merck, #1063820500
Sodium chloride (NaCl)	Roth, #3957.5
Sodium hydroxide (NaOH)	Merck, #106498
Sodium phosphate, dibasic (Na_2HPO4)	Roth, #P030.2
Sodium phosphate, monobasic (NaH_2PO4)	Merck, #1.06346.0500
Sodium thiosulfate pentahydrate	Merck, #6516.0500
Sorbitol	Sigma, #S1876
TEMED	Sigma, #T9281
Trichloroacetic acid (TCA)	Sigma, #T9159
Tris base	Sigma, #T1503
Triton X-100	Sigma, #T9284
Tryptone	Sigma, #95039
Tween-20	Sigma, #P1379
Yeast extract	Serva, #24540.03
Yeast nitrogen base without amino acid	Otto Nordwald, #291920
Yeast nitrogen with ammonium sulfate without amino acids	Invitrogen™, #Q30009
Yeast protease inhibitors	Sigma, #P8215
B-Mercaptoethanol	Sigma, #M3148
β-Nicotinamide adenine dinucleotide, (NAD)	VWR, #J62337.03

Table 9. List of consumables

Description	**Manufacturer, Catalogue No.**
0.2 mL PCR single cap 8er-soft strips	Biozym, #710988
0.2 mL PCR tube with flat cap	VWR, #PEQL82.0620A
0.5 mm Glass Beads	Biospec, #11079105
1.6 mL Cuvettes	Greiner Bio-One, #613101
Amicon® Ultra-4 Centrifugal Filter Devices with 50 kDa cut-off	Merck Millipore, #UFC805096
Econo-Pac® Chromatography Column	Bio-Rad, #7321010
Falcon® tube 15 mL and 50 mL	Falcon, #FALC352096 and #FALC352070
Glutathione Sepharose™ 4 Fast Flow	VWR, #17-5132-03
Luer-lock syringe 50 mL	Fisher Scientific, #300865
MF-Millipore membrane 0.22 µm	Merck, #GSWP04700

Micro Bio-Spin Chromatography Column	Bio-Rad, #7326204
Microcentrifuge tube 1.5 mL and 2 mL	Sarstedt, #72.690.001 and #72.691
Mini Bio-Spin® Chromatography column	Bio-Rad, #7326207
Minisart® Syringe Filter 0.22 µm sterile	Sartorius, #10686521
Minisart® Syringe Filter 0.45 µm sterile	Sartorius, #10109180
Ni-NTA Agarose	Qiagen, #30250
Omnifix syringes 1 mL, 3 mL, 20 mL	Fisher Scientific, #10017781, #10713047, #10666941
Parafilm® M Sealing Film	Parafilm, #9170002
Petri dish	Sarstedt, #82.1473
Pipette tips, 10 µL, 200 µL,1000 µL	Fisher Scientific, #11903466, #11963466, #11973466
Pipetting Reservoir 25 mL – Argos Technologies	Raptor Supplies, #B3125-100
Screw cap micro tube, 1.5 mL	Sarstedt, #72692
Serological pipette sterile for 2 mL	Sarstedt, #86.1252.001
Serological pipette sterile for 5 mL, 10 mL and 25 mL	Greiner Bio-One, #606180, #607180, #760180
Slide-A-Lyzer mini dialysis device	Thermo Scientific, #88402
Sterican needles 22G, 0.70 x 30 mm and 0.70 x 40 mm	Medpex, #2050812, #7463192

2.1.9 Buffers and solutions

Table 10. List of buffers and solutions

Description	Components
0.5 M Sodium phosphate (NaPO4) Buffer pH 6, 6.8, 7.5	0.5 M NaH_2PO_4, 0.5 M Na_2HPO_4
10x SDS Running Buffer	250 mM Tris, 1.92 M Glycine, 1% SDS
10x TBE	890 mM Tris, 890 Boric acid, 20 mM EDTA
10x TBS	0.2 M Tris pH 7.5, 1.5 M NaCl
1x TBST	20 mM Tris pH 7.5, 150 mM NaCl, 0.1% Tween 20
5x SDS Sample Buffer	250 mM Tris pH 6.8, 10% (w/v) SDS, 50% (v/v) Glycerol, 50 mM EDTA, 0.25 mg/mL Bromophenol blue
Amylose Pull-Down Buffer	50 mM Tris, 200 mM NaCl, 0.05% NP-40, 20% Glycerol, pH 8.0
ATP hydrolysis 20x Regenerating System Buffer	60 mM PEP, 12 mM NADH, 310 U/mL, 200 mM 14.3M β-Me, 1x Reaction Buffer
ATP hydrolysis 7x Reaction Buffer	175 mM HEPES-KOH pH 7.6, 10.5 mM MgOAc, 70% Glycerol, 700 mM KOAc, 1.4 mg/mL BSA
Calmodulin Binding Buffer	10 mM Tris pH 8.0, 10% (v/v) Glycerol, 150 mM KCl, 1 mM Magnesium acetate (MgOAc), 1 mM Imidazole, 2 mM CaCl2, 0.1% NP-40 and fresh supplemented with 1 mM DTT, 1 µg/mL Pepstatin A, 2 µg/mL Leupeptin, 1 mM PMSF, 5 mM Sodium Butyrate
Calmodulin Elution Buffer	10 mM Tris pH 8.0, 10% (v/v) Glycerol, 150 mM KCl, 1 mM Magnesium acetate (MgOAc), 1 mM Imidazole, 10 mM EDTA pH 8.0, 0.1% NP-40, fresh supplemented with 0.5 mM DTT, 1 µg/mL Pepstatin A, 2 µg/mL Leupeptin, 1 mM PMSF, 5 mM Sodium Butyrate
Calmodulin Modified Extraction Buffer	40 mM HEPES pH 7.5, 10% Glycerol, 350 mM NaCl, 1 mM Imidazole, 1 mM MgOAc, 2 mM CaCl2, 0.1% NP-40, fresh supplemented with 0.5 mM DTT, 1 mM PMSF, 2 µg/mL Leupeptin, 1 µg/mL Pepstatin A
Calmodulin Pull-Down Buffer	40 mM HEPES-KOH pH 7.5, 10% (v/v) Glycerol, 150 mM NaCl, 1 mM Imidazole, 1 mM MgOAc, 2 mM $CaCl_2$, 0.1% NP-40, fresh

	supplemented with 0.5 mM DTT, 1 mM PMSF, 2 µg/mL Leupeptin, 5 µg/mL Pepstatin, 5 mM Sodium Butyrate.
Coomassie Destaining Solution	40% (v/v) Methanol, 10% (v/v) Glacial Acetic Acid
Coomassie Staining Solution	50% (v/v) Methanol, 10% (v/v) Glacial Acetic Acid, 0.2% (w/v) Coomassie Brilliant Blue R250
EMSA Buffer D	50 mM Tris pH 7.5, 20% glycerol
GST Dialysis Buffer	50 mM Tris, 100 mM KCl, 10% Glycerol, fresh supplemented with 5 mM β-Mercaptoethanol, 0.5 mM PMSF, pH 8.0
GST Elution Buffer	50 mM Tris pH 8.0, 100 mM NaCl, 0.5 mM EDTA, 10% Glycerol, 100 mM Gluthathione, 10 mM β-Mercaptoethanol, 1 mM PMSF
GST Lysis Buffer	10 mM Tris pH 7.5, 20 mM $NaPO_4$ pH 6.8, 2 M NaCl, 0.01% NP-40, fresh supplemented with 2 µg/mL Leupeptin, 1 µg/mL Pepstatin, 1 mM Benzamidine HCl, 1 mM PMSF, 1 mM DTT
GST Wash Buffer 1	10 mM Tris pH 7.6, 20 mM $NaPO_4$ pH 6.8, 1 M NaCl, 0.01% NP-40
GST Wash Buffer 2	10 mM Tris, pH 7.6, 20 mM $NaPO_4$ pH 6.8, 0.1 M NaCl, 0.01% NP-40, fresh supplemented with 1 mM Benzamidine HCl, 1 mM PMSF, 10 mM β-Mercaptoethanol
Heparin Binding Buffer	20 mM sodium phosphate, monobasic (NaH_2PO_4), 50 mM NaCl, pH 7.0
Heparin Elution Buffer	20 mM sodium phosphate, monobasic (NaH_2PO_4), 2 M NaCl, pH 7.0
Ni-NTA 10x Stock Solution A	200 mM sodium phosphate, monobasic (NaH_2PO_4), 5 M NaCl
Ni-NTA 10x Stock Solution B	200 mM sodium phosphate, dibasic (Na_2HPO_4), 5 M NaCl
Ni-NTA 1x Native Binding Buffer	50 mM NaH_2PO_4, 0.5 M NaCl, 10 mM Imidazole, pH 8.0
Ni-NTA 1x Native Elution Buffer	50 mM NaH_2PO_4, 0.5 M NaCl, 250 mM Imidazole, pH 8.0
Ni-NTA 1x Native Purification Buffer	50 mM NaH_2PO_4, 0.5 M NaCl, pH 8.0
Ni-NTA 1x Native Wash Buffer	50 mM NaH_2PO_4, 0.5 M NaCl, 20 mM Imidazole, pH 8.0
Ni-NTA 3 M Imidazole pH 6.0	3 M Imidazole, 0.5 M NaCl, 20 mM Sodium Phosphate Buffer pH 6.0
Nucleosome reconstituted Final Dilution Buffer	10 mM Tris-HCl pH 7.5, 5 mM EDTA, 20% Glycerol, 0.1% NP-40, supplemented with 5 mM DTT, 0.5 mM PMSF and 100 µg/mL BSA
Nucleosome reconstituted Initial Dilution Buffer	10 mM HEPES pH 7.9, 1 mM EDTA, fresh supplemented with 0.5 mM PMSF
Nucleosome Sliding Buffer A	50 mM Tris pH 8.0, 10 mM $MgCl_2$, fresh supplemented with 0.5 mM PMSF
Nucleosome Sliding Stop Buffer	700 ng of competitor DNA, 0.7 M KCl
Oligo Annealing Buffer	1x TE Buffer pH 8.0, 50 mM NaCl
Ponceau S Staining Solution	0.2 %(w/v) Ponceau S, 5% Glacial Acetic Acid
Resolving Gel Buffer	1.5 M Tris-HCl pH 8.8, 0.4 % SDS
SDS Running Buffer	25 mM Tris, 192 Glycine, 0.1% SDS
SEC Running Buffer	50 mM sodium phosphate, monobasic (NaH_2PO_4), 150 mM NaCl, pH 7.0
Silver Staining Developer Buffer	6% (w/v) Na_2CO_3, 2 mL of 0.02% (w/v) $Na_2S_2O_3$ x $5H_2O$, 50 µL of 37% Formaldehyde in 10 mL
Silver Staining Fixation Buffer	50% Methanol, 12% Glacial Acetic Acid, 50 µL of 37% Formaldehyde in 10 mL
Silver Staining Reaction Buffer	0.2% (w/v) $AgNO_3$, 75 µL of 37% Formaldehyde in 10 mL
Silver Staining Sensitizer Buffer	0.02% (w/v) $Na_2S_2O_3$ x $5H_2O$
Silver Staining Stop Buffer	50 mM EDTA
Silver Staining Wash Buffer A	50% Ethanol
Stacking Gel Buffer	0.5 M Tris-HCl pH 6.8, 0.4 % SDS
TAP Extraction Buffer	40 mM HEPES-KOH pH 7.5, 10% (v/v) Glycerol, 350 mM NaCl, 0.1% Tween-20, fresh supplemented with 1 µg/mL Pepstatin A, 2 µg/mL Leupeptin, 1 mM PMSF, 5 mM Sodium Butyrate
TE Buffer	10 mM Tris-HCl pH 8.0, 1 mM EDTA

TEV Cleavage Buffer	10 mM Tris pH 8.0, 10% (v/v) Glycerol, 150 mM NaCl, 0.1% NP-40, 0.5 mM EDTA, fresh supplemented with 1 mM DTT, 1 µg/mL Pepstatin A, 2 µg/mL Leupeptin, 1 mM PMSF, 5 mM Sodium Butyrate
Zymoylase solution	2.5 mg/mL Zymoylase in 0.1 M Sodium Phosphate Buffer pH 7.5

2.1.10 *E. coli* and yeast media

Table 11. List of amino acids used for amino acid mix and drop-out amino acid minus mix

Description	Supplier, Catalogue No.
Adenine	Sigma, #A9126
Alanine	Sigma, #A7627
Arginine	Sigma, #A5006
Asparagine	Sigma, #A4159
Aspartic acid	Sigma, #A4534
Cysteine	Sigma, #C1276
Glutamic acid	Sigma, #G1251
Glutamine	Sigma, #G8540
Glycine	Sigma, #G8790
Histidine	Sigma, #H8000
Isoleucine	Sigma, #I5281
Leucine	ITW Reagents, #A1426
Lysine	Sigma, #L8662
Methionine	Sigma, #M9625
Myo-Inositol	Sigma, #I7508
para-Aminobenzoic acid	Sigma, #822312
Phenylalanine	Sigma, #P2126
Proline	Sigma, #P5607
Serine	Sigma, #S4500
Threonine	Sigma, #T8625
Tryptophan	Merck, #T0254
Tyrosine	ThermoFisher, #J63511
Uracil	Formedium, #DOC0214
Valine	Sigma, #V6504

Table 12. List of *E. coli* and yeast media

Description	Components
LB agar plate	10 g/L Tryptone, 10 g/L NaCl, 5g/L yeast extract, 20 g/L agar
LB medium	10 g/L Tryptone, 10 g/L NaCl, 5 g/L yeast extract
SC medium	6.7 g/L Yeast nitrogen base without amino acids and with ammonium sulfate, 2 g/L amino acid mix, 2% glucose
SC-MET medium	6.7 g/L Bact-yeast nitrogen base without amino acids, 2 g/L drop-out amino acid mix-minus MET, 2% glucose
SC-URA agar plate	6.7 g/L Bact-yeast nitrogen base without amino acids, 2 g/L drop-out amino acid mix-minus URA, 20g/L Bacto agar, 2% glucose
SC-URA medium	6.7 g/L Bact-yeast nitrogen base without amino acids, 2 g/L drop-out amino acid mix-minus URA, 2% glucose
YP medium	20 g/L Bacto peptone, 10 g/L yeast extract
YP with 2 % Raffinose	20 g/L Bacto peptone, 10 g/L yeast extract, 2% Raffinose
YP with 2% Galactose	20 g/L Bacto peptone, 10 g/L yeast extract, 2% Galactose
YPD agar plate	20 g/L Bacto peptone, 10 g/L yeast extract, 24 g/L Bacto agar, 2% glucose

YPD agar plate with G418	20 g/L Bacto peptone, 10 g/L yeast extract, 24 g/L agar, 2% glucose, 200 µg/mL G418
YPD medium	20 g/L Bacto peptone, 10 g/L yeast extract, 2% Glucose

2.1.11 Equipment or technical devices

Table 13. List of equipment or technical devices

Description	Supplier
ÄKTA Pure Protein Purification System	GE Healthcare
Analytical balance XS205DU	Mettler Toledo
Autoclave table top DX150	Systec
BioPhotometer	Eppendorf
Branson Ultrasonics™ Sonifier Model 250 CE	Fisher Scientific
Cell density meter, Ultrospec™10	Amersham Biosciences
Centrifuge Benchtop 5415D (RT, microcentrifuge tube)	Eppendorf
Centrifuge benchtop 5810R (Falcon tube)	Eppendorf
Centrifuge benchtop Mirofuge 20R (4°C, microcentrifuge tube)	Beckman Coulter
Centrifuge Standing Avanti-20XP with JLA-8.1000 rotor (1L)	Beckman Coulter
Centrifuge Standing Optima™ L-90K Ultracentrifuge	Beckman Coulter
ChemiDoc MP Imaging System	Bio-Rad
Christ Rotational Vacuum Concentrator System, RVC 2-25	Martin Christ
Freezer, -80°C	Thermo Scientific
Glass beads 0.5 mm	Roth
HiTrap™ Heparin HP affinity column	Cytiva, #17-0406-01
Incubator shaker Brunswick™ Innova® 44/44R	Eppendorf™
Incubators	Binder, Memmert
Infinite M1000 PRO plate reader	Tecan
Integra Pipetting robot	Integra
Millipore water systems	Elga Lab Water
Mini fridge and standing freezer, -20°C	Liebherr
Mini fridge and standing fridge, 4°C	Liebherr
NanoDrop™ One Spectrophotometer	Thermo Scientific™
Odyssey® CLx Imaging System	LI-COR
PCR machines – C1000 Touch™ Thermal Cycler	Bio-Rad
pH Meter	Schott instruments
Pipette boy acu 2	Integra Biosciences
Pipettes	Gilson
Precellys® 24 homogeniser	VWR
Precision balance Kern 572 series	Merck
SDS-PAGE electrophoresis system	Bio-Rad
Rocker shaker DRS-12	NeoLab
SPEX 6870 Freeze/Mill®	SPEX® SamplePrep
Sprout® Plus Mini Centrifuge (To spin down sample)	Heathrow Scientific
Superdex 200™ 10/300 GL column	Cytiva, #28-9909-44
The Eluator™ Vacuum Elution Device	Promega
ThermoMixer F1.5	Eppendorf
Trans-Blot® Turbo™ Transfer System	Bio-Rad
Tube Roller	Starlab
Typhoon™ FLA 9500	GE Healthcare
Vilber Quantum Gel Documentation Imaging	Vilber
Vortex-Genie 2	Scientific Industries

2.1.12 Software

Table 14. List of software

Software	Application
Affinity Designer	Scientific data merge for figures
ChimeraX-1.6.1	Protein structural analysis and visualization
Empiria Studio	Image analysis for LI-COR
GraphPad Prism 8.0	Statistical analysis and Graph
Image Quant TL 5.0	Image analysis for gel and blot images
Image Studio™	Image analysis for LI-COR
PyMOL	Protein structural analysis and visualization
UNICORN 6.4	Software in ÄKTA Pure Protein Purification System

2.2 Methods

2.2.1 Yeast strain generation

2.2.1.1 Promoter substitution using PCR-based tagging of yeast genes via transformation

The exchange of the native promoter of *ESC8* with various promoters was performed using the strategy of the previously published paper **(Janke et al., 2004)**. PCR cassettes with different promoter substitutions were generously gifted by Dr. Mathias Capella. To exchange the native promoter of *ESC8*, oligonucleotides with 42 bp homology upstream of the ATG of the gene, followed by S1-primer 5' -CGTACGCTGCAGGTCGAC- 3' as well as the downstream of the ATG of the gene (excluding ATG), followed by 5' -CATCGATGAATTCTCTGTCG- 3' were designed. After that, the gene of interest, containing the promoter and *KanMX4* selection marker, was amplified from the PCR cassettes using the respective primers. The amplified products were analyzed on a standard agarose gel, and the remaining products were purified using a mi-PCR Purification Kit (Metabion, #mi-PCR250), according to the manufacturer's instructions. Next, all constructs were transformed to an *ioc2*Δ *ioc3*Δ yeast strain. To validate the insertions in the genes and determine their sequences, it was confirmed by colony PCR and DNA sequencing, respectively.

2.2.1.2 Gene deletion or tagging through homologous recombination

To generate *ESC8* deletion mutants, either the N-terminus or C-terminus of *ESC8* was deleted. The C-terminus deletion of *ESC8* was replaced with *TAP-URA*, while the N-terminus deletion of *ESC8* was amplified and then cloned into a vector containing *TAP-URA* using Gibson assembly, followed by transformation into *E. coli* Dh5α. Upon transformation, colony PCR and DNA sequencing were further performed to verify the deletion. Following that, the oligonucleotides with 40 bp homology upstream of the start codon of the gene and downstream of the codon of the gene were designed. In addition, for C-terminus deletion, the oligonucleotides with 40 bp homology with *ESC8* upstream of the deletion region and downstream of the stop codon of the gene were designed. The targeted gene deletions were amplified using the appropriate primers. Subsequently, the PCR products were analyzed on a standard agarose gel, and the remaining products were purified using a mi-PCR Purification Kit (Metabion, #mi-PCR250) according to the manufacturer's instructions. After that, the *esc8*$_{\Delta N/C\text{-}}$*TAP-URA* were transformed into BY4741 and YMS249 yeast strains, respectively. To validate the deletion region, the modified loci were analyzed with colony PCR and DNA sequencing.

For *ISW1* mutants, the wild type and the yeast strains containing *ISW1*$_{\Delta SLIDE}$ or *ISW1*$_{\Delta SLIDESANT}$ were kindly gifted by Prof. Dr. Jane Mellor, which is based on the published paper **(Pinskaya et al., 2009)**. The *TAP-URA* was introduced at the 3' end of the *ESC8*. To achieve that, the oligonucleotides with 40 bp homology at the 3' end of the *ESC8* (without a stop codon) and the downstream of the gene were designed. The *TAP-URA* was amplified using PCR with the respective primers. Next, the amplified products were analyzed on agarose gel, and the remaining solution was purified using a mi-PCR Purification Kit (Metabion, #mi-PCR250). After that, the *TAP-*

URA was transformed into yeast strains of MPA64 (WT), MP3 (*ISW1*$_{\Delta SLIDE}$), and MP4 (*ISW1*$_{\Delta SANT\Delta SLIDE}$). The modified loci were further verified using colony PCR and DNA sequencing.

2.2.2 Molecular biology methods

2.2.2.1 *E. coli* plasmid isolation

Plasmid DNA from *E. coli* was extracted using a mi-Plasmid Miniprep Kit (Metabion, #mi-PMN250) or PureYield™ Plasmid Midiprep System (Promega, #A2495) according to the manufacturer's protocol. Before plasmid isolation, a single colony was inoculated in 5 mL (Miniprep scale) or 100 mL (Midiprep scale) LB broth containing appropriate antibiotics and grown overnight at 37°C with 150 rpm agitation. The cells were harvested the next day with centrifugation at 4,000 rpm for 5-10 min at room temperature and proceeded with DNA extraction. The eluted plasmid DNA was quantified using a NanoDrop™ One Spectrophotometer (Thermo Scientific™, #ND-One-W).

2.2.2.2 Yeast genomic DNA isolation

Genomic DNA from *S. cerevisiae* was isolated using the Yeast DNA Extraction Kit (Thermo Scientific, #78870) following the manufacturer's instructions. The yeast cells were grown overnight in the respective medium at 30°C. Then, the overnight yeast cultures were centrifuged at 4,000 rpm for 5 min at room temperature. After discarding the medium, the pellet was further processed for yeast genomic DNA isolation. The eluted yeast genomic DNA was quantified using a NanoDrop™ One Spectrophotometer (Thermo Scientific™, #ND-One-W).

2.2.2.3 Polymerase chain reaction (PCR)

The amplification of DNA was performed either using Phusion™ High-Fidelity DNA Polymerase (NEB, #M0530L), PCRBIO VeriFi™ Polymerase (PCRBIO, #PB10.42-05) or OneTaq® DNA Polymerase (NEB, #M0480L). Specifically, the Phusion™ DNA polymerase was used to amplify DNA for replacing the native promoter of *ESC8*, the VeriFi™ DNA Polymerase was employed to amplify DNA for generating *ESC8* and *ISW1* mutants, and the OneTaq® DNA Polymerase was utilized to prepare nucleosomal DNA for the reconstitution of mononucleosomes. The annealing temperatures of primers were calculated using the OligoAnalyzer Tool from the Integrated DNA Technologies (IDT) website. The PCR reaction mix with its thermocycling profile was described as follows:

a. Amplification of various promoter sequences from pYM plasmid

Table 15. PCR composition reagent to amplify various promoters

Component	50 µL rxn*	50 µL rxn	Final Conc.
5x Phusion™ HF Buffer	10 µL	10 µL	1X
100% DMSO	-	1.5 µL	3%
10 mM dNTPs	1 µL	1 µL	200 µM
10 µM Forward primer	1.25 µL	1.25 µL	0.25 µM
10 µM Reverse primer	1.25 µL	1.25 µL	0.25 µM
Template DNA	1 µL	1 µL	10 ng
Phusion™ High-Fidelity DNA Polymerase	0.5 µL	0.5 µL	1 unit/50 µL PCR
Sterile water	35 µL	33.5 µL	
Total	50 µL	50 µL	

*Note: This PCR reaction was prepared specifically for the pYM-N10 plasmid.

Table 16. PCR thermocycling condition to amplify various promoters

Cycle step	Temp. and Time	Cycles
Initial denaturation	98°C for 30 sec	1 Cycle
Denaturation Annealing Extension*	98°C for 10 sec 59°C for 30 sec 72°C for 1 min	5 Cycles
Denaturation Annealing Extension*	98°C for 10 sec 72°C for 30 sec 72°C for 1 min	25 Cycles
Final extension	72°C for 10 min	1 Cycle
Hold	8°C for ∞	

*Extension: 30 sec/kb

b. Amplification of DNA to generate *ESC8* and ISW1 mutants

Table 17. PCR composition reagent to amplify *TAP-URA* from plasmid pBS1539

Component	50 µL rxn	50 µL rxn	Final Conc.
	A	B	
5x PCRBIO VeriFI™ Buffer	10 µL	10 µL	1X
10x VeriMax Enhancer	5 µL	5 µL	1X
10 µM Forward primer	2 µL	2 µL	400 nM
10 µM Reverse primer	2 µL	2 µL	400 nM
100% DMSO [Optional]	1.5 µL	-	3%
Template DNA	1 µL	1-3 µL	10 ng
PCRBIO VeriFi™ Polymerase (2 U/µL)	0.5 µL	0.5 µL	1 unit/ 50 µL PCR
Sterile water	Add to 50 µL	Add to 50 µL	
Total volume	50 µL	50 µL	

A: Amplification of *TAP-URA* to generate *esc8*$_{\Delta C1/C2}$*-TAP-URA*
B: Amplification of *TAP-URA* to generate *esc8*$_{\Delta N1/N2}$-TAP-URA and *ESC8-TAP isw1*$_{\Delta SLIDE}$, *ESC8-TAP isw1*$_{\Delta SANT\Delta SLIDE}$

Table 18. PCR thermocycling condition to amplify *TAP-URA* for *esc8*$_{\Delta C1/C2}$*-TAP-URA*

Cycle step	Temp. and Time	Cycles
Initial denaturation	95°C for 1 min	1 Cycle
Denaturation Annealing Extension*	95°C for 15 sec 42°C for 15 sec 72°C for 2 min	5 Cycles
Denaturation Annealing Extension*	95°C for 15 sec 64°C for 15 sec 72°C for 2 min	25 Cycles
Final extension	72°C for 5 min	1 Cycle
Hold	8°C for ∞	

*Extension: 30 sec per kb

Table 19. PCR thermocycling condition to amplify *TAP-URA* for *esc8*$_{\Delta N1/N2}$*-TAP-URA*

Cycle step	Temp. and Time	Cycles
Initial denaturation	95°C for 1 min	1 Cycle
Denaturation Annealing Extension*	95°C for 15 sec 60°C for 30 sec 72°C for 3 min	30 Cycles
Final extension	72°C for 4 min	1 Cycles
Hold	8°C for ∞	

*Extension: 30 sec per kb

Table 20. PCR thermocycling condition to amplify *TAP-URA* for *ISW1* mutants

Cycle step	Temp. and Time	Cycles
Initial denaturation	95°C for 1 min	1 Cycle
Denaturation Annealing Extension*	95°C for 15 sec 65°C for 15 sec 72°C for 90 sec	30 Cycles
Final extension	72°C for 5 min	1 Cycle
Hold	8°C for ∞	

*Extension: 30 sec per kb

Table 21. PCR composition reagent to amplify *esc8*$_{\triangle N1/N2}$

Component	50 µL rxn	Final Conc.
5x PCRBIO VeriFI™ Buffer	10 µL	1x
10x VeriMax Enhancer	5 µL	1x
10 µM Forward primer	2 µL	400 nM
10 µM Reverse primer	2 µL	400 nM
Template DNA	1 µL	100-150 ng/µL
PCRBIO VeriFi™ Polymerase (2 U/µL)	0.5 µL	1 unit/ 50 µL PCR
Sterile water	29.5 µL	-
Total volume	50	-

Table 22. PCR thermocycling condition to amplify *esc8*$_{\triangle N1/N2}$

Cycle step	Temp. and Time	Cycles
Initial denaturation	95°C for 1 min	1 Cycle
Denaturation Annealing Extension	95°C for 15 sec 59°C for 30 sec 72°C for 1 min	30 Cycles
Final extension	72°C for 5 min	1 Cycle
Hold	8°C for ∞	

*Extension: 30 sec per kb

c. Amplification of nucleosomal DNA for reconstitution of mononucleosomes

Table 23. PCR composition reagent to amplify Cy5/IRD700/IRD800-194 bp, 218 bp and 147 bp dsDNA

Component	50 µL Rxn	Final Conc.
5x One*Taq* Standard Reaction Buffer	10 µL	1x
5% DMSO	2.5 µL	0.25%
10 mM dNTPs	1 µL	200 µM
50 µM Forward primer	0.5 µL	0.5 µM
50 µM Reverse primer	0.5 µL	0.5 µM
Template DNA	1-1.5 µL	1 ng
One*Taq*® DNA Polymerase	0.5 µL	2.5 U/ 50 µL
Sterile water	Add to 50 µL	-
Total volume	50 µL	-

Table 24. PCR thermocycling condition for Cy5/IRD700/IRD800-194bp dsDNA

Cycle step	Temp. and Time	Cycles
Initial denaturation	94°C for 2 min	1 Cycle
Denaturation Annealing Extension	94°C for 30 sec 55°C for 1 min 68°C for 30 sec	30 Cycles
Final extension	68°C for 5 min	1 Cycle
Hold	8°C for ∞	

Table 25. PCR thermocycling condition for Cy5-218 bp dsDNA

Cycle step	Temp. and Time	Cycles
Initial denaturation	94°C for 2 min	1 Cycle
Denaturation Annealing Extension	94°C for 30 sec 49°C for 1 min 68°C for 30 sec	5 Cycles
Denaturation Annealing Extension	94°C for 30 sec 62°C for 1 min 68°C for 30 sec	25 Cycles
Final extension	68°C for 5 min	1 Cycle
Hold	8°C for ∞	

Table 26. PCR thermocycling condition for Cy5-147 bp dsDNA

Cycle step	Temp. and Time	Cycles
Initial denaturation	94°C for 2 min	1 Cycle
Denaturation Annealing Extension	94°C for 30 sec 55°C for 1 min 68°C for 30 sec	30 Cycles
Final extension	68°C for 5 min	1 Cycle
Hold	8°C for ∞	

2.2.2.4 Phenol-chloroform extraction

DNA was purified and concentrated using phenol-chloroform extraction **(Gaillard & Strauss, 1990; Moore & Dowhan, 2002)**. To remove protein contaminants, an equal volume of phenol/chloroform/isoamyl alcohol (25:24:1) and DNA samples were mixed. The mixture was vortexed for 10 sec and subsequently centrifuged at top speed for 15 sec, RT. The DNA (aqueous phase) was transferred to a new 1.5 mL microcentrifuge tube. Next, to precipitate DNA and maximize the yield of the DNA, 1/10 volume of 3 M sodium acetate pH 5.2, 15 µg/mL of linear acrylamide,

and 2.5 volume of ice-cold 100% ethanol were added to DNA samples and mixed. The mixture was incubated at -20°C for at least 1 hour until overnight. On the next day, the sample was centrifuged at 13,000 rpm for 20 min at 4°C, and the supernatant was discarded. The DNA pellet was rinsed with 200 µL of 70% ethanol, followed by inverting the tube gently and centrifuging at 13,000 rpm for 5 min at 4°C. The supernatant was removed, and the pellet was allowed to air dry for 30-60 min in a lamina flow or a Christ rotary vacuum concentrator (Martin Christ). Lastly, DNA was dissolved in 15-30 µL of sterile water and subjected to DNA quantification using NanoDrop™ One Spectrophotometer (Thermo Scientific™, #ND-One-W).

2.2.2.5 Cloning via Gibson assembly

Gibson assembly method was conducted to clone the gene of interest into a vector **(Gibson et al., 2009)**. The modified version does not require the use of restriction enzymes and rather uses the overlapping sequence homology to insert a vector **(Miller, 2018)**. The genes of interest were amplified using PCRBIO VeriFi™ Polymerase (PCRBIO, #PB10.42-05), while the empty vector backbones were prepared either by PCR amplification or linearized by restriction enzyme digestion. All DNA fragments were analyzed on 1% agarose gel, and the remaining solutions were purified using a mi-PCR Purification Kit (Metabion, #mi-PCR250). Next, Gibson assembly was carried out using a master mix prepared in-house, and the assembly product was subsequently transformed into *E. coli* DH5α Competent cells. The successful correct clones were confirmed using colony PCR followed by DNA sequencing.

2.2.2.6 *E. coli* transformation

Transformation of plasmid DNA was performed using *E. coli* chemically competent cells. A total of 3-5 µL of plasmid DNA/ ligation mixture was added into *E. coli* competent cells, and then incubated on ice for 10 min. Next, the cells were subjected to heat shock at 42°C for 2 min at thermomixer (Eppendorf), followed by another incubation on ice for 10 min. A pre-warmed LB medium was added to the suspension culture and subsequently incubated at 37°C for 1 hour with agitation at 1,000 rpm. Then, a total of 50 µL and 200 µL of cell suspension were spread onto separate LB agar plates containing antibiotics. The LB agar plates were then incubated overnight at 37°C in the incubator. On the following day, the growth colonies were selected and proceeded to colony PCR and DNA sequencing to determine the coding frame orientation of the sequence.

2.2.2.7 *S. cerevisiae* transformation

Yeast transformation was carried out using the LiAc/SS carrier DNA/PEG method according to the published protocol **(Gietz & Schiestl, 2007)** with some modifications. In the preparation of yeast cells, a single colony was inoculated in 5 mL of YPD medium and incubated overnight at 30°C in a rotator. On the next day, the titer of the overnight culture was determined using a cell density meter **(**Ultraspec™10, Amersham Biosciences) measuring the OD at 600 nm. Next, the overnight culture was inoculated in 20 mL to an OD600 of 0.2 and subsequently incubated at the incubator shaker at 30°C with 150 rpm agitation until the cells completed at least 2 divisions (OD600 = 0.8). The culture was harvested by centrifugation at 3,000 rpm for 5 min at

4°C, and the medium was discarded. Next, the cell was resuspended in 25 mL sterile water and centrifuged at 3,000 rpm for 5 min at 4°C. After discarding the supernatant, the cell pellet was resuspended in 1 mL of 100 mM lithium acetate (LiAc). The cell suspension was transferred to a sterile 1.5 mL microcentrifuge tube and quickly centrifuged for about 20 sec at top speed. The LiAc solution was removed. Further, the pellet was resuspended with 833 µL of 100 mM lithium acetate when the titer of cell culture reached the OD600 of 1.0. A 50 µL samples were aliquoted into 1.5 mL microcentrifuge tubes and then centrifuged at a fast speed. The LiAc solution was removed from the tubes. For transformation, the cells were added with 240 µL of PEG solution (50% w/v), 36 µL of 1 M LiAc, 25 µL of 2 mg/mL single-stranded carrier DNA, and 50 µL sterile water containing 1-5 µg of DNA. The samples were mixed thoroughly until the pellet was completely dissolved. After that, it was incubated at the thermomixer (Eppendorf) at 30°C for 30 min with 1,000 rpm agitation. The cells were subjected to heat shock at 42°C for about 23 min and then pelleted with centrifugation at 7,000 rpm for 15 sec. The transformation mix was carefully removed with a micropipette. When the antibiotic gene selection was used instead of auxotrophic gene selection, the pellet was added with 500 µL of YPD and further incubated for about 2 hours at 30°C with 1,000 rpm agitation. Otherwise, the pellet was dissolved with 250 µL of sterile water and mixed gently by pipetting up and down. The transformation mix was plated onto the appropriate selection medium agar plate. The successful clones were confirmed using colony PCR as well as DNA sequencing.

2.2.2.8 Bacterial and yeast colony PCR

Colony PCR was carried out to validate the insertion or deletion after cloning and transformation. The compositions of colony PCR were the same as the standard PCR protocol for Phusion™ High-Fidelity DNA Polymerase (NEB, #M0530L) or PCRBIO VeriFi™ Polymerase (PCR Biosystems, #PB10.42-05). However, instead of using plasmid DNA or genomic DNA, a single colony on the agar plate was picked and processed before performing PCR. For *E. coli*, the colony was mixed with 20 µL sterile water, and about 1 µL of the solution was added to a 25 µL PCR reaction. For yeast, the colony was mixed with 15 µL of Zymoylase solution (2.5 mg/mL in 0.1 M sodium phosphate buffer pH 7.5) followed by incubation at 37°C for 20 min and heating at 95°C for 5 min. Next, the solution was diluted 1:10 with sterile water and used 2.5 µL as a DNA template in a 25 µL PCR reaction. Alternatively, the colony was mixed with 20 µL of 20 mM NaOH and heated at 95°C for 10 min. The mixture solution was centrifuged at 14,000 rpm for 2 min. A total of 1 µL supernatant was used as a DNA template in a 25 µL PCR reaction.

2.2.2.9 Agarose gel electrophoresis

Agarose gel electrophoresis is a method to analyze nucleic acids by size, purity, and concentration. For most of the time, 1% (w/v) agarose in 1x TAE Buffer with an addition of 0.5 µg/mL ethidium bromide was prepared. For sample preparation, the 6x DNA loading dye was diluted in 1:6 dilutions with the sample and loaded onto 1% (w/v) agarose gel. DNA markers such as 1 kb DNA Ladder (NEB, #N3232L) or 100 bp DNA Ladder (NEB, N3231L) were used as a standard to estimate the size of the DNA fragment. The agarose electrophoresis was run at 100 volts for 30 min. Then, DNA bands were visualized and photographed using a Vilber Quantum Gel Documentation Imaging (Vilber).

2.2.2.10 SDS-PAGE

Protein was analyzed by SDS-polyacrylamide gel electrophoresis. Gels with 10% resolving gel and 5% stacking gel were prepared routinely. For sample preparation, the protein was diluted 1:4 with 5x SDS Sample Buffer and subsequently incubated at 95°C for 5 min. Additionally, PageRuler™ Plus Prestained Protein Ladder, 10 to 250 kDa (Thermo Scientific™, #26620), was used as a marker to estimate the size of the proteins. Both protein samples and protein ladder were then loaded onto SDS-PAGE gel. The SDS-PAGE was run at 300 volts for 30 min in 1x Running Buffer. Furthermore, the gel was stained with Coomassie blue staining or silver staining. The detailed protocol for the staining is elaborated in the following section. After staining, protein bands were visualized and photographed using a ChemiDoc™ MP Imaging System (Bio-Rad).

2.2.2.11 Coomassie staining and silver staining

For Coomassie staining, the gel was stained with Coomassie Blue Staining Buffer for 3 hours at room temperature with low agitation. Next, the Staining Buffer was removed, and the gel was washed with the Destaining Buffer for about 4-5 hours at room temperature.

Silver staining was carried out most of the time due to its excellent sensitivity to low-concentrated protein. Here, all buffers were prepared in a total of 100 mL. First, the SDS-PAGE gel was fixated for 60 min in a Fixation Buffer containing 50% (v/v) methanol, 12% (v/v) glacial acetic acid, and 50 µL of 37% (v/v) formaldehyde. Then, the gel was washed twice with 50% (v/v) ethanol for 10 min each time and further incubated for 1 min with Sensitizer Buffer containing 0.02 % (w/v) sodium thiosulfate pentahydrate. Next, the gel was washed thrice with MilliQ water for 20 sec each time and continued incubated for 15 min with Reaction Buffer containing 0.2 % (w/v) silver nitrate and 75 µL of 37% (v/v) formaldehyde. After that, the gel was washed again twice with MilliQ water for 20 sec each time, followed by developing the gel with 5% (w/v) sodium carbonate, 2 mL of 0.02% (v/v) sodium thiosulfate pentahydrate, and 50 µL of 37% (v/v) formaldehyde for about 1 to 15 minutes, until the protein bands become visible. Lastly, the developing reaction was stopped by washing the gel with 50 mM EDTA for 15 min.

2.2.2.12 Western blot

Western blot was used to detect the presence of a specific protein in a complex mixture of proteins. Beforehand, the samples and a protein ladder were loaded onto the SDS-PAGE gel and run for about 30 min at a constant 300 volts in 1x Running Buffer. After protein separation, instead of proceeding to protein staining, the proteins were electrophoretically transferred from the gel to the nitrocellulose membrane using the Trans-Blot® Turbo™ Transfer System (Bio-Rad). Next, the membrane was stained with Ponceaus S Staining Solution for 5 min to evaluate the transfer efficiency. The Ponceau S staining on the gel was easily removed with MilliQ water. Afterward, the membrane was blocked with a Blocking Buffer containing 5% (w/v) non-fat dry milk (Frema, #4046006002033) in 1x TBST and incubated for 1 hour at room temperature. Subsequently, the membrane was washed with 1x TBST thrice with 5 min each incubation time at room temperature. Then, the membrane was incubated with the

primary antibody of either peroxidase-anti-peroxidase (PAP, #P1291) or anti-Isw1 (#3C4) for 1 hour at room temperature or overnight at 4°C, respectively. Peroxidase-anti-peroxidase (PAP) was used for TAP-tagged detection, whereas anti-Isw1 was used specifically for Isw1 detection. The membrane was washed with 1x TBST three times with 5 min incubation time. For the Isw1 antibody, the membrane was further incubated with a secondary antibody of Goat Anti-Rat IgG Antibody-HRP conjugated (Sigma-Aldrich, #AP136P) for 1 hour at room temperature, followed by washing with 1x TBST three times with 5 min incubation time. After washing, the membrane was developed by adding 1-2 mL of pre-incubated chemiluminescent HRP substrate mixture (Merck, #WBKLS0500) for 5 min at room temperature. The substrate was removed, and the membrane was photographed using the ChemiDoc MP Imaging System (Bio-Rad).

2.2.2.13 Native polyacrylamide electrophoresis

Native gels were used as a tool to analyze the newly reconstituted mononucleosomes, the shifted mononucleosomes, and the interaction of protein-nucleic acid or protein-mononucleosomes. In principle, it separates proteins and DNA fragments based on size, structure, and molecular weight. The 5% Native gels and 7% Native gels were prepared routinely. Orange G was used as a tracking dye for the length of separation in Native PAGE **(Eberharter et al., 2004)**. Before loading the samples, the Native PAGE was pre-run at 100 volts for 1 hour in 0.4x TBE Buffer at 4°C. After loading the samples onto the gels, the 5% Native PAGE was run at 300 volts for 1 hour in 0.4x TBE at 4°C, while the 7% Native PAGE was run at 300 volts for 2 hours in 0.4x TBE at 4°C. Next, the protein or DNA migration was visualized and photographed using Typhoon™ FLA 9500 (GE Healthcare) and Odyssey® CLx Imaging System (LI-COR), depending on the fluorescent dye used.

2.2.3 Protein expression and purification methods

2.2.3.1 Recombinant protein expression

In general, the constructs were overexpressed in *E. coli* using IPTG induction. A single colony was inoculated in an LB medium containing an appropriate antibiotic and incubated overnight at 37°C with 155 rpm agitation. On the next day, the overnight culture was added to a fresh LB medium containing an antibiotic and then incubated for 1-2 hours until it reached the log phase with an optical density of 0.5-0.8 at 600 nm. Afterward, the culture was inducted with the addition of IPTG and further incubated for protein overexpression. Next, the culture was harvested with centrifugation at 10,000 rpm for 5 min at RT. The supernatant was discarded, and the pellet was stored at -80°C until further use.

In this study, the constructs including pETDuet-1 6xHis-Esc8 and Isw1, pETDuet-1 6xHis-Esc8, pCoofy4 6xHis-MBP-Isw1, pCoofy4 6xHis-MBP-Esc8 and pGEX-6X-1 GST-Isw1 were overexpressed in *E. coli* Rosetta (DE3). Various overexpression conditions were carried out for each construct to obtain soluble high-yield protein. These included various temperatures and lengths of incubation, various IPTG concentrations, the addition of ethanol, high salt concentration, sorbitol, and heat shock treatment. During troubleshooting, some constructs were transformed and

expressed in other *E. coli*-competent cells, such as BL21 (DE3), BL21 (DE3) pLysS, and Rosetta (DE3) pLysS.

For the construct pETDuet-1 6xHis-Esc8 and Isw1, it was expressed at different temperatures of 24°C for 4 hours and 6 hours, 30°C for 4 hours, and 37°C for 4 hours. For pDuet-1 6xHis-Esc8, it was expressed at 24°C for 6 hours as well as overnight expression at 16°C with IPTG concentrations of 0.1 mM, 0.2 mM, and 0.5 mM. Additionally, heat shock treatment or the addition of additives such as 3% ethanol, 0.5 M NaCl, or 0.5 M sorbitol to the LB medium were employed with low and moderate IPTG concentrations. In this case, the cells were either subjected to heat shock treatment before IPTG induction or expressed in an LB medium containing 3% ethanol, 0.5 M NaCl, or 0.5 M sorbitol. Both pCoofy4 6xHis-MBP-Esc8 and pCoofy4 6xHis-MBP-Isw1 were expressed at various temperatures of 16°C for 20 hours, 24°C for 6 hours, 30°C for 4 hours, and 37°C for 4 hours. Moreover, troubleshooting was not required for pGEX-6P-1 GST-Isw1 as there was an established protocol in the Smolle Lab. To induce the pGEX-6P-1 GST-Isw1, the cell culture was inducted with the addition of 0.5 mM IPTG and further incubated at 16°C for 20 hours.

2.2.3.2 Preparation of cell lysate using a sonicator

The cell lysate was prepared before protein purification. The 50 mL culture of the overexpressed cell pellet was resuspended with 10 mL of the appropriate Buffer and an additional protease inhibitor PMSF of 0.5 mM. Next, the cell suspension was lysed using a sonicator (Branson Ultrasonics™ Sonifier Model 250 CE, Fisher Scientific) with a 25-second burst followed by a 30-second cooling down six times. After that, the lysate was centrifuged at 4,500 rpm for 15 min at 4°C. The supernatant was promptly used for protein purification. To check the protein solubility, both pellet and supernatant were added with 5x SDS Sample Buffer and incubated at 95°C for 5 min. Both protein samples and a protein ladder were then loaded onto SDS-PAGE gel.

2.2.3.3 Recombinant protein purification

Of all the recombinant proteins, the 6xHis-MBP-tagged Esc8, 6xHis-MBP-tagged Isw1, and GST-tagged Isw1 were subjected to purification. The attempt to purify 6xHis-tagged Esc8 and Isw1 was unsuccessful and not described in detail in this thesis. The following sections describe different purification systems that were used to purify 6xHis-MBP-tagged Esc8, 6xHis-MBP-tagged Isw1, and GST-tagged Isw1. The overview schematic of the purifications for each protein is shown in **Figure 16A**.

a. Ni-NTA purification

Purification of His-tagged proteins, including 6xHis-MBP-tagged Isw1 and 6xHis-MBP-tagged Esc8, was carried out following the procedure from the Ni-NTA Purification System (Invitrogen™, #K95001). All Buffers were prepared in-house. A total of 1.5 mL of Ni-NTA resin was added into a 15 mL Falcon tube. The ethanol storage solution was removed from the resin. The Ni-NTA resin was prewashed with 6 mL of sterile water and twice with 6 mL of 1x Native Binding Buffer. For each wash step, it was centrifuged at 2,000 rpm for 1 min at 4°C. After that, the lysate was loaded into the column containing Ni-NTA resin, and the mixture was incubated in a rotator

for 1 hour at 4°C. The resin was collected by centrifugation at 2,000 rpm for 1 min at 4°C. The supernatant was removed from the resin. Next, the resin was washed with 15 mL of 1x Native Binding Buffer and then 15 mL of 1x Native Wash Buffer. After adding 1 mL of 1x Native Wash Buffer to the resin, the mixture was transferred to the Econo-Pac® Chromatography Column (Bio-Rad, #7321010). Finally, 6 mL of 1x Native Elution Buffer was loaded into the column, and every 500 µL of eluate was collected as fractions. Each fraction was next analyzed by SDS-PAGE.

b. Heparin chromatography

Both 6xHis-MBP-tagged Isw1 and 6xHis-MBP-tagged Esc8 proteins were further purified using the Äkta Pure Protein Purification System (GE Healthcare) with HiTrap™ Heparin HP affinity columns (Cytiva, #17-0406-01) after Ni-NTA purification. Prior to purification, the sample was dialyzed overnight using Slide-A-Lyzer mini dialysis devices with 20 kDa cut-off (Thermo Scientific™, #88402) in 1 L of Heparin Binding Buffer at 4°C with stirring. For purification, the sample was loaded onto the pre-washed column. After that, the column was washed with 10 mL of Heparin Binding Buffer. At last, the protein was eluted with 10 mL of Heparin Elution Buffer. A 500 µL of each fraction was collected and analyzed by SDS-PAGE.

c. Size exclusion chromatography

The 6xHis-MBP-tagged Isw1 protein was further separated from other nonspecific proteins using the ÄKTA Pure Protein Purification System (GE Healthcare) with Superdex 200™ 10/300 GL column (Cytiva, #28-9909-44). Before purification, the protein was concentrated and exchanged buffer with the SEC Running Buffer using Amicon® Ultra-4 Centrifugal Filter Devices with 50 kDa cut-off (Merck Millipore, #UFC805096). For purification, the sample was loaded onto the pre-washed column, and the protein was eluted in 23 mL total volume. There was 1 mL solution per fraction. All fractions were analyzed by SDS-PAGE.

d. Glutathione affinity chromatography

Purification of GST-tagged Isw1 was performed using Glutathione Sepharose™ 4 Fast Flow (VWR, #17-5132-03). A total of 750 µL of Glutathione Sepharose was added into a 50 mL Falcon tube, and it was centrifuged at 2,000 rpm for 1 min at 4°C to remove the Storage Buffer. Next, the glutathione sepharose was washed twice with 10 mL of GST Wash Buffer 1. The resin was collected at 2,000 rpm for 1 min at 4°C, and the supernatant was removed. After pre-washing the resin, the cell lysate was loaded into the tube containing the glutathione sepharose and incubated by rotating for 3 hours at 4°C. After that, the sample was centrifuged at 2,000 rpm for 1 min at 4°C, and then the supernatant was discarded. The resin was washed thrice with 12 mL of GST Wash Buffer 1 and incubated for 5 min at 4°C by rotating per wash. The resin was collected by centrifugation at 2,000 rpm for 1 min at 4°C. The resin was washed twice with 12 mL of GST Wash Buffer 2. In the wash step, it was incubated for 5 min at 4°C by rotating, and then the resin was centrifuged at 2,000 rpm for 1 min at 4°C. To elute the protein, the sample was transferred to the Econo-Pac® Chromatography Column (Bio-Rad, #7321010). The purified protein was

eluted with 2 mL of GST Elution Buffer in which 500 µL of fraction were collected. Next, each fraction was analyzed by SDS-PAGE

2.2.3.4 Yeast protein expression

a. Expression of Esc8 from yeast strain containing the inducible promoter of *pCUP1-ESC8*, *pGAL1-ESC8,* and *pMET25-ESC8*

For a yeast strain containing *pCUP1-ESC8,* a single colony was inoculated in 5 mL of YPD medium and incubated overnight at 30°C with 150 rpm agitation. On the following day, the cell density of the overnight culture was determined using a cell density meter (Ultraspec™ 10, Amersham Biosciences) measuring the OD600. The overnight culture was inoculated in 50 mL of fresh YPD medium to an OD600 of 0.1-0.2 and further incubated for 4-6 hours at 30°C with 150 rpm agitation until it reached the late log phase of 1-2. To induce the Esc8 expression, the cell suspension was added with copper to a final concentration of 100 µM and continued incubated for 2 hours at 30°C with 150 rpm agitation. The cell suspension was pelleted with centrifugation at 4,000 rpm for 10 min at 4°C. The supernatant was removed, and the pellet was washed with 20 mL of Calmodulin-Modified Extraction Buffer. After that, it was centrifuged again at 4,000 rpm for 10 min at 4°C to collect the pellet. The pellet was snap-frozen and stored at -80°C until further use.

For a yeast strain containing *pGAL-ESC8*, a single colony was inoculated in 50 mL of YP medium containing 2% raffinose and incubated overnight at 30°C with 150 rpm agitation. Here, the cell culture was allowed to grow to reach the late log phase of 1-2. After that, the cell suspension was pelleted with centrifugation at 4,000 rpm for 10 min at 4°C. Next, the supernatant was removed. To induce the Esc8 expression from the galactose promoter, the cell pellet was resuspended with a fresh YP medium containing 2% galactose, and the culture was further incubated for 2 hours at 30°C. After induction, the cell was collected with centrifugation at 4,000 rpm for 10 min at 4°C. After the supernatant was discarded, the pellet was resuspended with 20 mL of Calmodulin-Modified Extraction Buffer. Next, the cell suspension was centrifuged at 4,000 rpm for 10 min at 4°C. The supernatant was discarded, and the pellet was snap-frozen and stored at -80°C.

For a yeast strain containing *pMET25-ESC8*, a single colony was inoculated in 50 mL of Synthetic Complete medium (SC) containing 2% glucose and incubated for about 19 hours at 30°C with 150 rpm agitation. After the cell culture reached the late log phase of 1-2, the cell suspension was pelleted with centrifugation at 4,000 rpm for 10 min at 4°C. The supernatant was discarded. To induce the expression of Esc8, the pellet was resuspended with 50 mL of SC-MET medium (minus methionine), and the cell suspension was incubated for 2 hours at 30°C with 150 rpm. Next, the cell was harvested with centrifugation at 4,000 rpm for 10 min at 4°C and washed with 20 mL of Calmodulin-Modified Extraction Buffer. After washing, the pellet was collected by centrifugation at 4,000 rpm for 10 min at 4°C. Then, the pellet was snap-frozen and stored at -80°C.

2.2.3.5 Preparation of cell lysate using a bead beater

The pellet was resuspended in 500 µL of Calmodulin-Modified Extraction Buffer. The cell suspension was added to a 1.7 mL screw cap tube containing 0.5 mm Glass Beads (Biospec, #11079105). Next, the cell suspension was lysed using a Precellys® 24 homogenizer (VWR) for 6 cycles, with each cycle having 30 seconds of homogenizer, followed by cooling down on ice for 5 min. The supernatant was collected by centrifugation at 10,000 rpm for 5 min at 4°C. Next, the whole cell extract was quantified using Bradford protein assay (Bio-Rad, #5000006) before proceeding to the SDS-PAGE.

2.2.3.6 Purification of Isw1c and Isw1a complexes from *S. cerevisiae*

Both Isw1c and Isw1a complexes were purified from the yeast strains containing *ESC8-TAP* with *ioc2*Δ *ioc3* and *IOC3-TAP*, respectively. For each time of purification, the total volume of yeast culture was about 72 liters for Isw1c and 12 liters for Isw1a. Since the associated subunit protein was conjugated with TAP-tagged, the tandem affinity purification (TAP) approach was performed to obtain the purified protein complex. Beforehand, the yeast strains were grown in 5 mL of YPD medium overnight at 30°C in a rotator. On the following day, 3-4 mL of overnight culture was inoculated in 60 mL fresh YPD medium and incubated for about 8 hours at 30°C with 150 rpm agitation. After that, 10 mL of day culture was transferred to 2 liters of fresh YPD medium and incubated overnight at 30°C with 150 rpm agitation. Next, the cells were harvested by centrifugation at 5,000 rpm for 10 min at 4°C (Avanti™ J-20XP with JLA-8.1000 rotor, Beckman Coulter). A total of 1L of cell culture was washed with 20 mL of cold 1x PBS and then centrifuged at 4,000 rpm for 10 min at 4°C (Benchtop centrifuge 5810 R, Eppendorf). The supernatant was removed, and the pellet was resuspended with TAP Extraction Buffer at a ratio of 1:1. Next, the cell suspension was frozen into liquid nitrogen dropped-by-dropped, making the cell popcorn. The cell popcorn was stored in a -80°C freezer until further use.

Further, the cells were lysed with a freezer mill (SPEX 6870 Freeze/Mill®, SPEX® SamplePrep) and resulted in powder form. The parameter for the freezer mill was 6 cycles with 2 min of homogenizing the cells and 1 min of cooling down. The cell was defrosted on ice. A 50 mL cell suspension was added with 100 µL yeast protease inhibitors (Sigma, #P8215), 50 µL of heparin (10 mg/mL) and 50 µL Benzonase nuclease (2.5U/µL). Next, the cell suspension was centrifuged at 4,000 rpm for 20 min at 4°C. The collected supernatant was centrifuged at high force (Optima™ L-90K Ultracentrifuge, Beckman Coulter) at 45,000 rpm for 60 min at 4°C. This ultracentrifuge was employed to separate the molecules in the sample based on their physical properties, such as size and mass. After centrifugation, the middle layer containing a soluble whole-cell extract was carefully collected.

The whole-cell extract was employed in the TAP purification system. This purification began with incubating the whole cell extract with 400 µL of pre-washed IgG Sepharose resin (Cytiva, #17096901) for 4 hours at 4°C. After that, the resin was collected with centrifugation at 1,200 rpm for 2 min at 4°C. The supernatant was discarded. The resin was washed four times with 10 mL of TAP Purification Buffer and one time with 6 mL of TEV Cleavage Buffer. The resin was collected by centrifugation at 1,200 rpm for 2 min at 4°C. Then, the resin was resuspended with 1 mL of TEV

Cleavage Buffer with the addition of 5 µL of acTEV™ Protease (Invitrogen™, #12575015). The solution was incubated for 16 hours at 4°C with rotation. This protease was used to cleave at the TEV protease cleavage site of the protein. After cleavage, the protein A bound to the resin and the protein-CBP-tagged with its protein interaction were expected to be detected in the supernatant. On the next day, the supernatant was collected by centrifugation at 1,200 rpm for 2 min at 4°C. Afterward, the resin was added with 6 mL of CBB and incubated by rotating at 5 min at 4°C. The supernatant was collected at 1,200 rpm for 2 min at 4°C. A total of 7 mL collected supernatant was added with 3 µL of 1 M $CaCl_2$. Then, the supernatant was added to 300 µL of pre-washed Calmodulin-Sepharose resin (Cytiva, #17-0529-01). The mixture was incubated in a rotator for 3 hours at 4°C. The resin was collected by centrifugation at 1,200 rpm for 2 min at 4°C. Subsequently, the resin was washed five times with 10 mL of CBB for 5 min at 4°C each time. After loading the resin into the Micro Bio-Spin Chromatography Column (Bio-Rad, #7326204), the resin was collected by gravity. At last, the purified protein was eluted with 300 µL of CEB four times. In the first elution step, the mixture was incubated for 1 hour at 4°C by rotating while the remaining elution steps were carried out without incubation.

2.2.3.7 Precipitation of protein using TCA

Protein with low concentration was concentrated using the Trichloroacetic acid (TCA) precipitation method. A 100% cold TCA was added to purified protein with a ratio of 1:4 volume. The mixture was incubated on ice for 30 min and then centrifuged at 14,000 rpm for 30 min at 4°C. The supernatant was carefully removed. The pellet was washed with cold acetone and centrifuged at 14,000 rpm for 5 min at 4°C. The supernatant was carefully discarded, whereas the pellet was air-dried for 30 min to 1 hour to remove the acetone. Furthermore, the pellet was resuspended with 20 µL of 5x SDS sample Buffer. The sample was analyzed by SDS-PAGE.

2.2.3.8 Desalting, buffer exchange, and concentrating protein

The protein was concentrated, and the buffer was exchanged using Amicon® Ultra-4 Centrifugal Filter Devices with a 50 kDa cut-off (Merck Millipore, #UFC805096) according to the manufacturer's instructions. The fractions containing purified protein were added to the Amicon® Device and centrifuged at 4,000 rpm for 10-30 min at 4°C. When buffer exchange was required, 4 mL of buffer was added to the Amicon® device and centrifuged at 4,000 rpm for 10-30 min at 4°C. The buffer exchange step was repeated. The device was inverted and centrifuged at 4,000 rpm to recover the purified protein for 5 mins.

2.2.3.9 Tag removal from protein

The 6xHis-MBP-tagged of the 6xHis-MBP-tagged Isw1 and 6xHis-MBP-tagged Esc8 was cleaved using Pierce™ HRV 3C Protease (Thermo Scientific™, #88946) according to the manufacturer's instructions with some modifications. HRV 3C protease (2 units) was added to the HRV 3C Reaction Buffer containing the protein. Further, the reaction was overnight incubated at 4°C to allow the process of tag cleaving. The uncleaved and cleaved protein samples were analyzed on the next day using SDS-PAGE.

2.2.4 Biochemical methods

2.2.4.1 Pull-down assay

The protein-protein interaction between 6xHis-MBP-tagged Esc8 and GST-tagged Isw1 was performed using a pull-down assay. Fundamentally, amylose resin (NEB, #E8021S) was employed to pull the 6xHis-MBP-tagged Esc8 interacting with GST-tagged Isw1. A 30 µL of amylose resin was added to a 1.5 mL microcentrifuge tube and washed twice with 1 mL of Amylose Pull-Down Buffer. The resin was collected by centrifugation at 3,000 rpm for 30 sec at 4°C. An equal protein amount of 6xHis-MBP-tagged Esc8 and GST-tagged Isw1 were mixed in an Amylose Pull-Down Buffer to a total volume of 100 µL. The mixture of proteins was added to amylose resin and further incubated at a rotator for 2 hours at 4°C. For negative control, only GST-tagged Isw1 was added to amylose resin. All samples were washed twice with 1 mL of Amylose Pull-Down Buffer. The resin was centrifuged at 3,000 rpm for 30 seconds at 4°C. To elute the protein, a total of 10 µL of 5x SDS Sample Buffer was added to the resin and incubated at 95°C for 5 min to release the proteins bound to the resin. Further, the samples were analyzed using SDS-PAGE.

2.2.4.2 Nucleosome reconstitution

The reconstitution of nucleosomes was conducted based on the protocol of reconstitution from histone octamers as described **(Owen-Hughes et al., 1999)**. Both DNA and histone octamer were required to perform the nucleosome reconstitution. In this study, histone octamers and distinct histone octamer PTMs were provided by Dr. Till Bartke, Dr. Philipp Voigt, and Dr. Michaela Smolle **(See Section 2.1.5, Table 5)**. In addition to that, the nucleosomal DNA labeled with fluorescence (Cy5, IRD700-, or IRD800-) was amplified from pGEM-3z/601 plasmid. To have end-positioned and mid-positioned nucleosomes, histone octamers were reconstituted onto 194 bp or 218 bp nucleosomal DNA, each containing the 601-positioning sequence. For nucleosome core particles (NCPs), histone octamers were reconstituted onto 147 bp nucleosomal DNA, also containing the 601-positioning sequence.

For the reconstitution of nucleosomes, a total of 10 µL of reactions containing a ratio of 1:1 of histone octamer/ distinct histone octamer PTMs and DNA in the Initial Dilution Buffer with a final concentration of 2 M NaCl was prepared and subsequently incubated at 37°C for 15 min. In the practical experiment, the optimum ratio between histone octamer/ distinct histone octamer PTMs and DNA for the reconstitution of nucleosomes might have varied; however, it was generally close to the ratio of 1:1. The reaction was transferred to 30°C and serially diluted with 3.3 µL, 6.7 µL, 5 µL, 3.6 µL, 4.7 µL, 6.7 µL, 10 µL, 30 µL and 20 µL Initial Dilution Buffer with a 15 min incubation per dilution. At last, a 100 µL Final Dilution Buffer was added to the reaction and further incubated at 30°C for another 15 min. Next, the quality of nucleosomes assembled with either histone octamers or distinct histone octamer PTMs, as well as the quantification of their amount, was assessed using Native PAGE electrophoresis. Approximately 5 µL of the reconstituted nucleosomes and nucleosomel DNA (at known amount of 10 µg, 20 µg, and 30 µg) were loaded onto 7% Native polyacrylamide gel in 0.4x TBE, and subsequently, the Native PAGE electrophoresis was run at 300 volt for 1 hour. The visualization of nucleosomes relied on the fluorescent-labeled DNA wrapped around the histone octamer. The Cy5-labeled nucleosomes and the IRD700-

/IRD800-labeled nucleosomes were detected and photographed using Typhoon™ FLA 9500 (GE Healthcare) and Odyssey® CLx Imaging System (LI-COR), respectively. The remaining sample containing the reconstituted nucleosomes was stored at 4°C until further use.

2.2.4.3 30 bp oligo annealing

To prepare the reaction, both 30 bp of Cy5-forward and 30 bp of unlabeled-reverse oligonucleotides were mixed in stoichiometric amounts with Oligo Annealing Buffer to a total volume of 50 µL. After that, the mixture was transferred to a Thermocycler (Bio-Rad) with a ready set-up program. To anneal the oligo, the mixture was heated at 95°C for 2 min, followed by the temperature dropped by 1°C every 2 min until it reached 25°C and the mixture was cooled at 4°C for temporary storage until it was collected.

2.2.4.4 ATP hydrolysis assay

The NADH-oxidation coupled ATPase assay was conducted as described **(Forne et al., 2012; Mueller-Planitz et al., 2013)**. The reaction of 30 µL containing pyruvate kinase (15.5 U/mL), PEP (3 mM), lactate dehydrogenase (15.5 U/mL), NADH (0.6 mM), remodeler (30 nM) and DNA/Histones/Long nucleosomes (0.1 mg/mL) in Remodeling Buffer were prepared and transferred to a 384-well plate (Greiner, #781101). After spinning down the plate, the reactions were supplemented with adding 1 mM Mg2+.ATP to start the ATP hydrolysis process. To measure the ATP hydrolysis activity, the NADH absorbance was monitored and recorded at 340 nm by Infinite M1000 PRO plate reader (Tecan).

2.2.4.5 Nucleosome sliding assay

A nucleosome sliding assay was carried out to investigate the ability of the remodeler to slide nucleosomes. To set up a nucleosome sliding assay, a 10 µL reaction containing 1 nM remodelers, 3 nM mononucleosomes, 1 µg BSA, and 44 mM KCl in Nucleosome Sliding Buffer A was prepared in a PCR tube. In the amount-dependent assay, varying quantities of remodeler were utilized, resulting in individually prepared reactions. Furthermore, the reaction was then incubated at 30°C for 30 min. On the other hand, a master mix with a total volume of 70 µL was prepared for the time-dependent assay. The reaction was incubated at 30°C for 0 min, 0.5 min, 1 min, 2 min, 5 min and 10 min. Alternatively, a different time incubation set was carried out with incubation of 0 min, 0.5 min, 2 min, 5 min, 10 min, and 20 min. To stop the reaction, 10 µL of the reaction was transferred to a cold Stop Buffer containing 700 ng plasmid competitor DNA and further incubated at 30°C for another 10 min. After that, the samples were added with 50% glycerol stock to a final concentration of 10% and then loaded on a 7% Native polyacrylamide gel in 0.4x TBE. The Native PAGE electrophoresis was then run at 300 volts for 3 hours at 4°C. Next, the shifted mononucleosomes were visualized and photographed using Typhoon™ FLA 9500 (GE Healthcare) for Cy5-labeled mononucleosomes or Odyssey® CLx Imaging System (LI-COR) for IRD700/IRD800-labeled mononucleosomes. Furthermore, the mononucleosome bands for each lane were quantified with ImageQuant TL (GE Healthcare). All lanes containing remodelers were normalized against the input lanes containing mononucleosomes only.

2.2.4.6 Competitive nucleosome sliding assay (cSliding Assay)

The ability of remodelers to slide a discrete nucleosome containing modified histone octamer or histone variant was investigated using a competitive nucleosome sliding assay (cSliding Assay). This assay is similar to the standard nucleosome sliding assay; however, one reaction contains two mononucleosomes instead. To distinguish the nucleosomes from the other, the mononucleosomes used were labeled with either IRD700 or IRD800. In a 10 µL reaction, the IRD700-labeled mononucleosomes and the IRD800-labeled mononucleosomes were mixed at a ratio of 1:1 with other components as described above. The concentration of each mononucleosome was 3 nM. After that, the samples were resolved on 7% Native PAGE gels in 0.4x TBE. After running the gel, it was scanned using Odyssey® CLx Imaging System (LI-COR) and subsequently photographed for dual channels as well as single channels. The quantification of the shifted mononucleosomes was performed using ImageQuant TL (GE Healthcare), which it was normalized with the input containing only mononucleosomes.

2.2.4.7 Electrophoretic mobility shift assay (EMSA)

The electrophoresis mobility shift assay (EMSA) was employed to detect the remodeler-nucleic acid interaction and remodeler-nucleosome interaction. Here, the 30 bp of dsDNA, 194 bp of dsDNA, or various nucleosomes were used as the substrates. Different protein concentration (0 nM, 2 nM, 4 nM, 8 nM and 16 nM) was added into a reaction containing 1 nM of mononucleosomes or 1 nM of dsDNA, 6.8 µg BSA, 0.5 mM $MgCl_2$ and 150 mM NaCl in EMSA Buffer D to a total volume of 15 µL. The reaction was incubated at 30°C for 30 min. Next, it was added with 50% glycerol to a final concentration of 10%. Subsequently, the samples were loaded onto a 5% Native polyacrylamide gel in 0.4x TBE. It was run at 300 volts for 1 hour at 4°C. After that, the gels were scanned using Typhoon™ FLA 9500 (GE Healthcare) for Cy5-labeled nucleosomes or Odyssey® CLx Imaging System (LI-COR) for IRD700/IRD800-labeled nucleosomes. After that, the DNA- or mononucleosome-bound remodeler was quantified using ImageQuant TL (GE Healthcare) by normalizing with the input containing only mononucleosomes.

2.2.4.8 Competitive electrophoretic mobility shift assay (cEMSA)

The competitive EMSA (cEMSA) was performed to determine the preferences of the remodelers to specific nucleosomes. Like the competitive nucleosome sliding assay, two nucleosomes labeled with different fluorescence (IRD700 or IRD800) were added to a reaction containing other components described above. Nevertheless, a lower concentration of each mononucleosome (0.5 nM) was used. After the samples were resolved on 5% Native PAGE gels in 0.4x TBE, the shifted mononucleosomes were detected using Odyssey® CLx Imaging System (LI-COR) and further quantified using ImageQuant TL (GE Healthcare).

2.2.4.9 Co-immunoprecipitation (Co-IP)

The protein-protein interactions between the Isw1 mutants with Esc8, as well as the Isw1 with Esc8 mutants, were determined by co-immunoprecipitation (Co-IP). The protein Esc8 conjugated with TAP-tagged was used as a bait protein that binds

to the resin and interacts with its protein interactor Isw1. The following were the detailed instructions for the co-immunoprecipitation assay, starting with the culture of yeast cells and continuing with the preparation of whole-cell lysate and Co-IP. The yeast strains containing either Isw1 mutants or Esc8 mutants were inoculated in 5 mL YPD medium and grown overnight at 30°C. Additionally, the wild-type and yeast strains containing the Isw1 and Esc8-TAP-tagged were used as negative and positive controls, respectively. On the following day, 3-4 mL of overnight culture was added into a 60 mL fresh YPD medium and incubated at 30°C for 8 hours with 150 rpm agitation. Next, 10 mL of day culture was inoculated into a 2 L fresh YPD medium and further incubated overnight at 30°C with 150 rpm agitation. A total of 6 L culture was prepared for each yeast strain. The cells were pelleted with centrifugation at 5,000 rpm for 10 min at 4°C. The 1 L of cell culture pellet was washed with 20 mL of cold 1x PBS and centrifuged at 4,000 rpm for 15 min at 4°C. The cell pellet was resuspended with Calmodulin Pull-Down Buffer with a ratio of 1:1. Subsequently, the cell suspension was carefully dropped-by-dropped into liquid nitrogen and caused the cell to freeze like popcorn. The cell popcorn was stored at -80°C until further use.

Furthermore, the cells were homogenized using a freezer mill (SPEX 6870 Freeze/Mill®). A total of 2 mL cell suspension was added with 2 µL of protease inhibitor cocktail (Sigma, #P8215), 2 µL of heparin (10 mg/mL), and 2 µL Benzonase (2.5U/µL). After that, the whole cell lysate in the supernatant was collected with centrifugation at 14,000 rpm for 20 min at 4°C and further quantified using Bradford protein assay (Bio-Rad, #5000006). A total of 4 mg of whole cell lysate was added into a 1.5 mL microcentrifuge tube containing 60 µL of pre-washed Calmodulin-Sepharose resin (Cytiva, #17-0529-01). The mixture was then incubated for 2 hours at 4°C on a rocker shaker (NeoLab) with slow agitation to allow the protein complex to bind with the resin via TAP-tagged conjugated to Esc8. The sample was centrifuged at 2,300 rpm for 30 seconds at 4°C, and the supernatant was discarded. Then, the sample was washed thrice with 0.5 mL Calmodulin Pull-Down Buffer and incubated on a shaker for 5 min at 4°C each wash before centrifugation at 2,300 rpm for 30 sec at 4°C. After the resin was collected, it was resuspended with 14 µL of 5x SDS Sample Buffer. Furthermore, both input and IP samples were resolved on 10% SDS-PAGE and continued with a western blot. For detection, the primary antibody peroxidase anti-peroxidase (1:1000) and the secondary antibody of goat anti-rat IgG antibody-HRP conjugated (1:5000) were used for Esc8-TAP protein and its mutants. Furthermore, the Isw1 antibody (1:50) was utilized for the Isw1 protein and its mutants.

2.2.4.10 Restriction enzyme accessibility assay

The restriction enzyme accessibility assay was carried out by Lorenz Spechtenhauser from Prof. Dr. Philipp Korber's research group, as described **(Krietenstein et al., 2016)** with some modifications. This assay is another technique approach used to test the ability of Isw1c to slide nucleosomes by detecting changes in DNA accessibility. Briefly, SGD chromatin, containing a 601-sequence positioned nucleosome at the KpnI, was prepared by mixing the DNA fragment and histone octamers under salt gradient dialysis (SGD). Then, the remodeler was added to the reconstitution reaction containing SGD chromatin. After incubation, the DNA was purified using protein K digestion, followed by phenol extraction and ethanol precipitation. The samples were then analyzed using a standard agarose gel.

2.2.4.11 Genome-wide *in vitro* reconstitution assay

The genome-wide *in vitro* reconstitution assay was performed by Drin Shabani from Prof. Dr. Philipp Korber's research group, as described **(Oberbeckmann et al., 2021)** with some modifications. This assay was used to determine whether Isw1c exhibits abilities to create spacing and phasing of nucleosomal arrays. This approach involves four steps. First, chromatin was prepared using salt gradient dialysis (SGD), which was then referred to as SGD chromatin. In this SGD chromatin, the nucleosomes were reconstituted at intrinsically preferred positions by mixing genomic plasmid libraries with purified histone octamers. Most of these nucleosomes are expected to be positioned at non-physiological locations. Second, a genome-wide remodeling reaction was performed by incubating the SGD chromatin with ATP, purified remodeler Isw1c, and the barrier Abf1 or the restriction enzyme KpnI. Third, the nucleosome pattern was analyzed using MNase-seq. Fourth, the data generated from MNase-seq was processed using bioinformatics.

2.2.5 AlphaFold structural analysis

The AlphaFold predicted structures of Isw1a and Isw1c were generated by Dr. Maren Heimhalt and further analyzed by me using UCSF ChimeraX-1.6.1 and PyMOL software. The quality and the accuracy of the AlphaFold predicted structures were assessed from the AlphaFold Error Plot. This included the pLDDT (Predicted local distance difference test) and the PAE (Predicted aligned error). To determine the similarities and differences between two proteins, two protein structures were superimposed using the matchmaker command in UCSF ChimeraX-1.6.1. Moreover, the potential residue pairs in the SLIDE domain of Isw1 interacting with Esc8 were identified by analyzing each residue pair that has a positive-negative surface charge interaction, hydrophobic contacts, or hydrogen bond. The cut-off distance between residues in hydrophobic contacts and hydrogen bonds was 4 Å and 3.6 Å, respectively.

3. Results

3.1 Expression and purification of Isw1c

3.1.1 Yeast proteins

3.1.1.1 The expression of Esc8 and purification of Isw1c complex from *S. cerevisiae*

Previously, tandem affinity purification and mass spectrometry identified protein interactors of Isw1. Among all, Esc8 is suggested to interact with Isw1 **(Gavin et al., 2002)**. In the Smolle Lab, Esc8 was also identified to interact with Isw1 by Isw1-TAP-tagged affinity purification and mass spectrometry **(Supplementary Table 1)**. To confirm that Isw1 and Esc8 interact, I further purified both proteins as a complex from *S. cerevisiae*. I used IgG and calmodulin sepharose affinity chromatography for the Esc8-TAP yeast strain. As a result, Isw1 and Esc8-CBP-tagged were shown as two distinct protein bands with molecular masses of 131 kDa and 100 kDa, respectively, as expected **(Fig. 11A)**. Although the molecular mass of Esc8-CBP-tagged is 86 kDa, it migrates slower and appears at around 100 kDa in SDS-PAGE gels. Nonetheless, this purification confirms that Isw1 binds to Esc8 and forms a protein complex, which we named Isw1c.

The purification of native Isw1c from yeast yielded low amounts of protein. Mass spectrometry analysis of Isw1-TAP-tagged showed that Esc8 was about 20 to 70 times less abundant than other associated Ioc subunits interacting with Isw1, based on the spectral count **(Supplementary Table 1)**.

The low abundance of Isw1c posed a significant obstacle to conducting subsequent experiments testing its function using biochemical assays. To increase the expression levels of Esc8 in yeast, I replaced its native promoter with a total of 6 constitutive or inducible promoters in an *ioc2*Δ *ioc3*Δ yeast strain. The constitutive promoters include glyceraldehyde-3-phosphate dehydrogenase (*GPD*), alcohol dehydrogenase (*ADH*), and translational elongation factor EF-1 alpha (*TEF*), whereas the inducible promoters include copper metallothionein (*CUP1*), galactokinase (*GAL1*), methionine 25 (*MET25*). The names and genotypes of the yeast strains are provided in section 2.1.2. After replacing the promoters, I determined the protein expression levels of Esc8. As a result, all promoters exhibited higher expression levels for Esc8 compared to its native promoter **(Fig. 11B)**. While all constitutive promoters yielded similar expression levels of Esc8, the inducible promoters displayed some variation in the expression levels. Upon comparative analysis of all the promoters, it was found that *pGAL1* had the highest amount of Esc8 protein, followed by *pADH*, *pGPD*, *pTEF*, *pMET25*, and *pCUP1* **(Fig. 11B)**. From all the promoters, I decided to select one constitutive promoter and one inducible promoter, namely *pADH* and *pCUP1*, respectively, for protein purification. This decision was based on the representative expression profile, wherein both promoters displayed a different moderate expression level from each other.

Furthermore, I purified Isw1c from yeast strains expressing Esc8-TAP-tagged from *ADH* and *CUP1* promoters. The yeast strain with *pCUP1-ESC8-TAP in ioc2*Δ *ioc3*Δ was induced with 100 µM copper for two hours in the late log phase. In contrast to the *CUP1* inducible promoter, the *ADH* constitutive promoter promotes a continuous transcription of the gene. Both yeast cultures were harvested, lysed, and processed using TAP purification. In the purified samples, both the Isw1 and Esc8-CBP proteins with molecular masses of 131 kDa and 100 kDa were observed **(Fig. 11C)**. Comparing these purified proteins, the Isw1c complex from the *pADH*-driven expression showed a higher amount of Isw1 and twice the amount of Esc8-CBP-tagged compared to the Isw1c complex from *pCUP1*-driven expression **(Fig. 11C)**. Ultimately, I successfully purified the Isw1c complex, yielding sufficient amounts of protein to characterize its functions using biochemical assays.

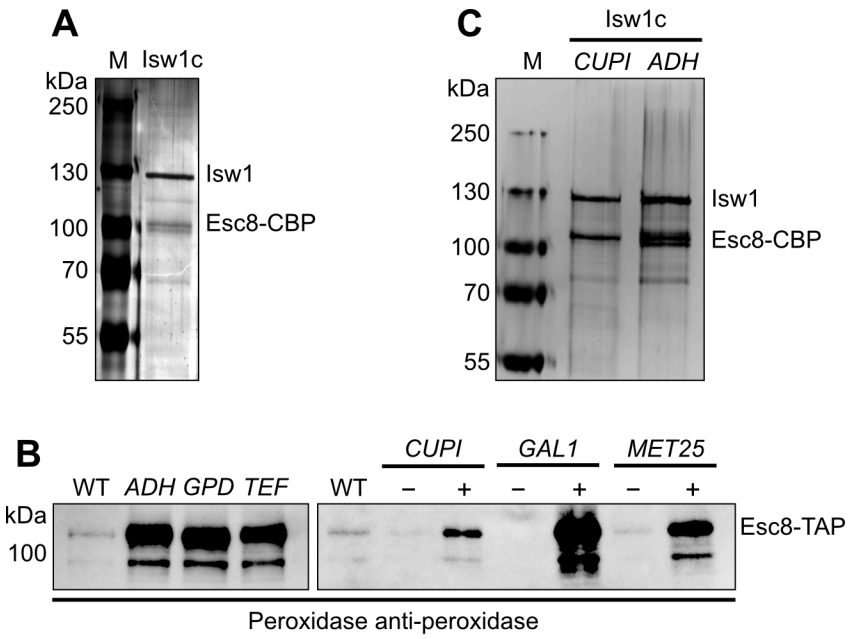

Figure 11. Expression levels of Esc8 from various promoters and purified Isw1c from *S. cerevisiae*. (A) Native purified Isw1c. **(B)** Whole-cell extracts from yeast strains containing modified promoters were resolved on 10% SDS-PAGE and analyzed by western blot using peroxidase anti-peroxidase antibody. **(C)** Purified Isw1c from yeast strains containing *pCUPI-ESC8* and *pADH-ESC8*. All purified Isw1c were separated on 10% SDS-PAGE and visualized by silver staining. Protein markers (M). Cultures were either not induced (-) or induced under respective conditions (+).

3.1.2 Recombinant proteins

In an attempt to obtain a large amount of Isw1c for further biochemical assays, I generated expression constructs of the recombinant Isw1c (rIsw1c) complex from *E. coli*. Throughout the process, two strategies were used to obtain the purified rIsw1c. One strategy involved using a co-expression vector for the dual expression of 6xHis-tagged Esc8 and Isw1. The other strategy involved overexpressing individual proteins from separate vectors, including 6xHis-tagged Esc8, 6xHis-MBP-tagged Isw1, 6xHis-MBP-tagged Esc8, and GST-tagged Isw1. All constructs were transformed into *E. coli* Rosetta (DE3) competent cells. Furthermore, I carried out many optimizations in protein overexpression and tested protein solubility, tag cleavage, and protein purification for each construct. These optimizations varied between the constructs but had the same objective to achieve a good expression level of the soluble protein and

obtain the purified proteins. Except for GST-tagged Isw1, the expression and purification strategies have been established in the Smolle Lab.

3.1.2.1 Overexpression and solubility test for recombinant Isw1c

Firstly, I used a co-expression vector that allows the expression of both 6xHis-tagged Esc8 and Isw1 from the same plasmid. Both proteins were expected to interact and form the rIsw1c complex. To determine optimal overexpression conditions for this construct together with a good amount of soluble protein, the recombinants were induced by 0.5 mM IPTG at various temperatures of 24°C for 4 and 6 hours, 30°C for 4 hours, and 37°C for 4 hours. After induction, overexpressed proteins were observed with two distinct bands representing Isw1 with molecular mass at 130 kDa and 6xHis-tagged Esc8 of 100 kDa **(Fig. 12A, B)**. In addition, both 6xHis-tagged Esc8 and Isw1 proteins showed an increase in expression proportional to the increment in temperature. More protein was expressed at 37°C for 4 hours, and less protein was expressed at 24°C for 4 hours. Since the expressed protein may form insoluble protein instead of forming soluble protein, I further tested protein solubility for each overexpression condition. Soluble protein was found in the supernatant, while the insoluble protein was detected in the pellet. Of all conditions, I discovered that both 6xHis-tagged Esc8 and Isw1 were most soluble when overexpressed at 24°C for 4 or 6 hours **(Fig. 12B, C)**. Notably, 6xHis-tagged Esc8 was more highly expressed compared to Isw1. Given that the disproportional protein amount between 6xHis-tagged Esc8 and Isw1 from this construct might affect the rIsw1c complex functions, I decided not to use this rIsw1c protein complex for biochemical assays.

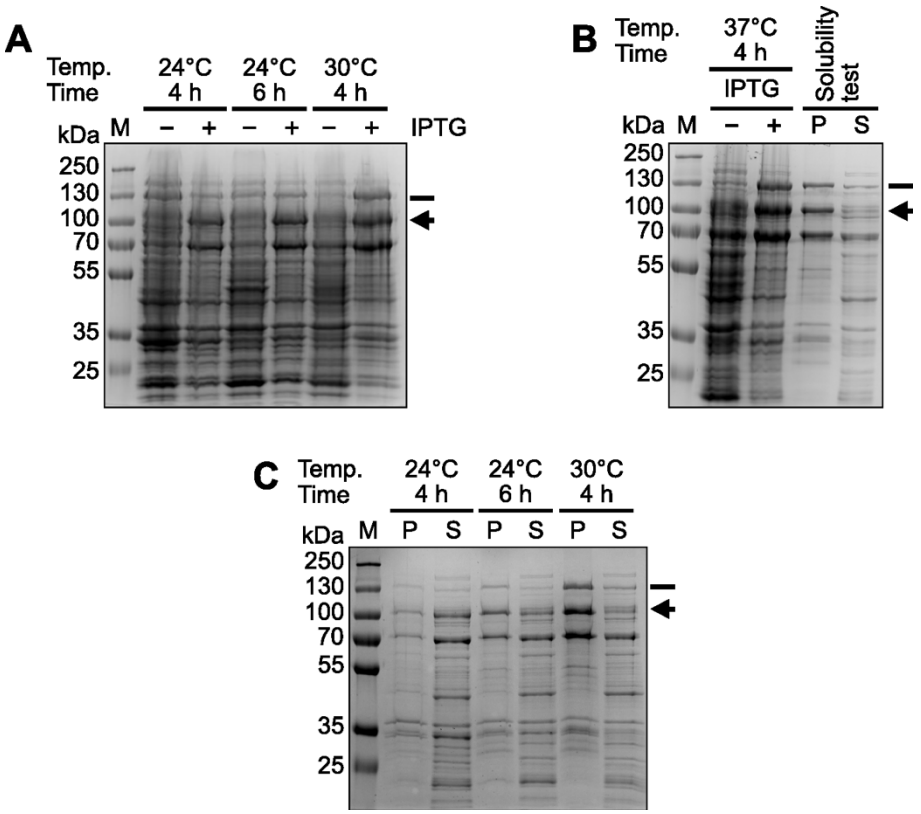

Figure 12. Optimization of protein overexpression and solubility test of co-expression 6xHis-tagged Esc8 and Isw1. (A) Protein expression was induced by the addition of 0.5 mM IPTG at 24°C for 4 hours and 6 hours, and 30°C for 4 hours. **(B)** Protein expression was induced by the addition of

0.5 mM IPTG at 37°C for 4 hours, followed by a solubility test. **(C)** Solubility test for the overexpression condition from Panel A. Protein markers (M). Cultures were not induced (-) or induced with IPTG (+). Pellet (P) and supernatant (S). Fractions are indicated. The arrow (←) represents 6xHis-tagged Esc8, while the line (—) represents Isw1.

Alternatively, I attempted to obtain rIsw1c by expressing both proteins from separate vectors. The first protein was 6x-His-tagged Esc8. Recombinant cells were induced with 0.5 mM IPTG at 24°C for 6 hours. This resulted in a good amount of expressed 6xHis-tagged Esc8 protein; however, the protein was mostly insoluble **(Fig. 13A)**. Furthermore, inducing protein expression with the addition of 0.1, 0.2, and 0.5 mM IPTG at a lower temperature of 16°C overnight led to lower protein expression levels, which were barely detectable in the gel **(Fig 13B)**. To improve protein expression and increase the yield of soluble proteins, I used strategies involving heat shock and osmotic stress. Implementing heat shock before induction can enhance the solubility of some recombinant proteins, though the mechanism is not fully understood **(Chen et al., 2002)**. For osmotic stress, I added additives such as high salt, sorbitol, or ethanol during the growth and induction of cells. Mechanistically, this stress triggers the increase in osmolytes that can act as “chemical chaperones” and thus increase the stability of the protein **(Bhatwa et al., 2021; Oganesyan et al., 2007)**. As a result of the experiments, adding 3% ethanol and 0.5M sorbitol increased the protein expression levels of 6xHis-tagged Esc8 **(Fig. 13C, D)**. Nonetheless, neither of these conditions improved the formation of soluble protein, as depicted in **Figure 13E**.

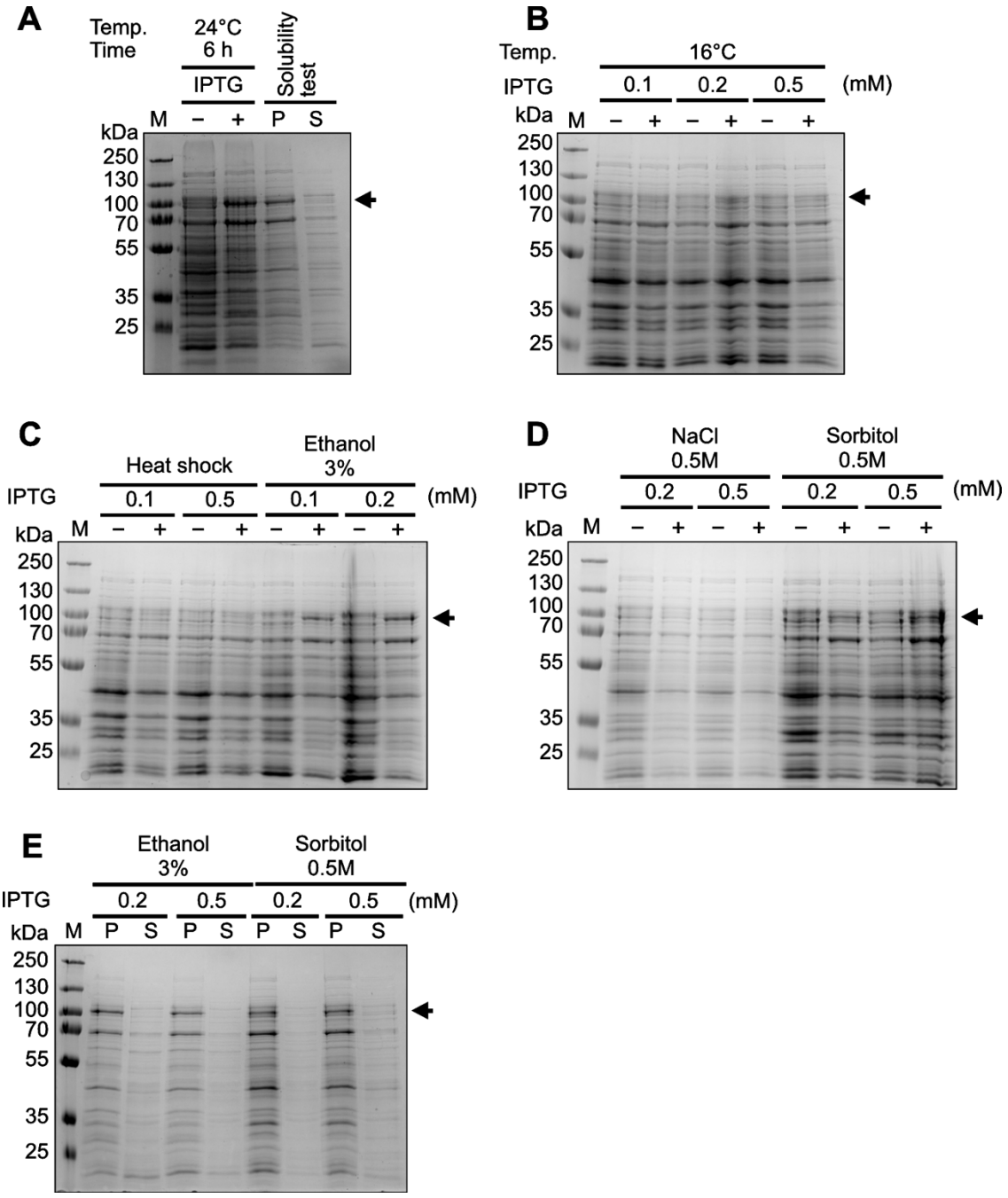

Figure 13. Optimization for protein overexpression and the solubility test of 6xHis-tagged Esc8. **(A)** Protein expression was induced by the addition of 0.5 mM IPTG at 24°C for 6 hours, and the protein solubility was tested. **(B)** Protein expression was induced with various IPTG concentrations at 16°C overnight. **(C, D)** Effect of heat shock and osmotic stress on the expression of 6xHis-tagged Esc8. **(E)** Solubility test. Protein markers (M). Cultures were not induced (-) or induced with IPTG (+). Pellet (P) and supernatant (S). The Arrow (←) represents 6xHis-tagged Esc8. Fractions are indicated.

Since the 6xHis-tagged Esc8 was insoluble, I next used a dual tag protein of 6xHis-MBP-tagged conjugated to either Esc8 or Isw1 to enhance the protein solubility. Specifically, the maltose-binding protein (MBP) has been well-recognized for enhancing protein solubility by promoting the proper folding of its fusion protein **(Kapust & Waugh, 1999; Raran-Kurussi & Waugh, 2017)**. Both constructs were induced by the addition of 0.5 mM IPTG at 16°C for 20 hours, at 24°C for 6 hours, at 30°C for 4 hours, and at 37°C for 4 hours. Both 6xHis-MBP-tagged Esc8 and 6xHis-MBP-tagged Isw1 have respective molecular masses of 122 kDa and 150 kDa. While the protein expression yield for both proteins increased from 16°C to 30°C, a slight drop in yield was observed at 37°C **(Fig. 14A-C)**. Subsequently, the cells were lysed and checked for protein solubility. As shown in **Figure 14D**, the 6xHis-MBP-tagged Esc8 yielded a substantial amount of soluble protein, particularly under the expression condition at 24°C for 6 hours. On the other hand, the 6xHis-MBP-tagged Isw1 resulted in more insoluble protein detected in the pellet for all expression conditions **(Figure 14E, F)**. After all, I continued with the purification for 6xHis-MBP-tagged Esc8 and 6xHis-MBP-tagged Isw1, which were expressed under a condition of 24°C for 6 hours.

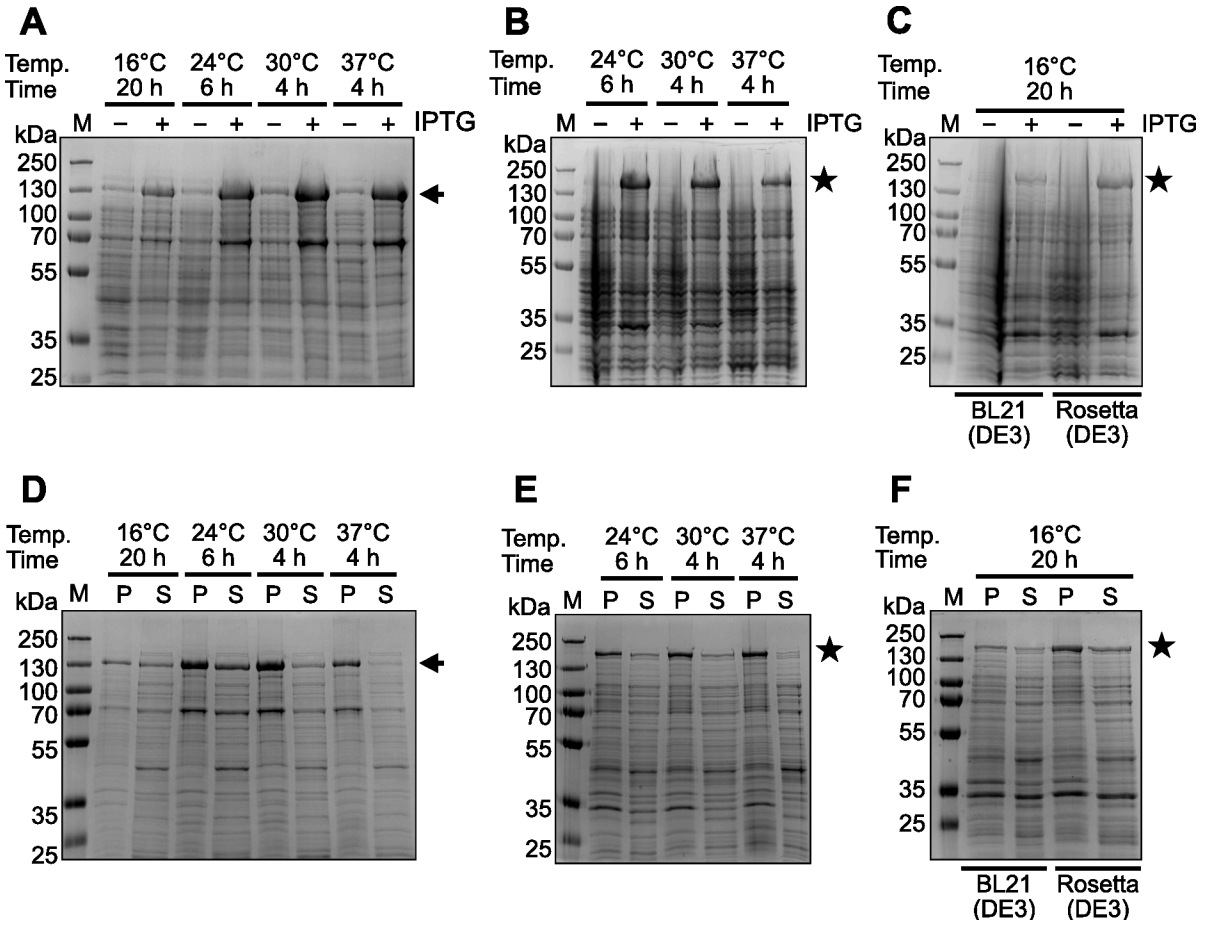

Figure 14. Optimization for overexpression and solubility test of 6xHis-MBP-tagged Esc8 and 6xHis-MBP-tagged Isw1. (A) Protein expression of 6xHis-MBP-tagged Esc8 was induced by the addition of 0.5 mM IPTG at various temperatures and respective incubation times. **(B, C)** Protein expression of 6xHis-MBP-tagged Isw1 was induced by the addition of 0.5 mM IPTG at various temperatures and respective incubation times. **(D)** Solubility test for 6xHis-MBP-tagged Esc8. **(E, F)** Solubility test for 6xHis-MBP-tagged Isw1. Protein markers (M). Cultures were not induced (-) or induced with IPTG (+). Pellet (P) and supernatant (S). The arrow (←) represents 6xHis-MBP-tagged Esc8, and the star represents 6xHis-MBP-tagged Isw1. Fractions are indicated.

In addition to the MBP tag, the glutathione S-transferase (GST) tag is also known to enhance protein solubility by acting as a chaperone to facilitate protein folding **(Harper & Speicher, 2011; Smith & Johnson, 1988)**. Due to the lower yield of soluble protein obtained with 6xHis-MBP-tagged Isw1, I subsequently utilized GST-tagged Isw1 as an alternative. Upon induction, GST-tagged Isw1 exhibited a high expression level, with half of the protein found to be soluble as detected in the supernatant **(Fig. 15)**. The molecular mass for GST-tagged Isw1 is about 151 kDa. The use of GST-tagged Isw1 significantly improved the solubility of Isw1.

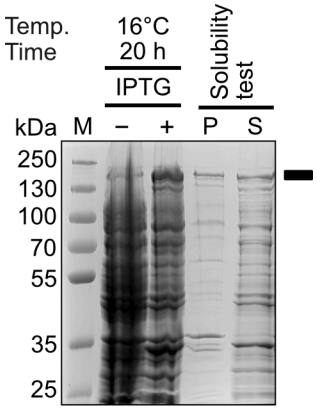

Figure 15. Overexpression and solubility of GST-tagged Isw1. Protein expression was induced by the addition of 0.5 mM IPTG at 16°C for 20 hours. Protein markers (M). Cultures were not induced (-) or induced with IPTG (+). Pellet (P) and supernatant (S). The rectangle (▬) represents GST-tagged Isw1.

3.1.2.2 Purification of recombinant Isw1 and Esc8

A total of 3 out of 5 proteins were subjected to purification. This included 6xHis-MBP-tagged Esc8, 6xHis-MBP-tagged Isw1 and GST-tagged Isw1. **Figure 16A** illustrates the schematic diagram for the different purification strategies employed for each protein. Multiple purification steps were used to enrich the target protein. Both 6xHis-MBP-tagged Esc8 and 6xHis-MBP-tagged Isw1 were subjected to Ni-NTA chromatography for the purification of 6xHis-tagged recombinant proteins. Both proteins were successfully purified; however, other non-specific proteins were still bound to the Ni-NTA agarose **(Fig. 16B, D)**. This purification strategy alone was not sufficient to remove all contaminants. Therefore, I used the eluted protein from Ni-NTA purification to conduct heparin affinity chromatography, which is commonly employed to purify DNA-binding proteins. In this step, I was able to remove many non-specific proteins and obtained both purified 6xHis-MBP-tagged Esc8 and 6xHis-MBP-tagged Isw1 **(Fig. 16C, E)**. Nevertheless, other proteins were detected in the elution fraction of 6xHis-MBP-tagged Isw1. Next, I performed size-exclusion chromatography of 6xHis-MBP-tagged Isw1 to separate the proteins by size further. Finally, both 6xHis-MBP-tagged Esc8 and 6xHis-MBP-tagged Isw1 were successfully purified with molecular masses of 122 kDa and 150 kDa, respectively **(Fig. 16C, F)**. Additionally, GST-tagged Isw1 was subjected to glutathione affinity chromatography, resulting in the purified GST-tagged Isw1 with a distinct band at 151 kDa **(Fig. 16G, H)**. In short, all the proteins were successfully purified.

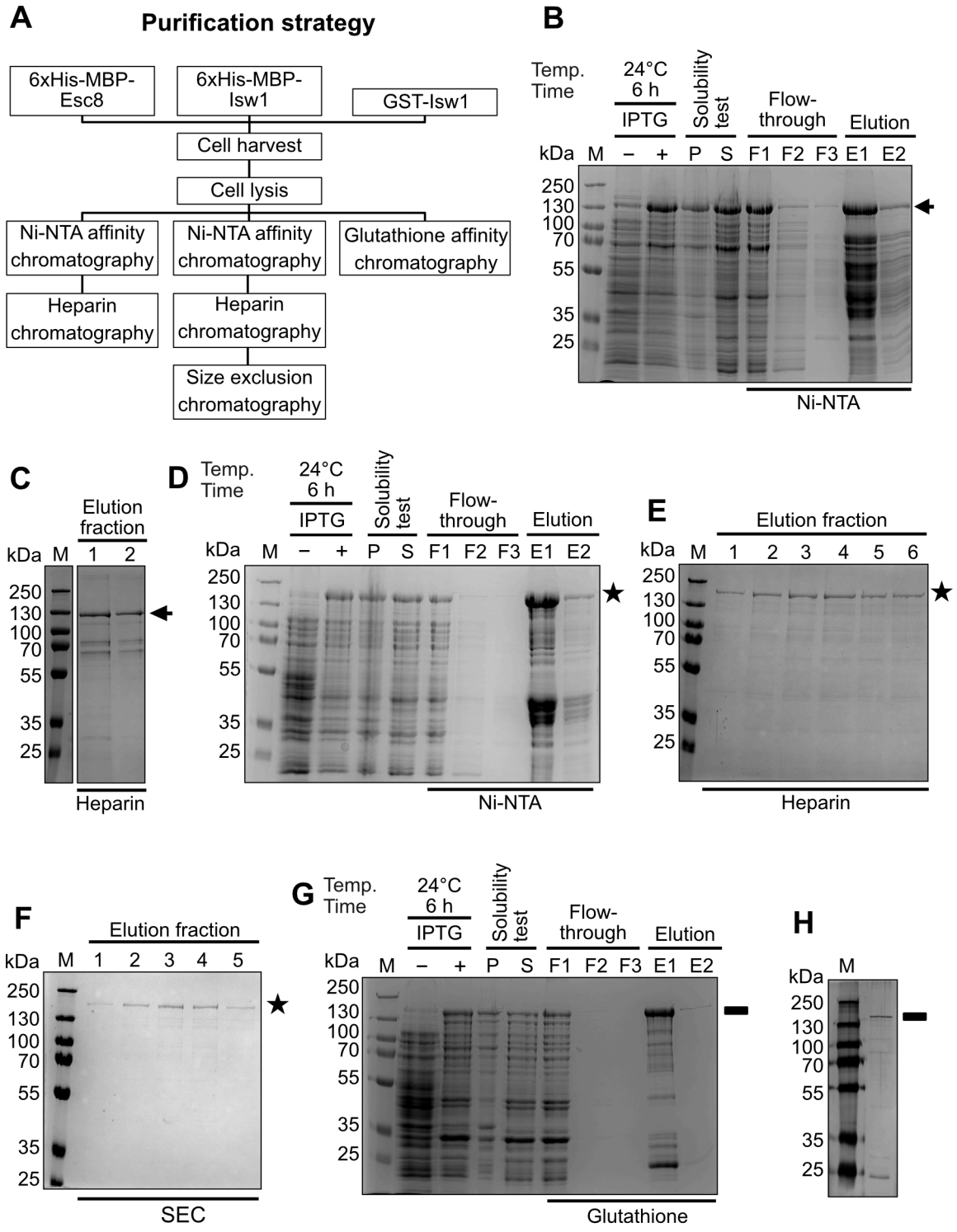

Figure 16. Purification of 6xHis-MBP-tagged Esc8, 6xHis-MBP-tagged Isw1 and GST-tagged Isw1. (A) Schematic representation of the purification strategy of 6xHis-MBP-tagged Esc8, 6xHis-MBP-tagged Isw1, and GST-tagged Isw1. **(B)** SDS-PAGE analysis of 6xHis-MBP-tagged Esc8 after Ni-NTA chromatography. **(C)** SDS-PAGE analysis of 6xHis-MBP-tagged Esc8 after heparin affinity chromatography. **(D)** SDS-PAGE analysis of 6xHis-MBP-tagged Isw1 after Ni-NTA chromatography. **(E)** SDS-PAGE analysis of 6xHis-MBP-tagged Isw1 after heparin affinity chromatography**. (F)** SDS-PAGE analysis of 6xHis-MBP-tagged Isw1 after size-exclusion chromatography. **(G)** SDS-PAGE analysis of GST-tagged Isw1 after glutathione affinity chromatography. **(H)** Purified protein GST-tagged Isw1. Protein markers (M). Cultures were not induced (-) or induced with IPTG (+). Pellet (P) and supernatant (S). Flow-through after protein binding to resin (F1), flow-through after washing steps (F2-

F3). Elution fractions (E1-E2). The arrow (🡐) represents 6xHis-MBP-tagged Esc8, the star (★) represents 6xHis-MBP-tagged Isw1 and the rectangle (▬) represents GST-tagged Isw1. Fractions are indicated.

3.1.2.3 Tag cleavage

Both 6xHis-MBP-tagged Isw1 and 6xHis-MBP-tagged Esc8 were conjugated with the same tag. Consequently, these proteins cannot be used in the same pull-down assay reaction for protein-protein interaction because both proteins will bind to the resin simultaneously. Therefore, cleaving the 6xHis-MBP-tag from one of the proteins was crucial. The tag cleavage is performed using HRV 3C protease, which recognizes a specific octapeptide sequence (LeuGluValLeuPheGlnGlyPro) and cleaves between Gln and Gly. In the assay, HRV 3C protease was added to the solution containing 6xHis-MBP-tagged Isw1/Esc8 to cleave the tag, and the mixture was incubated overnight at 4°C. As depicted in **Figure 17**, HRV 3C protease did not cleave 6xHis-MBP-tagged Isw1, resulting in the observation of an intact protein with a molecular mass of 150 kDa. The possible explanation for this was that the cleavage site was not accessible. Conversely, HRV 3C protease was able to cleave 6xHis-MBP-tagged Esc8, although it was not cleaved completely. Thus, Esc8 with a molecular mass of 100 kDa was observed in the gel **(Fig. 17)**. Furthermore, the attempt to obtain the Esc8 protein alone from the remaining proteins was not successful **(Data is not shown)**.

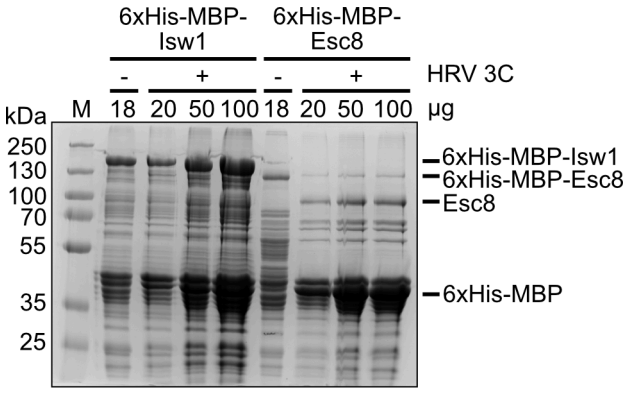

Figure 17. Tag cleavage of 6xHis-MBP-tagged Isw1 and 6xHis-MBP-tagged Esc8. Various amounts of purified protein were used for tag cleavage. Protein marker (M). Protein was uncleaved (-) or cleaved (+) with HRV 3C protease. Proteins are indicated.

3.1.2.4 Protein-protein interaction between Isw1 and Esc8

To acquire the rIsw1c complex, I performed a pull-down assay by incubating purified GST-tagged Isw1 and 6xHis-MBP-tagged Esc8 and then loaded the mixture onto amylose resin. The protein complex is expected to bind to the resin via 6xHisMBP-tagged Esc8 and then elute only in the elution fraction. However, I found that only 6xHis-MBP-tagged Esc8 was detected in the elution fraction, while GST-tagged Isw1 was found in the flow-through fraction **(Fig. 18)**. As a negative control, GST-tagged Isw1 alone did not bind to amylose resin as expected. This result revealed that 6xHis-MBP-tagged Esc8 and GST-tagged Isw1 did not form an Isw1c complex. Steric hindrance could be the cause of this interaction barrier, arising from the large size of both the MBP-tagged and GST-tagged, which obstructs binding access and

thereby impedes the formation of a protein complex. Ultimately, the attempts to obtain recombinant Isw1c complex from reconstitution were unsuccessful.

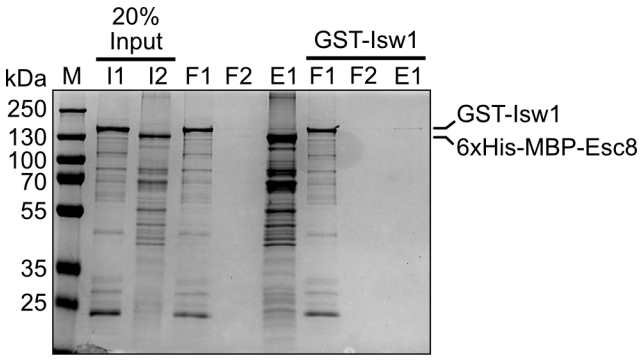

Figure 18. Protein-protein interactions between GST-tagged Isw1 and 6xHis-MBP-tagged Esc8. Protein markers (M). Input for GST-tagged Isw1 (I1) and input for 6xHis-MBP-tagged Esc8 (I2). Flowthrough after protein binding to amylose resin (F1) and flowthrough after washing step (F2). Elution fraction (E1).

3.2 Characterization of Isw1c as a chromatin remodeler

3.2.1 Isw1c hydrolyzes ATP in the presence of nucleosomes

The fundamental property of remodelers is their ability to hydrolyze ATP. Here, I carried out an NADH-coupled ATP hydrolysis assay to test whether Isw1c exhibits this ability. Additionally, I compared its activity to that of Isw1a, which served as a positive control. In principle, the assay measures the reduction rate of NADH absorbance at 340 nm, which is proportional to the rate of ATP hydrolysis **(Radnai et al., 2019; Sehgal et al., 2016)**. **Figure 19A** illustrates a schematic diagram of the NADH-coupled ATP hydrolysis assay used to measure the ATP hydrolysis activity of a remodeler. Specifically, equimolar amounts of the Isw1c or Isw1a complex were tested for ATPase activity in the presence of different substrates such as DNA, histone, or nucleosomes under saturating ATP conditions. In agreement with a published paper **(Vary et al., 2003)**, the ATPase activity of the Isw1a complex was strongly stimulated by the presence of nucleosomes but weakly stimulated by either DNA or histones **(Fig. 19B)**. Approximately 192 molecules of ATP were hydrolyzed per minute by Isw1a in the presence of nucleosomes. Similar to Isw1a, the Isw1c complex demonstrated ATPase activity stimulated by the presence of nucleosomes, albeit at a lower level of about 65 molecules of ATP hydrolyzed per minute **(Fig. 19B)**. Additionally, the ATPase activity of Isw1c with nucleosome was twofold higher than with DNA alone. However, when comparing the two remodelers, Isw1c showed a threefold lower ATPase activity rate than Isw1a. Nevertheless, Isw1c exhibits the ability to hydrolyze ATP when stimulated by the presence of nucleosomes.

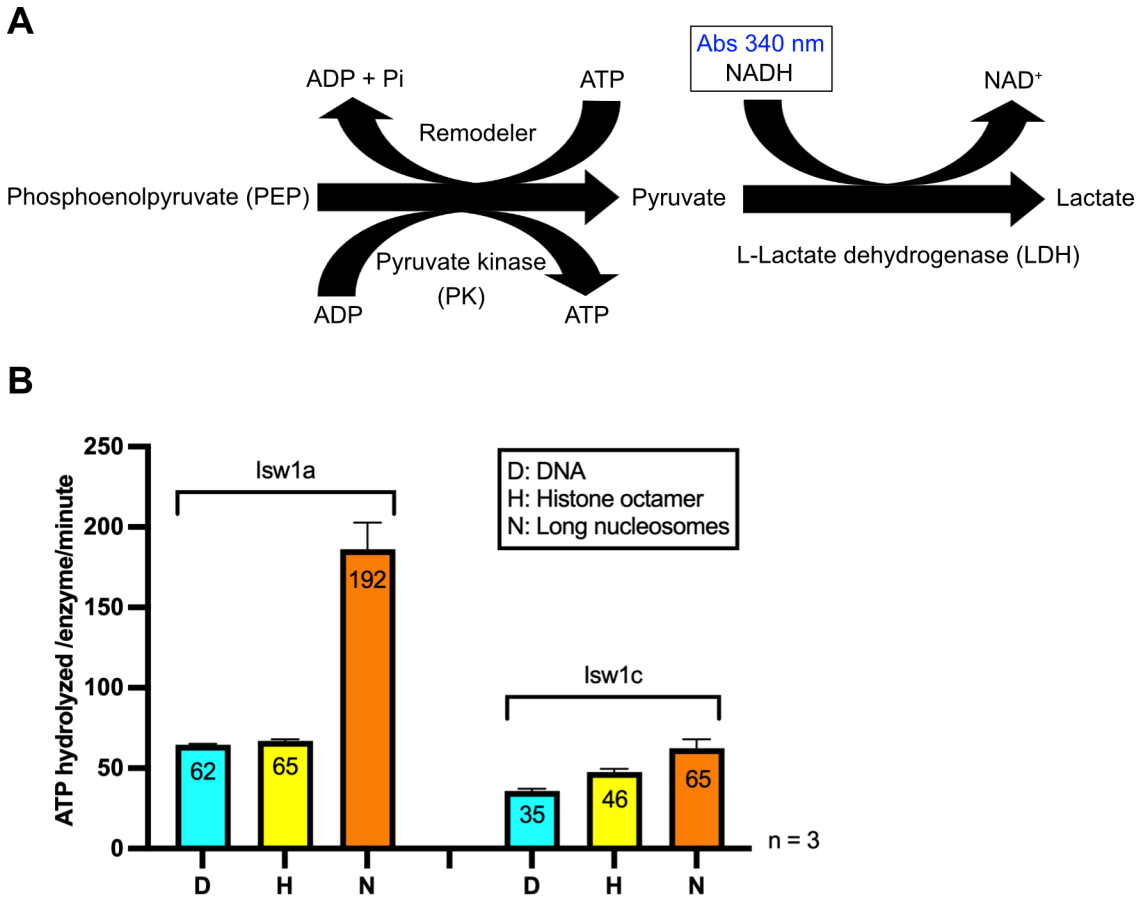

Figure 19. ATPase activities of Isw1a and Isw1c with various substrates. (A) Schematic diagram of the NADH-coupled ATP hydrolysis assay to measure ATP hydrolysis activity of a remodeler. Per cycle of ATP hydrolysis, this follows with a remodeler hydrolyzes ATP to ADP and phosphate (Pi), and subsequently, pyruvate kinase (PK) converts one molecule of phosphoenolpyruvate (PEP) to pyruvate wherein the ADP is converted back to ATP. After that, the L-lactate dehydrogenase (LDH) converts pyruvate to lactate, oxidizing one NADH molecule to NAD+. The decrease in NADH concentration is then measured at an absorbance of 340 nm, which is proportional to the rate of ATP hydrolysis. **(B)** ATPase assays for Isw1a and Isw1c complexes in the presence of DNA, histone octamer, or nucleosomes. Experiments were performed in triplicate. The schematic diagram in Panel A is inspired by Radnai et al., 2019; Sehgal et al., 2016.

3.2.2 Isw1c binds to both DNA and nucleosomes but not NCPs

I next investigated the ability of Isw1c to bind double-stranded DNA, nucleosome core particles (NCPs), and nucleosomes using gel electrophoretic mobility shift assay (EMSA). In this assay, Isw1c was incubated with fluorescently labeled DNA or nucleosomes, and the mixtures were subjected to electrophoresis under native conditions on a polyacrylamide gel. When binding occurs, the complex migrates more slowly than the substrate (DNA or nucleosome) alone. Notably, Isw1c demonstrated the ability to bind to longer rather than shorter dsDNA fragments **(Fig. 20A, B)**. Multiple binding events were observed between Isw1c with longer DNA fragments. However, no interaction was observed when NCPs were used as a substrate **(Fig. 20C)**. Instead, the interaction of Isw1c to nucleosomes occurred only when at least one overhang DNA was present on the nucleosomes **(Fig. 20D)**.

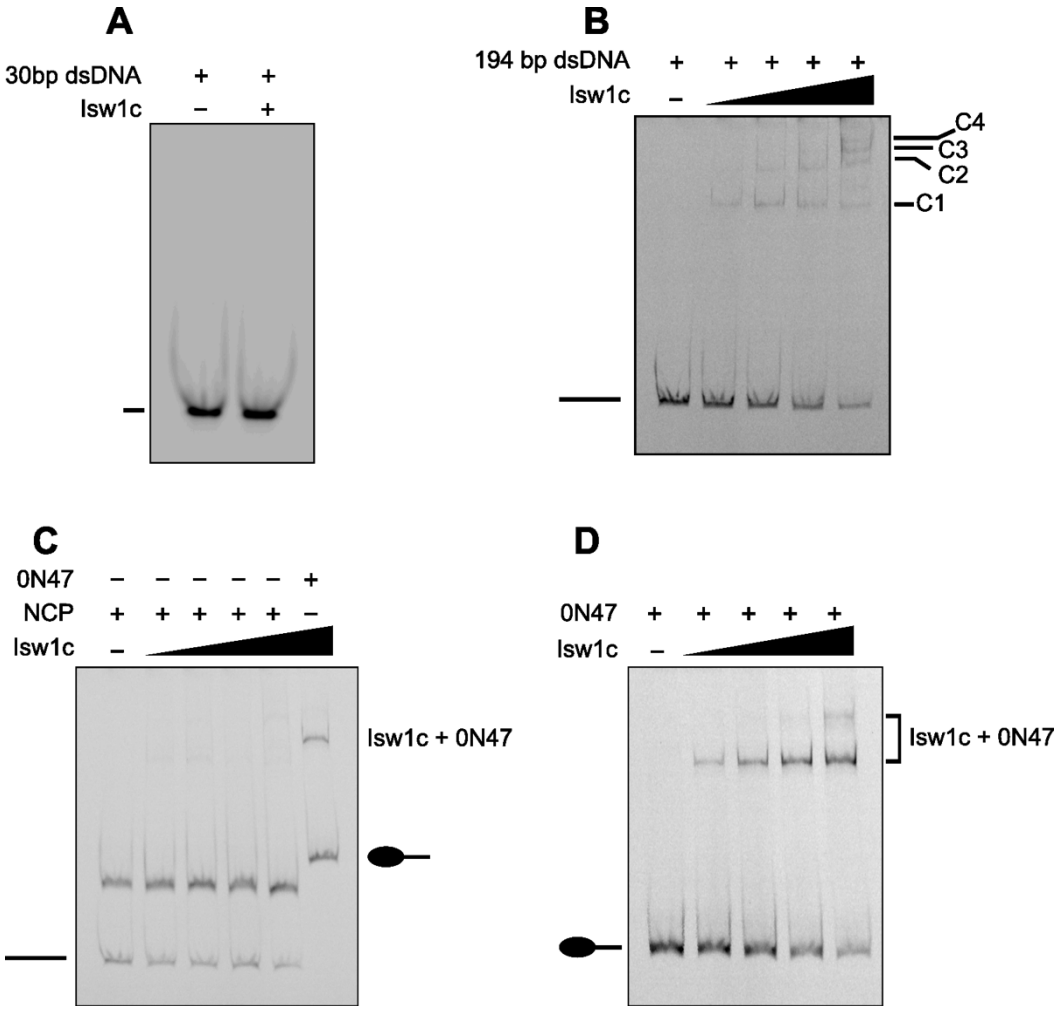

Figure 20. Binding activities of Isw1c with various substrates. (A) Native PAGE analysis of Isw1c binds to 30 bp dsDNA. **(B)** Native PAGE analysis of Isw1c binds to 194 bp dsDNA. **(C)** Native PAGE analysis of Isw1c binds to nucleosome core particles (NCPs). **(D)** Native PAGE analysis of Isw1c binds to end-positioned nucleosomes containing one overhang DNA (0N47). Free DNA (line), The reaction without Isw1c or substrates (-) and with Isw1c or substrates (+). Isw1c binds to DNA (C1-C4) or 0N47 nucleosomes (Isw1c + 0N47). For Panels B and D, experiments were performed in triplicate.

3.2.3 Isw1c preferably slides end-positioned nucleosomes over mid-positioned nucleosomes

At the beginning of the research, I first accessed the function of the native Isw1c in nucleosome sliding assays. The assay can be done in two different ways: time-dependent and concentration-dependent. For time-dependent assays, the purified Isw1c was incubated with reconstituted mononucleosomes and ATP for different lengths of time. Alternatively, various concentrations of purified Isw1c were used. In each assay, I used two differently positioned nucleosomes located at the 5' end of the DNA fragment (0N47) or at the middle position of the DNA fragment (34N37). The 0N47 nucleosomes have a 47 bp overhang, while the 34N37 nucleosomes have two overhangs on both sides, 34 bp on one side and 37 bp on the other side. Based on the observations from the sliding assays, the native Isw1c complex displayed sliding activity for the 5' end-positioned nucleosomes (0N47) towards the center position of the DNA **(Fig. 21A, B)**. This was shown with the appearance of a distinct band, implying the center-positioned nucleosomes that ran more slowly in the gel. Moreover,

the 0N47 nucleosomes were fully shifted with 8 fmol of purified native Isw1c in 10 minutes. Conversely, the native Isw1c showed very low remodeling activity on 34N37 nucleosomes **(Fig. 21A, B)**. Taken together, the native Isw1c can slide nucleosomes and demonstrates more efficiency in sliding the 0N47 nucleosomes than the 34N37 nucleosomes.

After testing the native Isw1c, I performed sliding assays using Isw1c purified from yeast containing *pCUP1-ESC8* or *pADH-ESC8* to determine whether these overexpressed proteins have a similar ability as the native Isw1c in sliding nucleosomes. Isw1c purified from yeast containing *pADH-ESC8* remodeled nucleosomes faster than that from *pCUP1-ESC8* cells, possibly due to higher levels of accessory Esc8 **(Fig. 21C)**. However, Isw1c purified from yeast containing *pCUP1-ESC8* more closely resembled wildtype Isw1c **(Fig. 21C)**.

To further ascertain that the Isw1c purified from yeast containing *pCUP1-ESC8* acts in a similar way in sliding nucleosomes as the native Isw1. I conducted additional nucleosome sliding assays with 0N37 and 34N37 nucleosomes. Consistent with the native Isw1c, the purified Isw1c (*pCUP1-ESC8*) mobilized the 0N47 nucleosomes more efficiently compared to 34N37 nucleosomes **(Fig. 21D)**. Nearly all the 0N47 nucleosomes were shifted, whereas only 50% of 34N37 nucleosomes were shifted **(Fig. 21E)**. This result confirmed that the Isw1c purified from yeast containing *pCUP1-ESC8* displayed similar efficiency in mobilizing end-positioned nucleosomes as the native Isw1c.

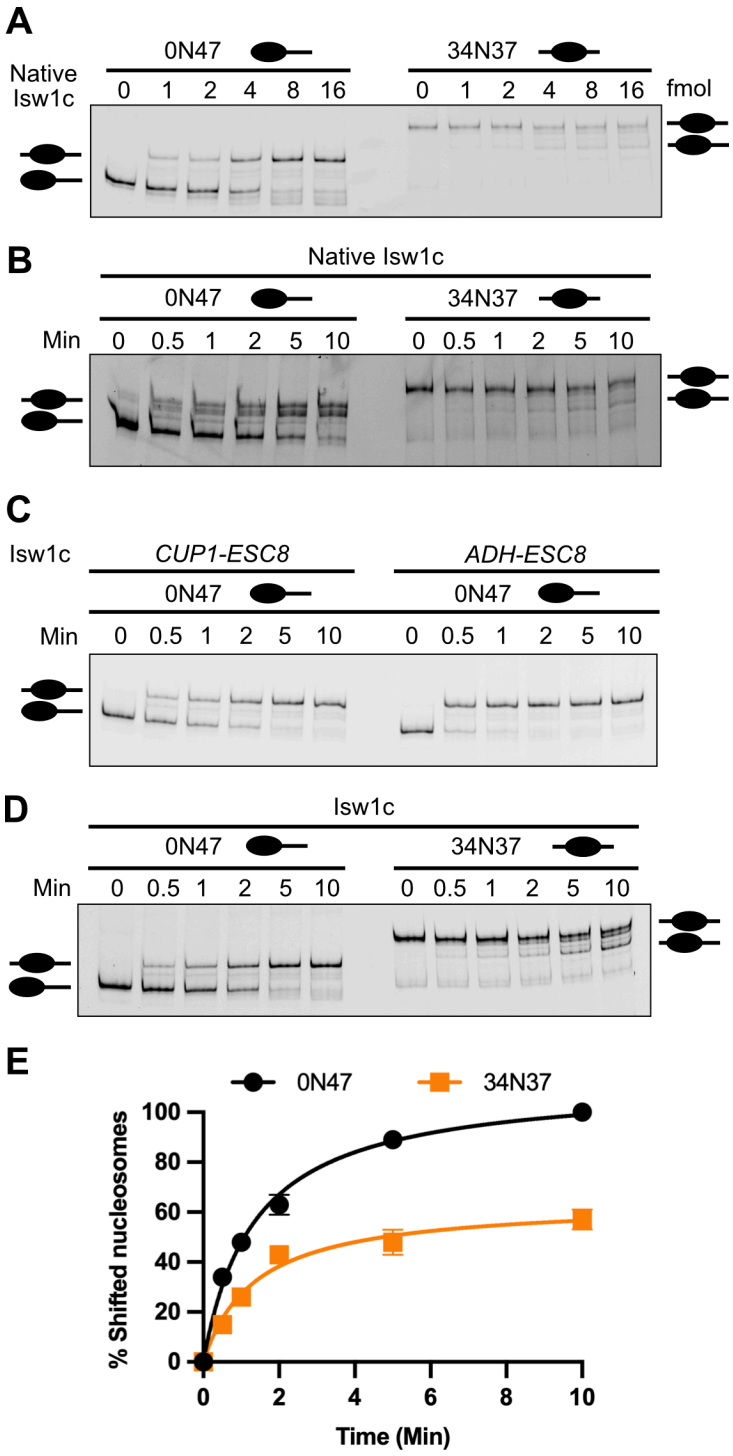

Figure 21. Sliding activities of native Isw1c and Isw1c purified from yeast containing *pCUP1-ESC8* or *pADH-ESC8*. (A) Sliding assays with various amounts of native Isw1c from 0 fmol to 16 fmol **(B)** Sliding assays of native Isw1c with different time points of incubation with nucleosomes: 0 sec, 30 sec, 1 min, 2 min, 5 min, and 10 min **(C)** sliding assays of purified Isw1c (*pCUP1-ESC8* or *pADH-ESC8*) with different time points of incubation with nucleosomes. **(D)** Sliding assays of purified Isw1c (*pCUP1-ESC8*) with two different positioned nucleosomes. **(E)** Quantification of the shifted nucleosomes in accordance with Panel D. Experiments in Panel A were performed in duplicate, while experiments in Panel B and D were carried out in triplicate. The 0N47 represents the end-positioned nucleosomes, and the 34N37 represents the middle-positioned nucleosomes.

3.2.4 Isw1c generates regularly spaced and phased nucleosome arrays

After testing the ability of Isw1c to slide nucleosomes, I collaborated with Drin Shabani and Lorenz Spechtenhauser from Prof. Dr Philipp Korber's research group to further characterize its role in nucleosome organization. First, we employed a restriction enzyme accessibility assay as an additional experimental approach to test the remodeling activity of purified Isw1a and Isw1c. In general, this assay evaluates remodeling activity by assessing changes in DNA accessibility at site-specific restriction enzyme (RE) before and after remodeling. Prior to remodeling, nucleosomes are positioned at specific DNA sequences, blocking access for restriction enzymes to cleave the DNA fragment. Thus, a single uncut DNA fragment with a size of 4929 bp can be observed **(Fig. 22A, Lane 1)**. However, upon remodeling, these RE sites become more accessible, resulting in the cutting of DNA. As illustrated in **Figure 22A,** there was the appearance of a cut DNA fragment with a size of about 3693 bp in both Isw1a **(Lane 2)** and Isw1c **(Lane 3)** samples. By comparing the two remodelers, Isw1a exhibited greater remodeling activity than Isw1c, as indicated by a higher amount of the cut fragment, which is in agreement with the results of the ATPase assay. This result confirmed that both purified Isw1a and Isw1c have active remodeling activities, as expected. The uncut DNA fragment remained either because a small number of nucleosomes were positioned over the RE site or the reaction did not proceed to completion.

Next, we determined whether Isw1c bears functions in spacing and phasing nucleosomes using a genome-wide *in vitro* reconstitution assay. In this assay, salt gradient dialysis (SGD) chromatin was incubated with ATP, purified remodeller, and the restriction enzyme KpnI or the barrier Abf1. Then, the nucleosome patterns were analyzed by MNase seq. Purified Isw1a remodeller was used as a positive control in the assay. Our findings revealed that Isw1c can generate spaced and phased nucleosome arrays, similar to Isw1a **(Fig. 22B, C)**. The activities of Isw1a detected here were also consistent with a previous study **(Krietenstein et al., 2016; Oberbeckmann et al., 2021)**. The observations of the spacing and phasing nucleosome arrays were based on the nucleosome peaks and positions in composite plots aligned to KpnI or Abf1 sites. Interestingly, Isw1c seems to position the flanking nucleosomes slightly closer to Abf1 sites than Isw1a **(Fig. 22C)**. Furthermore, in the absence of the Abf1, neither Isw1a nor Isw1c alone were capable of positioning *in vivo*-like +1 nucleosome on their own **(Fig. 22D)**. After all, we discovered that Isw1c has the ability to establish spaced and phased nucleosome arrays.

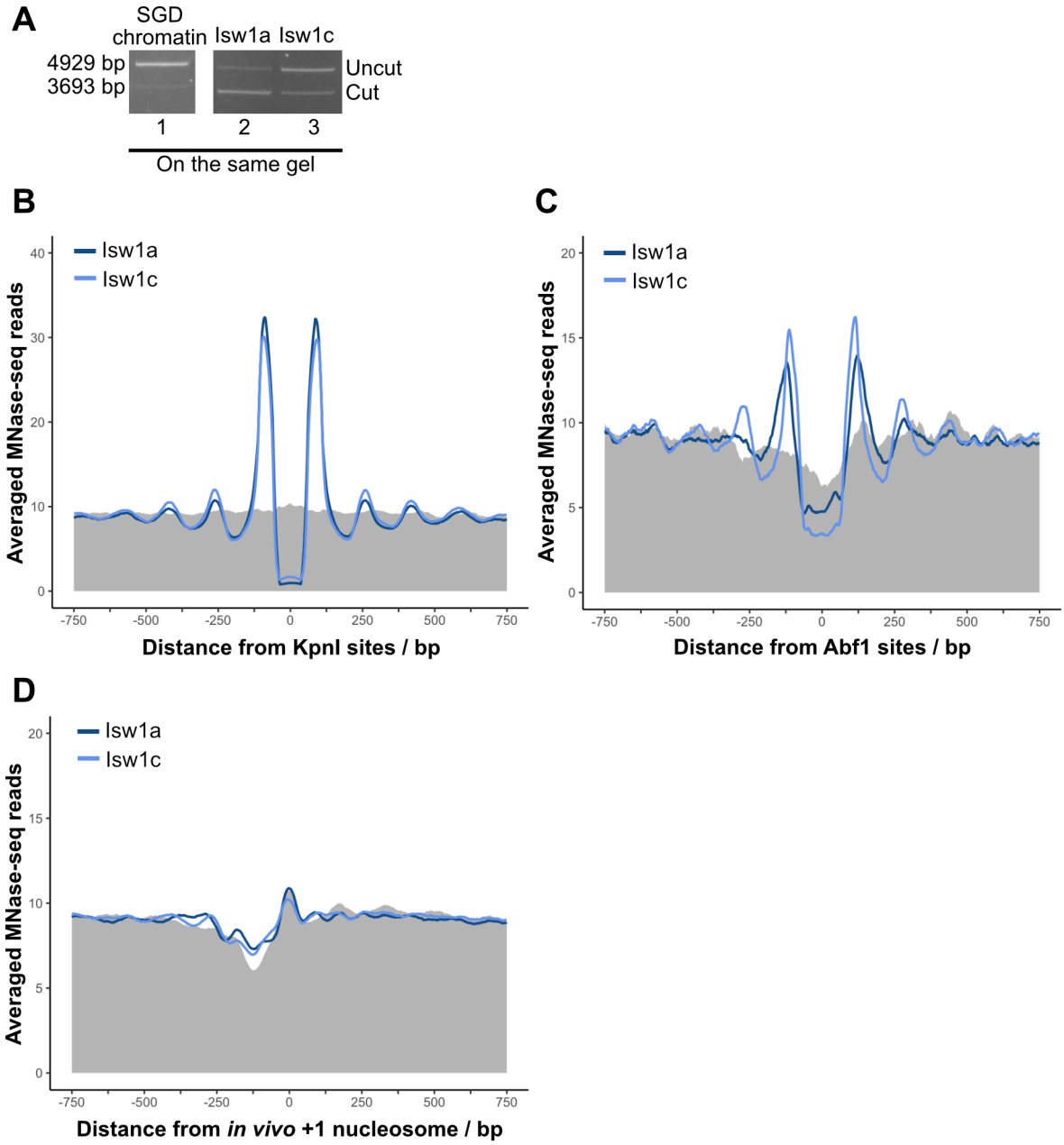

Figure 22. Isw1c generates evenly spaced and phased arrays. A) Restriction enzyme accessibility analysis of Isw1c and Isw1a. **(B)** Composite plot of averaged MNase-seq data for Isw1c and Isw1a in aligned at KpnI sites. **(C)** Composite plot of averaged MNase-seq data for Isw1c and Isw1a in aligned at Abf1 sites. **(D)** Composite plot of averaged MNase-seq data for Isw1c and Isw1a in aligned from *in vivo* +1 nucleosome positions. Isw1a is used as a positive control. Two replicates were performed for each experiment.

3.3 Influence of histone variants and modifications on Isw1c functions

The distinct functions of Isw1a and Isw1b in transcriptional coordination are known to depend on the associated Ioc proteins despite both complexes sharing the ATPase Isw1 subunit. Numerous *in vitro* and *in vivo* studies have elucidated how the Isw1 complex or its associated subunits can distinguish between differentially modified nucleosomes and influence remodeling activity based on the modification states.

Given this information, I investigated whether histone variants and common histone modifications might affect Isw1c sliding and binding activities. Basically, I compared the remodeling and binding activities of Isw1c by using two different nucleosome substrates in every experiment. These nucleosomes may contain canonical histone, histone variants, or certain histone modifications such as methylation or acetylation. The histone octamers used for reconstituting nucleosomes in this study were prepared using a peptide ligation strategy, which introduces precise modifications to the histone and ensures the accurate investigation of the effects of these modifications on remodeler function. Furthermore, histone variants and site-specific histone modifications were selected for testing in the assays due to their involvement in various cellular processes such as transcription, replication, or DNA repair. Additionally, some of these histones also has been reported to affect either Isw1a or Isw1b remodeling activities.

3.3.1 Isw1c has equivalent sliding activity towards histone H2A- and H2A.Z-containing nucleosomes

Only recently, a study employing *in vitro* biochemical assays demonstrated that Isw1a exhibits a preference for binding and sliding histone variant H2A.Z over histone H2A-containing nucleosomes **(Bergmann, 2021)**. Given the similarities between the associated subunit of Esc8 in Isw1c and the associated subunit Ioc3 in Isw1a, I conducted nucleosome sliding assays to examine the Isw1c remodeling activity on canonical histone H2A- and histone variant H2A.Z-containing nucleosomes. This comparison aims to elucidate whether Isw1c exhibits a similar preference for histone variant H2A.Z-containing nucleosomes. From the nucleosome sliding assays, Isw1c displayed a comparable sliding efficiency for both histone H2A and histone variant H2A.Z-containing nucleosomes **(Fig. 23)**. This finding unveils that neither histone H2A- nor histone variant H2A.Z-containing nucleosomes had an impact on the Isw1c remodeling activity.

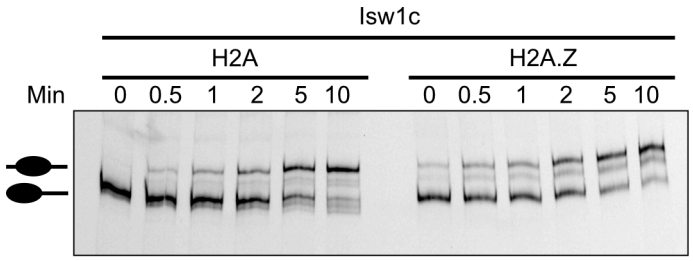

Figure 23. Isw1c slides both histone H2A- and histone variant H2A.Z-containing nucleosomes. All nucleosomes were reconstituted at the 5' end position of the DNA fragment. The reaction contains purified Isw1c (10 fmol) and reconstituted nucleosomes (30 fmol).

3.3.2 Isw1c does not distinguish between unmethylated and methylated-containing nucleosomes

To further determine whether specific histone modifications can affect Isw1c remodeling activity, I performed nucleosome sliding assays using unmethylated and methylated nucleosomes as substrates. Here, I particularly compared nucleosomes containing unmethylated histone H3K4 (H3K4me0) or trimethylated histone H3K4 (H3K4me3) as well as unmethylated histone H3K36 (H3K36me0) or trimethylated

histone H3K36 (H3K36me3). These nucleosomes were chosen in this study because Isw1a has been suggested to interact with histone H3K4me3, while Isw1b is known to have preferential interaction with histone H3K36me3, associated with transcription regulation **(Li et al., 2022; Smolle et al., 2012)**. After testing both sets of nucleosomes, I found that Isw1c demonstrated the ability to slide both histones H3K4me3-containing nucleosome or H3K36me3-containing nucleosome; however, there was no difference in sliding activity between unmethylated nucleosomes and methylated nucleosomes **(Fig. 24)**. Overall, these findings suggest that neither unmethylated nucleosomes containing histone H3K4me0 or histone H3K36me0 nor methylated nucleosomes containing histone H3K4me3 or histone H3K36me3 significantly affect the remodeling activity of isw1c.

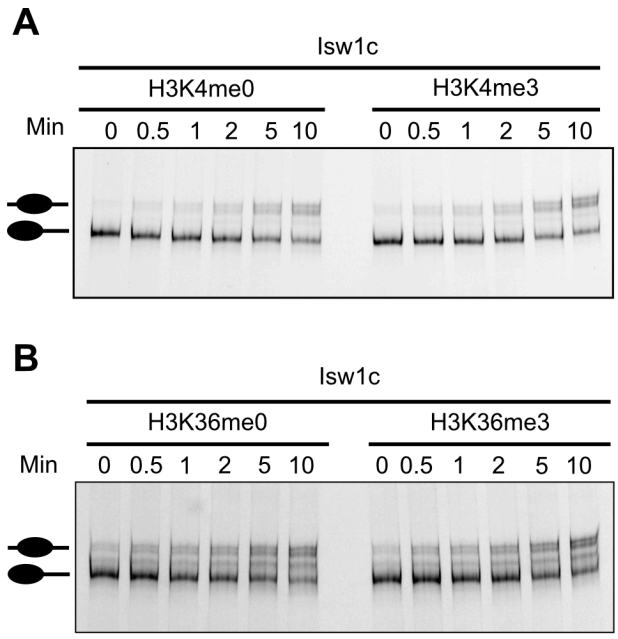

Figure 24. Native PAGE analysis of Isw1c mediated sliding on both unmethylated and methylated. All nucleosomes were reconstituted at the 5' end position of the DNA fragment. The reaction contains purified Isw1c (10 fmol) and reconstituted nucleosomes (30 fmol). Modified nucleosomes are indicated.

3.3.3 Isw1c preferentially remodels histone H4K5,8,12ac-containing nucleosomes over histone H4-containing nucleosomes

Histone acetylation has been extensively studied since it was first reported in 1964 **(Allfrey et al., 1964)**. This modification explicitly caught my interest because it can affect chromatin organization by neutralizing the positive charge of lysine residues, and it can also function as a docking platform to recruit chromatin remodelers to modify chromatin structure **(Bannister & Kouzarides, 2011)**. Given these mechanisms, histone acetylation commonly links to the establishment of the "open" chromatin states, facilitating accessibility to DNA and promoting cellular processes such as transcription, DNA replication, and repair **(Chen et al., 2022; Eberharter & Becker, 2002; Lee et al., 1993; Struhl, 1998; Vettese-Dadey et al., 1996)**. However, it is important to note that there is an exception for specific histone acetylation, such as H4K16ac, that has a role in the assembly of heterochromatin **(Kimura et al., 2002; Oppikofer et al., 2011; Suka et al., 2002)**. The opposite of histone acetylation,

histone deacetylation is associated with “closed” chromatin conformation, forming repressive structures that hinder these cellular processes **(Eberharter & Becker, 2002)**. Additionally, hypoacetylated nucleosomes are known to form in the heterochromatin region and are then referred to as silent chromatin **(Braunstein et al., 1993)**. By comparing whether unacetylated or acetylated nucleosomes can influence the remodeling activity of Isw1c, we could gain new insights into the involvement of Isw1c in a distinct chromatin state.

For that reason, I performed competitive nucleosome sliding assays using unacetylated and acetylated nucleosomes in one reaction. In these assays, I compared nucleosomes containing unacetylated histone H4 (H4) and acetylated histone H4K16 (H4K16ac); unacetylated histone H3 and acetylated H3K9,14 (H3K9,14ac); unacetylated histone H4 (H4) and acetylated histone H4K5,8,12ac (H4K5,8,12ac). Additionally, I compared nucleosomes containing histone H3K9,14ac and histone H4K5,8,12ac. Since multiple acetylation in histones H3 and H4 leads to a fuzzier appearance in gel electrophoresis, this competitive nucleosome sliding assay is more suitable for these modified nucleosomes **(Georgieva & Sendra, 1999; Wang et al., 2000)**. Moreover, the detection of nucleosomes shifted using this assay is more sensitive. To set up this assay, two proportions of nucleosomes and Isw1c were mixed with the addition of ATP in one reaction, followed by incubation at various time lengths. Since each nucleosome was reconstituted either with IRD700-labeled DNA or IRD800-labeled DNA, it was subsequently detected using Licor machines, which captured infrared signals emitted at 700 nm and 800 nm wavelengths.

Based on these remodeling assays, Isw1c demonstrated a comparable nucleosome sliding activity on histone H4-containing nucleosomes and histone H4K16ac-containing nucleosomes **(Fig. 25A, B)**. Both nucleosomes were shifted equally from the end position toward the center position. Similarly, Isw1c displayed the capability to slide both histone H3-containing nucleosomes and histone H3K9,14ac-containing nucleosomes to a similar extent **(Fig. 25C, D)**. Notably, Isw1c fully remodeled nucleosomes containing histone H4K5,8,12ac, while approximately 50% of the unacetylated nucleosomes containing histone H4 were shifted **(Fig. 25E, F)**. Considering that multiple histone acetylation may weaken DNA-histone contacts and cause a premature shift of nucleosomes, I performed additional nucleosome sliding assays to investigate whether Isw1 slides nucleosomes containing histone H4K5,8,12ac more efficiently than nucleosomes containing histone H3K9, 14ac, which has one less acetylation site. As a result, Isw1c showed an equivalent shift for both nucleosomes containing histone H3K9,14ac and histone H4K5,8,12ac **(Fig. 25G, H)**. Together, these experiments reveal that histone H4K5,8,12ac-containing nucleosomes significantly influence the remodeling activity of Isw1c, which may indicate the involvement of Isw1c in an “open” chromatin state to promote cellular processes.

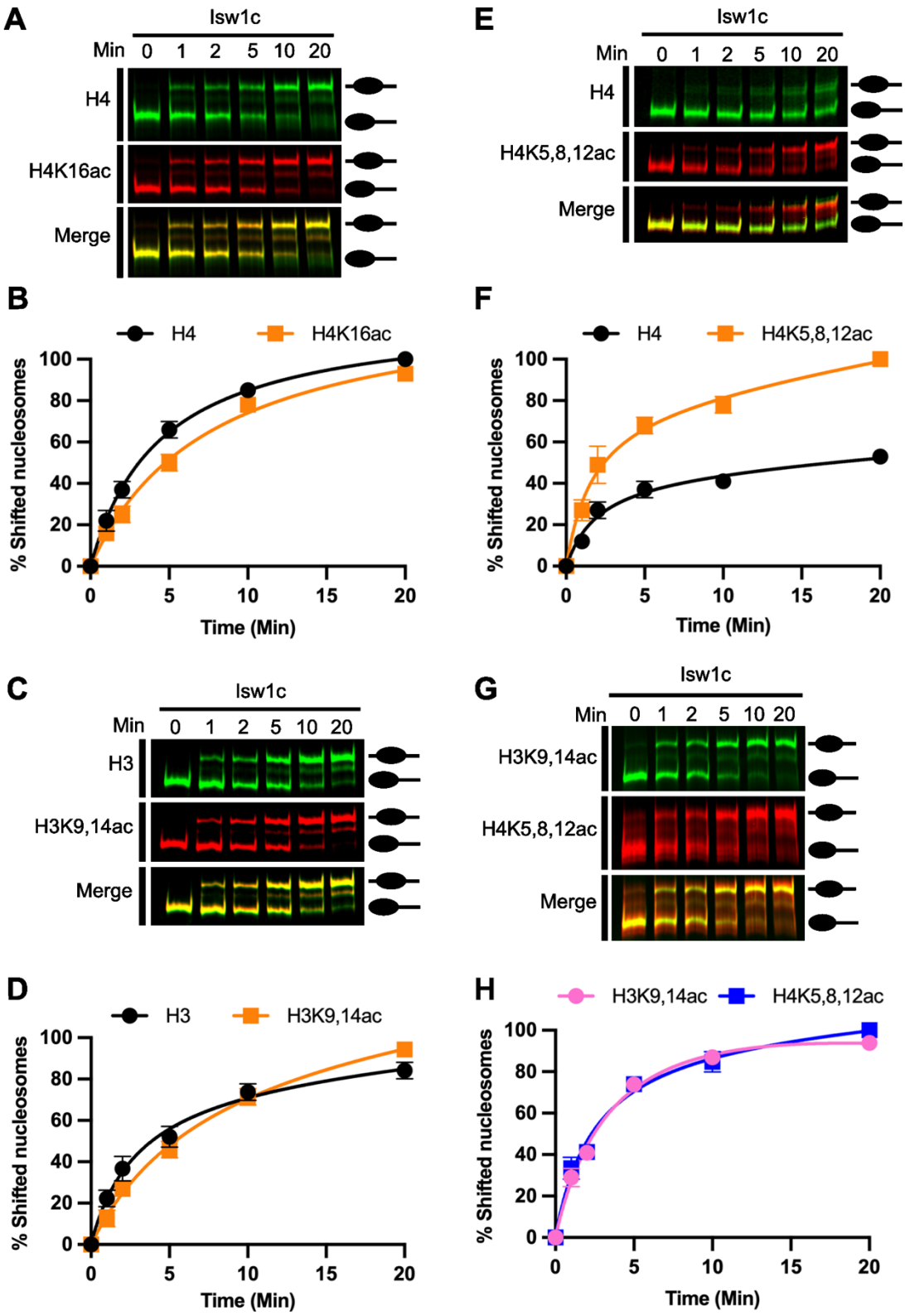

Figure 25. Isw1c sliding activities on unacetylated and acetylated nucleosomes. (A) Sliding analysis of Isw1c with nucleosomes containing histone H4 or histone H4K16ac. **(B)** Quantification of remodeled nucleosomes by Isw1c based on Panel A. **(C)** Sliding analysis Isw1c with nucleosomes containing histone H3 or histone H3K9,14ac. **(D)** Quantification of remodeled nucleosomes by Isw1c based on Panel C. **(E)** Sliding analysis of Isw1c with nucleosomes containing histone H4 or histone H4K5,8,12ac. **(F)** Quantification of remodeled nucleosomes by Isw1c based on Panel E. **(G)** Sliding analysis of Isw1c with nucleosomes containing histone H3K9,14ac or histone H4K5,8,12ac. **(H)**

Quantification of remodeled nucleosomes by Isw1c based on Panel G. Nucleosomes were reconstituted either with IRD800-labeled DNA (shown in green color) or IRD700-labeled DNA (shown in red color) at the 5' end position of the DNA fragment. The yellow color indicates an equal amount of two remodeled nucleosomes. Experiments were performed in triplicates.

3.3.4 Recruitment of Isw1c to unmodified nucleosomes

Given the earlier discovery that histone H4K5,8,12ac-containing nucleosomes enhance Isw1c remodeling efficiency compared to unacetylated nucleosomes, I proceeded to investigate whether this acetylated nucleosome can also impact the recruitment of Isw1c in comparison to unacetylated nucleosomes. To address this question, I conducted competitive EMSA using the same nucleosome substrates employed in the competitive sliding assay, comparing unacetylated nucleosomes with acetylated nucleosomes. Here, various amounts of Isw1c (from 2 nM to 16 nM) were incubated with both nucleosomes (0.5 nM) for 30 minutes without the presence of ATP. When Isw1c bound to nucleosomes, the complex migrated more slowly than the nucleosomes alone, as observed.

According to Isw1c binding activities data, when unacetylated histone H4 and acetylated histone H4K16-containing nucleosomes were present in a reaction, Isw1c bound to these two nucleosomes equally well **(Fig. 26A, D)**. Surprisingly, Isw1c displayed a slight preference to bind with unacetylated histone H3-containing nucleosomes over histone H3K9,14ac-containing nucleosomes **(Fig. 26B, E)**. Similarly, Isw1c also preferred to bind with unacetylated histone H4-containing nucleosomes than histone H4K5,8,12ac-containing nucleosomes **(Fig. 26C, F)**. Furthermore, the equal binding activity of Isw1c to both histone H4 and histone H4K5,8,12ac-containing nucleosomes was observed, indicating saturation of protein binding. Overall, these experiments suggest that unacetylated nucleosomes appear to recruit Isw1c more effectively than histones H3K9,14ac- or histone H4K5,8,12ac-containing nucleosomes.

Since the activities of Isw1c in binding and remodeling nucleosomes are impacted by unacetylated nucleosomes and specific acetylation nucleosomes, respectively, this may suggest that these activities are two independent mechanisms.

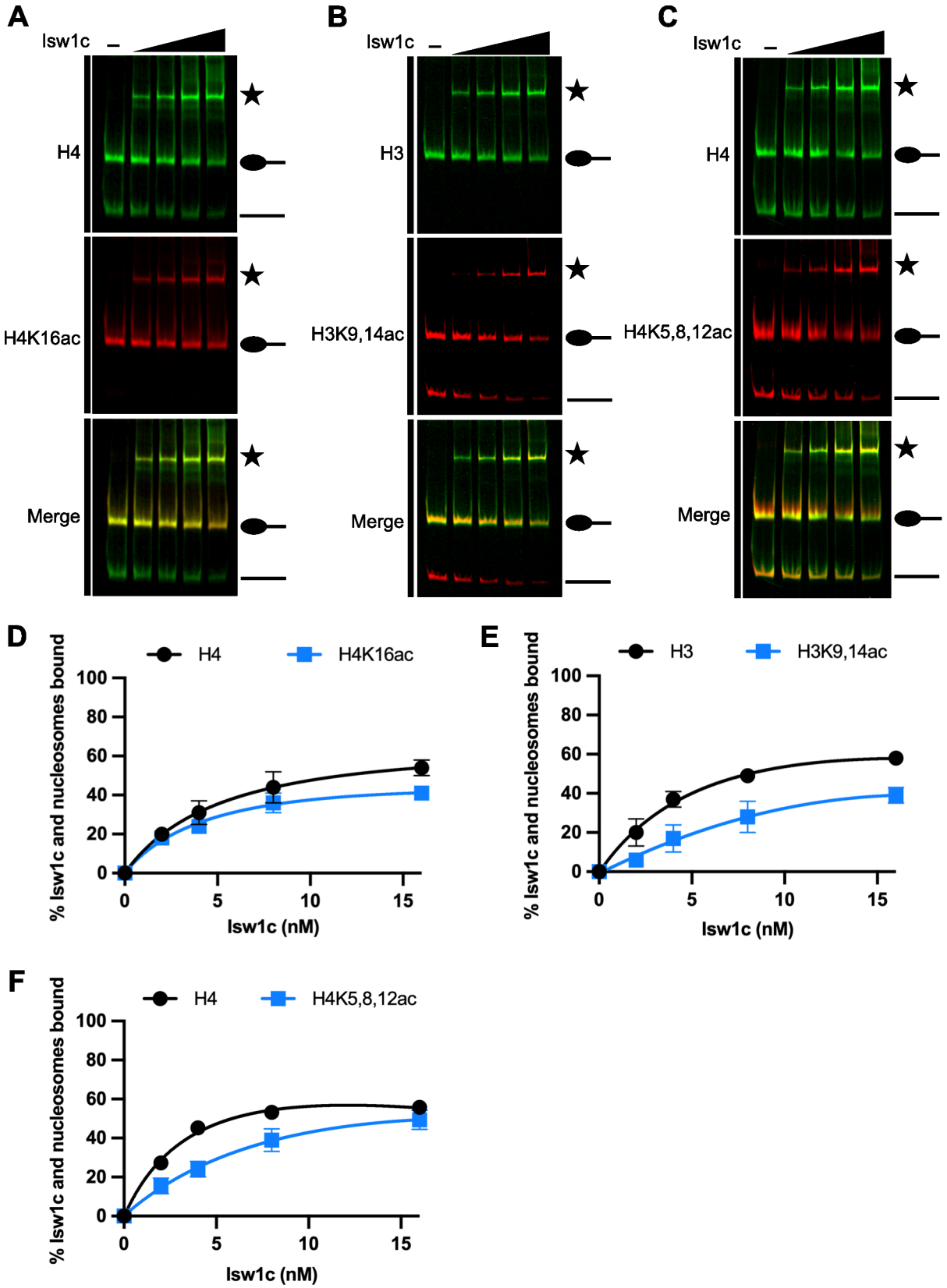

Figure 26. Isw1c binding activities on unacetylated and acetylated nucleosomes. (A) Binding analysis of Isw1c with nucleosomes containing histone H4 or histone H4K16ac. **(B)** Binding analysis of Isw1c with nucleosomes containing histone H3 and histone H3K9,14ac. **(C)** Binding analysis of Isw1c with nucleosomes containing histone H4 and histone H4K5,8,12ac. **(D)** Quantification of Isw1c-bound nucleosomes according to Panel A. **(E)** Quantification of Isw1c-bound nucleosomes according to Panel

B. **(F)** Quantification of Isw1c bound-nucleosomes according to Panel C. Nucleosomes were reconstituted either with IRD800-labeled DNA (shown in green color) or IRD700-labeled DNA (shown in red color) at the 5' end position of the DNA fragment. The yellow color indicates an equal amount of two remodeled nucleosomes. Experiments were performed in triplicates.

3.4 Mechanistic dissection of protein-protein interactions between Isw1 and Esc8, and vice versa

3.4.1 AlphaFold structures of Isw1c and Isw1a

The AlphaFold program has emerged as a premier computational method for generating highly accurate protein structure predictions from amino acid sequences **(Jumper et al., 2021)**. In collaboration with Dr. Maren Heimhalt, predicted structures of both Isw1c and Isw1a complexes were generated using the AlphaFold tool. By obtaining the Isw1c predicted structure, I gained insights into the overall view of the Isw1c complex and was able to conduct a detailed examination of the interactions between Isw1 and Esc8. Additionally, the predicted structure of Isw1a was used as a reference and comparison. Although the crystal structures of Isw1a were present at the time, I utilized the predicted structure of Isw1a to ensure an equivalent comparison with the predicted structure of Isw1c. Notably, the predicted structure of Isw1a, particularly the HSS-Ioc3 region, closely resembles the crystal structure of Isw1a **(Supplementary Fig. 2A)**, as expected, since it was generated based on the protein structure database.

Upon obtaining the AlphaFold structures prediction, I first assessed the predicted structures' quality and accuracy according to two confidence metrics provided by AlphaFold. First, pLDDT (predicted local distance difference test) is a local confidence metric to measure the per-residue score of the predicted model on a scale of 0 to 100 **(Tunyasuvunakool et al., 2021; Varadi et al., 2022)**. The confidence band is colored-coded for each residue where dark blue (pLDDT>90) represents very high confidence, light blue (90<pLDDT<70) indicates confidence, yellow (70<pLDDT<50) illustrates low confidence and orange (pLDDT<50) marks lowest confidence. Second, PAE (predicted aligned error) is known to measure the confidence in the relative position and orientation of the domains of the predicted model **(Varadi et al., 2022)**. The outcome of PAE can be visualized either by the 2D plot integrated with a 3D structure representation **(Elfmann & Stulke, 2023)**.

First, the predicted structure of Isw1a showed the interaction of Isw1 with Ioc3 to form a protein complex **(Fig. 27A)**. Here, I examined the model confidence of pLDDT, assessing the confidence of the predicted protein structure at each residue position **(Fig. 27B)**. Based on the analysis, the core structure of Isw1 and Ioc3 displayed a high confidence level in the residue structures (pLDDT>90, shown in dark blue). In assessing each domain, the ATPase, SANT, and SLIDE domains of Isw1 and the HLB domain of Ioc3 had high confidence scores (pLDDT >90, indicated in dark blue). All these domains represented highly accurate structures with correct domain packing **(Jumper et al., 2021)**. In addition, the HAND domain of Isw1 and the CLB and HSSB domains of Ioc3 were shown in yellow, indicating a low confidence score of pLDDT around 50 to 70. These domains were likely to have a pLDDT score of 70, which was just at the borderline for the lower cut-off of pLDDT >70 to be considered to have a correct backbone prediction **(Tunyasuvunakool et al., 2021)**. In this

scenario, these domains were suggested to be treated with caution during the interpretation. Moreover, the AutoN, NegC, and RA motif in Isw1 with the FH in Ioc3 showed the lowest confidence structure (pLDDT<50, depicted in orange). These regions were most likely linkers or intrinsically disordered protein domains **(Akdel et al., 2022; Ruff & Pappu, 2021; Tunyasuvunakool et al., 2021)**. Furthermore, I evaluated the accuracy of predicted protein structures based on the outcome of the PAE plot **(Fig. 27C)**. Notably, there was a high confidence in relative domain positions and orientations of the HAND-SANT-SLIDE domains of Isw1 when associated with Ioc3, as shown by the uniform distribution of purple color. Conversely, varying colors within the ATPase domain implied that its position and orientation were more likely to be random. Moreover, each Isw1 and Ioc3 subunit, with its domains, exhibited a correct structural conformation based on an interactive 2D plot of the PAE values **(Supplementary Figure 1B, C)**.

Second, the predicted structure of Isw1c revealed the interaction between Isw1 and Esc8, forming a protein complex **(Fig. 27D)**. Upon accessing the model confidence of pLDDT for this structure, it showed that the regions in Isw1 and Esc8 exhibited varying levels of confidence, ranging from low to high (shown in yellow and dark blue) **(Fig. 27E)**. Of all the regions, only the core structure of the ATPase domain and the SLIDE domain of Isw1 exhibited high confidence with pLDDT>90. Additionally, Esc8 residues 133-343 also showed high confidence. Moreover, the HAND and SANT domains of Isw1 appeared to have a confidence score of pLDDT around 70-90 (indicated in light blue), representing correct backbone prediction. Meanwhile, the NegC in Isw1 and the HLB domain in Esc8 were indicated in yellow, implying a low confidence score (70<pLDDT<50). Other domains, like the AutoN domain and RA motif, had the lowest confidence score (pLDDT<50)**.** Overall, the predicted structure of Isw1c exhibited a moderate level of confidence. Furthermore, the PAE plot of the predicted structure Isw1c unveiled that the HAND-SANT-SLIDE domain of Isw1 connected with Esc8 was highly confident based on their relative domain positions and orientations, similar to that of Isw1a **(Fig 27F)**. The interactive 2D plot of the PAE values also showed that Isw1 and Esc8 subunits have correct structural conformations **(Supplementary Fig 1E, F)**.

Based on the comparison between the analyses of both predicted structures, Isw1c exhibits a comparable structure to Isw1a. In this context, Isw1c demonstrated good structural accuracy with correct domain packing corresponding to Isw1a despite the difference in pLDDT values. Remarkably, the 3D PAE plots for both Isw1c and Isw1a displayed high similarity, especially in the formation of the HSS domain of Isw1 interacting with either the Ioc3 or Esc8 subunit protein. Given the prediction that the HSS domain of Isw1, in conjunction with the associated protein (Ioc3 or Esc8), would form a protein complex with accurate position and orientation, I then directed my focus toward investigating the protein-protein interactions in this complex formation.

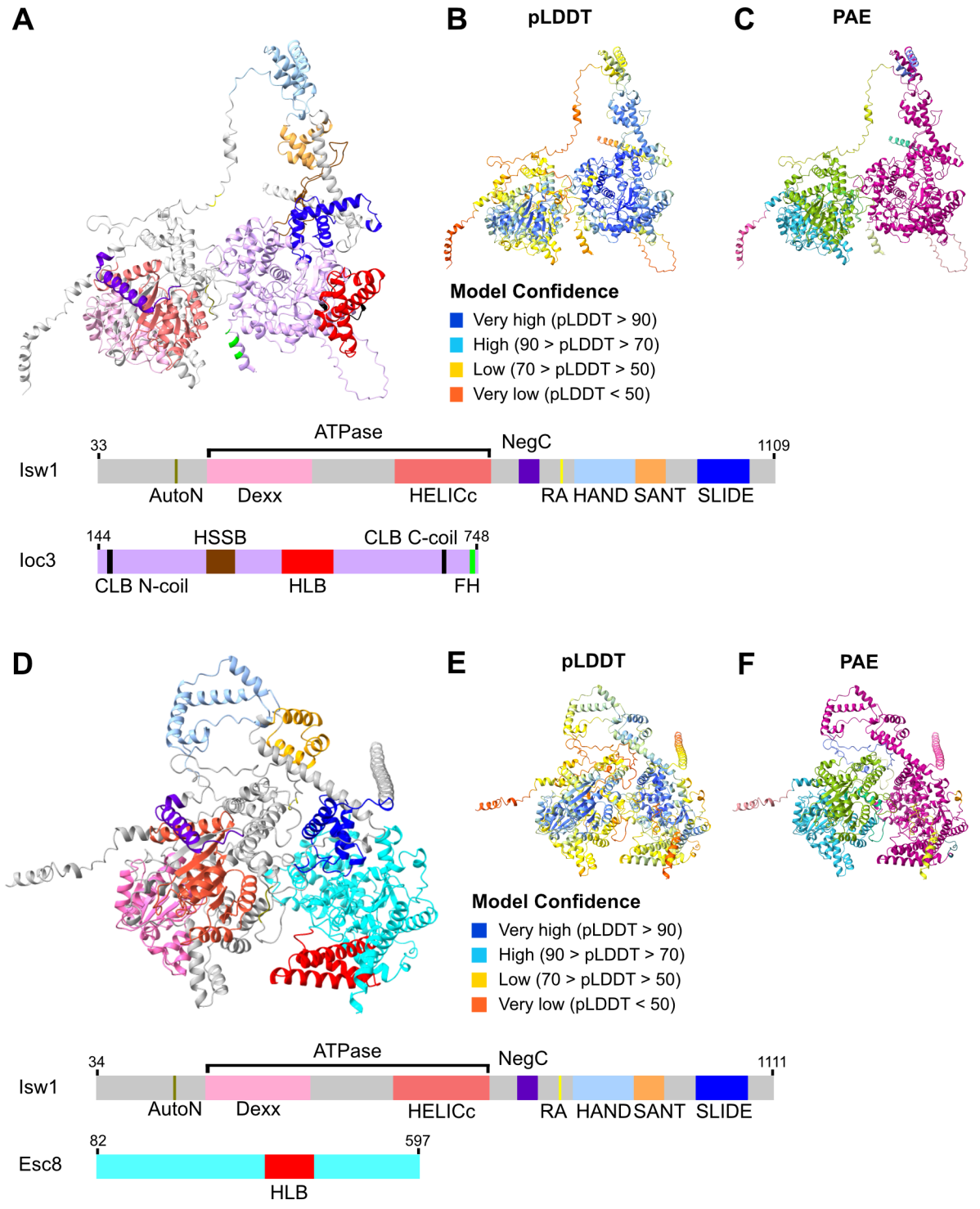

Figure 27. AlphaFold structures prediction of Isw1a and Isw1c. (A) Representations of the predicted structure of Isw1a with its domain organization. **(B)** PLDDT confidence metric of Isw1a. **(C)** Visualization of Isw1a predicted structures from PAE plot. **(D)** Representations of the predicted structure of Isw1c with its domain organization. **(E)** PLDDT confidence metric of Isw1c **(F)** Visualization of Isw1c predicted structures from PAE plot. For Panels A and D, the color regions in the predicted structures of Isw1a and Isw1c are in accordance with the color in the domain composition. In Panels B and E, each amino acid is colored according to its per-residue confidence score, known as pLDDT. In Panels C and F, the association between the HSS domain of Isw1 with the Ioc3 or Esc8 is predicted with high confidence, as indicated by the purple color.

3.4.2 Structural similarities and differences of the Isw1c and Isw1a complexes based on the structural alignment

I performed a structural alignment of the AlphaFold structure of Isw1a and the crystal structure of Isw1a **(Yamada et al., 2011),** which lacks its ATPase domain, to ensure the similarity between the two. Using the matchmaker command in ChimeraX software, I paired both structures based on the sequence and secondary structure, allowing them to be superimposed. The predicted structure of Isw1a is aligned well with the crystal structure of Isw1a, albeit missing residues aa 662-678 **(Supplementary Figure. 2A)**. Given this similarity, I decided to use the Alphafold predicted structure of Isw1a as a reference for unbiased comparison with the predicted structure of Isw1c.

I aligned both the predicted structures of Isw1c and Isw1a using the matchmaker command in ChimeraX. Following the alignment, no structural differences were observed for the HSS domain in Isw1 **(Fig. 28A-C)**. Instead, there were high structural similarities and few structural differences between the associated proteins of Esc8 and Ioc3 **(Fig. 28A-C)**. In general, the structure of Esc8 was well-aligned with the structure of Ioc3. Nevertheless, the HSS-binding loop (HSSB) of Ioc3, located in close proximity to Isw1, was absent in Esc8. In addition, Esc8 showed 3 of 4 helix structures at the helical linker DNA binding (HLB) domain, in agreement with the sequence alignment **(Yamada et al., 2011)**. Here, Esc8 lacked HLB- α9. Moreover, Esc8 also did not have the finger helix (FH), recently identified in Ioc3 **(Li et al., 2024)**. Collectively, Esc8 shares largely structural similarities with Ioc3 with some noticeable differences.

3.4.3 Esc8 forms a binding pocket specifically to the SLIDE domain of Isw1

Based on the structural predictions, I further analyzed the formation of Isw1c and Isw1a complexes. Consistent with the Isw1a crystal structure **(Yamada et al., 2011)**, the Ioc3 core not only formed a large pocket that interacts solely with the SLIDE domain but also there was an HSSB loop of Ioc3 projecting across the SLIDE domain to the SANT domain **(Fig. 28E)**. These two properties of Ioc3 seems to play a role in the interaction with Isw1, contributing to the formation of Isw1a complex. Nevertheless, the Isw1c complex formation was slightly different compared to the Isw1a. Based on the predicted structure, the Esc8 protein was found to form a binding pocket primarily associated with the SLIDE domain of Isw1 **(Fig. 28F)**. With this observation, I proposed that the SLIDE domain of Isw1 plays a crucial role in the association with Esc8, resulting in the formation of the Isw1c complex.

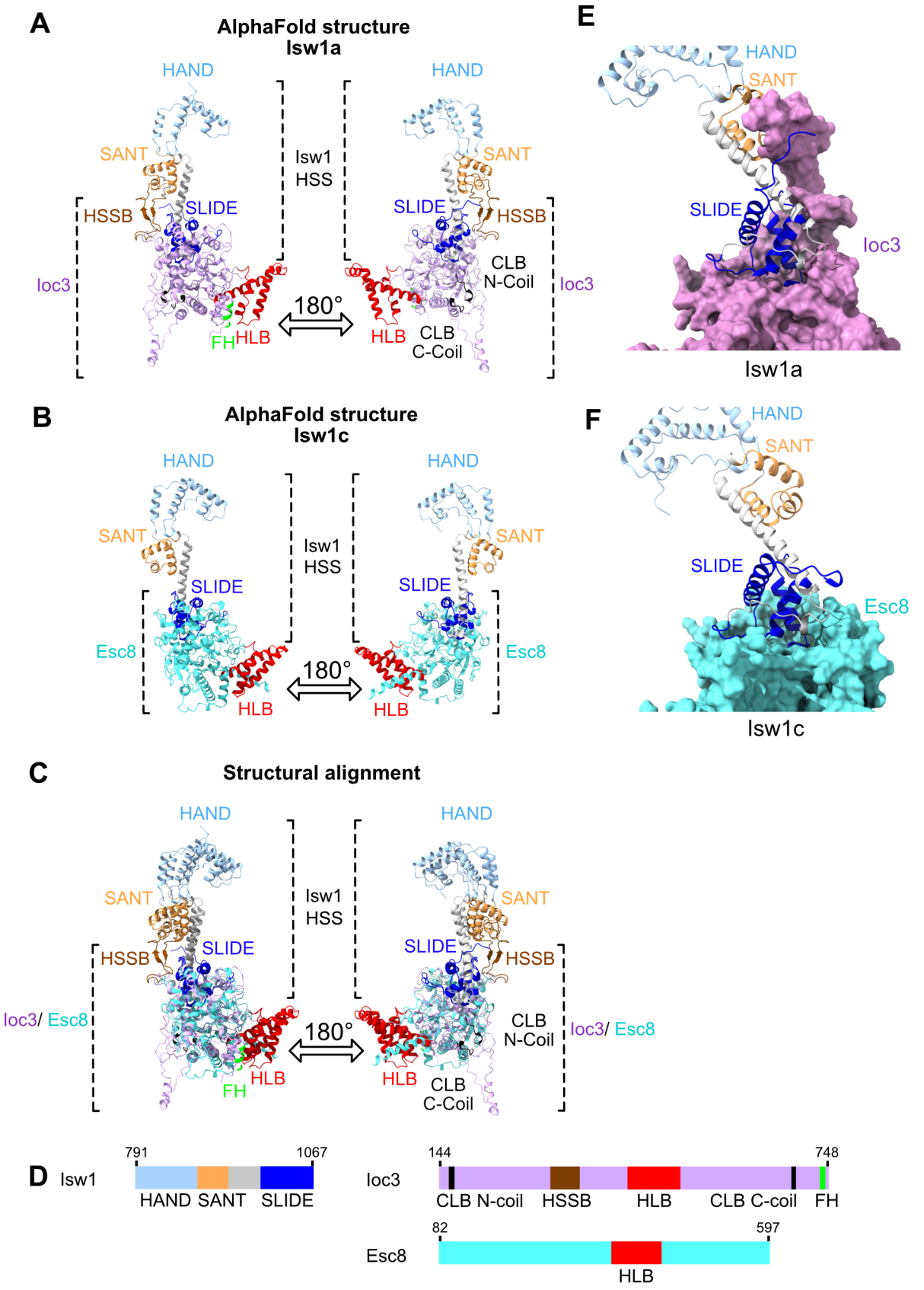

Figure 28. Structural alignment and formation of binding pockets of Ioc3 and Esc8 interacting with Isw1. (A) Two perspective views (front and back) of the predicted structures of Isw1a lacking the ATPase domain. **(B)** Two perspective views (front and back) of the predicted structures of Isw1c lacking the ATPase domain. **(C)** Three-dimensional superimpositions of Isw1a and Isw1c. **(D)** Domain

organization of the Isw1 protein complex. **(E)** Surface representation of Ioc3 forming a binding pocket to Isw1. **(F)** Surface representation of Esc8 forming a binding pocket to Isw1.

3.4.4 SLIDE domain of Isw1 is required for its interaction with Esc8

According to structural analysis, Esc8 was predicted to form a binding pocket solely to the SLIDE domain of Isw1. To dissect the interaction of Esc8 with the SLIDE domain of Isw1, I deleted the SLIDE domain alone or in combination with the SANT domain to generate *ISW1*$_{\Delta SLIDE}$ and *ISW1*$_{\Delta SANT\Delta SLIDE}$ yeast strains **(Fig. 29A)**. Deleting the SLIDE domain or in combination with SANT domain is expected to impede the interaction with Esc8, as illustrated in **Fig. 29B**. I performed co-immunoprecipitation to uncover the protein-protein interactions between the Isw1 mutants and Esc8. Untagged Esc8 and Esc8-TAP-tagged were used as negative and positive controls, respectively. To set this assay, I incubated cell extracts together with calmodulin sepharose, and the eluted protein was resolved by SDS-PAGE, followed by a western blot. For protein detection, peroxidase-anti-peroxidase (PAP) and anti-Isw1 were used to detect the Esc8-TAP-tagged and the Isw1 together with their mutants, respectively. As expected, I found that the deletion of the SLIDE domain alone in Isw1 resulted in no interaction with Esc8 **(Fig. 29C)**. This was observed as the Esc8-TAP-tagged was detected in the IP sample, but a loss of Isw1ΔSLIDE proteins in the immunoprecipitated sample. This finding is in line with the structural analysis that suggests that the SLIDE domain of Isw1 is responsible for the interaction with Esc8 to form a protein complex. Additionally, the deletion of SANT and SLIDE domains also showed no interaction with Esc8 **(Fig. 29C)**. Taken together, our results demonstrate that the SLIDE domain is essential for the interaction of Isw1 with Esc8, highlighting the importance of this domain for the formation of Isw1c complex.

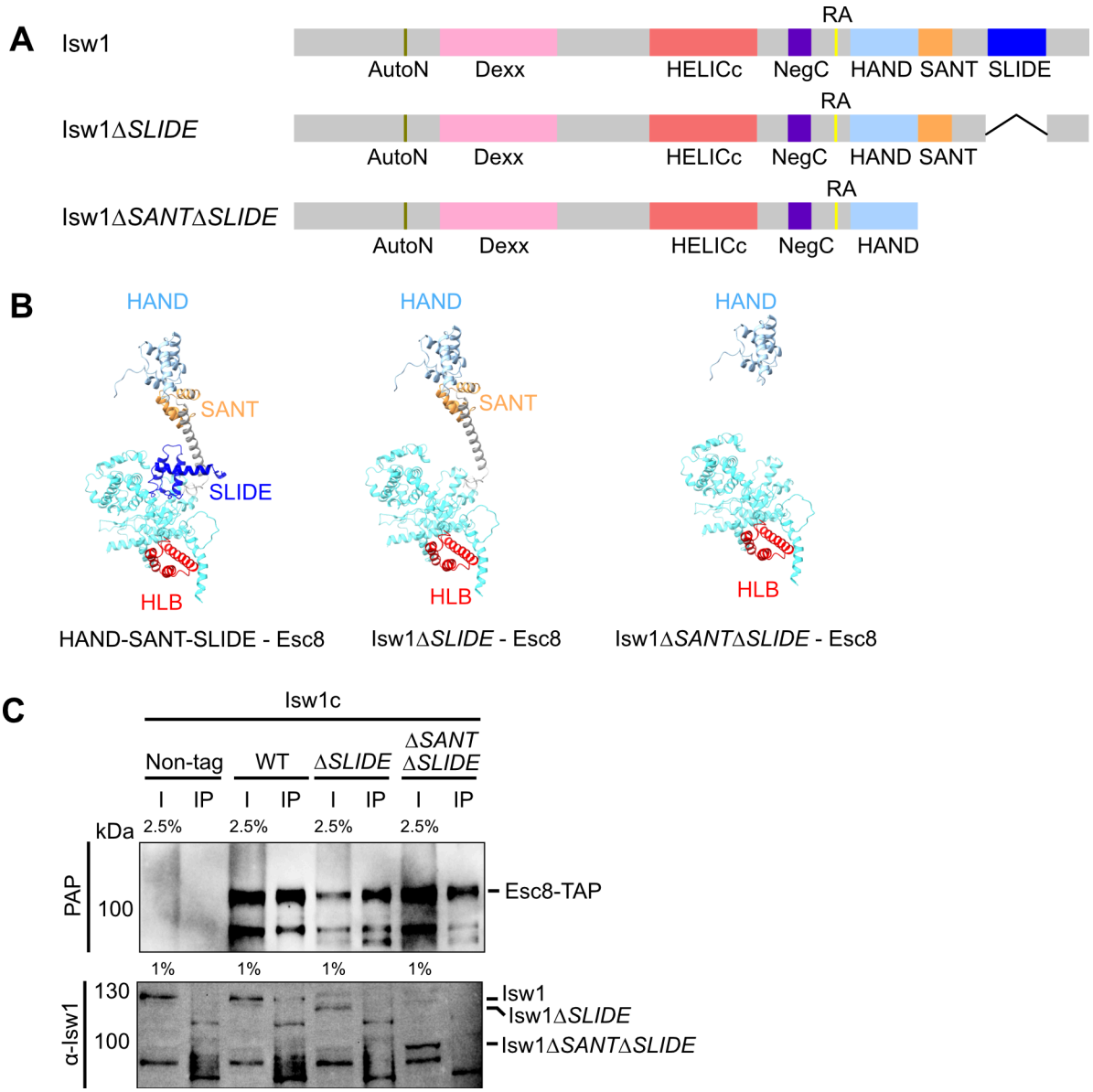

Figure 29. Deletion of the SLIDE domain and the SANT-SLIDE domain of Isw1 hinder the interaction with Esc8. (A) Domain organization of Isw1 and its mutants. **(B)** The representation of the AlphaFold predicted structures of Isw1 mutants. The regions are colored based on their domain composition. **(C)** Co-immunoprecipitation of Isw1$_{\Delta SLIDE}$ and Isw1$_{\Delta SANT\Delta SLIDE}$ with Esc8-TAP-tagged. The input sample (I) and immunoprecipitated samples (IP) are shown. The proteins of Esc8-TAP-tagged (120 kDa), Isw1 (130 kDa), Isw1$_{\Delta SLIDE}$ (123 kDa), and Isw1$_{\Delta SANT\Delta SLIDE}$ (102 kDa) are indicated.

3.4.5 Esc8$_{\Delta C2}$ mutant retains its interaction with Isw1

To investigate the specific region of Esc8 involved in its interaction with Isw1, I generated a total of four Esc8 deletion mutants conjugated with C-terminal TAP tags **(Fig. 30A)**. Two mutants featured N-terminal deletions (Esc8$_{\Delta N1/\Delta N2}$) while the other mutants had C-terminal deletions (Esc8$_{\Delta C1/\Delta C2}$). **Figures 30B-F** depict the AlphaFold predicted structures for each Esc8 mutant interacting with Isw1. Notably, among these structures, the absence of residues aa1-335 in Esc8 showed in the dissociation of the Isw1 and Esc8 protein complex structures **(Fig. 30D)**.

Additionally, I conducted co-immunoprecipitation assays to access the interaction of these Esc8 mutants with Isw1. Untagged Esc8 and Esc8-TAP-tagged were used as negative and positive controls, respectively. From this experiment, I found that the deletion of the N-terminus of Esc8 ($Esc8_{\Delta N1}$, aa1-203) resulted in a less stable protein. This was shown by more intensity of degraded protein at 35 kDa in the IP sample compared to the input sample **(Fig. 30G)**. Moreover, neither $Esc8_{\Delta N2}$ (aa1-335) nor $Esc8_{\Delta C1}$ (aa470-714) were detected in either the input or IP samples **(Fig 30G, H)**. The absence of residues aa1-335 or aa470-714 in Esc8 may lead to incorrect folding or protein instability, subsequently resulting in protein degradation. Lastly, the $Esc8_{\Delta C2}$ (aa606-714) demonstrated an interaction with Isw1, as evidenced by both proteins being immunoprecipitated **(Fig. 30H)**. This interaction likely occurs due to the smaller deletion in Esc8.

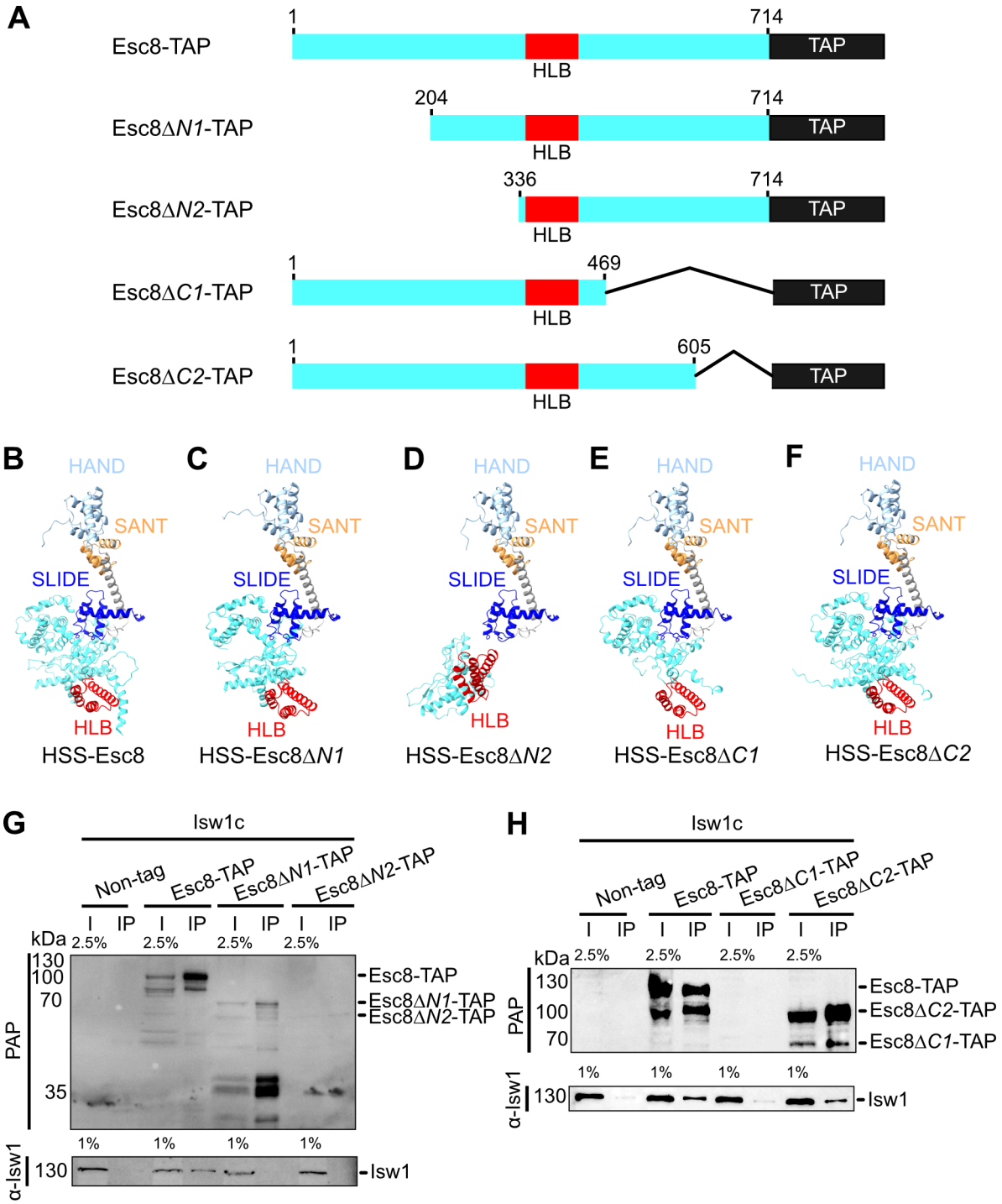

Figure 30. Protein-protein interactions between Esc8 mutants and Isw1. (A) Domain organizations of Esc8 and its mutants. **(B-F)** AlphaFold predicted structures of Esc8 mutants interacting with the HSS domains of Isw1. Regions are colored to correspond to their domain configurations. **(G)** Co-immunoprecipitation of Esc8 N-terminal deletions with Isw1. **(H)** Co-immunoprecipitation of Esc8 C-terminal deletions with Isw1. The proteins of Isw1 (130 kDa), Esc8-TAP-tagged (120 kDa), Esc8$_{\Delta N1}$-TAP-tagged (76 kDa), Esc8$_{\Delta N2}$-TAP-tagged (61 kDa), Esc8$_{\Delta C1}$-TAP-tagged (71.5 kDa) and Esc8$_{\Delta C2}$-TAP-tagged (86.5 kDa) are indicated.

3.4.6 Isw1c$_{\Delta C2}$ (Isw1-Esc8$_{\Delta C2}$) mutant demonstrates nucleosome sliding activity

Since Esc8$_{\Delta C2}$ can interact with Isw1, forming an Isw1c mutant complex, I next tested its function in remodeling nucleosomes. For the experiment, I purified both wild-type and Isw1c$_{\Delta C2}$ proteins **(Fig. 31A)** and subsequently performed nucleosome sliding assays with 0N47 nucleosomes. Unexpectedly, the Isw1c$_{\Delta C2}$ exhibited similar nucleosome sliding activities as the wild-type **(Fig. 31B)**. Furthermore, I also conducted a competitive nucleosome sliding assay with unacetylated histone H4-containing nucleosomes and acetylated histone H4K5,8,12ac-containing nucleosomes. Similarly, the Isw1c$_{\Delta C2}$ demonstrated equivalent nucleosome sliding activities as compared to the wild-type **(Fig. 31C)**. Both wild-type and Isw1c$_{\Delta C2}$ preferred to slide the histone H4K5,8,12ac-containing nucleosomes over histone H4-containing nucleosomes. In short, the absence of 106 amino acids at the C-terminus of Esc8 does not affect its interaction with Isw1, and the Isw1c$_{\Delta C2}$ complex has the ability to slide nucleosomes, which suggests that the Isw1c$_{\Delta C2}$ retains its function as a chromatin remodeler.

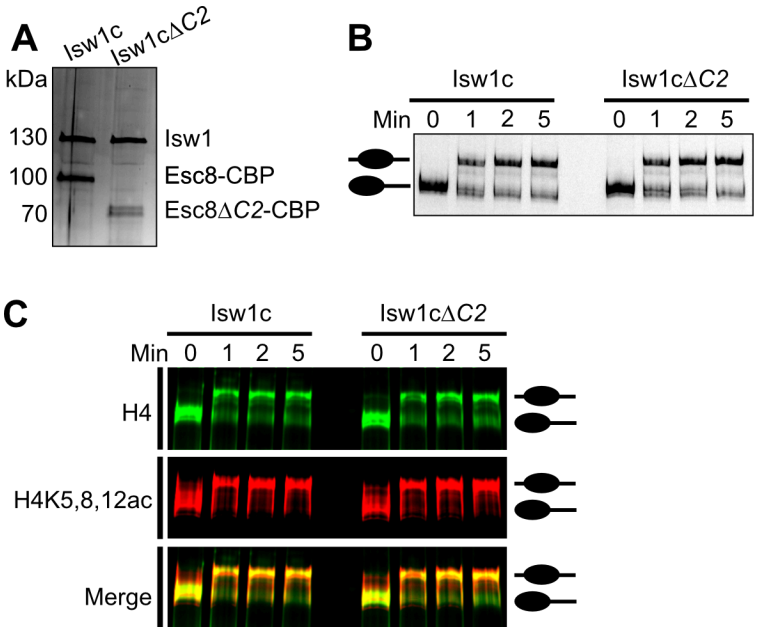

Figure 31. Purified Isw1c$_{\Delta C2}$ slides nucleosomes. **(A)** SDS-PAGE analysis of purified wild-type and Isw1c$_{\Delta C2}$. The proteins of Isw1 (130 kDa), Esc8-CBP-tagged (100 kDa), and Esc8$_{\Delta C2}$-CBP-tagged (86.5 kDa) are indicated. **(B)** Sliding assay of wild-type and Isw1c$_{\Delta C2}$ on 0N47 nucleosomes. **(C)** Competitive sliding assay of wild-type and Isw1c$_{\Delta C2}$ on histone H4-containing nucleosomes and histone H4K5,8,12ac-containing nucleosomes.

4. Discussion

In *Saccharomyces cerevisiae*, there are two known Isw1 remodeler complexes, namely Isw1a and Isw1b **(Tsukiyama et al., 1999; Vary et al., 2003)**. These complexes share the Isw1 catalytic ATPase subunit with different Ioc-associated subunits. Isw1a consists of Isw1 and Ioc3, whereas Isw1b comprises Isw1, Ioc2, and Ioc4 **(Vary et al., 2003)**. Interestingly, each of the Ioc-associated subunits is found to have distinct regulatory functions, contributing to the unique functionality of the Isw1 complex. These functions entail interactions with other proteins or chromatin components, localization to specific genomic loci, and modulation of the enzymatic activity of the remodeler complex **(Morillon et al., 2003; Smolle et al., 2012; Vary et al., 2003; Yen et al., 2012)**. Besides Ioc-associated subunits, the Esc8 protein has been proposed to interact with the Isw1, based on the analysis of the protein interaction complex in yeast and the homology to Ioc3 **(Cuperus & Shore, 2002; Gavin et al., 2002; Yamada et al., 2011)**. However, little is known about the interaction of Esc8 with Isw1 to form a protein complex and its functions in chromatin remodeling. Therefore, my PhD research focused on the Isw1-Esc8 (Isw1c) protein complex and characterized its functions as a chromatin remodeler.

4.1 *S. cerevisiae* Isw1 interacts with Esc8 *in vivo* to form the Isw1c complex

In this study, I have shown and confirmed that yeast Isw1 binds to the associated protein Esc8 and forms the Isw1c complex *in vivo*. This result was in line with identifying Esc8 as a protein interactor with Isw1 in *S. cerevisiae* **(Gavin et al., 2002)**. Moreover, mass spectrometry of the purified Isw1 and Isw1c complexes further confirmed that Isw1 binds to Esc8. After performing protein purification, native Isw1c yielded low amounts of protein. Mass spectrometry of the purified Isw1 showed that Esc8 protein was about 20-70 times less abundant than other associated Ioc subunits, based on the spectral count. With a very low yield of Esc8, it is therefore not surprising that Esc8 is undetected in the early identification of the ISWI complex. After all, our experiment suggests that Isw1c is a novel Isw1 complex in *S. cerevisiae*.

The low yield of purified Isw1c protein posed the biggest challenge in proceeding with the biochemical experiments to investigate its functions. Thus, the initial focus of the work was to establish expression and purification protocols to obtain higher amounts of the Isw1c protein complex. Initially, I utilized the *E. coli* system for protein expression. The attempt to co-express both Isw1 and Esc8 proteins simultaneously resulted in an unbalanced ratio between the two proteins and insufficient protein amounts. The alternative strategy involved expressing and purifying individual proteins and then reconstituting the protein complex from its purified constituent proteins. While the individual proteins were successfully purified, the Isw1c complex could not be reconstituted, likely due to steric hindrance. Encountered challenges obtaining the Isw1c complex using the *E. coli* system, I shifted my focus to using the *S. cerevisiae* system for protein expression and purification. By exchanging the endogenous promoter of *ESC8* with other promoters of different expression strengths, there was a significant increase in the expression of Esc8,

resulting in higher amounts of the Isw1c protein complex. Finally, using this strategy, I successfully obtained sufficient amounts of the Isw1c protein complex.

4.2 Isw1c complex is a novel ISW1 chromatin remodeler in *S. cerevisiae*

The interaction of Isw1 with Esc8 to form a protein complex, as well as the sequence homology of Esc8 with Ioc3, the associated subunit in the Isw1a complex, has prompted me to investigate the potential role of Isw1c as a chromatin remodeler.

In general, chromatin remodelers play an essential role in modulating chromatin organization. To function, remodelers are required to bind to nucleosomes, hydrolyze ATP, and then utilize the energy generated from ATP hydrolysis to move, eject, or reorganize nucleosomes **(Clapier & Cairns, 2009)**. By using established biochemical assays, I tested the abilities of Isw1c in binding DNA and nucleosomes, hydrolyzing ATP, and sliding nucleosomes as fundamental features of chromatin remodelers. I found that Isw1c exhibits all the basic hallmarks of a remodeler. First, Isw1c demonstrates the ability to bind to double-stranded DNA as well as nucleosomes. Notably, Isw1c can only bind to nucleosomes with at least one DNA overhang. It cannot directly interact with the nucleosome core particle. Thus, the presence of a single DNA overhang on nucleosomes seems to be crucial for Isw1c's binding activity. This binding mechanism of Isw1c is similar to Isw1a. This is evidenced by the fact that the Isw1a complex requires a minimum of 33 bp of overhang DNA on one side of the nucleosome **(Gangaraju & Bartholomew, 2007; Stockdale et al., 2006).** Second, Isw1c exhibits ATPase activity stimulated by nucleosomes but not histones or DNA alone. When I compared the ATPase activity of both Isw1c and Isw1a, it was noticeable that Isw1c displayed three-fold lower activity than Isw1a. Nonetheless, Isw1c and Isw1a can hydrolyze ATP in a nucleosome-dependent manner. Third, Isw1c efficiently mobilizes end-positioned nucleosomes toward the center rather than in the opposite direction. This nucleosome repositioning pattern also has been observed similarly to Isw1a rather than Isw1b **(Stockdale et al., 2006)**. Together, Isw1c is a novel chromatin remodeler, interacting with nucleosomes through a single DNA overhang and utilizing the energy from ATP hydrolysis to mobilize nucleosomes from the end position toward the middle position. The schematic representative of Isw1c as a chromatin remodeler is illustrated in **Figure 32**.

In addition to those basic features of chromatin remodeler, we further investigated whether Isw1c demonstrates nucleosome spacing and phasing activities akin to those observed in Isw1a. To address this question, we employed the genome-wide *in vitro* reconstitution assay, a technique previously used to characterize these activities for Isw1a **(Oberbeckmann et al., 2021).** Our findings show that Isw1c is capable of generating regular spacing, characterized by a constant distance between nucleosomes. Furthermore, we discovered that Isw1c, in combination with Abf1, can create regular nucleosome arrays at Abf1 sites. The phased nucleosome array is characterized by all nucleosomes in the cell population having a similar position relative to a given genomic alignment point, such as the transcription start site **(Baldi et al., 2018; Blank & Becker, 1996; Chereji & Clark, 2018; Singh & Mueller-Planitz, 2021)**. Here, the barrier Abf1 is used as the genomic alignment point, which is known to bind in the promoter region **(Gutin et al., 2018)** and plays a role in organizing nucleosomes together with other remodellers **(Krietenstein et al., 2016)**. Moreover, it

is noteworthy that Isw1c positions the flanking nucleosomes slightly closer at Abf1 sites than Isw1a. This suggests that Isw1c may play a role in positioning nucleosomes slightly tighter than Isw1a. Nonetheless, the function of Isw1c in setting the linker length between nucleosomes and the distance to the barrier remains to be determined. Ultimately, these findings show that Isw1c exhibits nucleosome spacing and phasing activities, which could suggest its potential function as a protein ruler to set the length of linker DNA, similar to Isw1a.

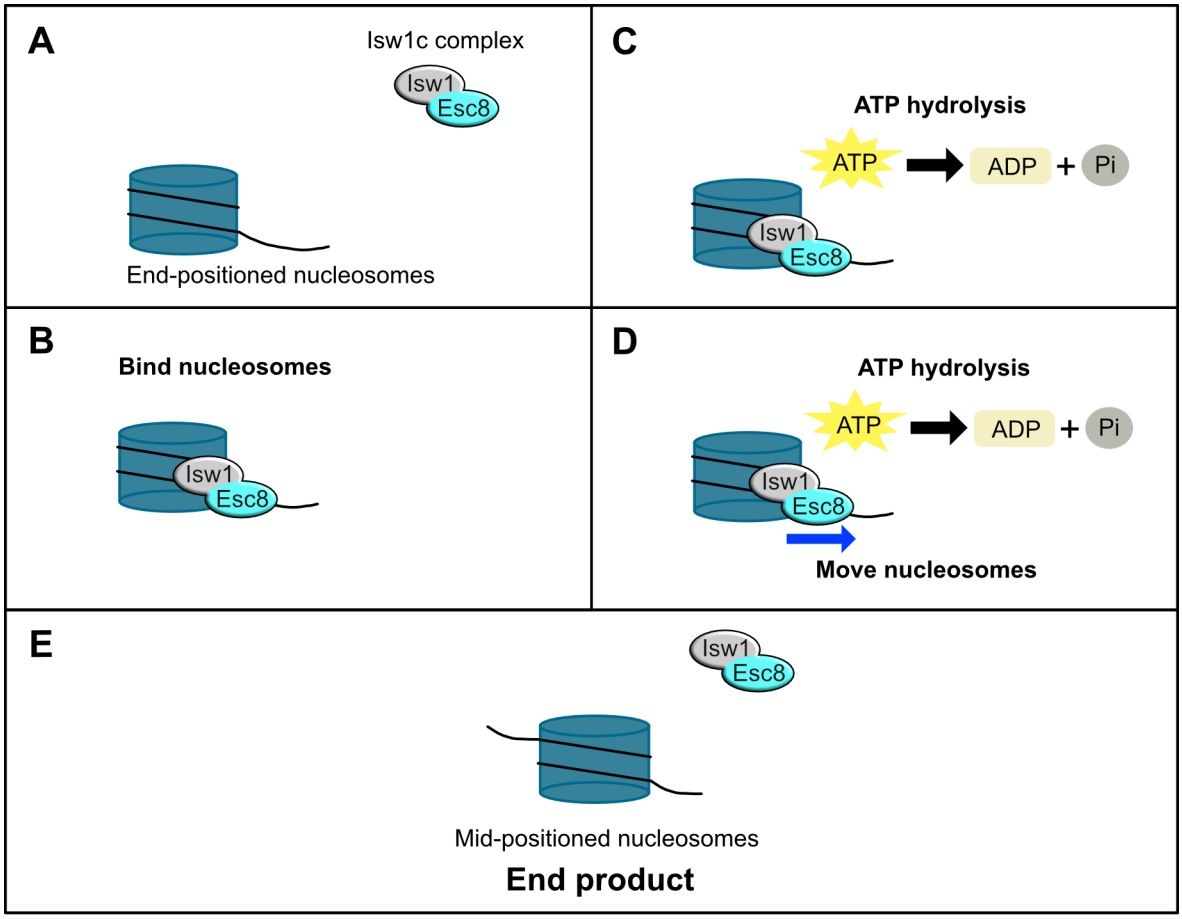

Figure 32. Mechanisms of Isw1c as a chromatin remodeler. (A) Isw1c recognizes nucleosomes. **(B)** Isw1c binds to nucleosomes containing one overhang DNA. **(C)** The ATPase subunit of Isw1 hydrolyzes ATP to ADP with inorganic phosphate. **(D)** Isw1c utilizes the energy from ATP hydrolysis to move nucleosomes from the end position toward the center. **(E)** Nucleosomes are shifted to the middle position.

4.3 Specific histone modifications impacting Isw1c chromatin remodeling

Specific histone modifications and histone variants can promote the recruitment of chromatin remodeling to nucleosomes and influence the efficiency of the remodeling activities. This can rely on the specialized domains in the chromatin remodelers to recognize specific histone modifications and histone variants. In fact, the Isw1a and Isw1b recruitment and remodeling activity are evidently reported to be influenced by histone variant H2AZ-containing nucleosomes and histone H3K36me3-containing nucleosomes **(Bergmann, 2021; Li et al., 2022; Smolle et al., 2012)**. Upon characterizing the function of Isw1c as a chromatin remodeler, I next asked which histone modifications and histone variants can influence the function of Isw1c, specifically in the binding and sliding nucleosomes.

I found that Isw1c slightly prefers interacting with unacetylated histone H3 or H4-containing nucleosomes over histones H3K9,14ac or H4K5,8,12ac-containing nucleosomes, respectively. The preference of the Isw1c complex for these unmodified nucleosomes appears to be aligned with the previously reported role of Esc8 in gene silencing and silent chromatin cohesion **(Chen et al., 2016; Cuperus & Shore, 2002)**. This correlation can be attributed to the characteristic absence of histone modifications in the silent chromatin state, which corresponds with Isw1c affinity binding for unmodified nucleosomes. Given these findings, the associated subunit of Esc8 is likely to be responsible for this binding preference of Isw1c for unmodified nucleosomes.

Moreover, in contrast with the binding preference, Isw1c demonstrates a sliding preference for histone H4K5,8,12ac-containing nucleosomes over unacetylated histone H4-containing nucleosomes. The sliding preference of Isw1c on this acetylated nucleosome may suggest that Isw1c has a role in facilitating cellular processes such as transcription, replication, or DNA repair. Apart from that, no nucleosome sliding preference was observed between histone H3-containing nucleosomes and histone H3K9,14ac-containing nucleosomes, as well as histone H4K16ac-containing nucleosome and histone H4-containing nucleosomes. These findings further highlight the substantial and specific preference of Isw1c to slide H4K5,8,12ac-containing nucleosomes. However, whether either one of these acetylation sites of histone H4K5,8,12ac might affect the Isw1c remodeler remains unclear.

In brief, unmodified nucleosomes slightly prefer to recruit the Isw1c complex, whereas nucleosomes containing acetylated histone H4K5,8,12ac enhance the remodeling activity of Isw1c. **Figure 33** depicts the schematic representation of Isw1c recruitment and sliding nucleosome preferences.

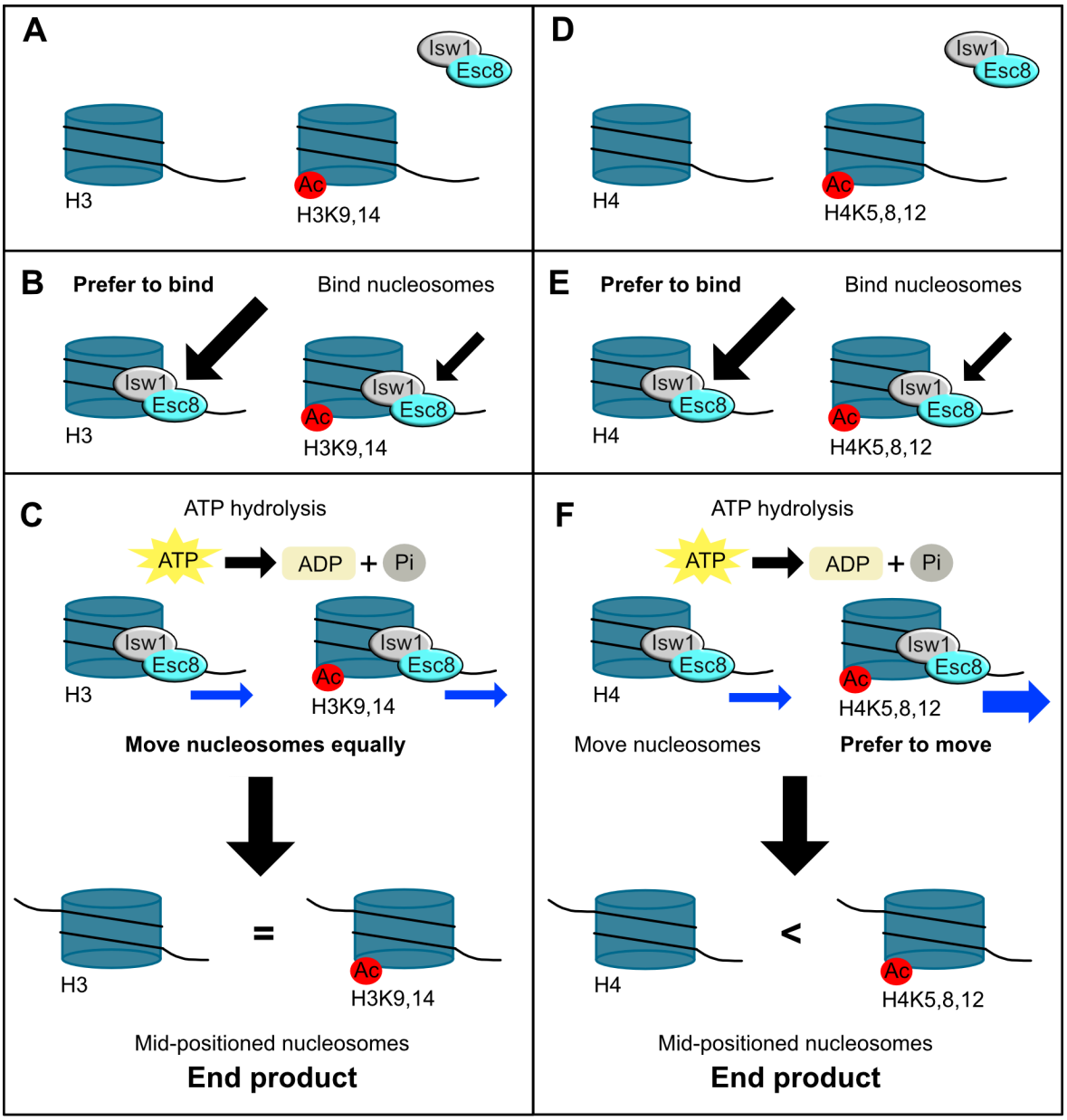

Figure 33. Model representative of Isw1c in recruitment and sliding nucleosome preferences. **(A)** Isw1c recognizes both histone H3-containing nucleosomes and histone H3K9,14ac-containing nucleosomes. **(B)** Isw1c exhibits a binding preference for histone H3-containing nucleosomes over histone H3K9,14ac-containing nucleosomes. **(C)**. Isw1c equally slides both histone H3-containing nucleosomes and histone H3K9,14ac-containing nucleosomes. **(D)** Isw1c recognizes both histone H4-containing nucleosomes and histone H4K5,8,12ac-containing nucleosomes. **(E)** Isw1c has a binding preference for histone H4-containing nucleosomes over histone H4K5,8,12ac-containing nucleosomes. **(F)** Isw1c prefers sliding histone H4K5,8,12ac-containing nucleosomes over histone H4-containing nucleosomes.

4.4 Formation of the Isw1c complex relies on the SLIDE domain of Isw1

A previous study discovered that Esc8 shares significant sequence similarity with Ioc3 **(Cuperus & Shore, 2002)**. Based on the sequence alignment, Esc8 is then found to exhibit the conserved regions of Ioc3 interacting with Isw1, strongly suggesting the interaction of Esc8 and Isw1 **(Yamada et al., 2011)**. Consistent with this sequence alignment, the AlphaFold predicted structure of Isw1c (HSS-Esc8) is well-aligned with the crystal structure of Isw1a (HSS-Ioc3) **(Supplementary Figure 2B)**. The two complexes are remarkably similar, with some differences observed between Ioc3 and Esc8 structures. After analyzing both aligned complexes, I confirmed that Esc8 retains the helical-linker-DNA-binding domain (HLB) structure (3 of 4 helix structures, α8, α10, and α11) but lacks the HSS-binding loop (HSSB) structure from Ioc3, which is in line with the previous sequence alignment **(Yamada et al., 2011)**. Additionally, Esc8 is missing the finger helix (FH), which consists of four positively charged arginine residues located at the C-terminal helix of Ioc3 and plays a role in interacting with the H2A-H2B acidic patch of the nucleosomes **(Li et al., 2024)**.

In Ioc3, the HLB domain consists of four α-helix structures from α8 to α11 **(Yamada et al., 2011)**. In the Isw1a complex, the HLB domain plays a crucial role in the recruitment of the complex with dinucleosomes instead of mononucleosomes through interactions with DNA **(Bhardwaj et al., 2020)**. In addition, the lack of the HLB domain does not intrude with the formation of Isw1a or the interaction of Isw1a with mononucleosomes **(Bhardwaj et al., 2020)**. Although the deletion of the HLB domain retains the formation of the Isw1a complex, it somewhat consequently impacts the ability of Isw1a to remodel dinucleosomes, space nucleosomes, and alter several gene transcriptions **(Bhardwaj et al., 2020)**. Given that Esc8 also contains the HLB domain similar to Ioc3, thus the likelihood of recruitment of the Isw1c to dinucleosomes appears plausible.

Based on the crystallography structure of Isw1a, the HSSB loop of Ioc3 extends across the SLIDE domain and reaches close to the SANT domain **(Yamada et al., 2011)**. Additionally, co-immunoprecipitation (co-IP) data revealed that deleting of only the SLIDE domain of Isw1 did not fully abolish the interaction with Ioc3 **(Pinskaya et al., 2009)**. Instead, a weak interaction between $Isw1_{\Delta SLIDE}$ and Ioc3 seems to rely on the HSSB loop, which is in close proximity to the SANT domain. This association can be observed from a surface representation structure of Ioc3-HSS in **Figure 28E**. In contrast to Isw1a, the absence of the HSSB loop in Esc8 suggests that the formation of Isw1c is primarily dependent on the interaction of Esc8 core protein to Isw1, particularly in the SLIDE domain **(Figure 28F)**. In agreement with this Isw1c structural analysis, the co-IP experiment revealed that there was no protein-protein interaction between Isw1c lacking SLIDE domain with Esc8 as expected.

I further determined which region of Esc8 is involved in an interaction with Isw1. Nevertheless, I found that deleting an average of approximately 261 amino acids in the Esc8 region resulted in an unstable protein. In addition, I discovered that only $Esc8_{\Delta C2}$ remains to interact with Isw1 to form the Isw1c complex mutant. Furthermore, this Isw1c mutant can efficiently slide nucleosomes similar to the wildtype Isw1c. Thus far, the region of Esc8 protein interacting with Isw1 remains unresolved.

Since the SLIDE domain of Isw1 is primarily found to bind with Esc8, I conducted preliminary data analysis to search for residue pairs from the SLIDE domain of Isw1 interacting with Esc8 through salt bridges (positive-negative charged), hydrophobic contacts, and hydrogen bonds. I listed all the potential residue pairs in **Supplementary Table 2.** Additionally, I showed the representative structural model containing the residue pairs from the SLIDE domain of Isw1 binding to Esc8 in **Supplementary Figure 3**.

To sum up, Esc8 protein shares significant similarities with Ioc3 based on the sequence and structural alignment, albeit with some differences. Notably, Esc8 contains a conserved region known as the HLB domain, suggesting the possibility of Isw1c interacting with dinucleosomes. Furthermore, the formation of the Isw1c complex relies on the interaction between the SLIDE domain of Isw1 and Esc8. Additionally, the N-terminus of Esc8 seems to have a role in stabilizing the protein, while deletion of the C-terminus of Esc8 does not impact the formation of the Isw1c complex and its remodeling nucleosome activity.

4.5 Outlook

In the present study, I have shown that the association of Isw1 with Esc8 is dependent on the SLIDE domain of Isw1. However, there are unresolved questions about how Esc8 interacts with Isw1. Particularly, which region of Esc8 interacts with Isw1? Since large deletion regions of Esc8 led to unstable protein in previous experiments, it would be worthwhile to delete a small fragment of Esc8 to minimize the misfolding protein and subsequently test its interaction with Isw1 using co-IP experiments. Another question is which residues in Esc8 are involved in the interaction with the SLIDE domain of Isw1? To assist with that question, I have analyzed the interaction between the two proteins through the AlphaFold predicted structure of the Isw1c complex, and resulted in listing all potential residue pairs for Esc8 interacting with the SLIDE domain of Isw1 as preliminary data in **Supplementary Table 2**. Given this data, Esc8 point mutation can be generated and further investigated for its interaction with Isw1 using co-IP experiments. If any of those Esc8 mutants remain to interact with Isw1, the binding and remodeling nucleosome abilities can also be further investigated. All these are to uncover the impacts of the mutation for Isw1c to function as a chromatin remodeler. After all, it would be interesting to understand the interaction of Esc8 with Isw1 in depth.

In the Isw1a complex, the HLB domain of Ioc3 has been known to play an important role in the Isw1a binding to dinucleosomes instead of mononucleosomes **(Bhardwaj et al., 2020)**. Besides this interaction, HLB appears to hold the key that somewhat impacts and determines the mechanisms of action of Isw1 as a chromatin remodeler. In this process, HLB not only associates with the preference of Isw1a for remodeling dinucleosomes but it further impacts the nucleosome spacing and transcription to many genes **(Bhardwaj et al., 2020)**. Interestingly, the HLB domain is also found in the associated subunit Esc8 of Isw1c. Having the HLB domain conserved in Esc8, I thus propose that Isw1c may potentially exhibit a binding and sliding preference for dinucleosomes rather than mononucleosomes. Additionally, truncating the HLB domain from Esc8 may loosen the ability of Isw1c to bind and slide dinucleosomes and further abrogate the nucleosome spacing activity.

Moreover, characterizing the functions of Isw1c *in vivo* will be the ultimate goal to gain insights into its biological roles. The yeast Isw1 complex chromatin remodeler has been reported to have a function to prevent cryptic initiation **(Smolle et al., 2012)**. However, by utilizing RNA-Seq and northern blot, the deletion of *ESC8* displayed no cryptic transcript **(Data is not shown)**. Given these findings, we need to explore the other potential functions of Isw1c *in vivo*. Our finding reveals that Isw1c demonstrates a sliding preference for histone H4K5,8,12ac-containing nucleosomes, which suggests that this Isw1c complex may facilitate cellular processes such as transcription, replication, or DNA repair. Since histone H4K5,8,12ac-containing nucleosomes are generally localized at the 5' end of the genes near the promoter, it would be particularly intriguing to investigate the *in vivo* localization of Esc8. Nevertheless, addressing this research question using ChIP-seq or Cut&RUN techniques can be very challenging due to the low abundance of Isw1c in the cell. In fact, our attempt to use Cut&RUN techniques to address this question was not successful. Therefore, the qPCR can be a good initial approach for determining the enrichment of Esc8 in the genes.

5. References

Akdel, M., Pires, D. E. V., Pardo, E. P., Janes, J., Zalevsky, A. O., Meszaros, B., Bryant, P., Good, L. L., Laskowski, R. A., Pozzati, G., Shenoy, A., Zhu, W., Kundrotas, P., Serra, V. R., Rodrigues, C. H. M., Dunham, A. S., Burke, D., Borkakoti, N., Velankar, S., . . . Beltrao, P. (2022). A structural biology community assessment of AlphaFold2 applications. *Nat Struct Mol Biol*, *29*(11), 1056-1067. https://doi.org/10.1038/s41594-022-00849-w

Allfrey, V. G., Faulkner, R., & Mirsky, A. E. (1964). Acetylation and Methylation of Histones and Their Possible Role in the Regulation of Rna Synthesis. *Proc Natl Acad Sci U S A*, *51*(5), 786-794. https://doi.org/10.1073/pnas.51.5.786

Allshire, R. C., & Ekwall, K. (2015). Epigenetic Regulation of Chromatin States in Schizosaccharomyces pombe. *Cold Spring Harb Perspect Biol*, *7*(7), a018770. https://doi.org/10.1101/cshperspect.a018770

Alper, B. J., Lowe, B. R., & Partridge, J. F. (2012). Centromeric heterochromatin assembly in fission yeast--balancing transcription, RNA interference and chromatin modification. *Chromosome Res*, *20*(5), 521-534. https://doi.org/10.1007/s10577-012-9288-x

Altaf, M., Auger, A., Monnet-Saksouk, J., Brodeur, J., Piquet, S., Cramet, M., Bouchard, N., Lacoste, N., Utley, R. T., Gaudreau, L., & Cote, J. (2010). NuA4-dependent acetylation of nucleosomal histones H4 and H2A directly stimulates incorporation of H2A.Z by the SWR1 complex. *J Biol Chem*, *285*(21), 15966-15977. https://doi.org/10.1074/jbc.M110.117069

Andersen, E. C., Lu, X., & Horvitz, H. R. (2006). C. elegans ISWI and NURF301 antagonize an Rb-like pathway in the determination of multiple cell fates. *Development*, *133*(14), 2695-2704. https://doi.org/10.1242/dev.02444

Arents, G., Burlingame, R. W., Wang, B. C., Love, W. E., & Moudrianakis, E. N. (1991). The nucleosomal core histone octamer at 3.1 A resolution: a tripartite protein assembly and a left-handed superhelix. *Proc Natl Acad Sci U S A*, *88*(22), 10148-10152. https://doi.org/10.1073/pnas.88.22.10148

Awad, S., & Hassan, A. H. (2008). The Swi2/Snf2 bromodomain is important for the full binding and remodeling activity of the SWI/SNF complex on H3- and H4-acetylated nucleosomes. *Ann N Y Acad Sci*, *1138*, 366-375. https://doi.org/10.1196/annals.1414.038

Badenhorst, P., Voas, M., Rebay, I., & Wu, C. (2002). Biological functions of the ISWI chromatin remodeling complex NURF. *Genes Dev*, *16*(24), 3186-3198. https://doi.org/10.1101/gad.1032202

Baldi, S., Jain, D. S., Harpprecht, L., Zabel, A., Scheibe, M., Butter, F., Straub, T., & Becker, P. B. (2018). Genome-wide Rules of Nucleosome Phasing in Drosophila. *Mol Cell*, *72*(4), 661-672 e664. https://doi.org/10.1016/j.molcel.2018.09.032

Bannister, A. J., & Kouzarides, T. (2011). Regulation of chromatin by histone modifications. *Cell Res*, *21*(3), 381-395. https://doi.org/10.1038/cr.2011.22

Bannister, A. J., Schneider, R., & Kouzarides, T. (2002). Histone methylation: dynamic or static? *Cell*, *109*(7), 801-806. https://doi.org/10.1016/s0092-8674(02)00798-5

Bannister, A. J., Zegerman, P., Partridge, J. F., Miska, E. A., Thomas, J. O., Allshire, R. C., & Kouzarides, T. (2001). Selective recognition of methylated lysine 9 on

histone H3 by the HP1 chromo domain. *Nature*, *410*(6824), 120-124. https://doi.org/10.1038/35065138

Bao, Y., & Shen, X. (2007). INO80 subfamily of chromatin remodeling complexes. *Mutat Res*, *618*(1-2), 18-29. https://doi.org/10.1016/j.mrfmmm.2006.10.006

Bartholomew, B. (2014). ISWI chromatin remodeling: one primary actor or a coordinated effort? *Curr Opin Struct Biol*, *24*, 150-155. https://doi.org/10.1016/j.sbi.2014.01.010

Beacon, T. H., Delcuve, G. P., López, C., Nardocci, G., Kovalchuk, I., van Wijnen, A. J., & Davie, J. R. (2021). The dynamic broad epigenetic (H3K4me3, H3K27ac) domain as a mark of essential genes. *Clinical Epigenetics*, *13*(1), 138. https://doi.org/10.1186/s13148-021-01126-1

Becker, P. B., & Workman, J. L. (2013). Nucleosome remodeling and epigenetics. *Cold Spring Harb Perspect Biol*, *5*(9). https://doi.org/10.1101/cshperspect.a017905

Bedford, M. T., & Richard, S. (2005). Arginine methylation an emerging regulator of protein function. *Mol Cell*, *18*(3), 263-272. https://doi.org/10.1016/j.molcel.2005.04.003

Bergmann, L. S. (2021). Elucidating the molecular mechanism of Isw1a and Isw1b chromatin remodeler recruitment.

Bernard, P., Maure, J. F., Partridge, J. F., Genier, S., Javerzat, J. P., & Allshire, R. C. (2001). Requirement of heterochromatin for cohesion at centromeres. *Science*, *294*(5551), 2539-2542. https://doi.org/10.1126/science.1064027

Bhardwaj, S. K., Hailu, S. G., Olufemi, L., Brahma, S., Kundu, S., Hota, S. K., Persinger, J., & Bartholomew, B. (2020). Dinucleosome specificity and allosteric switch of the ISW1a ATP-dependent chromatin remodeler in transcription regulation. *Nat Commun*, *11*(1), 5913. https://doi.org/10.1038/s41467-020-19700-1

Bhatwa, A., Wang, W., Hassan, Y. I., Abraham, N., Li, X. Z., & Zhou, T. (2021). Challenges Associated With the Formation of Recombinant Protein Inclusion Bodies in Escherichia coli and Strategies to Address Them for Industrial Applications. *Front Bioeng Biotechnol*, *9*, 630551. https://doi.org/10.3389/fbioe.2021.630551

Bi, X. (2014). Heterochromatin structure: lessons from the budding yeast. *IUBMB Life*, *66*(10), 657-666. https://doi.org/10.1002/iub.1322

Biswas, M., Voltz, K., Smith, J. C., & Langowski, J. (2011). Role of histone tails in structural stability of the nucleosome. *PLoS Comput Biol*, *7*(12), e1002279. https://doi.org/10.1371/journal.pcbi.1002279

Blank, T. A., & Becker, P. B. (1996). The effect of nucleosome phasing sequences and DNA topology on nucleosome spacing. *J Mol Biol*, *260*(1), 1-8. https://doi.org/10.1006/jmbi.1996.0377

Bowman, G. D. (2010). Mechanisms of ATP-dependent nucleosome sliding. *Curr Opin Struct Biol*, *20*(1), 73-81. https://doi.org/10.1016/j.sbi.2009.12.002

Bozhenok, L., Wade, P. A., & Varga-Weisz, P. (2002). WSTF-ISWI chromatin remodeling complex targets heterochromatic replication foci. *EMBO J*, *21*(9), 2231-2241. https://doi.org/10.1093/emboj/21.9.2231

Bradbury, E. M. (1977). Histone nomenclature. *Methods Cell Biol*, *16*, 179-181. https://www.ncbi.nlm.nih.gov/pubmed/886978

Braunstein, M., Rose, A. B., Holmes, S. G., Allis, C. D., & Broach, J. R. (1993). Transcriptional silencing in yeast is associated with reduced nucleosome acetylation. *Genes Dev*, *7*(4), 592-604. https://doi.org/10.1101/gad.7.4.592

Braunstein, M., Sobel, R. E., Allis, C. D., Turner, B. M., & Broach, J. R. (1996). Efficient transcriptional silencing in Saccharomyces cerevisiae requires a heterochromatin histone acetylation pattern. *Mol Cell Biol*, *16*(8), 4349-4356. https://doi.org/10.1128/MCB.16.8.4349

Briggs, S. D., Bryk, M., Strahl, B. D., Cheung, W. L., Davie, J. K., Dent, S. Y., Winston, F., & Allis, C. D. (2001). Histone H3 lysine 4 methylation is mediated by Set1 and required for cell growth and rDNA silencing in Saccharomyces cerevisiae. *Genes Dev*, *15*(24), 3286-3295. https://doi.org/10.1101/gad.940201

Buratowski, S., & Kim, T. (2010). The role of cotranscriptional histone methylations. *Cold Spring Harb Symp Quant Biol*, *75*, 95-102. https://doi.org/10.1101/sqb.2010.75.036

Carey, M., Li, B., & Workman, J. L. (2006). RSC exploits histone acetylation to abrogate the nucleosomal block to RNA polymerase II elongation. *Mol Cell*, *24*(3), 481-487. https://doi.org/10.1016/j.molcel.2006.09.012

Carrozza, M. J., Li, B., Florens, L., Suganuma, T., Swanson, S. K., Lee, K. K., Shia, W. J., Anderson, S., Yates, J., Washburn, M. P., & Workman, J. L. (2005). Histone H3 methylation by Set2 directs deacetylation of coding regions by Rpd3S to suppress spurious intragenic transcription. *Cell*, *123*(4), 581-592. https://doi.org/10.1016/j.cell.2005.10.023

Chen, G., Li, W., Yan, F., Wang, D., & Chen, Y. (2020). The Structural Basis for Specific Recognition of H3K14 Acetylation by Sth1 in the RSC Chromatin Remodeling Complex. *Structure*, *28*(1), 111-118 e113. https://doi.org/10.1016/j.str.2019.10.015

Chen, J., Acton, T. B., Basu, S. K., Montelione, G. T., & Inouye, M. (2002). Enhancement of the solubility of proteins overexpressed in Escherichia coli by heat shock. *J Mol Microbiol Biotechnol*, *4*(6), 519-524. https://www.ncbi.nlm.nih.gov/pubmed/12432951

Chen, K., Yuan, J., Sia, Y., & Chen, Z. (2023). Mechanism of action of the SWI/SNF family complexes. *Nucleus*, *14*(1), 2165604. https://doi.org/10.1080/19491034.2023.2165604

Chen, Y. C., Koutelou, E., & Dent, S. Y. R. (2022). Now open: Evolving insights to the roles of lysine acetylation in chromatin organization and function. *Mol Cell*, *82*(4), 716-727. https://doi.org/10.1016/j.molcel.2021.12.004

Chen, Y. F., Chou, C. C., & Gartenberg, M. R. (2016). Determinants of Sir2-Mediated, Silent Chromatin Cohesion. *Mol Cell Biol*, *36*(15), 2039-2050. https://doi.org/10.1128/MCB.00057-16

Chereji, R. V., & Clark, D. J. (2018). Major Determinants of Nucleosome Positioning. *Biophys J*, *114*(10), 2279-2289. https://doi.org/10.1016/j.bpj.2018.03.015

Chou, K. Y., Lee, J. Y., Kim, K. B., Kim, E., Lee, H. S., & Ryu, H. Y. (2023). Histone modification in Saccharomyces cerevisiae: A review of the current status. *Comput Struct Biotechnol J*, *21*, 1843-1850. https://doi.org/10.1016/j.csbj.2023.02.037

Choy, J. S., Acuña, R., Au, W. C., & Basrai, M. A. (2011). A role for histone H4K16 hypoacetylation in Saccharomyces cerevisiae kinetochore function. *Genetics*, *189*(1), 11-21. https://doi.org/10.1534/genetics.111.130781

Clapier, C. R., & Cairns, B. R. (2009). The biology of chromatin remodeling complexes. *Annu Rev Biochem*, *78*, 273-304. https://doi.org/10.1146/annurev.biochem.77.062706.153223

Clapier, C. R., & Cairns, B. R. (2012). Regulation of ISWI involves inhibitory modules antagonized by nucleosomal epitopes. *Nature*, *492*(7428), 280-284. https://doi.org/10.1038/nature11625

Clapier, C. R., Iwasa, J., Cairns, B. R., & Peterson, C. L. (2017). Mechanisms of action and regulation of ATP-dependent chromatin-remodelling complexes. *Nat Rev Mol Cell Biol*, *18*(7), 407-422. https://doi.org/10.1038/nrm.2017.26

Cuperus, G., & Shore, D. (2002). Restoration of silencing in Saccharomyces cerevisiae by tethering of a novel Sir2-interacting protein, Esc8. *Genetics*, *162*(2), 633-645. https://doi.org/10.1093/genetics/162.2.633

Cutler, S., Lee, L. J., & Tsukiyama, T. (2018). Chromatin Remodeling Factors Isw2 and Ino80 Regulate Chromatin, Replication, and Copy Number of the Saccharomyces cerevisiae Ribosomal DNA Locus. *Genetics*, *210*(4), 1543-1556. https://doi.org/10.1534/genetics.118.301579

Cutter, A. R., & Hayes, J. J. (2015). A brief review of nucleosome structure. *FEBS Lett*, *589*(20 Pt A), 2914-2922. https://doi.org/10.1016/j.febslet.2015.05.016

Davey, C. A., Sargent, D. F., Luger, K., Maeder, A. W., & Richmond, T. J. (2002). Solvent mediated interactions in the structure of the nucleosome core particle at 1.9 a resolution. *J Mol Biol*, *319*(5), 1097-1113. https://doi.org/10.1016/S0022-2836(02)00386-8

De Cian, A., Praly, E., Ding, F., Singh, V., Lavelle, C., Le Cam, E., Croquette, V., Pietrement, O., & Bensimon, D. (2012). ATP-independent cooperative binding of yeast Isw1a to bare and nucleosomal DNA. *PLoS One*, *7*(2), e31845. https://doi.org/10.1371/journal.pone.0031845

Deuring, R., Fanti, L., Armstrong, J. A., Sarte, M., Papoulas, O., Prestel, M., Daubresse, G., Verardo, M., Moseley, S. L., Berloco, M., Tsukiyama, T., Wu, C., Pimpinelli, S., & Tamkun, J. W. (2000). The ISWI chromatin-remodeling protein is required for gene expression and the maintenance of higher order chromatin structure in vivo. *Mol Cell*, *5*(2), 355-365. https://doi.org/10.1016/s1097-2765(00)80430-x

Dhalluin, C., Carlson, J. E., Zeng, L., He, C., Aggarwal, A. K., & Zhou, M. M. (1999). Structure and ligand of a histone acetyltransferase bromodomain. *Nature*, *399*(6735), 491-496. https://doi.org/10.1038/20974

Di Lorenzo, A., & Bedford, M. T. (2011). Histone arginine methylation. *FEBS Lett*, *585*(13), 2024-2031. https://doi.org/10.1016/j.febslet.2010.11.010

Diaz-Olmos, Y., Batista, M., Ludwig, A., & Marchini, F. K. (2020). Characterising ISWI chromatin remodeler in Trypanosoma cruzi. *Mem Inst Oswaldo Cruz*, *115*, e190457. https://doi.org/10.1590/0074-02760190457

Dirscherl, S. S., & Krebs, J. E. (2004). Functional diversity of ISWI complexes. *Biochem Cell Biol*, *82*(4), 482-489. https://doi.org/10.1139/o04-044

Donovan, D. A., Crandall, J. G., Truong, V. N., Vaaler, A. L., Bailey, T. B., Dinwiddie, D., Banks, O. G., McKnight, L. E., & McKnight, J. N. (2021). Basis of specificity for a conserved and promiscuous chromatin remodeling protein. *Elife*, *10*. https://doi.org/10.7554/eLife.64061

Downs, J. A., Allard, S., Jobin-Robitaille, O., Javaheri, A., Auger, A., Bouchard, N., Kron, S. J., Jackson, S. P., & Cote, J. (2004). Binding of chromatin-modifying activities to phosphorylated histone H2A at DNA damage sites. *Mol Cell*, *16*(6), 979-990. https://doi.org/10.1016/j.molcel.2004.12.003

Eberharter, A., & Becker, P. B. (2002). Histone acetylation: a switch between repressive and permissive chromatin. Second in review series on chromatin

dynamics. *EMBO Rep*, *3*(3), 224-229. https://doi.org/10.1093/embo-reports/kvf053

Eberharter, A., Ferrari, S., Langst, G., Straub, T., Imhof, A., Varga-Weisz, P., Wilm, M., & Becker, P. B. (2001). Acf1, the largest subunit of CHRAC, regulates ISWI-induced nucleosome remodelling. *EMBO J*, *20*(14), 3781-3788. https://doi.org/10.1093/emboj/20.14.3781

Eberharter, A., Langst, G., & Becker, P. B. (2004). A nucleosome sliding assay for chromatin remodeling factors. *Methods Enzymol*, *377*, 344-353. https://doi.org/10.1016/S0076-6879(03)77021-9

Elfmann, C., & Stulke, J. (2023). PAE viewer: a webserver for the interactive visualization of the predicted aligned error for multimer structure predictions and crosslinks. *Nucleic Acids Res*, *51*(W1), W404-W410. https://doi.org/10.1093/nar/gkad350

Elfring, L. K., Deuring, R., McCallum, C. M., Peterson, C. L., & Tamkun, J. W. (1994). Identification and characterization of Drosophila relatives of the yeast transcriptional activator SNF2/SWI2. *Mol Cell Biol*, *14*(4), 2225-2234. https://doi.org/10.1128/mcb.14.4.2225-2234.1994

Emelyanov, A. V., Vershilova, E., Ignatyeva, M. A., Pokrovsky, D. K., Lu, X., Konev, A. Y., & Fyodorov, D. V. (2012). Identification and characterization of ToRC, a novel ISWI-containing ATP-dependent chromatin assembly complex. *Genes Dev*, *26*(6), 603-614. https://doi.org/10.1101/gad.180604.111

Eustermann, S., Patel, A. B., Hopfner, K. P., He, Y., & Korber, P. (2023). Energy-driven genome regulation by ATP-dependent chromatin remodellers. *Nat Rev Mol Cell Biol*. https://doi.org/10.1038/s41580-023-00683-y

Fazzio, T. G., Gelbart, M. E., & Tsukiyama, T. (2005). Two distinct mechanisms of chromatin interaction by the Isw2 chromatin remodeling complex in vivo. *Mol Cell Biol*, *25*(21), 9165-9174. https://doi.org/10.1128/MCB.25.21.9165-9174.2005

Fazzio, T. G., Kooperberg, C., Goldmark, J. P., Neal, C., Basom, R., Delrow, J., & Tsukiyama, T. (2001). Widespread collaboration of Isw2 and Sin3-Rpd3 chromatin remodeling complexes in transcriptional repression. *Mol Cell Biol*, *21*(19), 6450-6460. https://doi.org/10.1128/MCB.21.19.6450-6460.2001

Fazzio, T. G., & Tsukiyama, T. (2003). Chromatin remodeling in vivo: evidence for a nucleosome sliding mechanism. *Mol Cell*, *12*(5), 1333-1340. https://doi.org/10.1016/s1097-2765(03)00436-2

Finch, J. T., Lutter, L. C., Rhodes, D., Brown, R. S., Rushton, B., Levitt, M., & Klug, A. (1977). Structure of nucleosome core particles of chromatin. *Nature*, *269*(5623), 29-36. https://doi.org/10.1038/269029a0

Flanagan, J. F., Blus, B. J., Kim, D., Clines, K. L., Rastinejad, F., & Khorasanizadeh, S. (2007). Molecular implications of evolutionary differences in CHD double chromodomains. *J Mol Biol*, *369*(2), 334-342. https://doi.org/10.1016/j.jmb.2007.03.024

Flanagan, J. F., Mi, L. Z., Chruszcz, M., Cymborowski, M., Clines, K. L., Kim, Y., Minor, W., Rastinejad, F., & Khorasanizadeh, S. (2005). Double chromodomains cooperate to recognize the methylated histone H3 tail. *Nature*, *438*(7071), 1181-1185. https://doi.org/10.1038/nature04290

Flaus, A., Martin, D. M., Barton, G. J., & Owen-Hughes, T. (2006). Identification of multiple distinct Snf2 subfamilies with conserved structural motifs. *Nucleic Acids Res*, *34*(10), 2887-2905. https://doi.org/10.1093/nar/gkl295

Flemming, W. (1882). Zellsubstanz, Kern und Zelltheilung. *Verlag von F. C. W. Vogel*.

Forne, I., Ludwigsen, J., Imhof, A., Becker, P. B., & Mueller-Planitz, F. (2012). Probing the conformation of the ISWI ATPase domain with genetically encoded photoreactive crosslinkers and mass spectrometry. *Mol Cell Proteomics*, *11*(4), M111 012088. https://doi.org/10.1074/mcp.M111.012088

Fyodorov, D. V., & Kadonaga, J. T. (2002). Dynamics of ATP-dependent chromatin assembly by ACF. *Nature*, *418*(6900), 897-900. https://doi.org/10.1038/nature00929

Gaillard, C., & Strauss, F. (1990). Ethanol precipitation of DNA with linear polyacrylamide as carrier. *Nucleic Acids Res*, *18*(2), 378. https://doi.org/10.1093/nar/18.2.378

Gangaraju, V. K., & Bartholomew, B. (2007). Dependency of ISW1a chromatin remodeling on extranucleosomal DNA. *Mol Cell Biol*, *27*(8), 3217-3225. https://doi.org/10.1128/MCB.01731-06

Gavin, A. C., Bösche, M., Krause, R., Grandi, P., Marzioch, M., Bauer, A., Schultz, J., Rick, J. M., Michon, A. M., Cruciat, C. M., Remor, M., Höfert, C., Schelder, M., Brajenovic, M., Ruffner, H., Merino, A., Klein, K., Hudak, M., Dickson, D., . . . Superti-Furga, G. (2002). Functional organization of the yeast proteome by systematic analysis of protein complexes. *Nature*, *415*(6868), 141-147. https://doi.org/10.1038/415141a

Gelbart, M. E., Rechsteiner, T., Richmond, T. J., & Tsukiyama, T. (2001). Interactions of Isw2 chromatin remodeling complex with nucleosomal arrays: analyses using recombinant yeast histones and immobilized templates. *Mol Cell Biol*, *21*(6), 2098-2106. https://doi.org/10.1128/MCB.21.6.2098-2106.2001

Georgieva, E. I., & Sendra, R. (1999). Mobility of acetylated histones in sodium dodecyl sulfate-polyacrylamide gel electrophoresis. *Anal Biochem*, *269*(2), 399-402. https://doi.org/10.1006/abio.1999.4050

Gerhold, C. B., Winkler, D. D., Lakomek, K., Seifert, F. U., Fenn, S., Kessler, B., Witte, G., Luger, K., & Hopfner, K. P. (2012). Structure of Actin-related protein 8 and its contribution to nucleosome binding. *Nucleic Acids Res*, *40*(21), 11036-11046. https://doi.org/10.1093/nar/gks842

Ghoneim, M., Fuchs, H. A., & Musselman, C. A. (2021). Histone Tail Conformations: A Fuzzy Affair with DNA. *Trends Biochem Sci*, *46*(7), 564-578. https://doi.org/10.1016/j.tibs.2020.12.012

Gibson, D. G., Young, L., Chuang, R. Y., Venter, J. C., Hutchison, C. A., 3rd, & Smith, H. O. (2009). Enzymatic assembly of DNA molecules up to several hundred kilobases. *Nat Methods*, *6*(5), 343-345. https://doi.org/10.1038/nmeth.1318

Gietz, R. D., & Schiestl, R. H. (2007). High-efficiency yeast transformation using the LiAc/SS carrier DNA/PEG method. *Nat Protoc*, *2*(1), 31-34. https://doi.org/10.1038/nprot.2007.13

Goldmark, J. P., Fazzio, T. G., Estep, P. W., Church, G. M., & Tsukiyama, T. (2000). The Isw2 chromatin remodeling complex represses early meiotic genes upon recruitment by Ume6p. *Cell*, *103*(3), 423-433. https://doi.org/10.1016/s0092-8674(00)00134-3

Grigoryev, S. A., & Woodcock, C. L. (2012). Chromatin organization - the 30 nm fiber. *Exp Cell Res*, *318*(12), 1448-1455. https://doi.org/10.1016/j.yexcr.2012.02.014

Grune, T., Brzeski, J., Eberharter, A., Clapier, C. R., Corona, D. F., Becker, P. B., & Muller, C. W. (2003). Crystal structure and functional analysis of a nucleosome recognition module of the remodeling factor ISWI. *Mol Cell*, *12*(2), 449-460. https://doi.org/10.1016/s1097-2765(03)00273-9

Guschin, D., Geiman, T. M., Kikyo, N., Tremethick, D. J., Wolffe, A. P., & Wade, P. A. (2000). Multiple ISWI ATPase complexes from xenopus laevis. Functional conservation of an ACF/CHRAC homolog. *J Biol Chem*, *275*(45), 35248-35255. https://doi.org/10.1074/jbc.M006041200

Gutin, J., Sadeh, R., Bodenheimer, N., Joseph-Strauss, D., Klein-Brill, A., Alajem, A., Ram, O., & Friedman, N. (2018). Fine-Resolution Mapping of TF Binding and Chromatin Interactions. *Cell Rep*, *22*(10), 2797-2807. https://doi.org/10.1016/j.celrep.2018.02.052

Hall, J. A., & Georgel, P. T. (2007). CHD proteins: a diverse family with strong ties. *Biochem Cell Biol*, *85*(4), 463-476. https://doi.org/10.1139/O07-063

Hamiche, A., Sandaltzopoulos, R., Gdula, D. A., & Wu, C. (1999). ATP-dependent histone octamer sliding mediated by the chromatin remodeling complex NURF. *Cell*, *97*(7), 833-842. https://doi.org/10.1016/s0092-8674(00)80796-5

Hanai, K., Furuhashi, H., Yamamoto, T., Akasaka, K., & Hirose, S. (2008). RSF governs silent chromatin formation via histone H2Av replacement. *PLoS Genet*, *4*(2), e1000011. https://doi.org/10.1371/journal.pgen.1000011

Harata, M., Oma, Y., Mizuno, S., Jiang, Y. W., Stillman, D. J., & Wintersberger, U. (1999). The nuclear actin-related protein of Saccharomyces cerevisiae, Act3p/Arp4, interacts with core histones. *Mol Biol Cell*, *10*(8), 2595-2605. https://doi.org/10.1091/mbc.10.8.2595

Harata, M., Zhang, Y., Stillman, D. J., Matsui, D., Oma, Y., Nishimori, K., & Mochizuki, R. (2002). Correlation between chromatin association and transcriptional regulation for the Act3p/Arp4 nuclear actin-related protein of Saccharomyces cerevisiae. *Nucleic Acids Res*, *30*(8), 1743-1750. https://doi.org/10.1093/nar/30.8.1743

Harper, S., & Speicher, D. W. (2011). Purification of proteins fused to glutathione S-transferase. *Methods Mol Biol*, *681*, 259-280. https://doi.org/10.1007/978-1-60761-913-0_14

Hassan, A. H., Neely, K. E., & Workman, J. L. (2001). Histone acetyltransferase complexes stabilize swi/snf binding to promoter nucleosomes. *Cell*, *104*(6), 817-827. https://doi.org/10.1016/s0092-8674(01)00279-3

Hassan, A. H., Prochasson, P., Neely, K. E., Galasinski, S. C., Chandy, M., Carrozza, M. J., & Workman, J. L. (2002). Function and selectivity of bromodomains in anchoring chromatin-modifying complexes to promoter nucleosomes. *Cell*, *111*(3), 369-379. https://doi.org/10.1016/s0092-8674(02)01005-x

Hecht, A., Laroche, T., Strahl-Bolsinger, S., Gasser, S. M., & Grunstein, M. (1995). Histone H3 and H4 N-termini interact with SIR3 and SIR4 proteins: a molecular model for the formation of heterochromatin in yeast. *Cell*, *80*(4), 583-592. https://doi.org/10.1016/0092-8674(95)90512-x

Hecht, A., Strahl-Bolsinger, S., & Grunstein, M. (1996). Spreading of transcriptional repressor SIR3 from telomeric heterochromatin. *Nature*, *383*(6595), 92-96. https://doi.org/10.1038/383092a0

Horn, P. J., & Peterson, C. L. (2002). Molecular biology. Chromatin higher order folding--wrapping up transcription. *Science*, *297*(5588), 1824-1827. https://doi.org/10.1126/science.1074200

Hughes, K., Wand, M., Foulston, L., Young, R., Harley, K., Terry, S., Ersfeld, K., & Rudenko, G. (2007). A novel ISWI is involved in VSG expression site downregulation in African trypanosomes. *EMBO J*, *26*(9), 2400-2410. https://doi.org/10.1038/sj.emboj.7601678

Hughes, T. R., Marton, M. J., Jones, A. R., Roberts, C. J., Stoughton, R., Armour, C. D., Bennett, H. A., Coffey, E., Dai, H., He, Y. D., Kidd, M. J., King, A. M., Meyer, M. R., Slade, D., Lum, P. Y., Stepaniants, S. B., Shoemaker, D. D., Gachotte, D., Chakraburtty, K., . . . Friend, S. H. (2000). Functional discovery via a compendium of expression profiles. *Cell*, *102*(1), 109-126. https://doi.org/10.1016/s0092-8674(00)00015-5

Hyun, K., Jeon, J., Park, K., & Kim, J. (2017). Writing, erasing and reading histone lysine methylations. *Exp Mol Med*, *49*(4), e324. https://doi.org/10.1038/emm.2017.11

Iida, T., & Araki, H. (2004). Noncompetitive counteractions of DNA polymerase epsilon and ISW2/yCHRAC for epigenetic inheritance of telomere position effect in Saccharomyces cerevisiae. *Mol Cell Biol*, *24*(1), 217-227. https://doi.org/10.1128/MCB.24.1.217-227.2004

Imai, S., Armstrong, C. M., Kaeberlein, M., & Guarente, L. (2000). Transcriptional silencing and longevity protein Sir2 is an NAD-dependent histone deacetylase. *Nature*, *403*(6771), 795-800. https://doi.org/10.1038/35001622

Ito, T., Bulger, M., Pazin, M. J., Kobayashi, R., & Kadonaga, J. T. (1997). ACF, an ISWI-containing and ATP-utilizing chromatin assembly and remodeling factor. *Cell*, *90*(1), 145-155. https://doi.org/10.1016/s0092-8674(00)80321-9

Ito, T., Levenstein, M. E., Fyodorov, D. V., Kutach, A. K., Kobayashi, R., & Kadonaga, J. T. (1999). ACF consists of two subunits, Acf1 and ISWI, that function cooperatively in the ATP-dependent catalysis of chromatin assembly. *Genes Dev*, *13*(12), 1529-1539. https://doi.org/10.1101/gad.13.12.1529

Iwasaki, H., Takahagi, M., Nakata, A., & Shinagawa, H. (1992). Escherichia coli RuvA and RuvB proteins specifically interact with Holliday junctions and promote branch migration. *Genes Dev*, *6*(11), 2214-2220. https://doi.org/10.1101/gad.6.11.2214

Iwasaki, W., Miya, Y., Horikoshi, N., Osakabe, A., Taguchi, H., Tachiwana, H., Shibata, T., Kagawa, W., & Kurumizaka, H. (2013). Contribution of histone N-terminal tails to the structure and stability of nucleosomes. *FEBS Open Bio*, *3*, 363-369. https://doi.org/10.1016/j.fob.2013.08.007

Jacobson, R. H., Ladurner, A. G., King, D. S., & Tjian, R. (2000). Structure and function of a human TAFII250 double bromodomain module. *Science*, *288*(5470), 1422-1425. https://doi.org/10.1126/science.288.5470.1422

Jae Yoo, E., Kyu Jang, Y., Ae Lee, M., Bjerling, P., Bum Kim, J., Ekwall, K., Hyun Seong, R., & Dai Park, S. (2002). Hrp3, a chromodomain helicase/ATPase DNA binding protein, is required for heterochromatin silencing in fission yeast. *Biochemical and Biophysical Research Communications*, *295*(4), 970-974. https://doi.org/https://doi.org/10.1016/S0006-291X(02)00797-0

Janke, C., Magiera, M. M., Rathfelder, N., Taxis, C., Reber, S., Maekawa, H., Moreno-Borchart, A., Doenges, G., Schwob, E., Schiebel, E., & Knop, M. (2004). A versatile toolbox for PCR-based tagging of yeast genes: new fluorescent proteins, more markers and promoter substitution cassettes. *Yeast*, *21*(11), 947-962. https://doi.org/10.1002/yea.1142

Jha, S., & Dutta, A. (2009). RVB1/RVB2: running rings around molecular biology. *Mol Cell*, *34*(5), 521-533. https://doi.org/10.1016/j.molcel.2009.05.016

Jiang, C., & Pugh, B. F. (2009a). A compiled and systematic reference map of nucleosome positions across the Saccharomyces cerevisiae genome. *Genome Biol*, *10*(10), R109. https://doi.org/10.1186/gb-2009-10-10-r109

Jiang, C., & Pugh, B. F. (2009b). Nucleosome positioning and gene regulation: advances through genomics. *Nat Rev Genet*, *10*(3), 161-172. https://doi.org/10.1038/nrg2522

Jin, Y. H., Yoo, E. J., Jang, Y. K., Kim, S. H., Kim, M. J., Shim, Y. S., Lee, J. S., Choi, I. S., Seong, R. H., Hong, S. H., & Park, S. D. (1998). Isolation and characterization of hrp1+, a new member of the SNF2/SWI2 gene family from the fission yeast Schizosaccharomyces pombe. *Mol Gen Genet*, *257*(3), 319-329. https://doi.org/10.1007/s004380050653

Jin, Y. H., Yoo, E. J., Jang, Y. K., Kim, S. H., Lee, C. G., Seong, R. H., Hong, S. H., & Park, S. D. (1998). Purification and characterization of Hrp1, a Homolog of Mouse CHD1 from the fission yeast schizosaccharomyces pombe. *Korean Journal of Biological Sciences*, *2*(4), 539-543. https://doi.org/10.1080/12265071.1998.9647457

Johnson, A., Li, G., Sikorski, T. W., Buratowski, S., Woodcock, C. L., & Moazed, D. (2009). Reconstitution of heterochromatin-dependent transcriptional gene silencing. *Mol Cell*, *35*(6), 769-781. https://doi.org/10.1016/j.molcel.2009.07.030

Jonsson, Z. O., Jha, S., Wohlschlegel, J. A., & Dutta, A. (2004). Rvb1p/Rvb2p recruit Arp5p and assemble a functional Ino80 chromatin remodeling complex. *Mol Cell*, *16*(3), 465-477. https://doi.org/10.1016/j.molcel.2004.09.033

Joti, Y., Hikima, T., Nishino, Y., Kamada, F., Hihara, S., Takata, H., Ishikawa, T., & Maeshima, K. (2012). Chromosomes without a 30-nm chromatin fiber. *Nucleus*, *3*(5), 404-410. https://doi.org/10.4161/nucl.21222

Jumper, J., Evans, R., Pritzel, A., Green, T., Figurnov, M., Ronneberger, O., Tunyasuvunakool, K., Bates, R., Zidek, A., Potapenko, A., Bridgland, A., Meyer, C., Kohl, S. A. A., Ballard, A. J., Cowie, A., Romera-Paredes, B., Nikolov, S., Jain, R., Adler, J., . . . Hassabis, D. (2021). Highly accurate protein structure prediction with AlphaFold. *Nature*, *596*(7873), 583-589. https://doi.org/10.1038/s41586-021-03819-2

Kang, J. G., Hamiche, A., & Wu, C. (2002). GAL4 directs nucleosome sliding induced by NURF. *EMBO J*, *21*(6), 1406-1413. https://doi.org/10.1093/emboj/21.6.1406

Kapust, R. B., & Waugh, D. S. (1999). Escherichia coli maltose-binding protein is uncommonly effective at promoting the solubility of polypeptides to which it is fused. *Protein Sci*, *8*(8), 1668-1674. https://doi.org/10.1110/ps.8.8.1668

Kasten, M., Szerlong, H., Erdjument-Bromage, H., Tempst, P., Werner, M., & Cairns, B. R. (2004). Tandem bromodomains in the chromatin remodeler RSC recognize acetylated histone H3 Lys14. *EMBO J*, *23*(6), 1348-1359. https://doi.org/10.1038/sj.emboj.7600143

Kent, N. A., Karabetsou, N., Politis, P. K., & Mellor, J. (2001). In vivo chromatin remodeling by yeast ISWI homologs Isw1p and Isw2p. *Genes Dev*, *15*(5), 619-626. https://doi.org/10.1101/gad.190301

Kimura, A., Umehara, T., & Horikoshi, M. (2002). Chromosomal gradient of histone acetylation established by Sas2p and Sir2p functions as a shield against gene silencing. *Nat Genet*, *32*(3), 370-377. https://doi.org/10.1038/ng993

Kizer, K. O., Phatnani, H. P., Shibata, Y., Hall, H., Greenleaf, A. L., & Strahl, B. D. (2005). A novel domain in Set2 mediates RNA polymerase II interaction and

couples histone H3 K36 methylation with transcript elongation. *Mol Cell Biol*, *25*(8), 3305-3316. https://doi.org/10.1128/MCB.25.8.3305-3316.2005

Klug, A., Rhodes, D., Smith, J., Finch, J. T., & Thomas, J. O. (1980). A low resolution structure for the histone core of the nucleosome. *Nature*, *287*(5782), 509-516. https://doi.org/10.1038/287509a0

Kornberg, R. D. (1974). Chromatin structure: a repeating unit of histones and DNA. *Science*, *184*(4139), 868-871. https://doi.org/10.1126/science.184.4139.868

Kouzarides, T. (2007). Chromatin modifications and their function. *Cell*, *128*(4), 693-705. https://doi.org/10.1016/j.cell.2007.02.005

Krietenstein, N., Wal, M., Watanabe, S., Park, B., Peterson, C. L., Pugh, B. F., & Korber, P. (2016). Genomic Nucleosome Organization Reconstituted with Pure Proteins. *Cell*, *167*(3), 709-721 e712. https://doi.org/10.1016/j.cell.2016.09.045

Krogan, N. J., Kim, M., Tong, A., Golshani, A., Cagney, G., Canadien, V., Richards, D. P., Beattie, B. K., Emili, A., Boone, C., Shilatifard, A., Buratowski, S., & Greenblatt, J. (2003). Methylation of histone H3 by Set2 in Saccharomyces cerevisiae is linked to transcriptional elongation by RNA polymerase II. *Mol Cell Biol*, *23*(12), 4207-4218. https://doi.org/10.1128/MCB.23.12.4207-4218.2003

Kurdistani, S. K., & Grunstein, M. (2003). Histone acetylation and deacetylation in yeast. *Nat Rev Mol Cell Biol*, *4*(4), 276-284. https://doi.org/10.1038/nrm1075

Kurdistani, S. K., Tavazoie, S., & Grunstein, M. (2004). Mapping global histone acetylation patterns to gene expression. *Cell*, *117*(6), 721-733. https://doi.org/10.1016/j.cell.2004.05.023

Kwon, S. Y., Grisan, V., Jang, B., Herbert, J., & Badenhorst, P. (2016). Genome-Wide Mapping Targets of the Metazoan Chromatin Remodeling Factor NURF Reveals Nucleosome Remodeling at Enhancers, Core Promoters and Gene Insulators. *PLoS Genet*, *12*(4), e1005969. https://doi.org/10.1371/journal.pgen.1005969

Ladurner, A. G., Inouye, C., Jain, R., & Tjian, R. (2003). Bromodomains mediate an acetyl-histone encoded antisilencing function at heterochromatin boundaries. *Mol Cell*, *11*(2), 365-376. https://doi.org/10.1016/s1097-2765(03)00035-2

Lafon, A., Petty, E., & Pillus, L. (2012). Functional antagonism between Sas3 and Gcn5 acetyltransferases and ISWI chromatin remodelers. *PLoS Genet*, *8*(10), e1002994. https://doi.org/10.1371/journal.pgen.1002994

Landry, J., Sutton, A., Tafrov, S. T., Heller, R. C., Stebbins, J., Pillus, L., & Sternglanz, R. (2000). The silencing protein SIR2 and its homologs are NAD-dependent protein deacetylases. *Proc Natl Acad Sci U S A*, *97*(11), 5807-5811. https://doi.org/10.1073/pnas.110148297

Langst, G., Bonte, E. J., Corona, D. F., & Becker, P. B. (1999). Nucleosome movement by CHRAC and ISWI without disruption or trans-displacement of the histone octamer. *Cell*, *97*(7), 843-852. https://doi.org/10.1016/s0092-8674(00)80797-7

Lee, D. Y., Hayes, J. J., Pruss, D., & Wolffe, A. P. (1993). A positive role for histone acetylation in transcription factor access to nucleosomal DNA. *Cell*, *72*(1), 73-84. https://doi.org/10.1016/0092-8674(93)90051-q

LeRoy, G., Orphanides, G., Lane, W. S., & Reinberg, D. (1998). Requirement of RSF and FACT for transcription of chromatin templates in vitro. *Science*, *282*(5395), 1900-1904. https://doi.org/10.1126/science.282.5395.1900

Li, B., Gogol, M., Carey, M., Pattenden, S. G., Seidel, C., & Workman, J. L. (2007). Infrequently transcribed long genes depend on the Set2/Rpd3S pathway for accurate transcription. *Genes Dev*, *21*(11), 1422-1430. https://doi.org/10.1101/gad.1539307

Li, B., Howe, L., Anderson, S., Yates, J. R., 3rd, & Workman, J. L. (2003). The Set2 histone methyltransferase functions through the phosphorylated carboxyl-terminal domain of RNA polymerase II. *J Biol Chem*, *278*(11), 8897-8903. https://doi.org/10.1074/jbc.M212134200

Li, B., Jackson, J., Simon, M. D., Fleharty, B., Gogol, M., Seidel, C., Workman, J. L., & Shilatifard, A. (2009). Histone H3 lysine 36 dimethylation (H3K36me2) is sufficient to recruit the Rpd3s histone deacetylase complex and to repress spurious transcription. *J Biol Chem*, *284*(12), 7970-7976. https://doi.org/10.1074/jbc.M808220200

Li, F., Huarte, M., Zaratiegui, M., Vaughn, M. W., Shi, Y., Martienssen, R., & Cande, W. Z. (2008). Lid2 is required for coordinating H3K4 and H3K9 methylation of heterochromatin and euchromatin. *Cell*, *135*(2), 272-283. https://doi.org/10.1016/j.cell.2008.08.036

Li, G., & Reinberg, D. (2011). Chromatin higher-order structures and gene regulation. *Curr Opin Genet Dev*, *21*(2), 175-186. https://doi.org/10.1016/j.gde.2011.01.022

Li, H., Ilin, S., Wang, W., Duncan, E. M., Wysocka, J., Allis, C. D., & Patel, D. J. (2006). Molecular basis for site-specific read-out of histone H3K4me3 by the BPTF PHD finger of NURF. *Nature*, *442*(7098), 91-95. https://doi.org/10.1038/nature04802

Li, J., Bergmann, L., Rafael de Almeida, A., Webb, K. M., Gogol, M. M., Voigt, P., Liu, Y., Liang, H., & Smolle, M. M. (2022). H3K36 methylation and DNA-binding both promote Ioc4 recruitment and Isw1b remodeler function. *Nucleic Acids Res*, *50*(5), 2549-2565. https://doi.org/10.1093/nar/gkac077

Li, L., Chen, K., Sia, Y., Hu, P., Ye, Y., & Chen, Z. (2024). Structure of the ISW1a complex bound to the dinucleosome. *Nat Struct Mol Biol*. https://doi.org/10.1038/s41594-023-01174-6

Li, Y., Gong, H., Wang, P., Zhu, Y., Peng, H., Cui, Y., Li, H., Liu, J., & Wang, Z. (2021). The emerging role of ISWI chromatin remodeling complexes in cancer. *J Exp Clin Cancer Res*, *40*(1), 346. https://doi.org/10.1186/s13046-021-02151-x

Lin, A., Du, Y., & Xiao, W. (2020). Yeast chromatin remodeling complexes and their roles in transcription. *Curr Genet*, *66*(4), 657-670. https://doi.org/10.1007/s00294-020-01072-0

Liu, C. L., Kaplan, T., Kim, M., Buratowski, S., Schreiber, S. L., Friedman, N., & Rando, O. J. (2005). Single-nucleosome mapping of histone modifications in S. cerevisiae. *PLoS Biol*, *3*(10), e328. https://doi.org/10.1371/journal.pbio.0030328

Liu, R., Wu, J., Guo, H., Yao, W., Li, S., Lu, Y., Jia, Y., Liang, X., Tang, J., & Zhang, H. (2023). Post-translational modifications of histones: Mechanisms, biological functions, and therapeutic targets. *MedComm (2020)*, *4*(3), e292. https://doi.org/10.1002/mco2.292

Luger, K., Mader, A. W., Richmond, R. K., Sargent, D. F., & Richmond, T. J. (1997). Crystal structure of the nucleosome core particle at 2.8 A resolution. *Nature*, *389*(6648), 251-260. https://doi.org/10.1038/38444

Maeshima, K., Hihara, S., & Eltsov, M. (2010). Chromatin structure: does the 30-nm fibre exist in vivo? *Curr Opin Cell Biol*, *22*(3), 291-297. https://doi.org/10.1016/j.ceb.2010.03.001

Maeshima, K., Hihara, S., & Takata, H. (2010). New insight into the mitotic chromosome structure: irregular folding of nucleosome fibers without 30-nm chromatin structure. *Cold Spring Harb Symp Quant Biol*, *75*, 439-444. https://doi.org/10.1101/sqb.2010.75.034

Maeshima, K., Ide, S., & Babokhov, M. (2019). Dynamic chromatin organization without the 30-nm fiber. *Curr Opin Cell Biol*, *58*, 95-104. https://doi.org/10.1016/j.ceb.2019.02.003

Maeshima, K., Ide, S., Hibino, K., & Sasai, M. (2016). Liquid-like behavior of chromatin. *Curr Opin Genet Dev*, *37*, 36-45. https://doi.org/10.1016/j.gde.2015.11.006

Maeshima, K., Imai, R., Tamura, S., & Nozaki, T. (2014). Chromatin as dynamic 10-nm fibers. *Chromosoma*, *123*(3), 225-237. https://doi.org/10.1007/s00412-014-0460-2

Maksimov, V., Oya, E., Tanaka, M., Kawaguchi, T., Hachisuka, A., Ekwall, K., Bjerling, P., & Nakayama, J. I. (2018). The binding of Chp2's chromodomain to methylated H3K9 is essential for Chp2's role in heterochromatin assembly in fission yeast. *PLoS One*, *13*(8), e0201101. https://doi.org/10.1371/journal.pone.0201101

Maltby, V. E., Martin, B. J., Schulze, J. M., Johnson, I., Hentrich, T., Sharma, A., Kobor, M. S., & Howe, L. (2012). Histone H3 lysine 36 methylation targets the Isw1b remodeling complex to chromatin. *Mol Cell Biol*, *32*(17), 3479-3485. https://doi.org/10.1128/MCB.00389-12

Marfella, C. G., & Imbalzano, A. N. (2007). The Chd family of chromatin remodelers. *Mutat Res*, *618*(1-2), 30-40. https://doi.org/10.1016/j.mrfmmm.2006.07.012

Marmorstein, R., & Trievel, R. C. (2009). Histone modifying enzymes: structures, mechanisms, and specificities. *Biochim Biophys Acta*, *1789*(1), 58-68. https://doi.org/10.1016/j.bbagrm.2008.07.009

Martin, B. J. E., Ablondi, E. F., Goglia, C., Mimoso, C. A., Espinel-Cabrera, P. R., & Adelman, K. (2023). Global identification of SWI/SNF targets reveals compensation by EP400. *Cell*, *186*(24), 5290-5307 e5226. https://doi.org/10.1016/j.cell.2023.10.006

Martin, C., & Zhang, Y. (2005). The diverse functions of histone lysine methylation. *Nat Rev Mol Cell Biol*, *6*(11), 838-849. https://doi.org/10.1038/nrm1761

Matangkasombut, O., & Buratowski, S. (2003). Different sensitivities of bromodomain factors 1 and 2 to histone H4 acetylation. *Mol Cell*, *11*(2), 353-363. https://doi.org/10.1016/s1097-2765(03)00033-9

Maurer-Stroh, S., Dickens, N. J., Hughes-Davies, L., Kouzarides, T., Eisenhaber, F., & Ponting, C. P. (2003). The Tudor domain 'Royal Family': Tudor, plant Agenet, Chromo, PWWP and MBT domains. *Trends Biochem Sci*, *28*(2), 69-74. https://doi.org/10.1016/S0968-0004(03)00004-5

McConnell, A. D., Gelbart, M. E., & Tsukiyama, T. (2004). Histone fold protein Dls1p is required for Isw2-dependent chromatin remodeling in vivo. *Mol Cell Biol*, *24*(7), 2605-2613. https://doi.org/10.1128/MCB.24.7.2605-2613.2004

McGinty, R. K., & Tan, S. (2015). Nucleosome structure and function. *Chem Rev*, *115*(6), 2255-2273. https://doi.org/10.1021/cr500373h

Mellor, J., & Morillon, A. (2004). ISWI complexes in Saccharomyces cerevisiae. *Biochim Biophys Acta*, *1677*(1-3), 100-112. https://doi.org/10.1016/j.bbaexp.2003.10.014

Meshorer, E., & Plath, K. (2020). Chromatin and Nuclear Architecture in Stem Cells. *Stem Cell Reports*, *15*(6), 1155-1157. https://doi.org/10.1016/j.stemcr.2020.11.012

Millan-Zambrano, G., Burton, A., Bannister, A. J., & Schneider, R. (2022). Histone post-translational modifications - cause and consequence of genome function. *Nat Rev Genet*, *23*(9), 563-580. https://doi.org/10.1038/s41576-022-00468-7

Millar, C. B., & Grunstein, M. (2006). Genome-wide patterns of histone modifications in yeast. *Nat Rev Mol Cell Biol*, *7*(9), 657-666. https://doi.org/10.1038/nrm1986

Millar, C. B., Kurdistani, S. K., & Grunstein, M. (2004). Acetylation of yeast histone H4 lysine 16: a switch for protein interactions in heterochromatin and euchromatin. *Cold Spring Harb Symp Quant Biol*, *69*, 193-200. https://doi.org/10.1101/sqb.2004.69.193

Miller, S. (2018). Gibson Assembly. https://pengxulab.weebly.com/uploads/7/9/3/5/79359982/gibson_assembly_%E2%80%93_samuel_miller_lab_uw_seattle.pdf

Miller, T., Krogan, N. J., Dover, J., Erdjument-Bromage, H., Tempst, P., Johnston, M., Greenblatt, J. F., & Shilatifard, A. (2001). COMPASS: a complex of proteins associated with a trithorax-related SET domain protein. *Proc Natl Acad Sci U S A*, *98*(23), 12902-12907. https://doi.org/10.1073/pnas.231473398

Misteli, T. (2020). The Self-Organizing Genome: Principles of Genome Architecture and Function. *Cell*, *183*(1), 28-45. https://doi.org/10.1016/j.cell.2020.09.014

Mizuguchi, G., Tsukiyama, T., Wisniewski, J., & Wu, C. (1997). Role of nucleosome remodeling factor NURF in transcriptional activation of chromatin. *Mol Cell*, *1*(1), 141-150. https://doi.org/10.1016/s1097-2765(00)80015-5

Moazed, D., Kistler, A., Axelrod, A., Rine, J., & Johnson, A. D. (1997). Silent information regulator protein complexes in Saccharomyces cerevisiae: a SIR2/SIR4 complex and evidence for a regulatory domain in SIR4 that inhibits its interaction with SIR3. *Proc Natl Acad Sci U S A*, *94*(6), 2186-2191. https://doi.org/10.1073/pnas.94.6.2186

Mohrmann, L., & Verrijzer, C. P. (2005). Composition and functional specificity of SWI2/SNF2 class chromatin remodeling complexes. *Biochim Biophys Acta*, *1681*(2-3), 59-73. https://doi.org/10.1016/j.bbaexp.2004.10.005

Moore, D., & Dowhan, D. (2002). Purification and concentration of DNA from aqueous solutions. *Curr Protoc Mol Biol*, *Chapter 2*, Unit 2 1A. https://doi.org/10.1002/0471142727.mb0201as59

Moretti, P., Freeman, K., Coodly, L., & Shore, D. (1994). Evidence that a complex of SIR proteins interacts with the silencer and telomere-binding protein RAP1. *Genes Dev*, *8*(19), 2257-2269. https://doi.org/10.1101/gad.8.19.2257

Morettini, S., Tribus, M., Zeilner, A., Sebald, J., Campo-Fernandez, B., Scheran, G., Worle, H., Podhraski, V., Fyodorov, D. V., & Lusser, A. (2011). The chromodomains of CHD1 are critical for enzymatic activity but less important for chromatin localization. *Nucleic Acids Res*, *39*(8), 3103-3115. https://doi.org/10.1093/nar/gkq1298

Morillon, A., Karabetsou, N., O'Sullivan, J., Kent, N., Proudfoot, N., & Mellor, J. (2003). Isw1 chromatin remodeling ATPase coordinates transcription

elongation and termination by RNA polymerase II. *Cell*, *115*(4), 425-435. https://doi.org/10.1016/s0092-8674(03)00880-8

Morrison, A. J. (2017). Genome maintenance functions of the INO80 chromatin remodeller. *Philos Trans R Soc Lond B Biol Sci*, *372*(1731). https://doi.org/10.1098/rstb.2016.0289

Motamedi, M. R., Hong, E. J., Li, X., Gerber, S., Denison, C., Gygi, S., & Moazed, D. (2008). HP1 proteins form distinct complexes and mediate heterochromatic gene silencing by nonoverlapping mechanisms. *Mol Cell*, *32*(6), 778-790. https://doi.org/10.1016/j.molcel.2008.10.026

Mueller-Planitz, F., Klinker, H., Ludwigsen, J., & Becker, P. B. (2013). The ATPase domain of ISWI is an autonomous nucleosome remodeling machine. *Nature Structural & Molecular Biology*, *20*(1), 82-89. https://doi.org/10.1038/nsmb.2457

Murawska, M., & Brehm, A. (2011). CHD chromatin remodelers and the transcription cycle. *Transcription*, *2*(6), 244-253. https://doi.org/10.4161/trns.2.6.17840

Musselman, C. A., & Kutateladze, T. G. (2011). Handpicking epigenetic marks with PHD fingers. *Nucleic Acids Res*, *39*(21), 9061-9071. https://doi.org/10.1093/nar/gkr613

Mutskov, V., Gerber, D., Angelov, D., Ausio, J., Workman, J., & Dimitrov, S. (1998). Persistent interactions of core histone tails with nucleosomal DNA following acetylation and transcription factor binding. *Mol Cell Biol*, *18*(11), 6293-6304. https://doi.org/10.1128/MCB.18.11.6293

Nakayama, J., Rice, J. C., Strahl, B. D., Allis, C. D., & Grewal, S. I. (2001). Role of histone H3 lysine 9 methylation in epigenetic control of heterochromatin assembly. *Science*, *292*(5514), 110-113. https://doi.org/10.1126/science.1060118

Navarathna, D. H., Pathirana, R. U., Lionakis, M. S., Nickerson, K. W., & Roberts, D. D. (2016). Candida albicans ISW2 Regulates Chlamydospore Suspensor Cell Formation and Virulence In Vivo in a Mouse Model of Disseminated Candidiasis. *PLoS One*, *11*(10), e0164449. https://doi.org/10.1371/journal.pone.0164449

Ng, H. H., Ciccone, D. N., Morshead, K. B., Oettinger, M. A., & Struhl, K. (2003). Lysine-79 of histone H3 is hypomethylated at silenced loci in yeast and mammalian cells: a potential mechanism for position-effect variegation. *Proc Natl Acad Sci U S A*, *100*(4), 1820-1825. https://doi.org/10.1073/pnas.0437846100

Nguyen, A. T., & Zhang, Y. (2011). The diverse functions of Dot1 and H3K79 methylation. *Genes Dev*, *25*(13), 1345-1358. https://doi.org/10.1101/gad.2057811

Nishino, Y., Eltsov, M., Joti, Y., Ito, K., Takata, H., Takahashi, Y., Hihara, S., Frangakis, A. S., Imamoto, N., Ishikawa, T., & Maeshima, K. (2012). Human mitotic chromosomes consist predominantly of irregularly folded nucleosome fibres without a 30-nm chromatin structure. *EMBO J*, *31*(7), 1644-1653. https://doi.org/10.1038/emboj.2012.35

Nodelman, I. M., & Bowman, G. D. (2021). Biophysics of Chromatin Remodeling. *Annu Rev Biophys*, *50*, 73-93. https://doi.org/10.1146/annurev-biophys-082520-080201

Nonaka, N., Kitajima, T., Yokobayashi, S., Xiao, G., Yamamoto, M., Grewal, S. I., & Watanabe, Y. (2002). Recruitment of cohesin to heterochromatic regions by

Swi6/HP1 in fission yeast. *Nat Cell Biol*, *4*(1), 89-93. https://doi.org/10.1038/ncb739

Oberbeckmann, E., Niebauer, V., Watanabe, S., Farnung, L., Moldt, M., Schmid, A., Cramer, P., Peterson, C. L., Eustermann, S., Hopfner, K. P., & Korber, P. (2021). Ruler elements in chromatin remodelers set nucleosome array spacing and phasing. *Nat Commun*, *12*(1), 3232. https://doi.org/10.1038/s41467-021-23015-0

Oganesyan, N., Ankoudinova, I., Kim, S. H., & Kim, R. (2007). Effect of osmotic stress and heat shock in recombinant protein overexpression and crystallization. *Protein Expr Purif*, *52*(2), 280-285. https://doi.org/10.1016/j.pep.2006.09.015

Oh, J., Yeom, S., Park, J., & Lee, J. S. (2022). The regional sequestration of heterochromatin structural proteins is critical to form and maintain silent chromatin. *Epigenetics Chromatin*, *15*(1), 5. https://doi.org/10.1186/s13072-022-00435-w

Olins, A. L., & Olins, D. E. (1974). Spheroid chromatin units (v bodies). *Science*, *183*(4122), 330-332. https://doi.org/10.1126/science.183.4122.330

Olins, D. E., & Olins, A. L. (2003). Chromatin history: our view from the bridge. *Nat Rev Mol Cell Biol*, *4*(10), 809-814. https://doi.org/10.1038/nrm1225

Oppikofer, M., Bai, T., Gan, Y., Haley, B., Liu, P., Sandoval, W., Ciferri, C., & Cochran, A. G. (2017). Expansion of the ISWI chromatin remodeler family with new active complexes. *EMBO Rep*, *18*(10), 1697-1706. https://doi.org/10.15252/embr.201744011

Oppikofer, M., Kueng, S., & Gasser, S. M. (2013). SIR-nucleosome interactions: structure-function relationships in yeast silent chromatin. *Gene*, *527*(1), 10-25. https://doi.org/10.1016/j.gene.2013.05.088

Oppikofer, M., Kueng, S., Martino, F., Soeroes, S., Hancock, S. M., Chin, J. W., Fischle, W., & Gasser, S. M. (2011). A dual role of H4K16 acetylation in the establishment of yeast silent chromatin. *EMBO J*, *30*(13), 2610-2621. https://doi.org/10.1038/emboj.2011.170

Oudet, P., Gross-Bellard, M., & Chambon, P. (1975). Electron microscopic and biochemical evidence that chromatin structure is a repeating unit. *Cell*, *4*(4), 281-300. https://doi.org/10.1016/0092-8674(75)90149-x

Owen-Hughes, T., Utley, R. T., Steger, D. J., West, J. M., John, S., Cote, J., Havas, K. M., & Workman, J. L. (1999). Analysis of nucleosome disruption by ATP-driven chromatin remodeling complexes. *Methods Mol Biol*, *119*, 319-331. https://doi.org/10.1385/1-59259-681-9:319

Padeken, J., Methot, S. P., & Gasser, S. M. (2022). Establishment of H3K9-methylated heterochromatin and its functions in tissue differentiation and maintenance. *Nat Rev Mol Cell Biol*, *23*(9), 623-640. https://doi.org/10.1038/s41580-022-00483-w

Parsons, C. A., Tsaneva, I., Lloyd, R. G., & West, S. C. (1992). Interaction of Escherichia coli RuvA and RuvB proteins with synthetic Holliday junctions. *Proc Natl Acad Sci U S A*, *89*(12), 5452-5456. https://doi.org/10.1073/pnas.89.12.5452

Paweletz, N. (2001). Walther Flemming: pioneer of mitosis research. *Nat Rev Mol Cell Biol*, *2*(1), 72-75. https://doi.org/10.1038/35048077

Pinskaya, M., Nair, A., Clynes, D., Morillon, A., & Mellor, J. (2009). Nucleosome remodeling and transcriptional repression are distinct functions of Isw1 in

Saccharomyces cerevisiae. *Mol Cell Biol*, *29*(9), 2419-2430. https://doi.org/10.1128/MCB.01050-08

Pokholok, D. K., Harbison, C. T., Levine, S., Cole, M., Hannett, N. M., Lee, T. I., Bell, G. W., Walker, K., Rolfe, P. A., Herbolsheimer, E., Zeitlinger, J., Lewitter, F., Gifford, D. K., & Young, R. A. (2005). Genome-wide map of nucleosome acetylation and methylation in yeast. *Cell*, *122*(4), 517-527. https://doi.org/10.1016/j.cell.2005.06.026

Pray-Grant, M. G., Daniel, J. A., Schieltz, D., Yates, J. R., 3rd, & Grant, P. A. (2005). Chd1 chromodomain links histone H3 methylation with SAGA- and SLIK-dependent acetylation. *Nature*, *433*(7024), 434-438. https://doi.org/10.1038/nature03242

Qin, S., & Min, J. (2014). Structure and function of the nucleosome-binding PWWP domain. *Trends Biochem Sci*, *39*(11), 536-547. https://doi.org/10.1016/j.tibs.2014.09.001

Radnai, L., Stremel, R. F., Sellers, J. R., Rumbaugh, G., & Miller, C. A. (2019). A Semi-High-Throughput Adaptation of the NADH-Coupled ATPase Assay for Screening Small Molecule Inhibitors. *J Vis Exp*(150). https://doi.org/10.3791/60017

Raran-Kurussi, S., & Waugh, D. S. (2017). Expression and Purification of Recombinant Proteins in Escherichia coli with a His(6) or Dual His(6)-MBP Tag. *Methods Mol Biol*, *1607*, 1-15. https://doi.org/10.1007/978-1-4939-7000-1_1

Rawal, Y., Chereji, R. V., Qiu, H., Ananthakrishnan, S., Govind, C. K., Clark, D. J., & Hinnebusch, A. G. (2018). SWI/SNF and RSC cooperate to reposition and evict promoter nucleosomes at highly expressed genes in yeast. *Genes Dev*, *32*(9-10), 695-710. https://doi.org/10.1101/gad.312850.118

Renauld, H., Aparicio, O. M., Zierath, P. D., Billington, B. L., Chhablani, S. K., & Gottschling, D. E. (1993). Silent domains are assembled continuously from the telomere and are defined by promoter distance and strength, and by SIR3 dosage. *Genes Dev*, *7*(7A), 1133-1145. https://doi.org/10.1101/gad.7.7a.1133

Reyes, A. A., Marcum, R. D., & He, Y. (2021). Structure and Function of Chromatin Remodelers. *J Mol Biol*, *433*(14), 166929. https://doi.org/10.1016/j.jmb.2021.166929

Richmond, T. J. (2012). Nucleosome recognition and spacing by chromatin remodelling factor ISW1a. *Biochem Soc Trans*, *40*(2), 347-350. https://doi.org/10.1042/bst20110748

Richmond, T. J., & Davey, C. A. (2003). The structure of DNA in the nucleosome core. *Nature*, *423*(6936), 145-150. https://doi.org/10.1038/nature01595

Richmond, T. J., Finch, J. T., Rushton, B., Rhodes, D., & Klug, A. (1984). Structure of the nucleosome core particle at 7 A resolution. *Nature*, *311*(5986), 532-537. https://doi.org/10.1038/311532a0

Rona, G. B., Eleutherio, E. C. A., & Pinheiro, A. S. (2016). PWWP domains and their modes of sensing DNA and histone methylated lysines. *Biophys Rev*, *8*(1), 63-74. https://doi.org/10.1007/s12551-015-0190-6

Roth, S. Y., Denu, J. M., & Allis, C. D. (2001). Histone acetyltransferases. *Annu Rev Biochem*, *70*, 81-120. https://doi.org/10.1146/annurev.biochem.70.1.81

Ruff, K. M., & Pappu, R. V. (2021). AlphaFold and Implications for Intrinsically Disordered Proteins. *J Mol Biol*, *433*(20), 167208. https://doi.org/10.1016/j.jmb.2021.167208

Ruiz, C., Escribano, V., Morgado, E., Molina, M., & Mazon, M. J. (2003). Cell-type-dependent repression of yeast a-specific genes requires Itc1p, a subunit of the Isw2p-Itc1p chromatin remodelling complex. *Microbiology (Reading)*, *149*(Pt 2), 341-351. https://doi.org/10.1099/mic.0.25920-0

Ruthenburg, A. J., Li, H., Milne, T. A., Dewell, S., McGinty, R. K., Yuen, M., Ueberheide, B., Dou, Y., Muir, T. W., Patel, D. J., & Allis, C. D. (2011). Recognition of a mononucleosomal histone modification pattern by BPTF via multivalent interactions. *Cell*, *145*(5), 692-706. https://doi.org/10.1016/j.cell.2011.03.053

Sadaie, M., Iida, T., Urano, T., & Nakayama, J. (2004). A chromodomain protein, Chp1, is required for the establishment of heterochromatin in fission yeast. *EMBO J*, *23*(19), 3825-3835. https://doi.org/10.1038/sj.emboj.7600401

Sadaie, M., Kawaguchi, R., Ohtani, Y., Arisaka, F., Tanaka, K., Shirahige, K., & Nakayama, J. (2008). Balance between distinct HP1 family proteins controls heterochromatin assembly in fission yeast. *Mol Cell Biol*, *28*(23), 6973-6988. https://doi.org/10.1128/mcb.00791-08

Sanchez, R., & Zhou, M. M. (2011). The PHD finger: a versatile epigenome reader. *Trends Biochem Sci*, *36*(7), 364-372. https://doi.org/10.1016/j.tibs.2011.03.005

Santoro, R., Li, J., & Grummt, I. (2002). The nucleolar remodeling complex NoRC mediates heterochromatin formation and silencing of ribosomal gene transcription. *Nat Genet*, *32*(3), 393-396. https://doi.org/10.1038/ng1010

Saravanan, M., Wuerges, J., Bose, D., McCormack, E. A., Cook, N. J., Zhang, X., & Wigley, D. B. (2012). Interactions between the nucleosome histone core and Arp8 in the INO80 chromatin remodeling complex. *Proc Natl Acad Sci U S A*, *109*(51), 20883-20888. https://doi.org/10.1073/pnas.1214735109

Scacchetti, A., Brueckner, L., Jain, D., Schauer, T., Zhang, X., Schnorrer, F., van Steensel, B., Straub, T., & Becker, P. B. (2018). CHRAC/ACF contribute to the repressive ground state of chromatin. *Life Sci Alliance*, *1*(1), e201800024. https://doi.org/10.26508/lsa.201800024

Schaft, D., Roguev, A., Kotovic, K. M., Shevchenko, A., Sarov, M., Shevchenko, A., Neugebauer, K. M., & Stewart, A. F. (2003). The histone 3 lysine 36 methyltransferase, SET2, is involved in transcriptional elongation. *Nucleic Acids Res*, *31*(10), 2475-2482. https://doi.org/10.1093/nar/gkg372

Schalch, T., Duda, S., Sargent, D. F., & Richmond, T. J. (2005). X-ray structure of a tetranucleosome and its implications for the chromatin fibre. *Nature*, *436*(7047), 138-141. https://doi.org/10.1038/nature03686

Sehgal, P., Olesen, C., & Moller, J. V. (2016). ATPase Activity Measurements by an Enzyme-Coupled Spectrophotometric Assay. *Methods Mol Biol*, *1377*, 105-109. https://doi.org/10.1007/978-1-4939-3179-8_11

Separovich, R. J., & Wilkins, M. R. (2021). Ready, SET, Go: Post-translational regulation of the histone lysine methylation network in budding yeast. *J Biol Chem*, *297*(2), 100939. https://doi.org/10.1016/j.jbc.2021.100939

Shen, X., Mizuguchi, G., Hamiche, A., & Wu, C. (2000). A chromatin remodelling complex involved in transcription and DNA processing. *Nature*, *406*(6795), 541-544. https://doi.org/10.1038/35020123

Shen, X., Ranallo, R., Choi, E., & Wu, C. (2003). Involvement of actin-related proteins in ATP-dependent chromatin remodeling. *Mol Cell*, *12*(1), 147-155. https://doi.org/10.1016/s1097-2765(03)00264-8

Shi, Y. G., & Tsukada, Y. (2013). The discovery of histone demethylases. *Cold Spring Harb Perspect Biol*, *5*(9). https://doi.org/10.1101/cshperspect.a017947

Simic, R., Lindstrom, D. L., Tran, H. G., Roinick, K. L., Costa, P. J., Johnson, A. D., Hartzog, G. A., & Arndt, K. M. (2003). Chromatin remodeling protein Chd1 interacts with transcription elongation factors and localizes to transcribed genes. *EMBO J*, *22*(8), 1846-1856. https://doi.org/10.1093/emboj/cdg179

Sims, J. K., & Wade, P. A. (2011). SnapShot: Chromatin remodeling: CHD. *Cell*, *144*(4), 626-626 e621. https://doi.org/10.1016/j.cell.2011.02.019

Sims, R. J., 3rd, Chen, C. F., Santos-Rosa, H., Kouzarides, T., Patel, S. S., & Reinberg, D. (2005). Human but not yeast CHD1 binds directly and selectively to histone H3 methylated at lysine 4 via its tandem chromodomains. *J Biol Chem*, *280*(51), 41789-41792. https://doi.org/10.1074/jbc.C500395200

Singh, A., Modak, S. B., Chaturvedi, M. M., & Purohit, J. S. (2023). SWI/SNF Chromatin Remodelers: Structural, Functional and Mechanistic Implications. *Cell Biochem Biophys*, *81*(2), 167-187. https://doi.org/10.1007/s12013-023-01140-5

Singh, A. K., & Mueller-Planitz, F. (2021). Nucleosome Positioning and Spacing: From Mechanism to Function. *J Mol Biol*, *433*(6), 166847. https://doi.org/10.1016/j.jmb.2021.166847

Smith, D. B., & Johnson, K. S. (1988). Single-step purification of polypeptides expressed in Escherichia coli as fusions with glutathione S-transferase. *Gene*, *67*(1), 31-40. https://doi.org/10.1016/0378-1119(88)90005-4

Smolle, M., Venkatesh, S., Gogol, M. M., Li, H., Zhang, Y., Florens, L., Washburn, M. P., & Workman, J. L. (2012). Chromatin remodelers Isw1 and Chd1 maintain chromatin structure during transcription by preventing histone exchange. *Nat Struct Mol Biol*, *19*(9), 884-892. https://doi.org/10.1038/nsmb.2312

Soares, L. M., He, P. C., Chun, Y., Suh, H., Kim, T., & Buratowski, S. (2017). Determinants of Histone H3K4 Methylation Patterns. *Mol Cell*, *68*(4), 773-785 e776. https://doi.org/10.1016/j.molcel.2017.10.013

Stanne, T., Narayanan, M. S., Ridewood, S., Ling, A., Witmer, K., Kushwaha, M., Wiesler, S., Wickstead, B., Wood, J., & Rudenko, G. (2015). Identification of the ISWI Chromatin Remodeling Complex of the Early Branching Eukaryote Trypanosoma brucei. *J Biol Chem*, *290*(45), 26954-26967. https://doi.org/10.1074/jbc.M115.679019

Stockdale, C., Flaus, A., Ferreira, H., & Owen-Hughes, T. (2006). Analysis of nucleosome repositioning by yeast ISWI and Chd1 chromatin remodeling complexes. *J Biol Chem*, *281*(24), 16279-16288. https://doi.org/10.1074/jbc.M600682200

Stokes, D. G., & Perry, R. P. (1995). DNA-binding and chromatin localization properties of CHD1. *Mol Cell Biol*, *15*(5), 2745-2753. https://doi.org/10.1128/MCB.15.5.2745

Strahl-Bolsinger, S., Hecht, A., Luo, K., & Grunstein, M. (1997). SIR2 and SIR4 interactions differ in core and extended telomeric heterochromatin in yeast. *Genes Dev*, *11*(1), 83-93. https://doi.org/10.1101/gad.11.1.83

Strohner, R., Nemeth, A., Jansa, P., Hofmann-Rohrer, U., Santoro, R., Langst, G., & Grummt, I. (2001). NoRC--a novel member of mammalian ISWI-containing chromatin remodeling machines. *EMBO J*, *20*(17), 4892-4900. https://doi.org/10.1093/emboj/20.17.4892

Struhl, K. (1998). Histone acetylation and transcriptional regulatory mechanisms. *Genes Dev*, *12*(5), 599-606. https://doi.org/10.1101/gad.12.5.599

Sudarsanam, P., & Winston, F. (2000). The Swi/Snf family nucleosome-remodeling complexes and transcriptional control. *Trends Genet*, *16*(8), 345-351. https://doi.org/10.1016/s0168-9525(00)02060-6

Suka, N., Luo, K., & Grunstein, M. (2002). Sir2p and Sas2p opposingly regulate acetylation of yeast histone H4 lysine16 and spreading of heterochromatin. *Nat Genet*, *32*(3), 378-383. https://doi.org/10.1038/ng1017

Szerlong, H., Hinata, K., Viswanathan, R., Erdjument-Bromage, H., Tempst, P., & Cairns, B. R. (2008). The HSA domain binds nuclear actin-related proteins to regulate chromatin-remodeling ATPases. *Nat Struct Mol Biol*, *15*(5), 469-476. https://doi.org/10.1038/nsmb.1403

Szerlong, H., Saha, A., & Cairns, B. R. (2003). The nuclear actin-related proteins Arp7 and Arp9: a dimeric module that cooperates with architectural proteins for chromatin remodeling. *EMBO J*, *22*(12), 3175-3187. https://doi.org/10.1093/emboj/cdg296

Tan, L. M., Liu, R., Gu, B. W., Zhang, C. J., Luo, J., Guo, J., Wang, Y., Chen, L., Du, X., Li, S., Shao, C. R., Su, Y. N., Cai, X. W., Lin, R. N., Li, L., Chen, S., Du, J., & He, X. J. (2020). Dual Recognition of H3K4me3 and DNA by the ISWI Component ARID5 Regulates the Floral Transition in Arabidopsis. *Plant Cell*, *32*(7), 2178-2195. https://doi.org/10.1105/tpc.19.00944

Thoma, F., Koller, T., & Klug, A. (1979). Involvement of histone H1 in the organization of the nucleosome and of the salt-dependent superstructures of chromatin. *J Cell Biol*, *83*(2 Pt 1), 403-427. https://doi.org/10.1083/jcb.83.2.403

Thompson, J. S., Ling, X., & Grunstein, M. (1994). Histone H3 amino terminus is required for telomeric and silent mating locus repression in yeast. *Nature*, *369*(6477), 245-247. https://doi.org/10.1038/369245a0

Tirosh, I., Sigal, N., & Barkai, N. (2010). Widespread remodeling of mid-coding sequence nucleosomes by Isw1. *Genome Biol*, *11*(5), R49. https://doi.org/10.1186/gb-2010-11-5-r49

Tosi, A., Haas, C., Herzog, F., Gilmozzi, A., Berninghausen, O., Ungewickell, C., Gerhold, C. B., Lakomek, K., Aebersold, R., Beckmann, R., & Hopfner, K. P. (2013). Structure and subunit topology of the INO80 chromatin remodeler and its nucleosome complex. *Cell*, *154*(6), 1207-1219. https://doi.org/10.1016/j.cell.2013.08.016

Tremethick, D. J. (2007). Higher-order structures of chromatin: the elusive 30 nm fiber. *Cell*, *128*(4), 651-654. https://doi.org/10.1016/j.cell.2007.02.008

Trujillo, J. T., Long, J., Aboelnour, E., Ogas, J., & Wisecaver, J. H. (2022). CHD Chromatin Remodeling Protein Diversification Yields Novel Clades and Domains Absent in Classic Model Organisms. *Genome Biol Evol*, *14*(5). https://doi.org/10.1093/gbe/evac066

Tse, C., Sera, T., Wolffe, A. P., & Hansen, J. C. (1998). Disruption of higher-order folding by core histone acetylation dramatically enhances transcription of nucleosomal arrays by RNA polymerase III. *Mol Cell Biol*, *18*(8), 4629-4638. https://doi.org/10.1128/MCB.18.8.4629

Tsukiyama, T. (2002). The in vivo functions of ATP-dependent chromatin-remodelling factors. *Nat Rev Mol Cell Biol*, *3*(6), 422-429. https://doi.org/10.1038/nrm828

Tsukiyama, T., Palmer, J., Landel, C. C., Shiloach, J., & Wu, C. (1999). Characterization of the imitation switch subfamily of ATP-dependent chromatin-remodeling factors in Saccharomyces cerevisiae. *Genes Dev*, *13*(6), 686-697. https://doi.org/10.1101/gad.13.6.686

Tsukiyama, T., & Wu, C. (1995). Purification and properties of an ATP-dependent nucleosome remodeling factor. *Cell*, *83*(6), 1011-1020. https://doi.org/10.1016/0092-8674(95)90216-3

Tunyasuvunakool, K., Adler, J., Wu, Z., Green, T., Zielinski, M., Zidek, A., Bridgland, A., Cowie, A., Meyer, C., Laydon, A., Velankar, S., Kleywegt, G. J., Bateman, A., Evans, R., Pritzel, A., Figurnov, M., Ronneberger, O., Bates, R., Kohl, S. A. A., . . . Hassabis, D. (2021). Highly accurate protein structure prediction for the human proteome. *Nature*, *596*(7873), 590-596. https://doi.org/10.1038/s41586-021-03828-1

Tyagi, M., Imam, N., Verma, K., & Patel, A. K. (2016). Chromatin remodelers: We are the drivers!! *Nucleus*, *7*(4), 388-404. https://doi.org/10.1080/19491034.2016.1211217

van Attikum, H., Fritsch, O., Hohn, B., & Gasser, S. M. (2004). Recruitment of the INO80 complex by H2A phosphorylation links ATP-dependent chromatin remodeling with DNA double-strand break repair. *Cell*, *119*(6), 777-788. https://doi.org/10.1016/j.cell.2004.11.033

van Holde, K., & Zlatanova, J. (1995). Chromatin higher order structure: chasing a mirage? *J Biol Chem*, *270*(15), 8373-8376. https://doi.org/10.1074/jbc.270.15.8373

van Holde, K., & Zlatanova, J. (2007). Chromatin fiber structure: Where is the problem now? *Semin Cell Dev Biol*, *18*(5), 651-658. https://doi.org/10.1016/j.semcdb.2007.08.005

Varadi, M., Anyango, S., Deshpande, M., Nair, S., Natassia, C., Yordanova, G., Yuan, D., Stroe, O., Wood, G., Laydon, A., Zidek, A., Green, T., Tunyasuvunakool, K., Petersen, S., Jumper, J., Clancy, E., Green, R., Vora, A., Lutfi, M., . . . Velankar, S. (2022). AlphaFold Protein Structure Database: massively expanding the structural coverage of protein-sequence space with high-accuracy models. *Nucleic Acids Res*, *50*(D1), D439-D444. https://doi.org/10.1093/nar/gkab1061

Varga-Weisz, P. D., Wilm, M., Bonte, E., Dumas, K., Mann, M., & Becker, P. B. (1997). Chromatin-remodelling factor CHRAC contains the ATPases ISWI and topoisomerase II. *Nature*, *388*(6642), 598-602. https://doi.org/10.1038/41587

Vary, J. C., Jr., Gangaraju, V. K., Qin, J., Landel, C. C., Kooperberg, C., Bartholomew, B., & Tsukiyama, T. (2003). Yeast Isw1p forms two separable complexes in vivo. *Mol Cell Biol*, *23*(1), 80-91. https://doi.org/10.1128/MCB.23.1.80-91.2003

Venkatesh, S., & Workman, J. L. (2013). Set2 mediated H3 lysine 36 methylation: regulation of transcription elongation and implications in organismal development. *Wiley Interdiscip Rev Dev Biol*, *2*(5), 685-700. https://doi.org/10.1002/wdev.109

Verdel, A., Jia, S., Gerber, S., Sugiyama, T., Gygi, S., Grewal, S. I., & Moazed, D. (2004). RNAi-mediated targeting of heterochromatin by the RITS complex. *Science*, *303*(5658), 672-676. https://doi.org/10.1126/science.1093686

Vettese-Dadey, M., Grant, P. A., Hebbes, T. R., Crane- Robinson, C., Allis, C. D., & Workman, J. L. (1996). Acetylation of histone H4 plays a primary role in

enhancing transcription factor binding to nucleosomal DNA in vitro. *EMBO J*, *15*(10), 2508-2518. https://www.ncbi.nlm.nih.gov/pubmed/8665858

Wald, J., Fahrenkamp, D., Goessweiner-Mohr, N., Lugmayr, W., Ciccarelli, L., Vesper, O., & Marlovits, T. C. (2022). Mechanism of AAA+ ATPase-mediated RuvAB-Holliday junction branch migration. *Nature*, *609*(7927), 630-639. https://doi.org/10.1038/s41586-022-05121-1

Wang, X., Moore, S. C., Laszckzak, M., & Ausio, J. (2000). Acetylation increases the alpha-helical content of the histone tails of the nucleosome. *J Biol Chem*, *275*(45), 35013-35020. https://doi.org/10.1074/jbc.M004998200

West, S. C., & Connolly, B. (1992). Biological roles of the Escherichia coli RuvA, RuvB and RuvC proteins revealed. *Mol Microbiol*, *6*(19), 2755-2759. https://doi.org/10.1111/j.1365-2958.1992.tb01454.x

Widom, J., & Klug, A. (1985). Structure of the 300A chromatin filament: X-ray diffraction from oriented samples. *Cell*, *43*(1), 207-213. https://doi.org/10.1016/0092-8674(85)90025-x

Williams, S. P., Athey, B. D., Muglia, L. J., Schappe, R. S., Gough, A. H., & Langmore, J. P. (1986). Chromatin fibers are left-handed double helices with diameter and mass per unit length that depend on linker length. *Biophys J*, *49*(1), 233-248. https://doi.org/10.1016/S0006-3495(86)83637-2

Wood, K., Tellier, M., & Murphy, S. (2018). DOT1L and H3K79 Methylation in Transcription and Genomic Stability. *Biomolecules*, *8*(1). https://doi.org/10.3390/biom8010011

Woodage, T., Basrai, M. A., Baxevanis, A. D., Hieter, P., & Collins, F. S. (1997). Characterization of the CHD family of proteins. *Proc Natl Acad Sci U S A*, *94*(21), 11472-11477. https://doi.org/10.1073/pnas.94.21.11472

Woodcock, C. L., & Dimitrov, S. (2001). Higher-order structure of chromatin and chromosomes. *Curr Opin Genet Dev*, *11*(2), 130-135. https://doi.org/10.1016/s0959-437x(00)00169-6

Woodcock, C. L., Frado, L. L., & Rattner, J. B. (1984). The higher-order structure of chromatin: evidence for a helical ribbon arrangement. *J Cell Biol*, *99*(1 Pt 1), 42-52. https://doi.org/10.1083/jcb.99.1.42

Woodcock, C. L., Grigoryev, S. A., Horowitz, R. A., & Whitaker, N. (1993). A chromatin folding model that incorporates linker variability generates fibers resembling the native structures. *Proc Natl Acad Sci U S A*, *90*(19), 9021-9025. https://doi.org/10.1073/pnas.90.19.9021

Woodcock, C. L., Safer, J. P., & Stanchfield, J. E. (1976). Structural repeating units in chromatin. I. Evidence for their general occurrence. *Exp Cell Res*, *97*, 101-110. https://doi.org/10.1016/0014-4827(76)90659-5

Worcel, A., Strogatz, S., & Riley, D. (1981). Structure of chromatin and the linking number of DNA. *Proc Natl Acad Sci U S A*, *78*(3), 1461-1465. https://doi.org/10.1073/pnas.78.3.1461

Wozniak, G. G., & Strahl, B. D. (2014). Hitting the 'mark': interpreting lysine methylation in the context of active transcription. *Biochim Biophys Acta*, *1839*(12), 1353-1361. https://doi.org/10.1016/j.bbagrm.2014.03.002

Wysocka, J., Swigut, T., Xiao, H., Milne, T. A., Kwon, S. Y., Landry, J., Kauer, M., Tackett, A. J., Chait, B. T., Badenhorst, P., Wu, C., & Allis, C. D. (2006). A PHD finger of NURF couples histone H3 lysine 4 trimethylation with chromatin remodelling. *Nature*, *442*(7098), 86-90. https://doi.org/10.1038/nature04815

Xiao, H., Sandaltzopoulos, R., Wang, H. M., Hamiche, A., Ranallo, R., Lee, K. M., Fu, D., & Wu, C. (2001). Dual functions of largest NURF subunit NURF301 in

nucleosome sliding and transcription factor interactions. *Mol Cell*, *8*(3), 531-543. https://doi.org/10.1016/s1097-2765(01)00345-8

Xiao, T., Hall, H., Kizer, K. O., Shibata, Y., Hall, M. C., Borchers, C. H., & Strahl, B. D. (2003). Phosphorylation of RNA polymerase II CTD regulates H3 methylation in yeast. *Genes Dev*, *17*(5), 654-663. https://doi.org/10.1101/gad.1055503

Yadon, A. N., & Tsukiyama, T. (2011). SnapShot: Chromatin remodeling: ISWI. *Cell*, *144*(3), 453-453 e451. https://doi.org/10.1016/j.cell.2011.01.019

Yamada, K., Frouws, T. D., Angst, B., Fitzgerald, D. J., DeLuca, C., Schimmele, K., Sargent, D. F., & Richmond, T. J. (2011). Structure and mechanism of the chromatin remodelling factor ISW1a. *Nature*, *472*(7344), 448-453. https://doi.org/10.1038/nature09947

Yamada, T., Fischle, W., Sugiyama, T., Allis, C. D., & Grewal, S. I. (2005). The nucleation and maintenance of heterochromatin by a histone deacetylase in fission yeast. *Mol Cell*, *20*(2), 173-185. https://doi.org/10.1016/j.molcel.2005.10.002

Yan, L., & Chen, Z. (2020). A Unifying Mechanism of DNA Translocation Underlying Chromatin Remodeling. *Trends Biochem Sci*, *45*(3), 217-227. https://doi.org/10.1016/j.tibs.2019.09.002

Yan, L., Wang, L., Tian, Y., Xia, X., & Chen, Z. (2016). Structure and regulation of the chromatin remodeller ISWI. *Nature*, *540*(7633), 466-469. https://doi.org/10.1038/nature20590

Yan, L., Wu, H., Li, X., Gao, N., & Chen, Z. (2019). Structures of the ISWI-nucleosome complex reveal a conserved mechanism of chromatin remodeling. *Nat Struct Mol Biol*, *26*(4), 258-266. https://doi.org/10.1038/s41594-019-0199-9

Yang, J. G., Madrid, T. S., Sevastopoulos, E., & Narlikar, G. J. (2006). The chromatin-remodeling enzyme ACF is an ATP-dependent DNA length sensor that regulates nucleosome spacing. *Nat Struct Mol Biol*, *13*(12), 1078-1083. https://doi.org/10.1038/nsmb1170

Yang, X., Zaurin, R., Beato, M., & Peterson, C. L. (2007). Swi3p controls SWI/SNF assembly and ATP-dependent H2A-H2B displacement. *Nat Struct Mol Biol*, *14*(6), 540-547. https://doi.org/10.1038/nsmb1238

Yen, K., Vinayachandran, V., Batta, K., Koerber, R. T., & Pugh, B. F. (2012). Genome-wide nucleosome specificity and directionality of chromatin remodelers. *Cell*, *149*(7), 1461-1473. https://doi.org/10.1016/j.cell.2012.04.036

Zhang, P., Torres, K., Liu, X., Liu, C. G., & Pollock, R. E. (2016). An Overview of Chromatin-Regulating Proteins in Cells. *Curr Protein Pept Sci*, *17*(5), 401-410. https://doi.org/10.2174/1389203717666160122120310

Zhao, Y., & Garcia, B. A. (2015). Comprehensive Catalog of Currently Documented Histone Modifications. *Cold Spring Harb Perspect Biol*, *7*(9), a025064. https://doi.org/10.1101/cshperspect.a025064

Zhou, C. Y., Johnson, S. L., Gamarra, N. I., & Narlikar, G. J. (2016). Mechanisms of ATP-Dependent Chromatin Remodeling Motors. *Annu Rev Biophys*, *45*, 153-181. https://doi.org/10.1146/annurev-biophys-051013-022819

Zhou, K., Gaullier, G., & Luger, K. (2019). Nucleosome structure and dynamics are coming of age. *Nat Struct Mol Biol*, *26*(1), 3-13. https://doi.org/10.1038/s41594-018-0166-x

Zhou, Y., Santoro, R., & Grummt, I. (2002). The chromatin remodeling complex NoRC targets HDAC1 to the ribosomal gene promoter and represses RNA polymerase I transcription. *EMBO J*, *21*(17), 4632-4640. https://doi.org/10.1093/emboj/cdf460

Zofall, M., & Grewal, S. I. (2006). Swi6/HP1 recruits a JmjC domain protein to facilitate transcription of heterochromatic repeats. *Mol Cell*, *22*(5), 681-692. https://doi.org/10.1016/j.molcel.2006.05.010

Appendix

Appendix A

Supplementary Table 1. List of proteins identified in tandem affinity purification of Isw1-TAP

Protein name	Ordered locus name	Peptide	Spectral count
Isw1	YBR245C	98	4383
Ioc2	YLR095C	29	545
Ioc3	YFR013W	33	1984
Ioc4	YMR044W	14	592
Esc8	YOL017W	8	27

Appendix B

Supplementary Table 2. List of residue pairs of Esc8 interacts with the SLIDE domain of Isw1 (Preliminary data)

Interaction	Residue at Isw1	Residue at Esc8
Salt bridge	E995	R137
	R1019	E269
	D1020	R277
	E1021	R277
	D1024	K274, K277
	E1029	H538, K171, R517
	E1041	H320
Hydrophobic contact	F999	L526
	L1002	L526
	M1003	L526
	L1027	F340, I523, L526
	F1028	F340, L526
	L1030	M170, F340,
	F1032	F175, F179, I309, I323, L442
Hydrogen bond	K898	H328, L329
	L991	R443
	E995	Y138, Y339
	E996	R443
	R1019	E269
	R1023	S314, W270
	D1024	R277
	P1026	R517
	E1029	R517, W539
	S1036	S314
	R1037	Q324

Appendix C

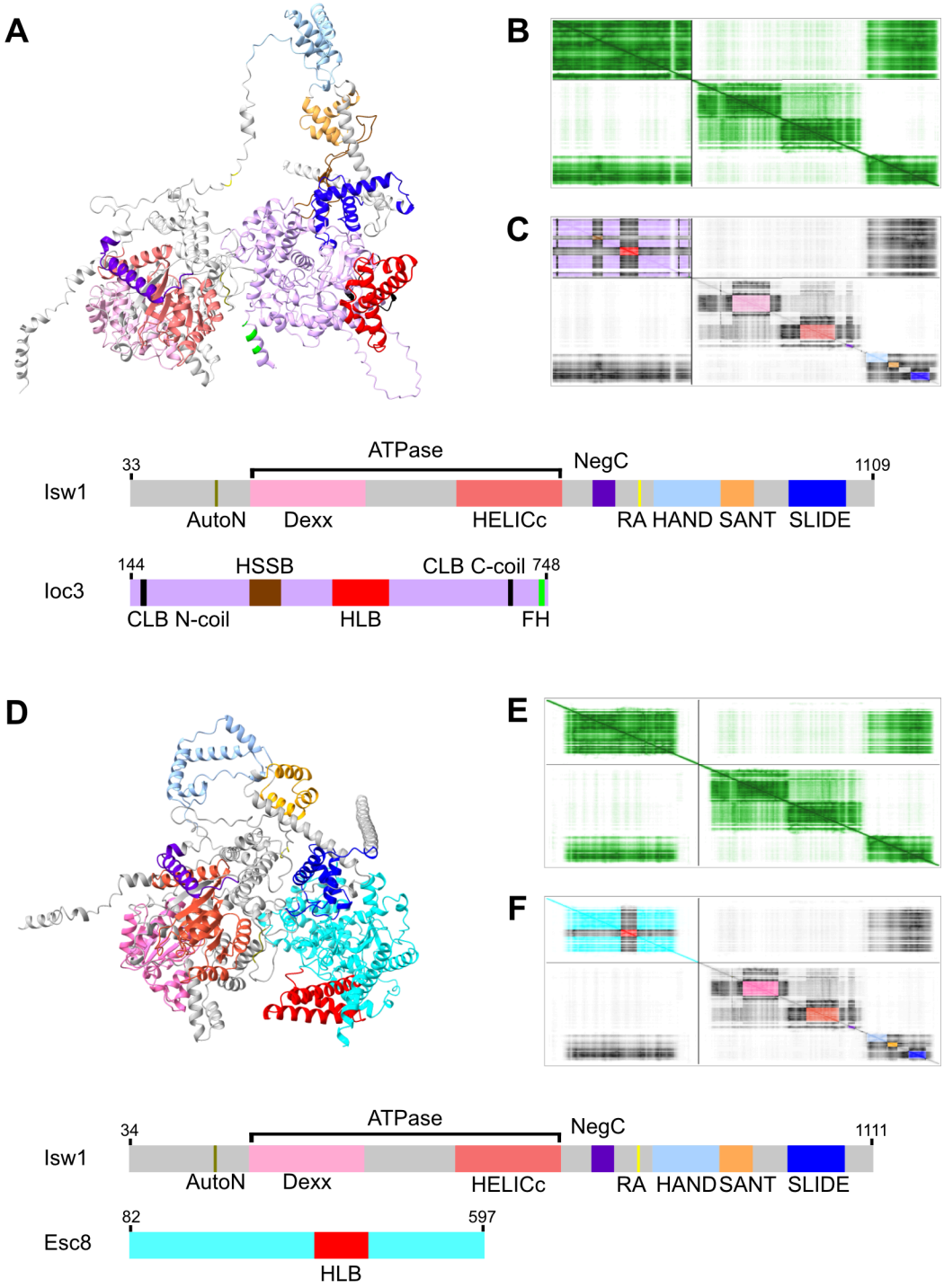

Supplementary Figure 1. AlphaFold structural proteins of Isw1a and Isw1c with their PAE plots. **(A)** AlphaFold predicted structure Isw1a with its domain compositions. **(B)** Interactive 2D PAE plot of Isw1a in green color-based. **(C)** Interactive 2D PAE plot of Isw1a in accordance with its structural domain color. **(D)** AlphaFold predicted structure Isw1c with its domain compositions. **(E)** Interactive 2D PAE plot of Isw1c in green color-based. **(F)** Interactive 2D PAE plot of Isw1c in accordance with its structural domain color.

Appendix D

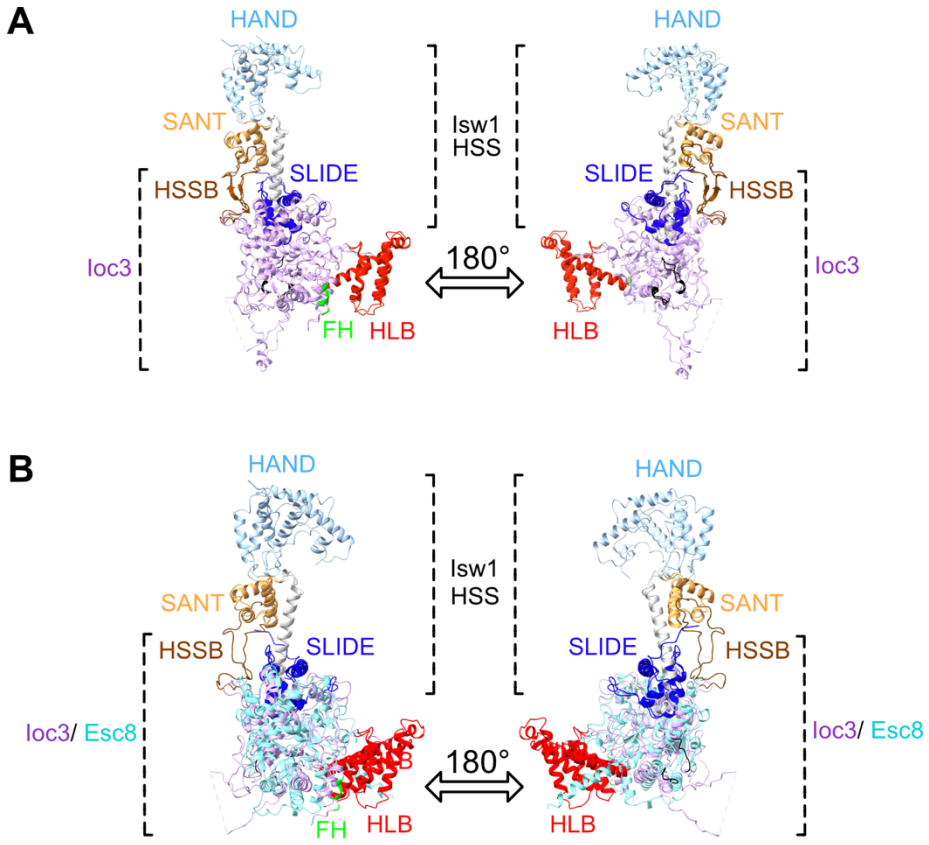

Supplementary Figure 2. Structural superimposed of the crystal structure of Isw1a with the AlphaFold structures of either Isw1a or Isw1c. (A) Three-dimensional superimpositions between the crystal structure of Isw1a with the AlphaFold predicted structure of Isw1a. **(B)** Three-dimensional superimpositions between the crystal structure of Isw1a with the AlphaFold predicted structure of Isw1c. The crystal structure of Isw1a is adapted from Yamada et al., 2011.

Appendix E

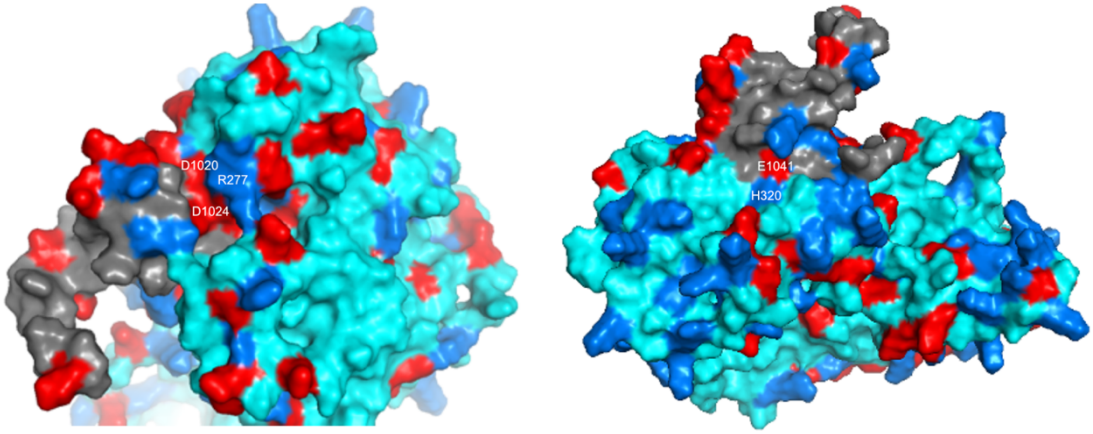

Supplementary Figure 3. Representative model structure for residue pairs of the SLIDE domain of Isw1 interacting with Esc8. On the left structure, negatively charged residues D1020 and D1024 of Isw1 interact with positively charged residue R277 of Esc8. On the right structure, negatively charged residue E1041 of Isw1 binds to positively charged residue H320 of Esc8. The Isw1-based color is grey color, and the Esc8-based color is cyan. The regions with positive charge residues are indicated with red color while the regions with negative charged residues are indicated with blue color. The amino acids of aspartic acid (D), glutamic acid (E), histidine (H), and arginine (R) are indicated.

Acknowledgments

First and foremost, I would like to sincerely thank my direct supervisor and mentor, Dr. Michaela Smolle, for giving me the opportunity to pursue my doctoral research in your laboratory. I truly appreciate your guidance, advice, encouragement, and endless support throughout my PhD journey. Thank you for helping me grow both as a scientist and as a person. You have taught me to think critically, persevere in the face of challenges, and appreciate the value of collaborative work.

Next, I would like to thank Prof. Dr. Andreas Ladurner, my doctorvater, and the head Department of Physiological Chemistry, for mentoring and providing support, valuable discussion, and feedback during my PhD. Moreover, I am grateful to Prof. Dr. Andreas Ladurner and Dr. Carla Margulies for accepting me to participate in their group research discussion. This experience enabled me to broaden my understanding of the research and think from diverse perspectives.

I also would like to say many thanks to my Thesis Advisory Committee (TAC) members, Prof. Dr. Peter Becker and Dr. Christoph Kurat, for your feedback, suggestions, and support in guiding me through my PhD research and helping me refine my thesis. Your expertise and encouragement have significantly contributed to the quality of my work. Thank you for your kindness and for always keeping your door open to me for advice.

I would like to extend my sincere gratitude to all my collaborators. Thank you to Dr. Maren Heimhalt for generating the AlphaFold predicted structures of the Isw1c, Isw1c mutants, and Isw1a. You guided me through the predicted structures and shared your invaluable insights into analyzing the protein structure. Thank you to Prof. Dr. Philipp Korber, Drin Shabani, and Lorenz Spechtenhauser for their contributions to elucidating the function of Isw1c in nucleosome positioning and remodeling. I really appreciate your input and great engaging discussion that have significantly improved the quality of the research. Also, I enjoy and appreciate working with such great scientists like many of you. Without all of your contribution, support, and guidance, this thesis would not have been possible.

In addition, thank you to Prof. Dr. Felix Müller-Planitz, Dr. Petra Vizjak, and Dr. Ashish Kumar Singh for sharing their expertise, the established procedure of the ATP hydrolysis assay, and the Isw1 antibody. Thank you to Dr, Till Bartke and Dr. Philipp Voight for generously providing me with various histone octamers that enabled me to uncover the influence of histone variants and common histone modifications in Isw1c functions. Thank you to Prof. Dr. Jane Mellor for generously giving me the Isw1 yeast strain mutants that allowed me to uncover the protein-protein interactions between Isw1 and Esc8. Thank you to Dr. Mathias Capella for kindly giving me the plasmids containing various promoter genes. Thank you to Dr. Gunnar Knobloch for giving me the plasmid competitor DNA used in nucleosome sliding assay and competitive nucleosome sliding assay.

Then, I would like to thank the members of the Smolle lab, including Julia Schluckebier, Dr. Lena Bergmann, Andreia Almeida, and Lingling Yang, for the discussion. You cultivated a diverse environment within the group. A special thanks

to Julia Schluckebier for your contribution in performing CUT&RUN and qPCR as part of an experimental attempt to determine the localization of *ESC8* in the genome. Since we were unable to successfully address this research question, the data are not included in the results section. Nevertheless, I deeply appreciate your strong support, encouragement, effort, and insightful discussions throughout my PhD. I have greatly enjoyed your presence, great energy, and enthusiasm.

I am grateful to all the members of the Physiological Chemistry Department. My PhD journey and life in Germany have been very enjoyable and fulfilling. I am also thankful to all the members of the Siegel lab, Ladurner lab, and Margulies lab groups for the warm welcome and for embracing me as a team member. Connecting with many people in this department throughout my PhD journey has taught me many valuable lessons in science and life. They have all profoundly shaped me into the researcher and the person I am today.

In addition, I would like to extend special thanks to Dr. Elizabeth Schroeder-Reiter, the IRTG-CRC-1064 Program Coordinator, for your kindness, support, and encouragement throughout the entire duration of my PhD Program. Your positive energy has greatly influenced how I have managed to navigate many of the challenges in my PhD.

I also wish to acknowledge the Deutscher Akademischer Austauschdienst (DAAD) for funding my PhD studies in Germany. This opportunity is very valuable for me, as it allows me to gain invaluable experience in conducting research in Germany.

Finally, I would like to express my gratitude to my family. Their unwavering love, faith in me, and support have enabled me to overcome all the challenges in life. Their belief in me has been my strength, and their sacrifices have paved the way for my success. I am grateful for their presence in my life.

Affidavit

Affidavit

Ameirika

Surname, first name

Großhaderner Str. 9

Street

82152, Planegg-Martinsried, Germany

Zip code, town, country

I hereby declare, that the submitted thesis entitled:

Characterization of a novel ISWI chromatin remodeler in *Saccharomyces cerevisiae*

is my own work. I have only used the sources indicated and have not made unauthorised use of services of a third party. Where the work of others has been quoted or reproduced, the source is always given.

I further declare that the dissertation presented here has not been submitted in the same or similar form to any other institution for the purpose of obtaining an academic degree.

Planegg, 7 January 2025 — Ameirika

place, date — Signature doctoral candidate

Confirmation of Congruency

LMU LUDWIG-MAXIMILIANS-UNIVERSITÄT MÜNCHEN | Promotionsbüro Medizinische Fakultät | MMRS

Confirmation of congruency between printed and electronic version of the doctoral thesis

Ameirika
Surname, first name

Großhaderner Str. 9
Street

82152, Planegg-Martinsried, Germany
Zip code, town, country

I hereby declare, that the submitted thesis entitled:

Characterization of a novel ISWI chromatin remodeler in *Saccharomyces cerevisiae*

is congruent with the printed version both in content and format.

Planegg, 7 January 2025
place, date

Ameirika
Signature doctoral candidate